

ISSN 2187-2260

**Proceedings of the 21st Meeting of
Japan CF Research Society
JCF 21**

December 11-12, 2020

Virtual Meeting

Japan CF-Research Society

Edited by Shinya Narita

Copyright © 2021 by Japan CF Research Society

All rights reserved. No part of this publication may be reproduced, stored in a retrieval system, or transmitted, in any form or by any means, electronic, mechanical, photocopying, recording or otherwise, without the prior permission of the copyright owner.

PREFACE

This is the proceedings of the 21st Meeting of Japan CF-Research Society (JCF21), which was organized by Professor Katsuaki Tanabe (Kyoto University). Due to pandemic of COVID-19, the meeting was held in online format. In this meeting, 10 presentations were given and 8 papers were submitted to the editorial board. They have been peer reviewed by the referees, and revised for the publication as the proceedings.

For all meetings, JCF1 through JCF20, we published the Proceedings. For the meetings after JCF4, we published electronic versions of the proceedings on our web-site http://jcfrs.org/proc_jcf.html in addition to their printed versions. In view of low efficiency and low effectiveness in distributing information, we decided to discontinue the printed version for the meetings, JCF12. Only the electronic versions have been published thereafter. Any comment and questions from the scientists all over the world are welcomed.

Finally, we would like to thank all the participants and the people who have collaborated in organizing this meeting.

Editor-in-Chief

Shinya Narita, Iwate University

July 2021

CONTENTS

Preface: S. Narita	i
Evidence for Surface Heat Release Reaction over Nano-sized Multilayer Metal Composite with Hydrogen Gas <i>Y. Iwamura, T. Itoh, M. Saito, S. Murakami, J. Kasagi</i>	1
Optical Observation on Anomalous Heat Generation from Nano-sized Metal Composite <i>T. Itoh, Y. Shibasaki, J. Kasagi, S. Murakami, M. Saito, Y. Iwamura</i>	15
Simulation Study of Heat Conduction in Deuterium Desorption Experiment <i>N. Kishimoto, M. Endo, A. Kikuchi, K. Matsushashi, K. Negishi, S. Narita</i>	26
Thermodynamic analysis of Pd–H electrode: $H/Pd > \beta_{\min}$ during repeated cathodic and anodic electrolysis in an acidic solution <i>H. Numata</i>	40
A theoretical study on the possible change of the phonon dispersion relation due to the nuclear reaction in two-dimensional lattice III <i>K. Tsuchiya</i>	47
Cold Fusion Phenomenon in the Composite CF Materials – Mixed Hydrogen Isotopes, Alloys, Ceramics, and Polymers – <i>H. Kozima</i>	54
Cold Fusion Phenomenon in the Compound CF Materials – Effects of Interfaces – <i>H. Kozima</i>	112
Neutron Energy Bands in the Compound and Composite CF Materials – Speculation on the Bases of the TNCF and ND Models – <i>H. Kozima</i>	188

Evidence for Surface Heat Release Reaction over Nano-sized Multilayer Metal Composite with Hydrogen Gas

Yasuhiro Iwamura¹, Takehiko Itoh^{1,2}, Mari Saito², Shoichi Murakami²
and Jirohta Kasagi¹

¹Research Center for Electron Photon Science, Tohoku University, Sendai, 982-0826, Japan

²CLEAN PLANET Inc., Tokyo, 105-0022, Japan

E-mail: iwamura@lms.tohoku.ac.jp

Abstract

Excess energy generation using a nano-sized multilayer metal composite with hydrogen gas has been investigated. Two nano-sized metal multilayer composite samples, which were composed of Ni, Cu, CaO thin films on bulk Ni (25 mm×25 mm×0.1 mm), were used. These samples were fabricated by Ar ion beam or magnetron sputtering method. Heat burst and excess energy generation were observed during the experiments using nano-sized metal multilayer composite on Ni substrate and hydrogen gas. Maximum average released energy per absorbed total hydrogen was 21 keV/H or 2.0 GJ/H-mol up to now.

Heat burst phenomena were simultaneously detected by two radiation thermometers looking at both surfaces (A and B) of the multilayer thin films and a thermocouple (TC) located near the metal composite. An experimental example showed that heat burst reaction occurred at the surface A at first and propagated to the TC and afterwards heat burst reaction occurred at the surface B. This type of clear evidence that heat release reactions occur in the near surface region of the nano-sized multilayer metal composite with hydrogen gas was often obtained during recent experiments. It also demonstrates that observed excess energy in our experiments was due to real heat generation and cannot be attributed to the artifact like variation of a calibration curve on the relationship between electrical input and TC. These experimental results cannot be explained by any known chemical process and implies that the observed heat generation must be of nuclear origin.

1. Introduction

New type of excess heat experiments using a nano-sized metal multilayer composite and hydrogen gas have been performed based on the permeation-induced transmutation experiments with multilayer thin film and excess heat experiments with nano particles. Figure 1 shows the background of the present experimental method.

The permeation-induced transmutation phenomenon, which is completely different from conventional transmutation by nuclear reactors or accelerators, was first reported in 2002 [1]. D₂ gas permeation through a nano-structured multilayer thin film composed of Pd and CaO thin film and Pd substrate with a target element induces nuclear transmutation reactions [2]-[4]. Permeation-induced nuclear transmutation reactions were firstly observed at Mitsubishi Heavy Industries and were successfully replicated by other institutes such as Toyota R&D center [5]. Typical target element is Cs and produced element is Pr. Transmutation reactions of Sr, Ba, W into Mo, Sm, Pt were also observed

by this method. In this research, deuterium diffusion through nano-sized multilayer thin film was a key factor and the elemental analysis was important technique.

Collaborative Research Project between six Japanese organizations funded by NEDO (New Energy and Industrial Technology Development Organization) on anomalous heat effects was done from Oct. 2015 to Oct. 2017 using Ni, Pd, Cu, Zr nano particles. Anomalous heat generation, which is too much to be explained by any known chemical process, was observed. Qualitative reproducibility was confirmed between the Kobe University and Tohoku University [6]-[9]. The authors replicated the experiments using nano Pd/Ni fabricated by glow discharge with D₂ gas developed by Dr. Mizuno [10]. In these experiments, nano-sized particles and diffusion of hydrogen and deuterium were one of key factors to observe the heat effects and precise heat estimation was crucial.

Combining above important factors and methods to induce transmutation and heat generation reactions, we developed a present method using a nano-sized metal multilayer composite and hydrogen gas. Larger excess energy per H was obtained using the present experimental method.

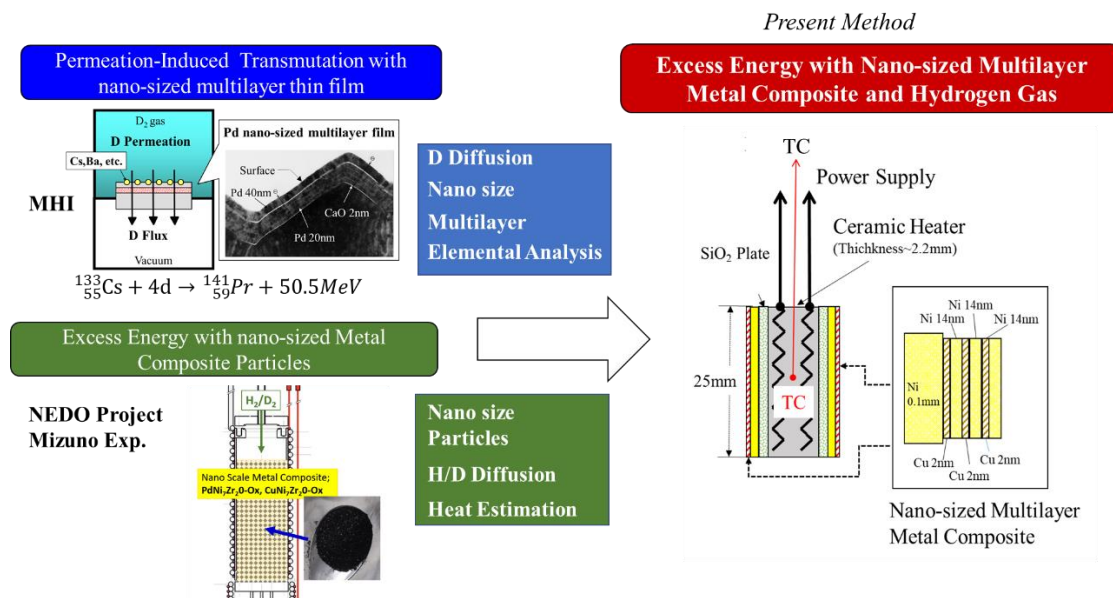


Figure.1 Background and Motivation of the Present Experimental Method.

2. Experimental

Schematic of our experimental apparatus is shown in Fig.2(a). It is basically the same with the paper [11]-[14] and improved in some points. Two nano-sized metal multilayer composite samples, which were composed of Ni, Cu, CaO thin films on bulk Ni (25 mm×25 mm×0.1 mm), were used. H₂ gas and its pressure were monitored by a Pirani gauge. The chamber could be evacuated by a turbo molecular pump. The multilayer samples could be heated up by a ceramic heater in which a thermocouple (TC; Pt-PtRh13 %) was embedded.

In the paper [11], surface temperature of a sample was evaluated by an infrared radiation thermometer (IR-CAQ3CS; Chino Corp.). Recently, we have introduced additional radiation thermometers and surface temperature measurement for the two nano-sized metal multilayer composite samples became possible. The detector was made of InGaAs and two wavelengths, 1.55 μm and 1.35 μm , were used in this work. Heater input power was supplied by a DC power source with constant voltage mode. The input voltage and current were measured both by voltage and current monitors provided by the power supply and an independent voltmeter and amperemeter, respectively.

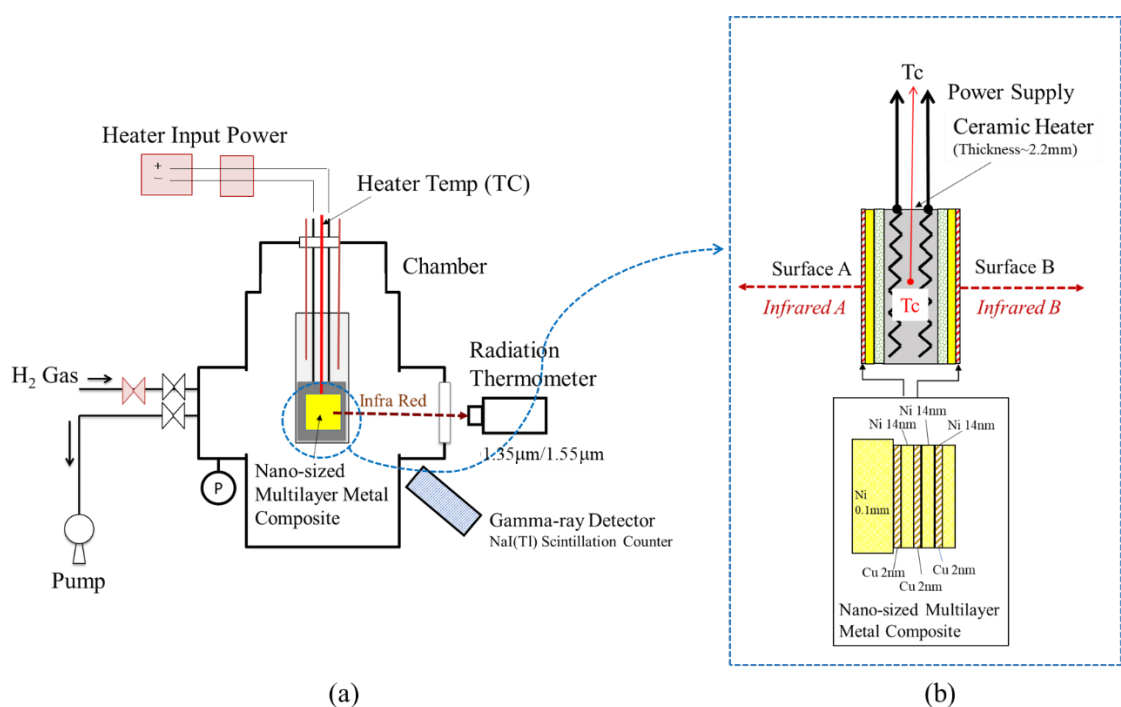


Figure 2. Experimental Set-up; (a) Schematic of Experimental Apparatus, (b) Detail Drawing around Nano-sized Multilayer Metal Composite.

A detailed drawing of the Ni based nano-sized metal multilayer composite is shown in Fig.2 (b). It was composed of a Ni Plate (25 mm square and 0.1 mm thickness) and Cu-Ni multilayer thin film (20 mm diameter circle and about 100 nm thickness). These samples were fabricated by Ar ion beam or magnetron sputtering method. Two nano-sized metal multilayer composite samples were heated by the ceramic heater (25 mm square and 2.2 mm thickness) through SiO₂ plates (0.3 mm thickness). If certain energy generation reactions would happen on the surface of samples, the temperature of the embedded thermocouple (Tc) would rise. Simultaneously, infrared emission detected by the radiation thermometer, which corresponds to surface temperature of the sample, would increase.

The experimental procedure is as follows. Two nano-sized metal multilayer composites were placed in the chamber and baked for 1-2 days at temperature more than 200 °C to remove H₂O on the surface under vacuum condition. After baking, H₂ gas was introduced into the chamber up to about 200 Pa at 250 °C. Usually H₂ gas was loaded for

about 16 hours. Then, H₂ gas was evacuated by the turbo molecular pump and simultaneously the samples were heated up by the ceramic heater up to 600-950 °C. These process triggers heat generation reactions and observed excess heat. Typically, after 8 hours, the heater input was turned down and the samples were made cool down to 250 °C. These processes (H₂ loading, heating up and cooling down samples) were repeated several times changing heating temperature.

During the above experimental procedure, hydrogen atoms are supposed to diffuse from the Ni plate through the nano-sized metal multilayer to the surface. The diffusion mechanism of hydrogen atoms is well known as “quantum diffusion” at low temperature [15]. Hydrogen atoms are hopping from a site to another site in metal. We assume that hydrogen flux is one of the key factors to induce condensed matter nuclear reactions and the hydrogen flux is intentionally arranged by the present experimental method. Hydrogen flux *J* from the nano-sized metal multilayer composite to the chamber is caused by gradient of hydrogen concentration and gradient of temperature as shown in eq. (1)[16].

$$J = -nD \left(\nabla c + \frac{cQ^*\nabla T}{k_B T^2} \right), \quad (1)$$

where *n* is the number of lattice atoms per unit volume, *c* is hydrogen concentration defined as the hydrogen/host-metal atom ratio, *D* is diffusion coefficient and *Q** is the heat of transport.

3. Results and Discussion

3.1 Excess Heat Evaluation

Excess Heat is evaluated based on the model described in Fig.3(a) and the following equation (2).

$$k_{eff} \frac{T_C - T_W}{L_{eff}} A_{eff} + A_S \sigma \{ \varepsilon_A (T_{SA}^4 - T_W^4) + \varepsilon_B (T_{SB}^4 - T_W^4) \} + A_{Rloss} \varepsilon_{Rloss} \sigma (T_{Rloss}^4 - T_W^4) = P_{in} + H_{ex}, \quad (2)$$

where *k_{eff}* is equivalent thermal conductivity, *T_c* is the thermocouple temperature embedded in the ceramic heater, *T_w* is wall temperature of the chamber, *L_{eff}* and *A_{eff}* are effective length and effective surface area between the sample holder and wall, respectively. *A_s* is surface area of the sample, *T_s* is the surface temperature, *ε* is the emissivity of the sample, *σ* is the Stefan–Boltzmann constant. subscript A and B means surface A and B, respectively. *A_{Rloss}*, *ε_{Rloss}* and *T_{Rloss}* are effective surface area; effective emissivity and effective surface temperature for radiation loss except from the sample surface, which is mainly derived from the sample holder. *P_{in}* is the electrical heater input and *H_{ex}* is excess power. This equation is obtained under the following assumptions.

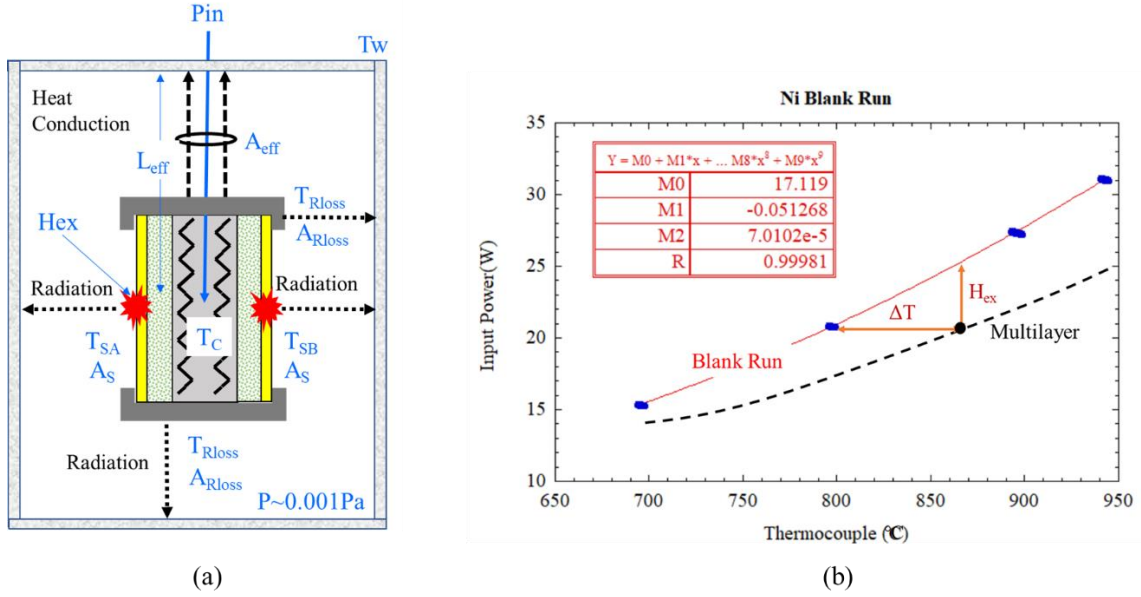


Figure 3. Excess Heat Evaluation; (a) Model of Excess Heat Evaluation, (b) Relationship between Input Power(W) and Thermocouple Temperature (°C) for a Blank Run and a Multilayer Run.

- 1) Thermal conduction via H₂ gas is negligible as H₂ pressure is low enough.
- 2) Radiation from chamber wall is negligible because T_w is room temperature.
- 3) The electrical input power is constant.

A blank run, in which same sized Ni bulk samples without multilayer thin films were used, was performed with the same procedure described above. Figure 3(b) shows the relationship between input power given to the ceramic heater and heater temperature detected by the thermocouple. As the radiation loss term from the sample holder is the same for Ni bulk and multilayer samples for the same temperature, generated excess heat power is supposed to be evaluated based on the blank run result as shown in Fig.3(b). Equation (2) for Ni bulk (subscript “0”) is written as

$$k_{eff} \frac{T_{C0} - T_W}{L_{eff}} A_{eff} + A_S \sigma \{ \epsilon_{A0} (T_{SA0}^4 - T_W^4) + \epsilon_{B0} (T_{SB0}^4 - T_W^4) \} + A_{Rloss} \epsilon_{Rloss} \sigma (T_{Rloss0}^4 - T_W^4) = P_{in}. \quad (3)$$

In the papers [11]-[14], excess heat analysis was done based on the assumption that ϵ is constant for Ni based nano-sized metal multilayer composite and Ni bulk as a first step of data analysis.

Emissivity ϵ can be measured by switching two wavelengths mode and single wavelength mode. Actual measured emissivity was in the range of 0.1-0.2 at surface

temperature 700-750 °C, depending on the condition of the sample such as oxidation of surface or surface roughness, the vacuum of the experimental apparatus. However, the difference in emissivity between Ni bulk and Ni multilayer composite samples is within 0.05 (< 5 %), and the assumed condition is satisfied. It would be possible to consider that emissivity was almost the same for the Ni bulk and multilayer composite samples.

Excess heat H_{ex} is written based on the equations (2) for multilayer composite and Ni bulk (subscript “0”) samples.

$$\begin{aligned}
H_{ex} &= k_{eff} \frac{T_c - T_{c0}}{L_{eff}} A_{eff} + A_S \sigma \{ \varepsilon_A T_{SA}^4 - \varepsilon_{A0} T_{SA0}^4 + \varepsilon_B T_{SB}^4 - \varepsilon_{B0} T_{SB0}^4 - T_W^4 (\varepsilon_A - \varepsilon_{A0}) \} + \\
&A_{Rloss} \varepsilon_{Rloss} \sigma (T_{Rloss}^4 - T_{Rloss0}^4) \\
&\approx k_{eff} \frac{T_c - T_{c0}}{L_{eff}} A_{eff} + A_S \sigma \{ \varepsilon_A T_{SA}^4 - \varepsilon_{A0} T_{SA0}^4 + \varepsilon_B T_{SB}^4 - \varepsilon_{B0} T_{SB0}^4 \} + A_{Rloss} \varepsilon_{Rloss} \sigma (T_{Rloss}^4 - \\
&T_{Rloss0}^4) \quad \because T_{SA,B}^4 \gg T_W^4 \quad (4)
\end{aligned}$$

Now, we assume the following relations based on our experimental data. It is possible that T_{SA} and T_{SB} can be expressed as liner function of T_c within the experimental parameters.

$$\varepsilon_A \sim \varepsilon_{A0}, \varepsilon_B \sim \varepsilon_{B0}, T_{SA} \sim \alpha_A T_c + \beta_A, T_{SB} \sim \alpha_B T_c + \beta_B, T_{Rloss} \sim \alpha_{Rloss} T_c + \beta_{Rloss}.$$

ΔT is defined as

$$\Delta T = T_c - T_{c0}. \quad (5)$$

Therefore, the following expression is obtained.

$$\begin{aligned}
H_{ex} &\approx \Delta T \left\{ \frac{k_{eff}}{L_{eff}} A_{eff} + A_S \varepsilon_{A0} \sigma \alpha_A (T_{SA} + T_{SA0}) (T_{SA}^2 + T_{SA0}^2) + A_S \varepsilon_{B0} \sigma \alpha_B (T_{SB} + \right. \\
&T_{SB0}) (T_{SB}^2 + T_{SB0}^2) + A_{Rloss} \varepsilon_{Rloss} \sigma (T_{Rloss} + T_{Rloss0}) (T_{Rloss}^2 + T_{Rloss0}^2) \left. \right\}. \quad (6)
\end{aligned}$$

This equation shows that excess heat can be written as a function of ΔT . Therefore, excess heat evaluation by the Ni bulk calibration curve shown in Fig.3(b) is valid under the assumptions described above.

3.2 Experimental Results

Heat burst phenomena were observed by a single radiation thermometer and the thermocouple in the heater simultaneously as shown in Fig.4 published already in [11]-[13]. A significant simultaneous increase of surface and heater temperature were observed twice, while no significant changes for input electrical power and room temperature were detected during these burst events.

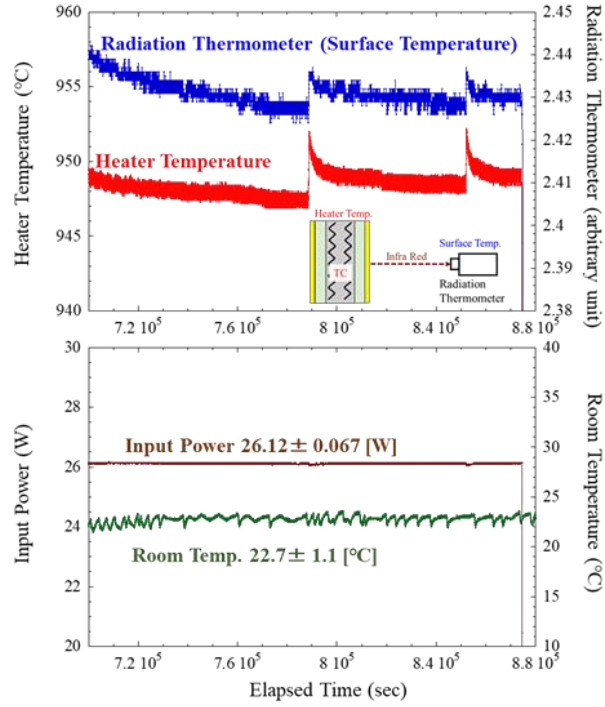


Figure 4. Simultaneously detected by a radiation thermometer looking at the surface of the multilayer thin film and a thermocouple located in the center of heater [11].

In this study, we have introduced additional radiation thermometers and surface temperature measurement for the two nano-sized metal multilayer composite samples became possible. By using the two independent radiation thermometers, interesting phenomena could be obtained.

Figure 5 shows temperature time variations for Tc, surface A and B. It is possible to see that heat release reaction occurred at the surface A at first and afterwards at the surface B. Their heat bursts propagated to the thermocouple. Input power and room temperature were constant during these events. Therefore, these events did not be caused by the change of electrical input power or heat income from environment. The samples consisted of 6 layers of Cu (2 nm) and Ni (14 nm) fabricated by magnetron sputtering method on Ni bulk same as in [11]-[14].

Delay time from the burst-like heat release at surface A to the thermocouple is about 33 sec as shown in Fig.5. Delay time from the heat burst at surface B is supposed to be about 40 sec, as inflection point of Tc can be recognized as shown in Fig.5. Although 3-dimensional heat analysis would be desirable, rough estimation of time constant for the observed burst phenomena. Figure 6 shows numerical model for one dimensional non-steady state heat conduction analysis. Time constant τ is given as the following equation.

$$\tau = \rho C_p V \frac{L}{k_{Al_2O_3+SiO_2} A} \quad (7)$$

where ρ is the density, C_p is the specific heat, and V is the volume for the sample holder. And k is the thermal conductivity for the mixture of Al_2O_3 and SiO_2 , A is the surface area and L is the distance between the surface and center of the heater. As Ni is thin and thermal conductivity is larger than Al_2O_3 and SiO_2 , contribution of Ni for τ is negligible. Based on the rough estimation, τ is calculated as 36 sec. It agrees with the experimental results, therefore the obtained delay times are supposed to be reasonable. This example gives us clear evidence that heat release reactions occurred in the near surface region of the nano-sized multilayer metal composite with hydrogen gas.

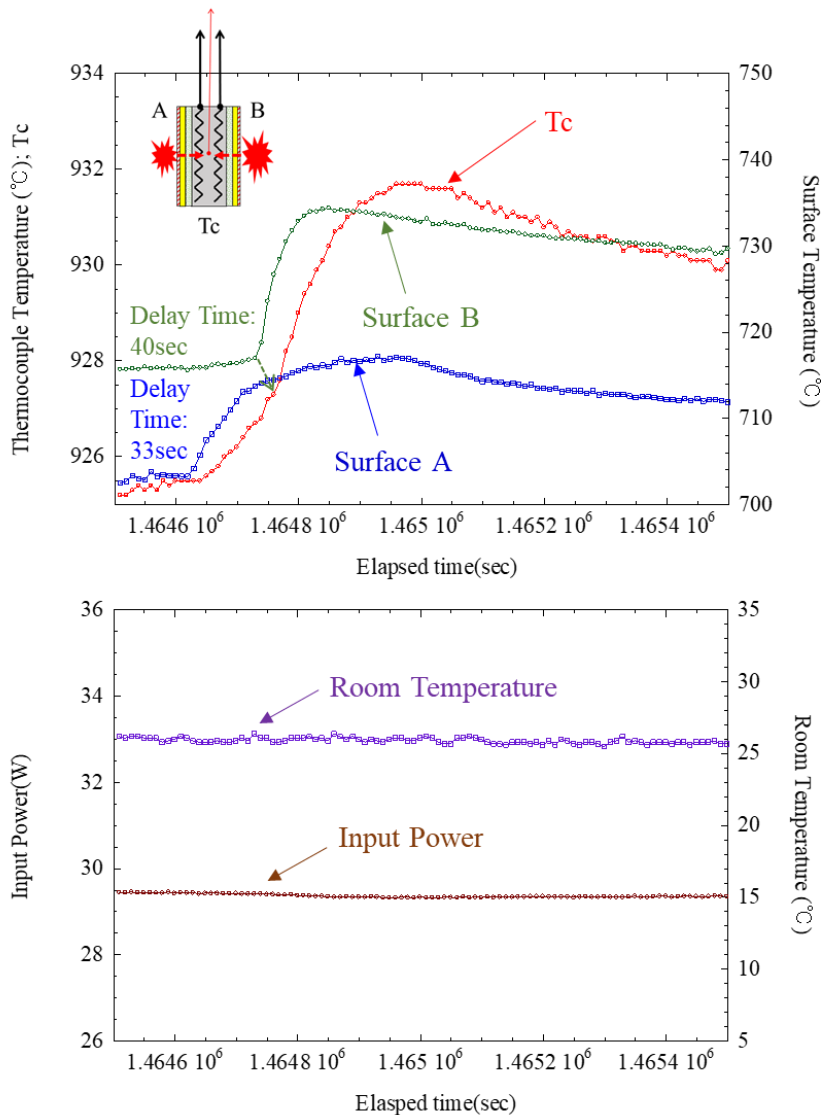


Figure 5. Heat burst reactions occurred at the surface A at first and afterwards at the surface B. Their heat bursts induced the rise of Tc. Input power and room temperature were constant during these events.

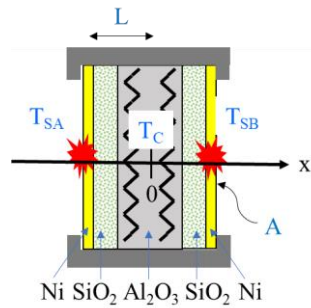


Figure 6. Numerical model for one dimensional non-steady state heat conduction analysis.

The above is an example of heat burst occurring on two surfaces, but it is more common for a heat burst to occur on only one surface. Figure 7 shows an example that a heat burst generated at surface B only. The samples for this experiment consisted of 6 layers of Cu (2 nm) and Ni (14 nm). In this case, the heat burst generated at surface B reached the thermocouple with a delay time of about 24 seconds and was further transmitted to surface A, but the temperature rise at surface A is small. Input power and room temperature were also constant during the heat burst event. These two examples demonstrate that observed excess energy in our experiments was due to real heat generation and cannot be attributed to the artifact like variation of a calibration curve on the relationship between electrical input and T_c .

Excess heat of this example is plotted in Fig.8. At the beginning of these experimental cycles, H_2 gas was evacuated and simultaneously each sample was heated up by the ceramic heater. After that, excess heat more than input power was observed for each experimental cycle as shown in Fig.8. Above each excess power plots, the value of the electrical input and the approximate thermocouple temperature are noted. During each experimental cycle, the input was almost constant. However, since the power supply was operating in constant voltage mode, when the sample temperature decreased, the resistance of the heater decreased: the input electrical power increased. As in the previous experiments, the excess heat tended to decrease gradually compared to immediately after the temperature rise at the beginning of each experimental cycle. We can see that some heat bursts occurred in this experiment as shown in Fig.8.

As a verification of the uncertainty in this excess heat calculation, we describe the effect of emissivity variation on the excess heat evaluation. In Eq. (2) and Fig. 3, the heat conduction loss and the heat loss from the sample holder are constant whether the sample is Ni bulk or Ni multilayer. Measured emissivity values in the temperature region where the heat burst phenomenon occurred shown in Fig. 7 were 0.16 for side A and 0.18 for side B, respectively. Based on these values, the energy released by radiation from surface A and B was about 2.8 W and 3.4 W, while electrical input power was 26.7 W. Thus, the radiant energy from the sample surface is not dominant to the input energy. The excess heat is evaluated to be about 6.7 W, as shown in Figure 9. Even though the error would be about half of the radiant energy from the surface A and B, about 3.6 W of excess energy would be being released from the Ni based nano-sized multilayer metal composite.

Released excess energies per hydrogen for this example is evaluated. The total amount of absorbed hydrogen for all the experimental cycles was 5.9×10^4 mol. The amount of released excess energy was calculated by the time integration of excess powers for each experimental cycle. Total released energy is calculated as 1.2 MJ. Although it

seems highly unlikely that all the absorbed hydrogen atoms reacted, we can still estimate that average released energies per absorbed total hydrogen. Total excess energy per absorbed hydrogen is 2.0 GJ/H-mol or 21 keV/H-atom. Obviously, it is too large to be explained by any known chemical reactions.

Even if the excess heat were 1/10 of this value, it would be 0.2 GJ/H-mol or 2.1 keV/H-atom, which means that energy that could not be explained by known chemical reactions must have been generated. Therefore, the uncertainty of the excess heat evaluation does not significantly affect the conclusion that observed phenomena cannot be explained by known chemical reactions.

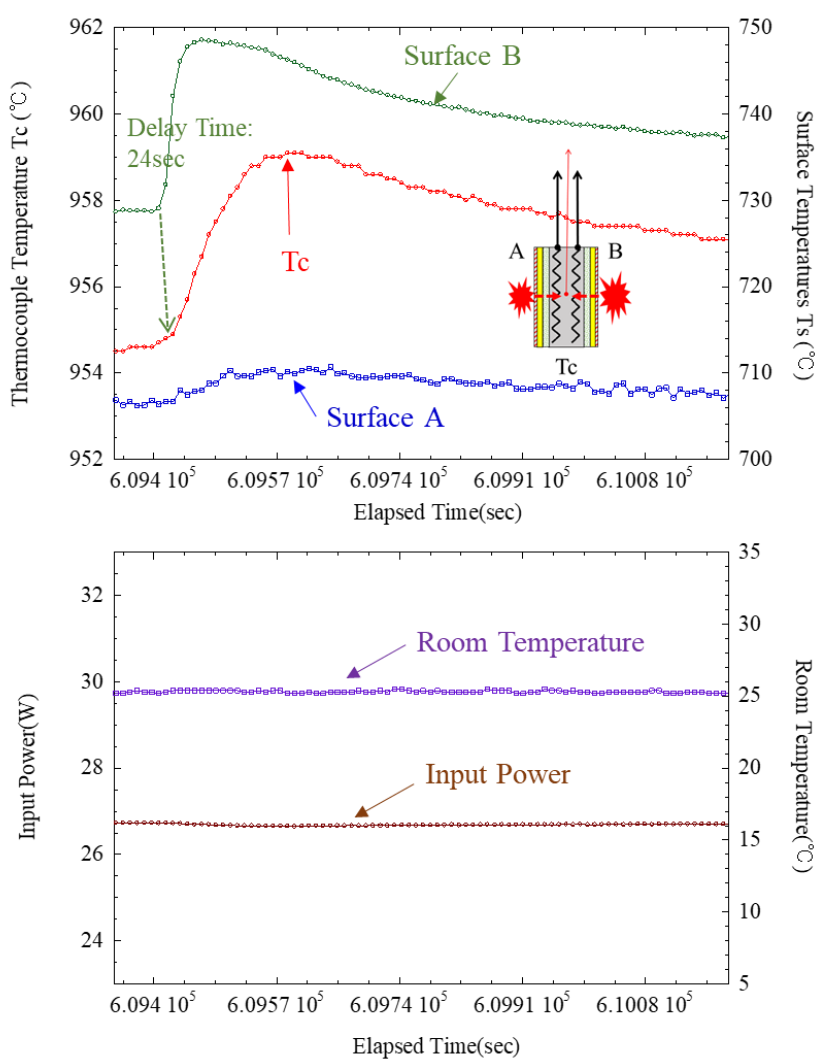


Figure 7. Heat burst reactions occurred at the surface at the surface B only and propagated to the TC. Input power and room temperature were constant during these events.

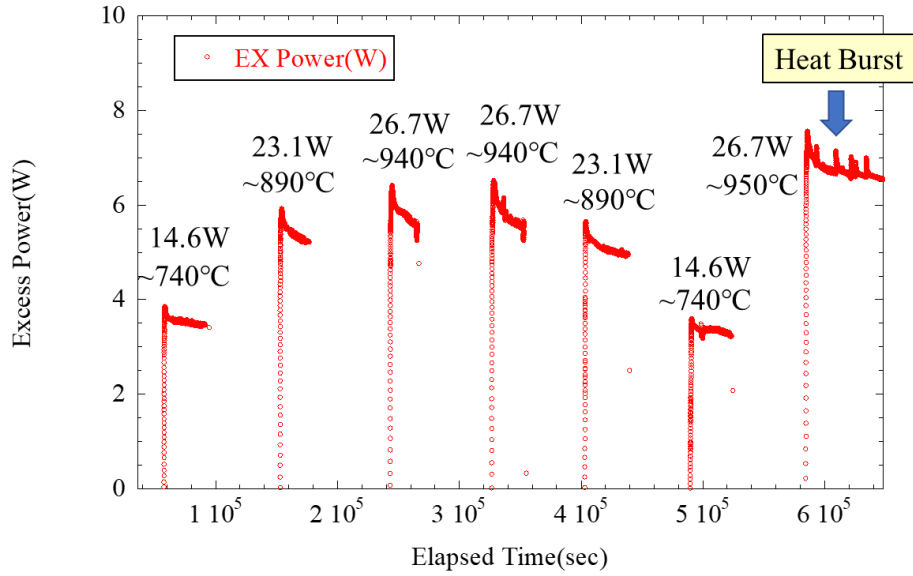


Figure 8. Excess power for this example. The heat burst phenomenon shown in Fig. 7 is an expansion of the time zone indicated by the arrows in this graph.

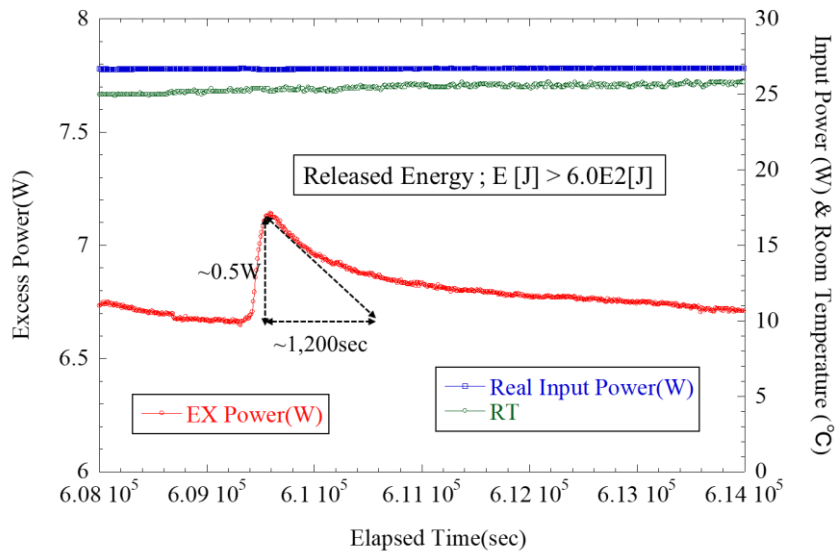


Figure 9. Estimation of Released Energy by the Heat Burst described in Fig.7.

Next, we examine the possibility that the observed heat burst phenomenon was caused by some chemical reactions. Figure 9 plots the change in excess heat during the heat burst shown in Figure 7 of this experimental example. At 6.094×10^5 sec, a heat burst of excess heat occurred. The peak increase of excess power was about 0.5 W and the

excess increase due to the burst lasted for at least 1200 seconds. This means that the excess heat increased by the heat burst is more than 600 J.

Consider the following chemical reactions that may cause a thermal burst for some reason.

- (1) If all the residual gas would be oxygen and the absorbed hydrogen would be oxidized and generates heat.
- (2) If the residual gas would be oxygen, and the Ni metal would be oxidized by it.
- (3) If the residual gas would consist of mixed gas ($H_2:O_2 = 2:1$), and the combustion energy would give energy to the surface of the two samples.

During the heat release experimental cycle, all the hydrogen introduced for absorption was evacuated, and the degree of vacuum was less than 1×10^{-4} Pa when the heat burst phenomenon was observed. Therefore, the number of moles of residual gas was less than 4×10^{-10} mol. It is known that the combustion reaction of hydrogen is about 290 kJ/mol and the heat of formation of nickel oxide is about 240 kJ/mol. Based on the number of moles of residual gas in the chamber, the heat generated in each case can be calculated as (1) 5.1×10^{-5} J, (2) 1.7×10^{-4} J and (3) 6.8×10^{-5} J. Comparing these values to the energy increased by the heat burst, 600 J, shows that they are completely negligible. This clearly shows that at least the chemical reactions (1)-(3) cannot explain the heat burst phenomenon observed in this study.

Above experimental results and discussions strongly suggests that some condensed matter nuclear reactions were induced in our experiments. According to the results, about 10^{-3} of the absorbed hydrogen might react if the condensed matter nuclear reactions would release energy order from 1MeV to 10MeV. Identification of reaction products is very important future work, in addition to more precisely excess heat evaluation, respectively.

4. Concluding Remarks

We have developed a new experimental method that combines the experiments of hydrogen permeation through multilayer films with those of hydrogen storage in nano-sized metals and temperature rise. As reported at JCF20 in 2019, we observed heat generation that cannot be explained by chemical reactions using Cu/Ni and Cu/Ni with CaO and Y_2O_3 in multilayer metal composites. Recently, we introduced a radiation thermometer, which enables us to measure the surface temperature of the sample, and we can frequently observe bursts of surface temperature. Examples of burst phenomena observed on only one side and on both sides of the two samples used in the experiment were reported. When the surface temperature of the sample increased, the heat was transmitted to the thermocouple in the center and to the sample on the opposite side, indicating that the exothermic reaction occurred near the surface. The burst phenomenon cannot be explained by known chemical reaction, and strongly suggests that the observed heat generation must be of nuclear origin.

Acknowledgements

The authors acknowledge Mr. H. Yoshino, Mr. S. Hirano, Mr. M. Dr. T. Hioki and Mr. T. Takahashi, who are the members of CLEAN PLANET Inc., for their significant assistance. The authors also thank Mr. Y. Shibasaki and Prof. H. Kikunaga of Tohoku University for their support. This work is supported by CLEAN PLANET Inc., Research Center for Electron Photon Science of Tohoku University Electron Photon, Tanaka Kikinzoku Memorial Foundation and The Thermal & Electric Energy Technology Foundation.

References

- [1] Y. Iwamura, M. Sakano and T. Itoh, Elemental Analysis of Pd Complexes: Effects of D₂ Gas Permeation, *Jpn. J. Appl. Phys.* **41** (2002) 4642-4650.
- [2] Y. Iwamura, T. Itoh, N. Gotoh and I. Toyoda, Detection of Anomalous Elements, X-ray and Excess Heat in a D₂-Pd System and its Interpretation by the Electron-Induced Nuclear Reaction Model, *Fusion Technology*, **33** (1998) 476-492.
- [3] Y. Iwamura, T. Itoh, M. Sakano, N. Yamazaki, S. Kuribayashi Y. Terada, T. Ishikawa, D. Sekiba, H. Yonemura and K. Fukutani, Observation of Low Energy Nuclear Transmutation Reactions Induced by Deuterium Permeation through Multilayer Pd and CaO thin Film, *J. Condensed Matter Nucl. Sci.* **4** (2011) 132–144.
- [4] Y. Iwamura, T. Itoh and S. Tsuruga, Transmutation Reactions Induced by Deuterium Permeation through Nano-structured Pd Multilayer Thin Film, *Current Science*, Vol. 108, NO. 4 (2015) 628-632.
- [5] T. Hioki et.al, Inductively Coupled Plasma Mass Spectrometry Study on the Increase in the Amount of Pr Atoms for Cs-Ion-Implanted Pd/CaO Multilayer Complex with Deuterium Permeation, *Jpn. J. Appl. Phys.* **52** (2013) 107301.
- [6] A. Kitamura, A. Takahashi, R. Seto, Y. Fujita, A. Taniike and Y. Furuyama, “Effect of Minority Atoms of Binary Ni-Based Nano-Composites on Anomalous Heat Evolution under Hydrogen Absorption”, *J. Condensed Matter Nucl. Sci.*, **19** (2016) 1-10.
- [7] A. Kitamura, A. Takahashi, K. Takahashi, R. Seto, T. Hatano, Y. Iwamura, T. Itoh, J. Kasagi, M. Nakamura, M. Uchimura, H. Takahashi, S. Sumitomo, T. Hioki, T. Motohiro, Y. Furuyama, M. Kishida, H. Matsune, “Excess heat evolution from nanocomposite samples under exposure to hydrogen isotope gases”, *International Journal of Hydrogen Energy* **43** (2018) 16187-16200.
- [8] Y. Iwamura, T. Itoh, J. Kasagi, A. Kitamura, A. Takahashi and K. Takahashi, “Replication Experiments at Tohoku University on Anomalous Heat Generation Using Nickel-Based Binary Nanocomposites and Hydrogen Isotope Gas”, *J. Condensed Matter Nucl. Sci.* **24** (2017) 191–201.
- [9] Y. Iwamura, T. Itoh, J. Kasagi, A. Kitamura, A. Takahashi, K. Takahashi, R. Seto, T. Hatano, T. Hioki, T. Motohiro, M. Nakamura, M. Uchimura, H. Takahashi, S. Sumitomo, Y. Furuyama. M. Kishida and H. Matsune, Anomalous Heat Effects Induced by Metal Nano-composites and Hydrogen Gas, *J. Condensed Matter Nucl. Sci.* **29** (2019) 119–128.
- [10] T. Itoh, Y. Iwamura, J. Kasagi and H. Shishido, Anomalous Excess Heat Generated by the Interaction between Nano-structured Pd/Ni surface and D₂/H₂ gas, *J. Condensed Matter Nucl. Sci.* **24** (2017) 179–190.
- [11] Y. Iwamura, T. Itoh, J. Kasagi, S. Murakami and M. Saito, “Excess Energy

- Generation using a Nano-sized Multilayer Metal Composite and Hydrogen Gas”, *J. Condensed Matter Nucl. Sci.* **33** (2020) 1–13.
- [12] Y. Iwamura, “Heat generation experiments using nano-sized metal composite and hydrogen gas”, *Cold Fusion: Advances in Condensed Matter Nuclear Science*, Ed. Jean-Paul Biberian, Elsevier, Amsterdam, (2020)157-165.
- [13] S. Murakami, T. Itoh, Y. Iwamura, M. Saito and J. Kasagi, “Excess Energy Generation Experiments using a Nano-sized Multilayer Metal Composite and Hydrogen Gas”, *Proceedings of the 20th Meeting of Japan CF Research Society, JCF20*, December 13-14, 2019, Reference Hakata Eki-Higashi Rental Room, Fukuoka, Japan p.86-96.
- [14] M. Saito, T. Itoh, Y. Iwamura, S. Murakami and J. Kasagi, “Elemental Analysis for Elucidation of the Anomalous Heat Generation Phenomena”, *Proceedings of the 20th Meeting of Japan CF Research Society, JCF20*, December 13-14, 2019, Reference Hakata Eki-Higashi Rental Room, Fukuoka, Japan p.74-85.
- [15] Y. Fukai, Evidence for Quantum Diffusion of Hydrogen in Ta: Quench-Recovery Experiments Revisited, *Japanese Journal of Applied Physics*, Vol.23, No.8 (1984) 596-598.
- [16] H. Wipf, Electro- and Thermo-Transport of Hydrogen in Metals, *Hydrogen in Metals II*, Ed. by G. Alefeld and J. Völkl, Springer-Verlag, Berlin, Heidelberg (1978) 273-304.

Optical Observation on Anomalous Heat Generation from Nano-sized Metal Composite

Takehiko Itoh^{1,2}, Yoshinobu Shibasaki^{1,2}, Jirohta Kasagi¹,
Shouichi Murakami², Mari Saito² and Yasuhiro Iwamura¹

1 Research Center for Electron Photon Science, Tohoku University, 982-0826 Japan

2 CLEAN PLANET Inc., 105-0022 Japan

E-mail: itoh@lms.tohoku.ac.jp

Abstract

We describe the first measurement of optical spectrum correlated with the anomalous excess heat generation from the NiCu multilayer foil with H₂ gas. The method to induce the anomalous excess heat is the one we have been developing: the anomalous excess heat occurs when a nano-sized metal composite film that has absorbed H₂ is forcibly evacuated and heated up for the gas to discharge. Spectra of the visible light of photon energy between 1.3 and 1.9 eV were measured, in addition to the temperature measurement near the heater at the sample core, which has been performed so far. Two types of samples, Ni plate and NiCu multilayer thin film, were examined under the conditions in which the sample was in vacuum (without H₂) and during desorption of H₂ (with H₂). It turns out that the measured spectrum is understood as that of gray-body radiation. Surface temperature and radiant intensity of the sample are deduced from the spectrum. For the NiCu multilayer sample which shows anomalous excess heat that is evaluated only from Tc, corresponding excessive radiant emission is clearly shown. Although the deduced quantities from the optical radiation qualitatively follow the evaluated values of excess heat, it is indicated that more sophisticated analysis that takes into account the radiation information is highly required for more reliable evaluation of the excess heat. Furthermore, we discuss that the optical measurement plays an important role in the analysis of the heat burst event observed during long-term observation. Our future experimental plans are also discussed.

1. Introduction

Recently, anomalous heat generation, producing much larger energy than ordinary chemical reactions produce, has been reported in a system consisting of nanostructured metals (Ni, Cu, etc.) and hydrogen (or deuterium) gas ^{[1]-[3]}. Such a system that produces a large amount of energy without CO₂ emissions is very promising as a future energy source; the realization of clean, powerful and inexpensive energy will have a great social and economic impact.

We have been working on development of a new experimental method that emphasizes the role of hydrogen diffusion in nano-sized metal multilayer composite ^{[4]-[6]}. The method currently under development is to induce a reaction of H₂ (or D₂) gas with the thin film layer structure of Ni and Cu metal ^{[4]-[6]} instead of the composite amorphous metal powder developed in the joint project of NEDO. We have already published some results using multi-layer foil with good reproducibility suggesting anomalous excess heat generation ^{[3]-[6]}, it is still necessary to develop experimental equipment for new measurement which may provide more accurate and quantitative discussions. In the previous measurements, the quantity of generated heat was evaluated only by the temperature of the sample core although together with the radiation temperature of the surface was also measured preliminarily.

Accurate excess heat measurement is highly required to discuss the phenomena more quantitatively, to clarify quantities that correlate with the energy generated, and, then, to explore the mechanism. In this work, we describe the first experiment performed with an optical spectroscopic measurement as the next step towards a more complete measurement.

2. Importance of optical measurement

Fig.1 shows a basic structure of a sample installed in a vacuum chamber; two sheets of Ni plate coated with NiCu multilayer are placed on both sides of a ceramic heater (25mm square ; MS-1000R; Sakaguchi E. H Voc Corp.) which has an R-type thermocouple (Tc) in the center. In the previous reports, values of the excess heat were evaluated only by temperature measured Tc. When the sample is heated up (typically between 700 and 900 °C), the heat generated by the heater (and the excess one) becomes a heat flow and is transferred to the low temperature region by the three processes as shown in Fig. 2; (1) conduction heat transfer through supporting rods (connected with the chamber wall) and wires of the heater and thermocouple, (2) radiation heat transfer from surfaces of heated element to the wall, and (3) convection heat transfer by gas. Since the pressure in the chamber is 1×10^{-4} Pa or less during measurements, the process (3) can be ignored. In processes (1) and (2), the latter contributes most of the heat flow, because a large heat-insulating substance (photveel) is used to support the sample. Thus, the measurement of radiant heat plays an essential role to improve the accuracy of excess heat measurement by measuring radiation.

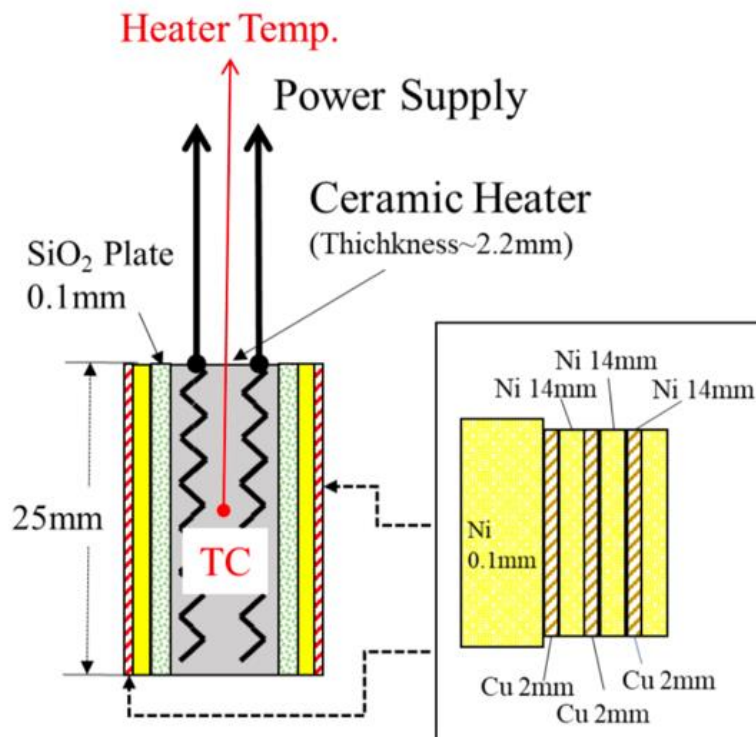


Fig.1 Schematic of components around Nano-sized Multilayer Metal Composite.

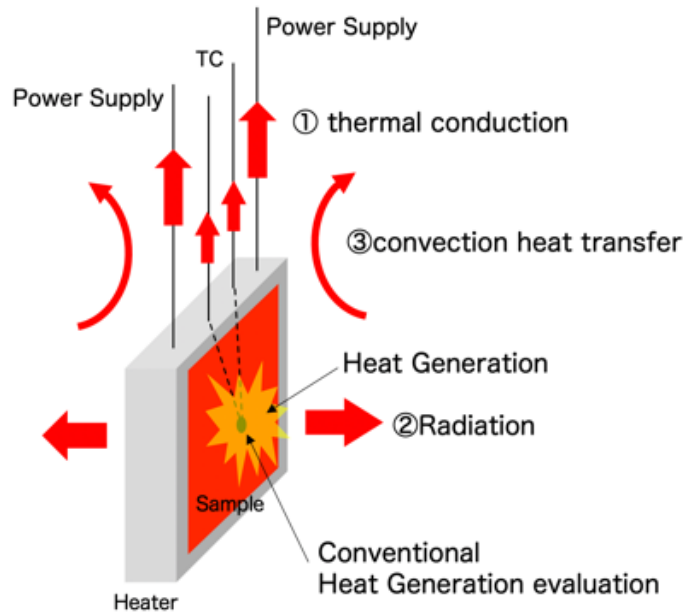


Fig.2 Heat transfer path when a heat generation phenomenon occurs.

Spectroscopic measurements contribute to search for any transitions of special electronic states that accompany the generation of excess heat [7]. In addition, it provides important information on temperature and emissivity, even if it is a continuous thermal spectrum. As an example of the latter, hotspot (local high-temperature region) observation is one of the challenges we are pursuing as discussed at JCF20. Consider the case where a reaction that produces high energy, such as a nuclear reaction, occurs in the sample as shown in Fig. 3(a). If the energy is deposited to several to many electrons immediately after the reaction occurs, those electrons may move in a random direction in the sample and lose their kinetic energies as shown in Fig. 3(b). This region may locally form a hot thermal equilibrium, temperature much higher than that the region heated up only by the heater. One can expect a radiation spectrum to have two temperature components (Fig.3(c)).

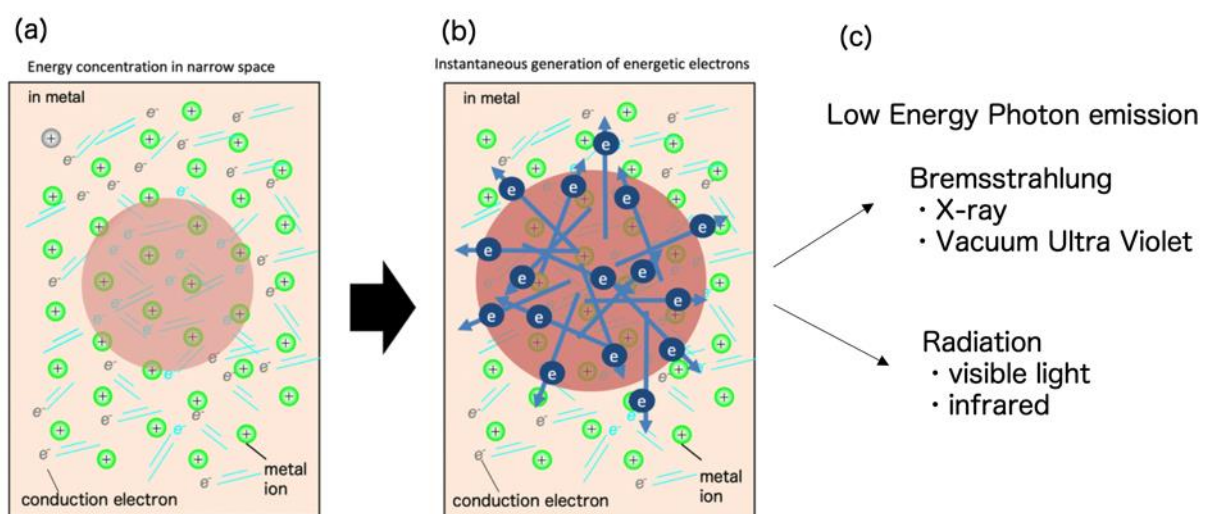


Fig.3 Schematic of energy distribution to electrons when energy is generated locally. (a)Energy concentration in narrow space, such as a nuclear reaction, (b)Instantaneous generation of energetic electrons, (c)Low Energy Photon Emission due to energetic electrons

3. Experimental procedure

The experimental apparatus is shown in Fig 4. A vacuum chamber is made of stainless steel and the volume inside the gate valve is 4.6 liters. It is evacuated with a turbo molecular pump down to 3×10^{-6} Pa. The sample with the structure shown in Fig. 1 is set in the chamber. H₂ gas was introduced from the lower port (gas inlet) and its pressure were monitored by a Pirani gauge. Heater input power is supplied by a DC power supplier with constant voltage mode. The voltage and current values indicated by the device are monitored and those of independently measured are recorded during the measurement.

The sample is placed at an angle of 45 degrees with respect to the direction of the center of the quartz window as shown in Fig. 4; this geometry enables us to put an X-ray detector behind the Be window. The light emitted from the sample goes out through the quartz window, is focused on the optical fiber by a focus lens, and is guided to the spectroscope (C10027-01; Hamamatsu Photonics K.K.) that has a measurement range of 200-950 nm and a wavelength resolution of 2 nm. In order to make the signal-to-noise ratio improve, we decided to obtain a spectrum that averaged 50 measurements with an exposure time of 1 second.

In the present work, we measured two types of samples: (1) nanostructured Ni-Cu multilayer film deposited on a Ni plate and (2) Ni plate (each side of 25 mm and a thickness of 0.1 mm) which is used as a substrate. For the Ni-Cu multilayer film, Cu and Ni are alternately deposited 6 times each on the substrate by the sputtering method. By this way, the sample with a laminated 6-layer structure of 2nm-Cu and 14nm-Ni is prepared. The Scanning Transmission Electron Microscope (STEM) image of the sample structure is shown in Fig. 5.

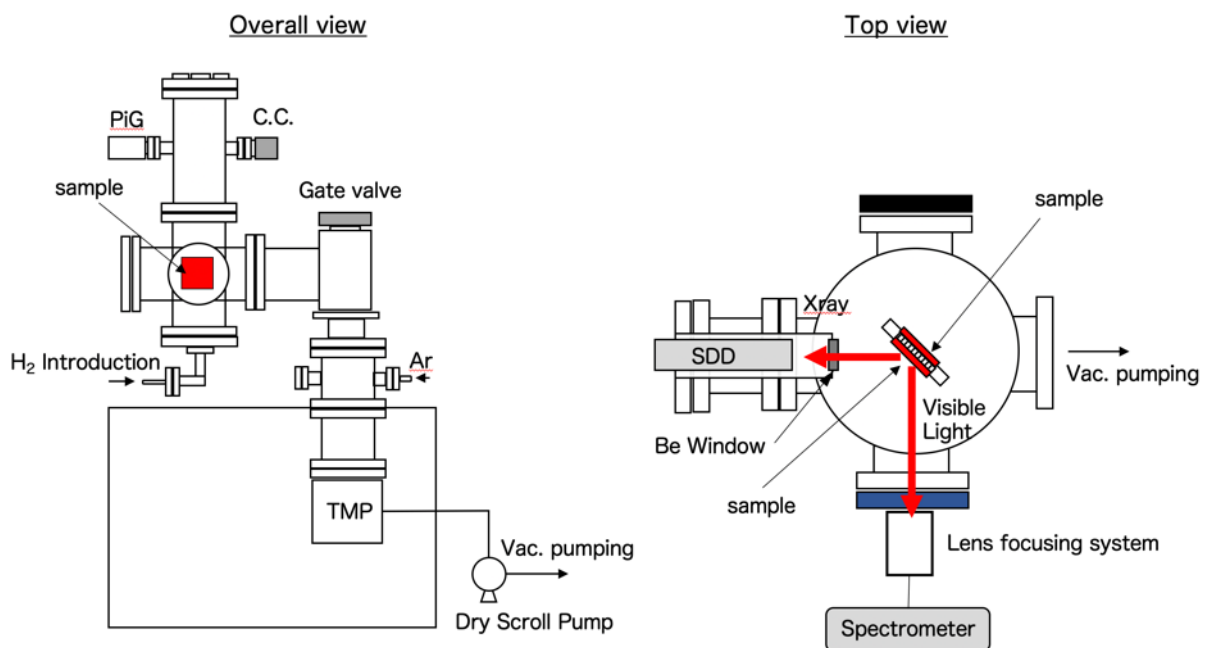


Fig.4 Schematic of Experimental apparatus.

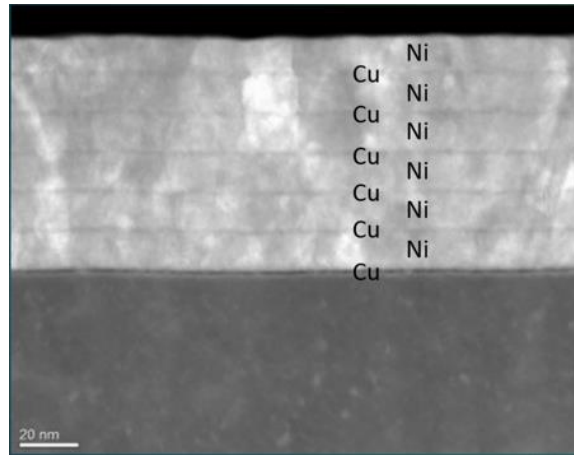


Fig. 5 Scanning Transmission Electron Microscope (STEM) Image of Cu-Ni Multilayer Thin Film.

The present experiment has been carried out as follows.

- (1) Setting sample: Two sheets of sample are fixed on both sides of a ceramic heater and placed at the right position in the vacuum chamber, which is evacuated for a vacuum bake-out. After about 3 days baking out, the heater is turned off.
- (2) Measurement without H₂ gas: In a vacuum condition (i.e., without H₂ gas introduction), the voltage of the power supply of the heater is set at various values (between 20 and 48 V) and measured are the temperature inside the heater (T_c) and the optical spectrum. These are regarded as the reference data corresponding to no excess heat.
- (3) Measurement during desorption of H₂ gas: The sample absorbs H₂ gas by filling the chamber with H₂ gas to 200-300 Pa and keeping the temperature at about 250 °C for 12 -15 hours. At the same time as setting the heater input voltage to the value of the measurement condition, the evacuation of the vacuum chamber is started. The sample temperature (T_c), chamber wall temperature, heater input voltage and current, and vacuum chamber pressure are read and recorded every second. In addition to this, optical spectral measurements in the visible light region are taken every 5 to 30 minutes and saved as data. Data collection continues for at least 6 hours after the voltage once set, since H₂ desorption is expected to continue sufficiently. For measurement under different conditions by changing the set voltage, return to the beginning of (3) and start from H₂ absorption.

4. Results and Discussion

As discussed in Section 2, the heat, including the one from heater and the other generated by reactions between the sample and the H₂ gas, is dissipated as a heat flow from the sample: a radiant heat transfer and a conduction heat transfer. However, the present experiment cannot be a complete measurement of above quantities because of a narrow and limited wavelength range of optical radiation. Thus, discussing more accurate values of excess heat must wait for future experiments. Here, we show the optical spectrum newly introduced, and discuss its change as the excess heat was produced.

Fig.6 shows simple estimates of excess heat from (a) the NiCu multilayer sample and (b) the Ni substrate sample. Each dot against the elapsed time represents the input power of the heater (black dot) and the excess power (orange dot). The time regions without dots correspond to the time for the sample to absorb H₂ gas. Note that the evaluation of the excess heat is based only on the temperature T_c as reported in our previous reports ^[3-6], and is not a quantitative evaluation with

the addition of radiant heat flow. As seen in Fig.6, excess heat of about 2 ± 1 W is observed for the NiCu multilayer sample, while for the Ni plate, almost no excess heat is detected.

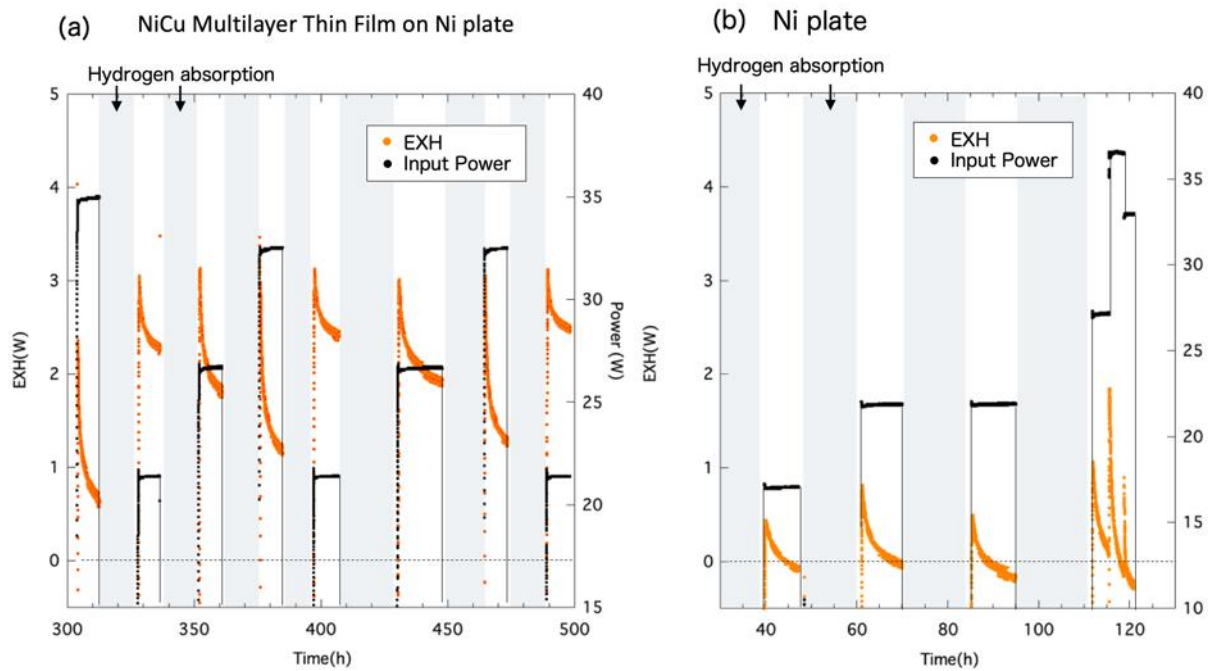


Fig. 6 Excess heat and Input power.
 (a) Experiment with NiCu Multilayer Thin Film on Ni plate,
 (b) Experiment with Ni plate.

Fig.7 shows intensity spectra of emitted light photon with energy above 1.2 eV from the NiCu multilayer sample: the sample clearly shows the excess heat generation as indicated in Fig.6. The vertical axis corresponds to the radiation energy observed per second (i.e., photon energy times number of photons /sec). In the figure, the spectrum measured during H₂ desorption (red dot) and that without H₂ (blue dot) for heater input power of 21, 27 and 35 W are compared.

The first point to be emphasized is the fact that the radiation intensity is clearly increased by desorption of H₂ as compared without H₂. This is a clear indication of the excess heat: the greater the amount of heat, the greater the brilliance. That is, it is shown that the radiant energy is increased by increasing the temperature of the sample surface due to heat generation. Moreover, the amount of yield increases as the input power increases. This is different from the behavior of excess heat in Fig.6. This indicates that more sophisticated analysis that takes into account the radiation information is highly required in order to obtain accurate value of the excess heat.

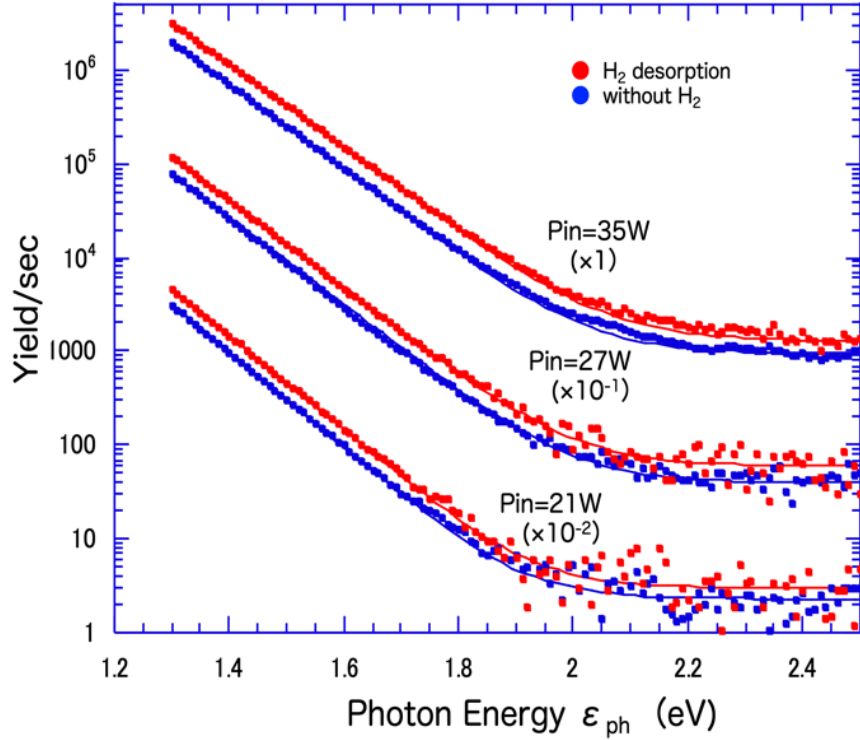


Fig. 7 Photon emission from NiCu Multilayer Thin Film.

Second, the measured spectrum is well understood as the gray-body radiation, at least in this energy region. Since the photon energy ε we measure is much larger than the radiation temperature ($\varepsilon \gg kT_s$), Planck's radiation equation can be approximated as follows.

$$Y(\varepsilon) = A\varepsilon^3 \frac{1}{\exp\left(\frac{\varepsilon}{kT}\right) - 1} = \sim A\varepsilon^3 \exp(-\varepsilon/k_B T)$$

The solid curves in Fig.7 are the best fitting curves calculated to explain the experimental data with 3 parameters under the assumption that the emissivity of the sample does not depend on energy. We used the following approximate function for the intensity $Y(\varepsilon)$:

$$Y(\varepsilon) = A\varepsilon^3 \exp\left(-\frac{\varepsilon}{kT_s}\right) + C, \quad (1)$$

where A is the normalization factor, ε is photon energy, k is the Boltzmann constant, T_s is the surface temperature of the sample and C represents the background yield due to the dark current of the device: the 3 parameters are A , T_s and C . In this way, the important values A and T_s can be obtained: the total (integral) radiation power from the sample is proportional to AT_s^4 , if the emissivity is a constant. The radiant power mentioned below refers to the AT_s^4 .

Figure 8 shows a comparison of the emitted radiation from the two samples. Fig.8 (a) and (b) show the radiant power and the surface temperature, respectively, obtained for the NiCu multilayer film, and Fig.8 (c) and (d) show those for the Ni plate sample. Red circles correspond to the foreground experiment with H_2 storage, and open circle to the reference experiment without H_2 .

The comparison of (a) and (c) in Fig.8 shows more clearly that the NiCu multilayer sample generates a large amount of excess heat as compared with the Ni plate sample. In the NiCu multilayer sample, the radiant power during H_2 desorption is always higher than without H_2 , demonstrating the presence of the excess radiation which increases as the input power increases. In the Ni plate sample, on the other hand, no significant difference is observed; i.e., no excess radiation in the Ni plate. The same behavior can be clearly seen in the comparison of (b) and (d) in

Fig.8. Observed temperatures, both T_c and T_s , are always larger during desorption of H_2 for the NiCu multilayer sample, while no change in temperature for the Ni plate sample.

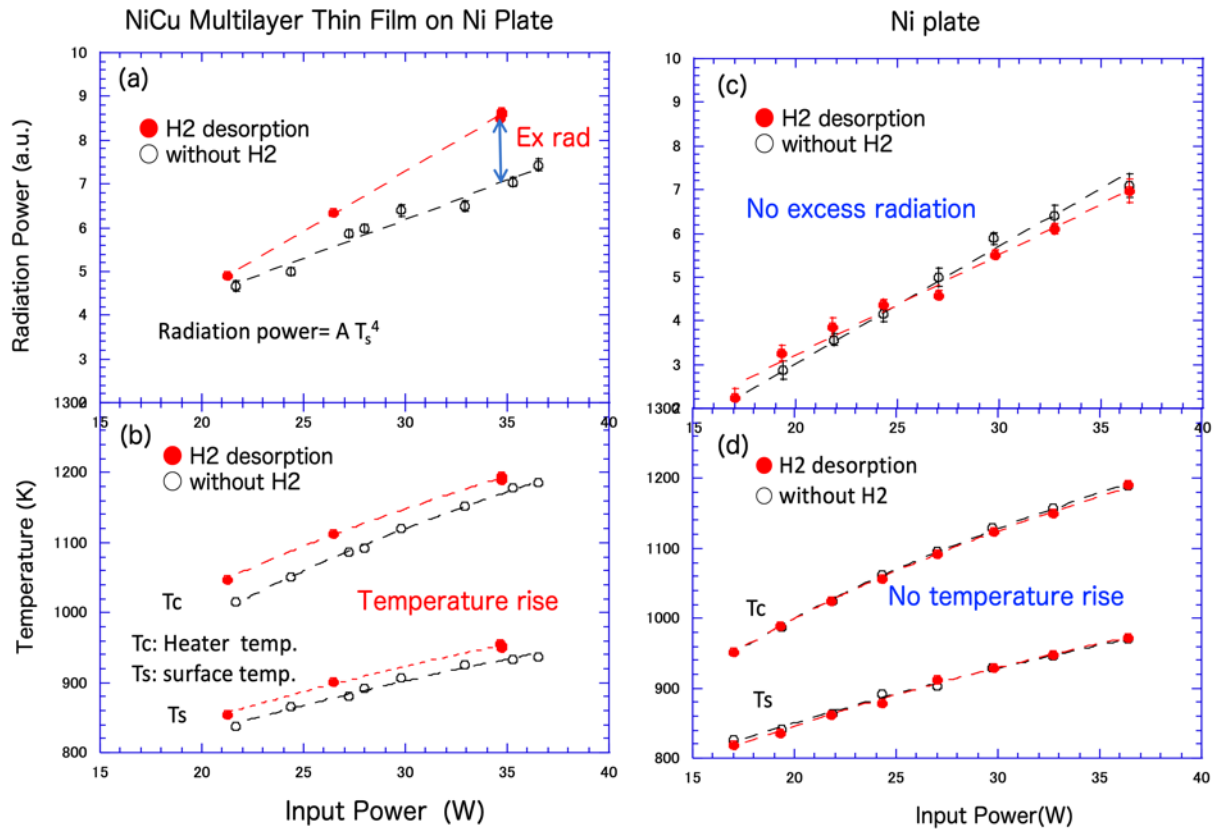


Fig. 8. Comparison of emitted radiations between NiCu Multilayer Thin Film on Ni Plate and Ni Plate. (a) Radiation Power and (b) Temperature of experiment using NiCu Multilayer Thin Film (c) Radiation Power and (d) Temperature of experiment using Ni Plate.

When the H_2 desorption experiment with the NiCu multilayer sample was conducted for several hours continuously, a phenomenon in which T_c rises suddenly did occur as reported in [4,5,8]. We call it heat burst. Fig.9 shows two such events observed simultaneously with measurements of optical spectra, for the first time. As seen in Fig.9 (a) where heater temperature (T_c) is plotted against elapsed time, the heat burst events are recorded at 8.5 and 22 hours after the start of the experiment. Fig. 9 (b) shows corresponding excess heat evaluated based solely on T_c . The surface temperature (T_s) and integrated yield between 1.2 and 1.5 eV (proportional to radiant intensity) deduced from light spectrum are shown in Fig. 9 (c). The bump structures corresponding to those of T_c are clearly confirmed in both T_s and the radiant intensity. However, the data were not obtained immediately before and after the bump, since the number of sampling of the optical measurement is small for the elapsed time after 15.5 h. Fig.9 (d) and 9 (e) show the spectra before and after the first burst and the second burst, respectively.

One may interpret the time sequence of the bump events observed in Fig.9 as follows: A heat burst occurs locally on the surface of the NiCu multilayer sample, part of the power is dissipated immediately from the surface as the radiant power, and at the same time, the generated heat is transferred to the core of the sample, then, temperature T_c raises. It is considered that investigating the heat burst in more detail, for example, to obtain precise time correlation between

the busts in T_c and in the radiant power, might lead to the elucidation of the mechanism of the excess heat generation.

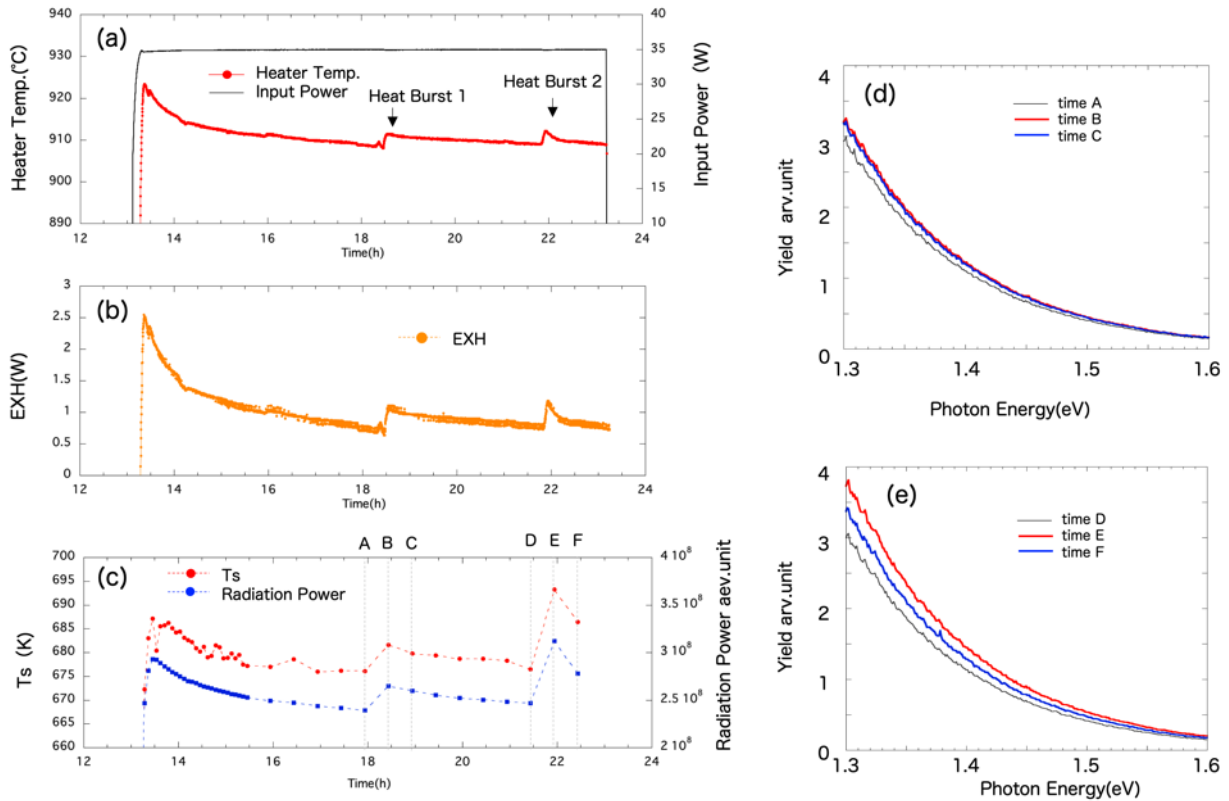


Fig. 9 Simultaneously detection of Heat Burst by Radiation of spectrometer Looking at the Surface of the Multilayer Thin Film and a Thermocouple Located in the center of Heater. (a)Heater Temperature and Input Power, (b)Excess Heat, (c) Surface temperature and Radiation Power by Spectrometer, (d)Radiation Spectrum of 1st Heat Burst, (e) Radiation Spectrum of 2nd Heat Burst.

5. Future Plan

In the present experiment, we were able to observe the anomalous heat generation phenomenon from the observation of radiation, although the observed region is very narrow as 1.3-1.9 eV. Also, we discussed, in Section 2, the importance of the radiation measurement to explore the mechanism of the anomalous excess heat. Thus, it is natural to extend the region of the wavelength to be measured. This is our future plan as a next step.

In Fig.10, calculated spectra of the black-body radiation are shown for temperatures from 800 to 1100 K, expected temperatures in our experiments. Shown in the lower part of Fig.10 are the detectable energy regions of the detectors under consideration. Since region 1 is already introduced in this work, we will extend our measurements to low energy regions using a near-infrared spectrometer (1.1-2.5 μm) and a mid-infrared detector (3-5.6 μm). It is expected, then, to grasp the whole picture of the radiation: This is equivalent to a sophisticated calorimeter measurement, and the reliability of the excess heat is dramatically increased.

In addition, in order to elucidate the mechanism related to the existence of hot spots, it is necessary to measure the visible light region on the high energy side more carefully. We are also considering ways to reduce the effects of radiation and improve S/N for measurement in higher energy side of region ①

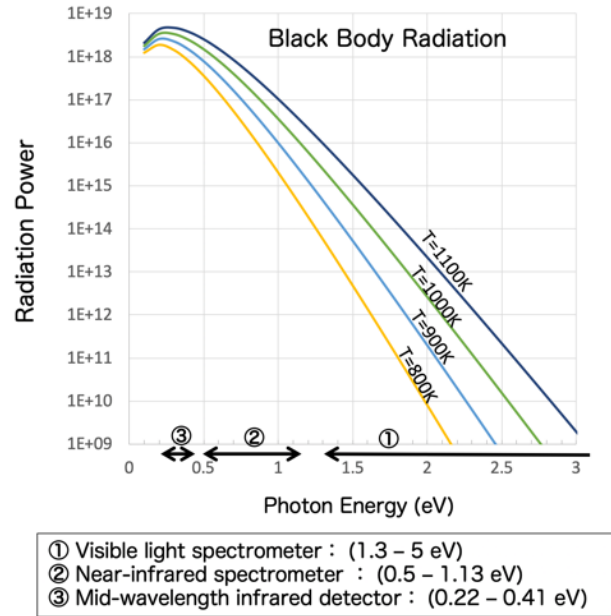


Fig.10 Extended spectra; from Visible light to infrared.

6. Summary

In the present work, we aimed to improve the accuracy of measurement of the anomalous excess heat generation observed in Ni-hydrogen system by adding optical measurement to the conventional measurement system. This is the first measurement of optical spectrum correlated with the anomalous excess heat generation from the NiCu multilayer sample with H₂ gas.

In the experiment with the Ni substrate sample, the temperature and radiation intensity deduced from the light spectrum hardly changed before and after hydrogen absorption, but with the NiCu multilayer sample, they showed clearly excessive radiations.

The heat burst phenomenon was observed multiple times in the measurement with the NiCu multilayer sample. When heat burst phenomena occurs, sudden increase in the radiation intensity together with the surface temperature was observed at the same time as the heater temperature increases.

In conclusion, we have constructed the measurement system for the optical spectroscopy by adding the previously used one. The optical measurement is found out to be an important one for the study of anomalous excess heat generation. Although the deduced quantities from the optical radiation qualitatively follow the evaluated values of excess heat, it is indicated that more sophisticated analysis that takes into account the radiation information is highly required for more reliable evaluation of the excess heat.

Acknowledgements

This work is partially supported by CLEAN PLANET Inc. The authors acknowledge also the members of CLEAN PLANET Inc., Mr. H.Yoshino, Mr. S.Hirano, Mr. T.Takahashi, and Mr. H.Shimokawa, for their significant assistance.

References

- [1] A. Kitamura, A. Takahashi, R. Seto, Y. Fujita, A. Taniike and Y. Furuyama, “Effect of Minority Atoms of Binary Ni-Based Nano-Composites on Anomalous Heat Evolution under Hydrogen Absorption”, *J. Condensed Matter Nucl. Sci.*, **19** (2016) 1-10.
- [2] A. Kitamura, A. Takahashi, K. Takahashi, R. Seto, T. Hatano, Y. Iwamura, T. Itoh, J. Kasagi, M. Nakamura, M. Uchimura, H. Takahashi, S. Sumitomo, T. Hioki, T. Motohiro, Y. Furuyama, M. Kishida, H. Matsune, “Excess heat evolution from nanocomposite samples under exposure to hydrogen isotope gases”, *International Journal of Hydrogen Energy* **43** (2018) 16187-16200.
- [3] Y. Iwamura, T. Itoh, J. Kasagi, A. Kitamura, A. Takahashi, K. Takahashi, R. Seto, T. Hatano, T. Hioki, T. Motohiro, M. Nakamura, M. Uchimura, H. Takahashi, S. Sumitomo, Y. Furuyama, M. Kishida and H. Matsune, Anomalous Heat Effects Induced by Metal Nano-composites and Hydrogen Gas, *J. Condensed Matter Nucl. Sci.* **29** (2019) 119-28.
- [4] Y. Iwamura, T. Itoh, J. Kasagi, S. Murakami and M. Saito, “Excess Energy Generation using a Nano-sized Multilayer Metal Composite and Hydrogen Gas”, *J. Condensed Matter Nucl. Sci.* **33** (2020) 1-13.
- [5] S. Murakami, T. Itoh, Y. Iwamura, M. Saito and J. Kasagi, “Excess Energy Generation Experiments using a Nano-sized Multilayer Metal Composite and Hydrogen Gas”, *Proceedings of the 20th Meeting of Japan CF Research Society*, JCF20, December 13-14, 2019, Reference Hakata Eki-Higashi Rental Room, Fukuoka, Japan p.86-96.
- [6] M. Saito, T. Itoh, Y. Iwamura, S. Murakami and J. Kasagi, “Elemental Analysis for Elucidation of the Anomalous Heat Generation Phenomena”, *Proceedings of the 20th Meeting of Japan CF Research Society*, JCF20, December 13-14, 2019, Reference Hakata Eki-Higashi Rental Room, Fukuoka, Japan p.74-85.
- [7] J. Kasagi, “Possible radiation from thin metallic multilayers with hydrogen-permeated anomalous excess heat: Can we observe hot spots or Bremsstrahlung?”, *Abstract of ICCF22* 8-13 Sep, 2019 Assisi Italy p.10
- [8] Y. Iwamura, T. Itoh, M. Saito, S. Murakami and J. Kasagi, “Evidence for Surface Heat Release Reaction over Nano-sized Multilayer Metal Composite with Hydrogen Gas”, *Proceedings of the 21th Meeting of Japan CF Research Society*, JCF21, to be published.

Simulation Study of Heat Conduction in Deuterium Desorption Experiment

N. Kishimoto, M. Endo, A. Kikuchi, K. Matsuhashi, K. Negishi,
S. Narita¹

Iwate University
Morioka, Iwate, 020-8551, Japan

Abstract

We conducted deuterium absorption and desorption experiments using a Pd foil coated with a metal membrane. We observed anomalies in the temperature pattern during the desorption process. We estimated the heat energy balance in the unique phenomena considering possible processes—especially the occurrence of a nuclear reaction—that may have been the source of these anomalies. However, we did not observe significant heat of any unknown origin. Furthermore, to accurately identify the anomalous phenomena, we still need to improve the heat balance calculation from the temperature variation of the sample. In this study, we simulated the heat transfer in the sample; using the finite-element-analysis tool (ANSYS Mechanical APDL), we illustrated the mechanism behind heat transfer as well as radiation when local heat evolution occurred in the sample. Additionally, we evaluated heat conduction and radiation quantitatively based on our experimental setup. We observed that under our experimental conditions, the empirical heat value deviated from the actual calorific value, possibly by a few Joules.

1. INTRODUCTION

We conducted deuterium absorption and desorption experiments using a Pd foil coated with Pd–Ni (at the interface) and Pd–Ni–Zr; these alloys have a fine structure. We observed peculiarities in thermal flux in the desorption process, such as short-lived temperature fluctuations and substantial instantaneous heat evolution [1–4]. Accordingly, we estimated the heat balance in the unique phenomena to specify the cause/s of these irregularities; we did not observe significant heat of entirely unknown origin. We still need to improve the calculation of the heat balance from the temperature variation of the sample to accurately identify the anomalous phenomena. In this study, we simulated heat transfer as well as radiation when heat evolution occurred locally in the sample; further, we quantitatively evaluated thermal conduction and radiation. We then compared the calorific values obtained from the experiment with those from the simulation.

2. SIMULATION METHOD

We simulated thermal conduction and radiation using ANSYS Mechanical APDL, a finite-element-analysis tool. We modeled radiation based on the "radiosity" method, one of the methods used to calculate the radiant heat between two or more surfaces [5]. When using this method, it is necessary to define the "surface-effect element" set as a film on the surface of a solid to provide the boundary conditions. In this simulation, the SURF252 element was applied to the surface of the Pd foil model to account for the flux in radiant and incident heat from other components. *i.e.* the chamber wall. In SURF252, the net

¹ narita@iwate-u.ac.jp

radiant-heat flux is calculated as follows:

$$\text{Net radiant-heat flux } \left(\frac{\text{W}}{\text{m}^2} \right) = \sigma \varepsilon T^4 + (1 - \varepsilon)q - q, \quad (1)$$

where σ is the Stefan–Boltzmann constant, ε is the emissivity, and q is the incident-heat flux. $\sigma \varepsilon T^4$ represents the radiant-heat flux, and $(1 - \varepsilon)q$ represents the reflection-heat flux. A schematic model of heat radiation is shown in Fig. 1.

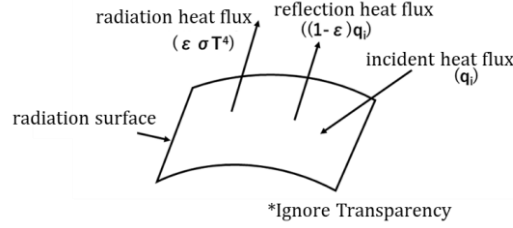


Figure 1: Heat radiant model.

The heat conduction is calculated from heat transfer Q using the following equation:

$$q = \frac{dQ}{dA} = -k_{nn} \frac{dT}{dn}, \quad (2)$$

where A is the cross-sectional area, k_{nn} is the thermal conductivity, and dT/dn is the temperature gradient in the n ($n = x, y, z$) direction.

The model was created according to the dimensions of the Pd foil and the chamber used in the actual deuterium desorption experiment, as shown in Fig. 2. The dimensions of the chamber and the Pd foil sample are shown in Fig. 3. The temperature of the sample was measured every 2.5 s using a thermocouple. SOLID70, an 8-node 3D solid, was employed in the simulation of heat transfer of the Pd foil sample and the stainless chamber [5]. Table 1 shows the element model and the physical properties of the material used in the simulation. Given that the inside of the stainless chamber was assumed to be vacuum, the heat transfer coefficient was not defined in the Pd foil model. In addition, a temperature-dependent heat transfer coefficient was applied to the stainless chamber, as shown in Table 2.

The heat generation was simulated at a spot on the Pd sample by applying a constraint temperature at the node. The simulation conditions are presented in Table 3. The initial temperature was set to 50 °C, considering the experimental conditions. In this simulation, heat conduction and radiation were investigated for 2.5 s when the Pd sample was heated to 100 °C, 200 °C, 300 °C, 400 °C, and 500 °C for 0.1 s at the center, midpoint, and edges. Figure 4 shows the positions heated during the simulation. A thermocouple was attached to the center position during the experiment. This analysis time of 2.5 s corresponds to the interval of temperature measurement in the experiment. The temperature outside the chamber was taken into consideration by applying 20 °C to the external node.

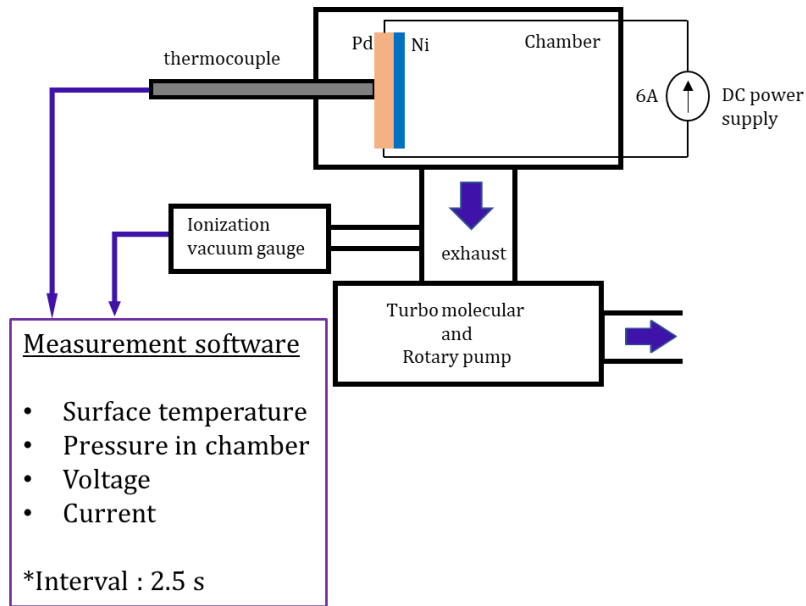


Figure 2: Experimental setup for desorption experiment.

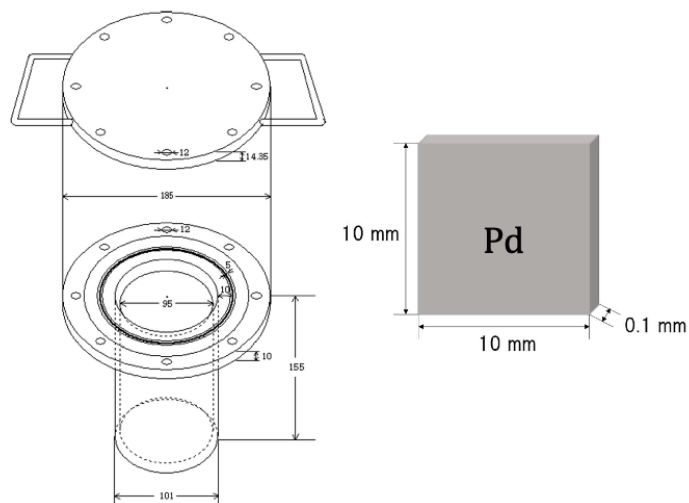


Figure 3: Dimensions of desorption chamber and Pd foil.

Table 1: Element model and material properties.

Model	Pd foil	Stainless chamber
Finite element	SOLID70	SOLID70
	SURF252	SURF252 (inside)
		SURF152
Thermal conductivity (W/m°C)	70	16.7
Specific heat (J/kg°C)	247	590
Density (kg/m ³)	11400	7930
Emissivity	0.05	0.35

Table 2: Heat transfer coefficient applied to stainless chamber model

Stainless temperature (°C)	Heat transfer coefficient (W/m ² °C)
20	0
21	2.2
22	2.6
23	2.9
24	3.1
25	3.1

Table 3: Simulation condition

Initial temperature of Pd (°C)	50
Heat generation temperature (°C)	100, 200, 300, 500
Temperature of the outside of the chamber (°C)	20
Heat generation position	center, midpoint, edge
Duration (s)	0.1 s
Analysis time (s)	2.5 s

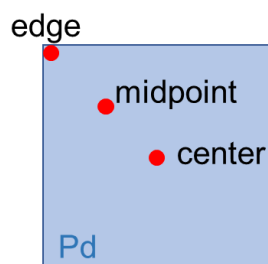


Figure 4: Heated positions in the simulation.

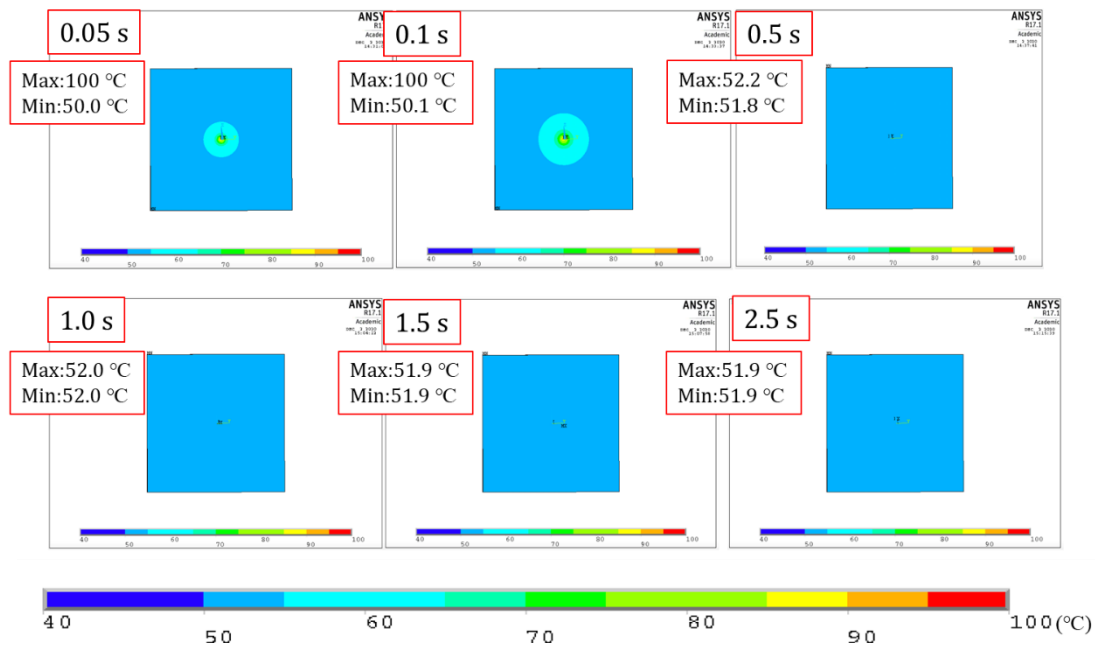


Figure 5: Thermal conduction behavior when the center of the Pd foil was heated to 100 °C.

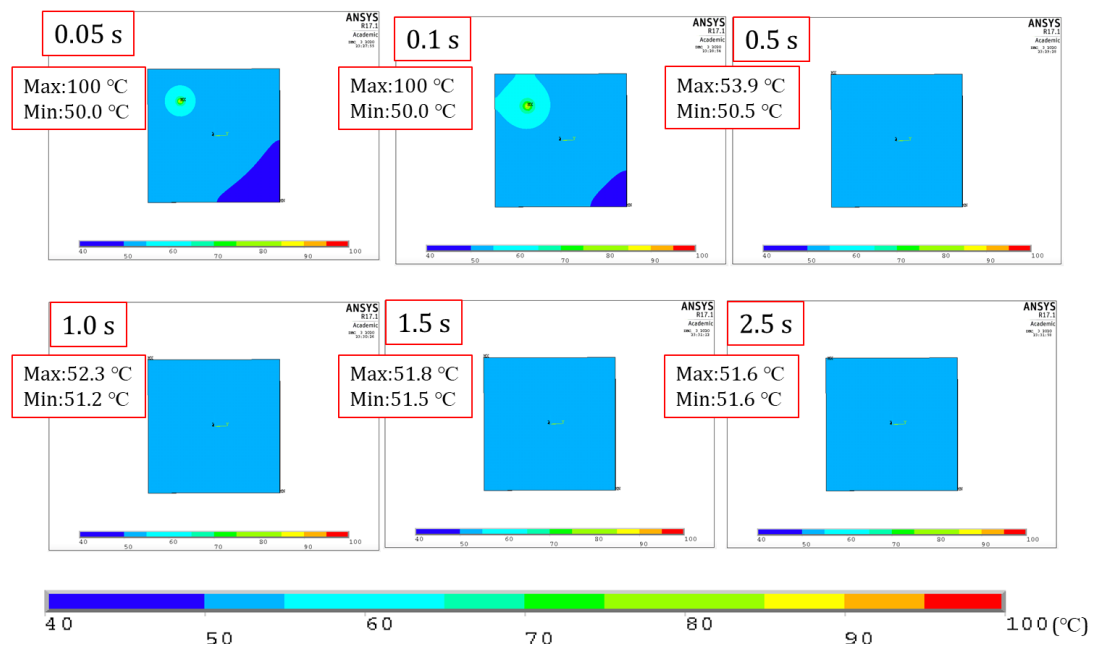


Figure 6: Thermal conduction behavior when the midpoint of the Pd foil model was heated to 100 °C.

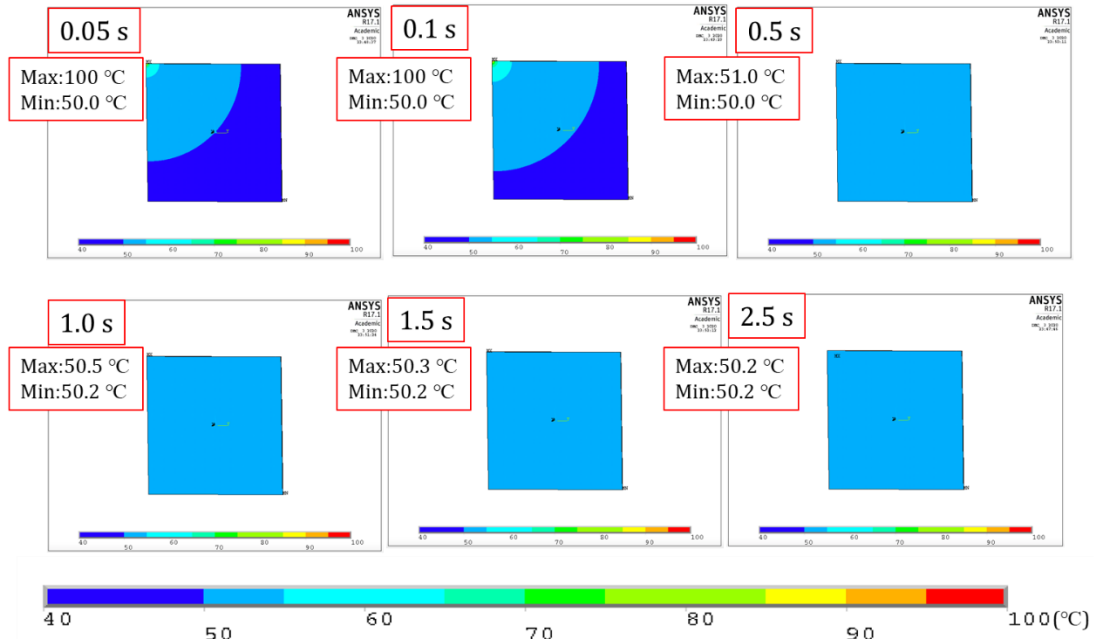


Figure 7: Thermal conduction behavior when the edge of the Pd foil model was heated to 100 °C.

3. RESULTS AND DISCUSSION

Figure 5 depicts heat conduction when the center of the Pd foil was heated to 100 °C at 0.05 s, 0.1 s, 0.5 s, 1.0 s, 1.5 s, and 2.5 s. During 0 to 0.1 s, the maximum temperature was 100 °C. Note that, in this simulation, the heat constraint of 100 °C was given to the node corresponding to the center, midpoint, or edge on the Pd sample from 0 to 0.1 s, then it was removed and the temperature of the node was given back to the initial temperature, 50 °C. Between 1 and 2.5 s, the Pd-foil temperature distribution was almost uniform. When the midpoint was heated up to 100 °C, the distribution was almost homogenous after 2.5 s, as shown in Fig. 6. Figure 7 shows the temperature behavior of the sample when the edge reaches 100 °C. The Pd foil temperature was 50.2 °C in the steady state. From the above results, the Pd foil has an almost uniform temperature distribution after 2.5 s, regardless of the heat generation position.

As mentioned above, the temperature was measured using a thermocouple attached to the center of the sample. The time change in temperature at the center of the model was investigated along with the calorific value obtained from the temperature variation.

Figure 8 illustrates the time variation of the temperature of the Pd foil while heating the center. Table 4 shows the temperatures at the measurement point (center of Pd foil model) and the respective calorific values calculated from $mc\Delta T$, which we evaluate as the amount of heat generated from the temperature measurement in the experiment. Here, m is the mass of the Pd foil, c is the specific heat, and ΔT is the temperature change. In the simulation, the heating point was heated for 0.1 s, so that when the center — which was the measurement point — was heated, the temperature there was identical to the given temperature up to 0.1 s. The temperatures measured after 0.15 s were 57.5 °C and 117 °C

when the heat applied was 100 °C and 500 °C, respectively.

Figure 9 shows the time-course variation in the temperature of the Pd foil while heating the midpoint. The temperatures at the measurement point and calorific value at each instance are shown in Table 5. At 100 °C, the temperature is almost constant after approximately 0.5 s and the generated heat is approximately 0.04 J. At 500 °C, the temperature is constant at approximately 65 °C and the generated heat is 0.4 J.

Figure 10 shows the time variation in the temperature of the Pd foil when the edge is heated. The temperature at the measurement point and calorific value for each instance are shown in Table 6. When the edge was heated, temperature at the measurement point increased to approximately 53 °C at the maximum.

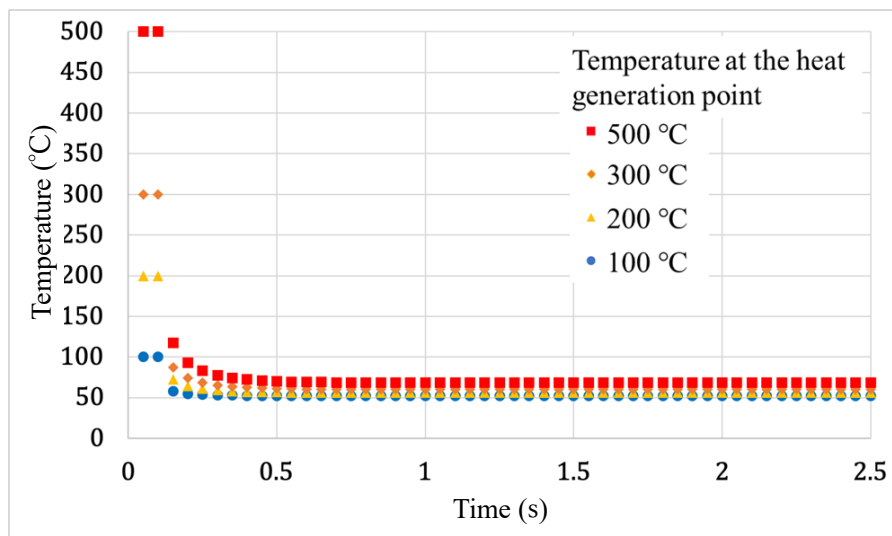


Figure 8: Time variation of temperature of Pd foil when heating the center.

Table 4: The temperature at the measurement point and calorific value calculated from $mc\Delta T$ for each temperature given at the center.

Given temperature (°C)	Time (s)	Temp (°C)	$mc\Delta T$ (J)
100	0.15	57.5	2.11×10^{-1}
	1.0	52.0	5.60×10^{-2}
	2.5	51.9	5.27×10^{-2}
200	0.15	72.5	6.33×10^{-1}
	1.0	56.1	1.72×10^{-1}
	2.5	56.0	1.68×10^{-1}
300	0.15	87.5	1.05
	1.0	60.2	2.88×10^{-1}
	2.5	60.1	2.83×10^{-1}
500	0.15	117	1.90
	1.0	68.5	5.20×10^{-1}
	2.5	68.3	5.14×10^{-1}

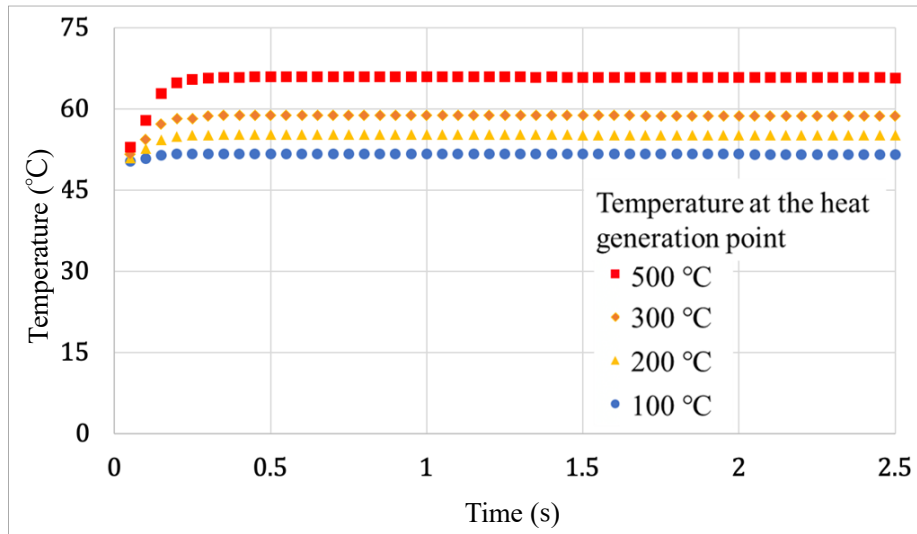


Figure 9: Time variation of temperature of Pd foil when heating the midpoint.

Table 5: The temperature at the measurement point and calorific value calculated from $mc\Delta T$ for each temperature given at the midpoint.

Given temperature (°C)	Time (s)	Temp (°C)	$mc\Delta T$ (J)
100	0.15	51.4	4.01×10^{-2}
	1.0	51.7	4.81×10^{-2}
	2.5	51.6	4.48×10^{-2}
200	0.15	54.3	1.21×10^{-1}
	1.0	55.3	1.48×10^{-1}
	2.5	55.1	1.45×10^{-1}
300	0.15	57.2	2.01×10^{-1}
	1.0	58.8	2.48×10^{-1}
	2.5	58.7	2.44×10^{-1}
500	0.15	62.9	3.63×10^{-1}
	1.0	65.9	4.49×10^{-1}
	2.5	65.8	4.44×10^{-1}

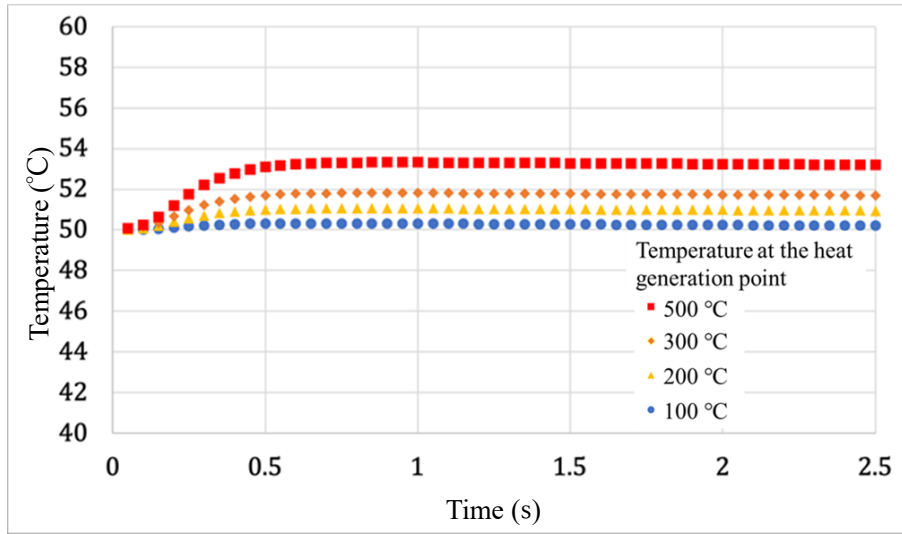


Figure 10: Time variation of temperature of Pd foil when heating the edge.

Table 6: The temperature at the measurement point and calorific value calculated from $mc\Delta T$ for each constraint temperature (Edge)

Given temperature (°C)	Time (s)	Temp (°C)	$mc\Delta T$ (J)
100	0.15	50.1	1.72×10^{-3}
	1.0	50.3	8.59×10^{-3}
	2.5	50.2	5.52×10^{-3}
200	0.15	50.2	5.77×10^{-3}
	1.0	51.1	2.98×10^{-2}
	2.5	50.9	2.67×10^{-2}
300	0.15	50.3	9.83×10^{-3}
	1.0	51.8	5.10×10^{-2}
	2.5	51.7	4.78×10^{-2}
500	0.15	50.6	1.79×10^{-2}
	1.0	53.3	9.34×10^{-2}
	2.5	53.2	9.01×10^{-2}

From these results, it was seen that even when there was a large amount of heat generated at any point, the thermocouple measured the temperature and calorific value correctly.

To obtain the total calorific value originally given, we also have to consider radiant heat in addition to the effect of thermal conduction discussed above. The total calorific value (J_{total}) is calculated by adding the energy used for heat conduction (calculated from $mc\Delta T$) and the energy from the integrated radiant heat emitted from the Pd foil at 2.5 s:

$$J_{total} = mc\Delta T + \int_0^{2.5} \Delta Q_r dt, \quad (3)$$

where ΔQ_r is the radiant heat per unit time. In this calculation, $mc\Delta T$ was calculated from the difference between the initial temperature and the temperature at the measurement point after 2.5 s, assuming that the temperature of the entire sample was uniform.

Figure 11 shows the integrated radiant heat up to each time, where heat is generated at the center, midpoint, and edge. It can be observed that the values increase linearly. In the experiment, the temperature was measured at a point between 0 and 2.5 s, and the calorific value was calculated based on the assumption that the measured temperature was uniform across the sample. In reality, however, there is a difference between the actual amount of heat generated and the actual amount of heat generated due to the effects of heat conduction and radiation, depending on the time difference between the heat generation and the timing of measurement and the location of the heat generation.

The total calorific values and its each term, conduction heat and radiant heat for each simulation conditions are summarized in Table 7.

We then estimated the time difference between the heat generation (J_{total}) and the location of the heat generation (J_{meas}). The results are shown in Fig. 12. When heat generation occurs at the center of the sample, the calorific value obtained from the temperature just after the heat generation is higher than the actual heat value. On the other hand, when heat is generated at the midpoint or edge, the heat is estimated to be lower than the actual heat when the temperature is measured immediately after heat generation. The difference is in the range of -0.1 to 10 J. The difference in heat generation for any condition is almost negligible after approximately 0.5 s. Note that these values also depended on the duration of the heating; this study covered only a duration of 0.1 s.

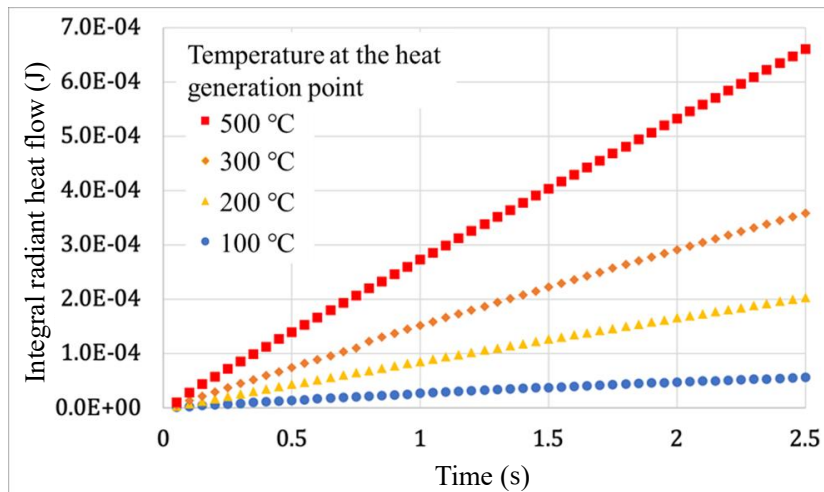
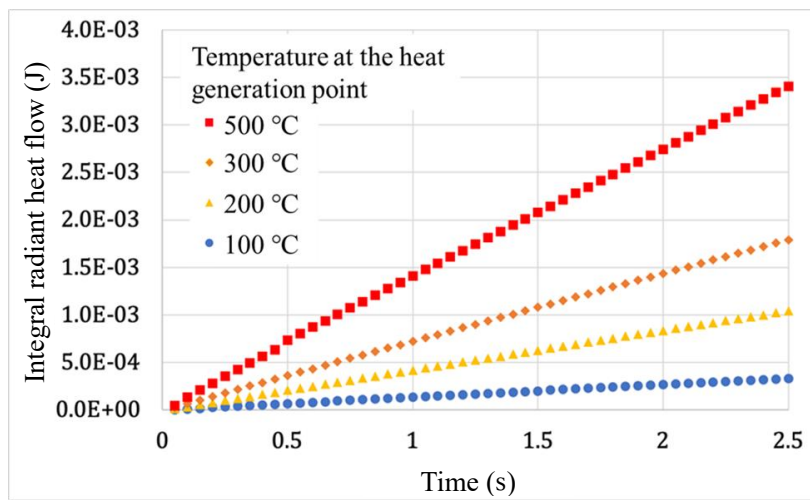
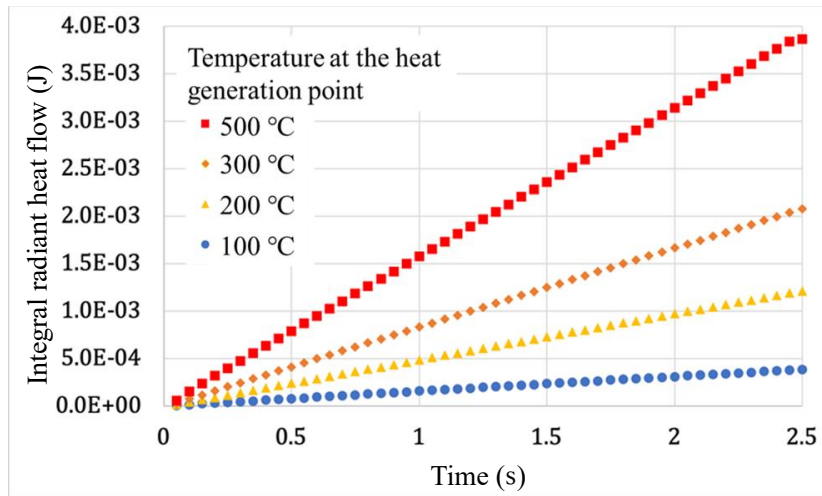


Figure 11: Integral radiant heat for heat generation at center (top), midpoint (middle), and edge (bottom) of the sample, respectively.

Table 7: Total calorific value J_{total} , the conduction heat, and the radiant heat for each condition; heat generation at center (top), midpoint (middle), and edge (bottom) of the sample, respectively.

	Center			
Given temperature	100 °C	200 °C	300 °C	500 °C
Conduction heat (J)	5.27×10^{-2}	1.68×10^{-1}	2.83×10^{-1}	5.14×10^{-1}
Radiant heat (J)	3.82×10^{-4}	1.21×10^{-3}	2.07×10^{-3}	3.86×10^{-3}
J_{total} (J)	5.30×10^{-2}	1.69×10^{-1}	2.86×10^{-1}	5.18×10^{-1}

	Midpoint			
Given temperature	100 °C	200 °C	300 °C	500 °C
Conduction heat (J)	4.48×10^{-2}	1.45×10^{-1}	2.44×10^{-1}	4.44×10^{-1}
Radiant heat (J)	3.29×10^{-4}	1.04×10^{-3}	1.79×10^{-3}	3.41×10^{-3}
J_{total} (J)	4.52×10^{-2}	1.46×10^{-1}	2.46×10^{-1}	4.47×10^{-1}

	Edge			
Given temperature	100 °C	200 °C	300 °C	500 °C
Conduction heat (J)	5.52×10^{-3}	2.67×10^{-2}	4.78×10^{-2}	9.01×10^{-2}
Radiant heat (J)	5.54×10^{-5}	2.03×10^{-4}	3.58×10^{-3}	6.60×10^{-4}
J_{total} (J)	5.57×10^{-3}	2.69×10^{-2}	4.82×10^{-2}	9.08×10^{-2}

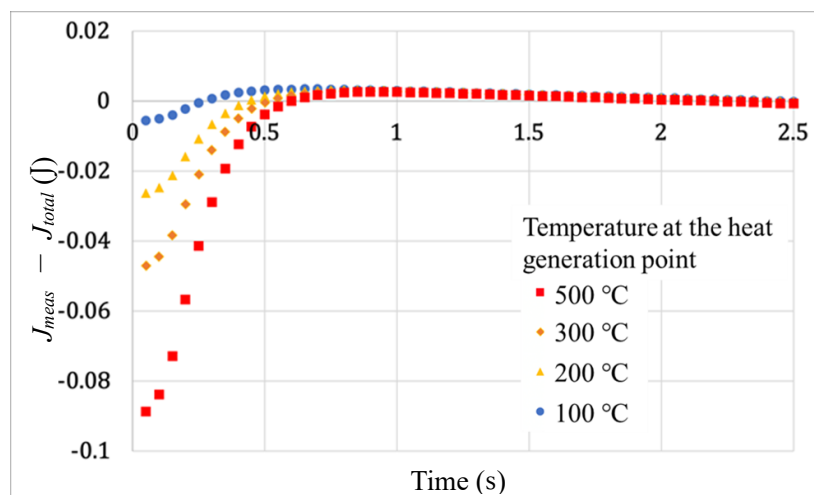
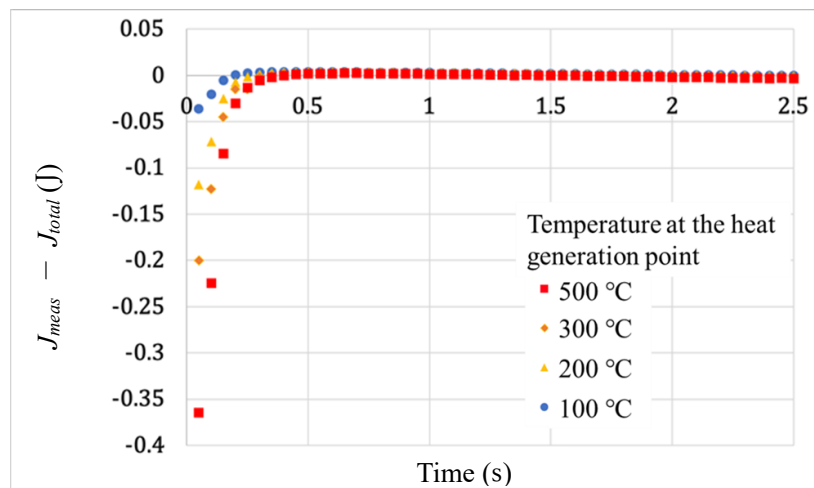
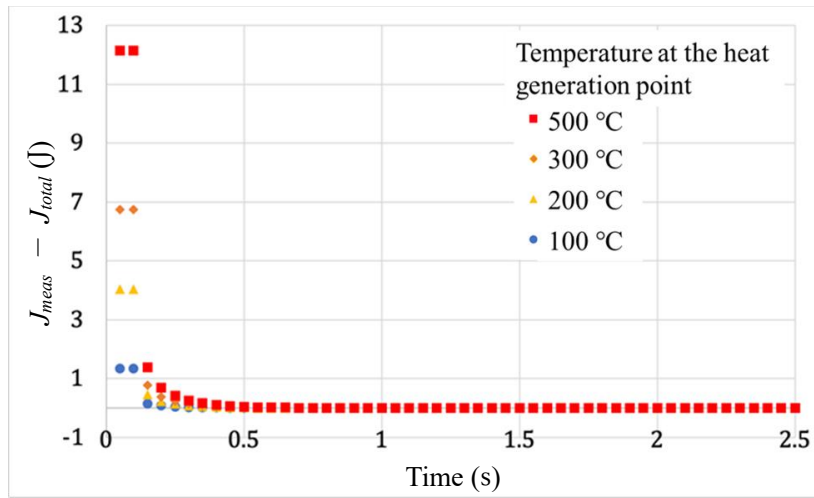


Figure 12: Difference from the value obtained in the experiment for the heat generation at center (top), midpoint (middle), and edge (bottom) of the sample, respectively.

4. SUMMARY

In this study, we successfully simulated how heat is transmitted in the sample at certain areas. We also evaluated radiant heat when localized heat evolution occurred in the sample; the conducted and radiated heat were evaluated quantitatively to understand the anomalous temperature trend in our experiment. As a result, we noted that, under our experimental conditions, there was a difference between the empirical heat value and the actual heat value. The magnitude of this discrepancy depended on the location of heat generation and the timing of measurement from the moment of heat generation. The difference was expected to be of the order of a few Joules, considering the uncertainties inherent in discussing the anomalous phenomenon. For further study, it is imperative to improve the simulation conditions to reproduce the temperature anomalies in the experiment and to more accurately measure the original heat generated. In addition, we should consider improving the temperature-measurement system to enable us to monitor the temperature more frequently.

References

- [1] H. Kudou et al., Proc. of JCF15, (2015) 20.
- [2] Y. Sato et al., Proc. of JCF18, (2018) 1.
- [3] M. Endo et al., Proc. of JCF19, (2019) 53.
- [4] M. Endo et al., Proc. of JCF20, (2020) 61.
- [5] CYBERNET, ANSYS Heat transfer analysis seminar.

Thermodynamic analysis of Pd –H electrode: $H/Pd > \beta_{\min}$ during repeated cathodic and anodic electrolysis in an acidic solution

Hiroo NUMATA

60 Higashidai Kaneyama-machi Iwaki City Fukushima 974-8211 Japan

Abstract

To understand loading behavior of hydrogen in a Pd electrode *in situ* potentiometric, resistance, and dilation measurements were performed during galvanostatic pulse mode electrolysis. This study is a continuation of the reported work[1]. With an increase of H concentration, over H/Pd ratio $> \beta_{\min}$ the electrode potential exhibits non Nernstian behavior: the potential deviates from a straight line whose slope is coincident with -62 mV/decade vs. logarithmic scale of H/Pd ratio.

The characteristic values of α_{\max} , β_{\min} of phase transition and equivalent hydrogen pressure p_{H_2} of two phase coexistence are consistent with that of the Pd-H isotherm obtained by the gas equilibrium method. In H/Pd ratio $> \beta_{\min}$, further comparison of thermodynamic parameters: the standard free energy of formation with those obtained by electrochemical method will be considered. Prior to these calculations, it is suggested that an effect is possible on the free energy through a base compound incorporated with lattice defects.

Key words: Pd-H phase diagram, H concentration, electrode potential, vacancy, thermodynamic calculation

1. Introduction

Metal hydrides have been intensively attracted fundamental and application research interests[2]. As for Pd-H phase diagram, it exhibits the α phase, two phase coexistence and β phase regions along with an increase of H concentration. As far as the author knows, there has been a lack of precise analyses with respect to the phases over β_{\min} . This issue is of special importance for researchers from experimental and theoretical aspects.

Besides many studies concerning metal hydrides, hydrogen insertion can be achieved by electrolysis where H concentration is calculated by the charges (current multiplied by time of electrolysis), in accordance with Faraday's law. However, there is the ambiguous point with respect to solute atom's homogeneity in a specimen because of retardation of the diffusion process and possible surface reaction. It is also noted that lattice defects induced by hydrogen insertion interact with hydrogen resulting its local accumulation on the defects. Although excellent works have been reported, the studies with respect to the hydrogen interactions is not included in this study.

The aim of this study is to present a miscellaneous consideration before a systematic study of physico-chemical property and phase changes due to hydrogen insertion in Pd. The contents include comparative description of equilibrium hydrogen occlusion in a gaseous chamber and in an aqueous solution using electrolysis. Furthermore, the electrode potentials obtained by the latter method are analyzed using thermodynamic parameters estimated by well-known thermo chemical calculation.

2. Experimental results and discussion

2.1 Experimental method

In a binary (two components system) phase diagram it has independent 3 variants: the temperature, pressure and composition of the system as a whole. As for

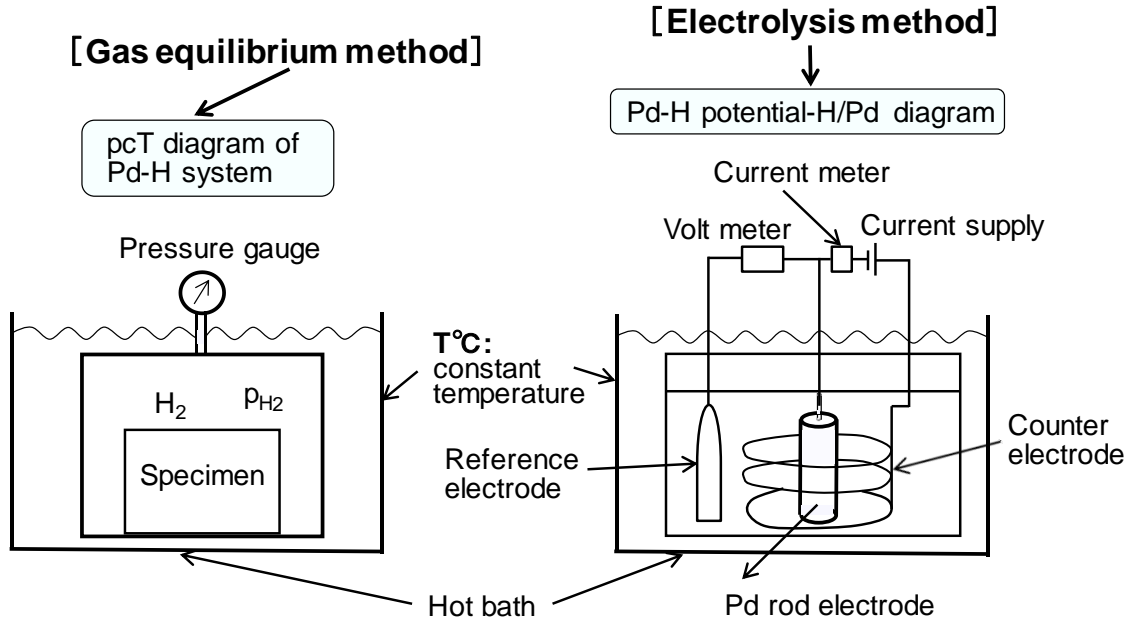


Fig. 1 Schematic of experimental apparatuses for measuring pcT and electrode potential-H/Pd ratio diagrams.

the binary phase diagram, we use a two-dimensional phase diagram: temperature–composition diagram at a fixed pressure or pressure–composition diagram at a fixed temperature.

The Pd-H phase diagram (e.g., pressure-concentration diagram) can be determined by Pd equilibration with gaseous hydrogen in a chamber, as shown in Fig. 1. Here, H concentration is for example determined by a decrease of hydrogen pressure in a gas tight chamber. Similarly shown in the right figure, the hydrogen pressure converted by equilibrium electrode potential constructs the Pd-H phase diagram where the H concentration is calculated from the charge thrown in each electrolysis. If homogeneity and equilibration of hydrogen in Pd in both the cases are ensured at a given temperature, the obtained two phase diagrams by different hydrogen equilibration methods can be coincident, as shown later.

2.2 Electrode potential corresponding to hydrogen absorbed in Pd

Figure 2 shows a plot of the electrode potential vs. logarithmic H/Pd ratio where the dotted line is theoretical one whose slope is calculated by the Nernst equation according to an equilibrium between proton ion and hydrogen absorbed. The Nernst equation can be written as

$$E = E^\circ - RT/F \ln a_{\text{H}_{\text{ab}}} - 2.3RT/F \cdot \text{pH} \quad (1)$$

where $a_{\text{H}_{\text{ab}}}$ represents the activity of hydrogen absorbed. The other symbols have their usual meanings. As shown in Fig. 2, the electrode potential obeys the Nernst Eq. showing a straight line with a slope of $-2.3 RT/F$. In $\text{H/Pd} < \beta$ single phase, $a_{\text{H}_{\text{ab}}}$ can be approximated as H concentration: C_{ab} . Thus, the electrode potential behaves the Nernst potential. Then the H/Pd ratios are calculated assuming 100% absorption of evolved hydrogen atoms and solute homogeneity in a Pd electrode.

Figure 3 shows a plot of electrode potential as a function of logarithmic H concentration until H/Pd 1.0. When the H/Pd ratio exceeds 0.01, the electrode potential

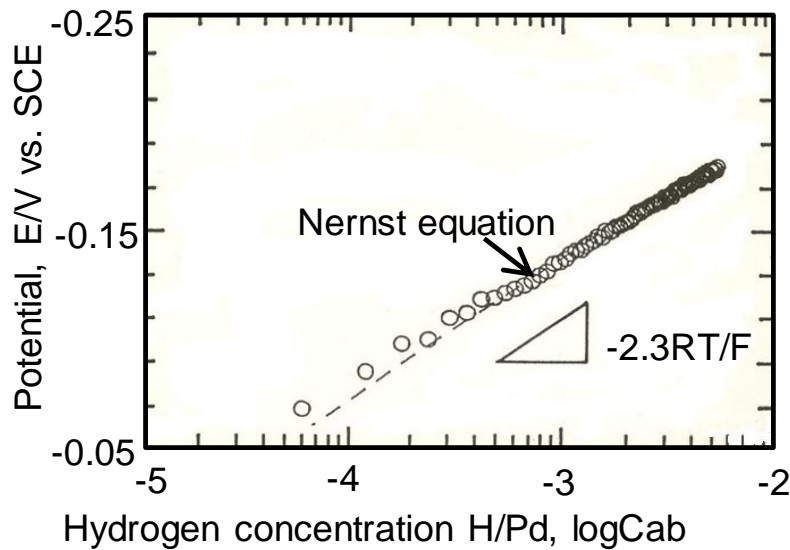


Fig. 2 Hydrogen electrode potential vs. $\log(H/Pd)$ in the α phase at 40°C .

becomes constant showing the $\alpha + \beta$ coexistence region. As shown in Fig. 3, over H/Pd 0.55 it exhibits a gradual decrease not obeying the Nernst Eq. These potentials correspond to the β single phase due to the deviation from two phase coexistence region.

Since the thermodynamic characteristic values of the Pd-H system becomes available between gas phase equilibrium and electrochemical methods.

As for the characteristic H/Pd ratio of individual phase boundary, for α phase: α_{max} , and solvus concentrations with the $\alpha + \beta$ two phase coexistence or the onset of β phase: β_{min} are determined, as shown in Fig. 3.

On the other hand, Fig. 4 shows the Pd-H phase diagram measured by gas equilibrium method where longitudinal axis represents temperature and lateral one H/Pd ratio. From this diagram the characteristic values of α_{max} and β_{min} are obtained as 0.01 and 0.55, respectively. These values coincide quite well with that indicated in Fig. 3 measured by electrochemical method.

As for an equilibrium partial pressure of hydrogen, above consideration is performed. As above mentioned the electrode potential obeys the Nernst potential, the hydrogen pressure of p_{H_2} can be calculated from the electrode potential under limited conditions [3, 4]:

$$p_{H_2} = \exp[-(E + E_{SCE}) / (2F/RT)] \quad (2)$$

where E_{SCE} is the potential of the reference

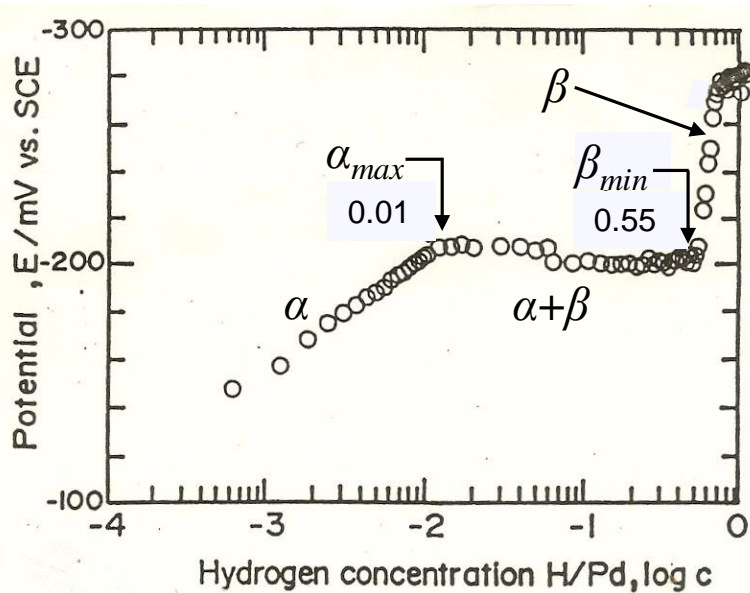


Fig. 3 Hydrogen electrode potential vs. $\log(H/Pd)$ in the β phase at 40°C .

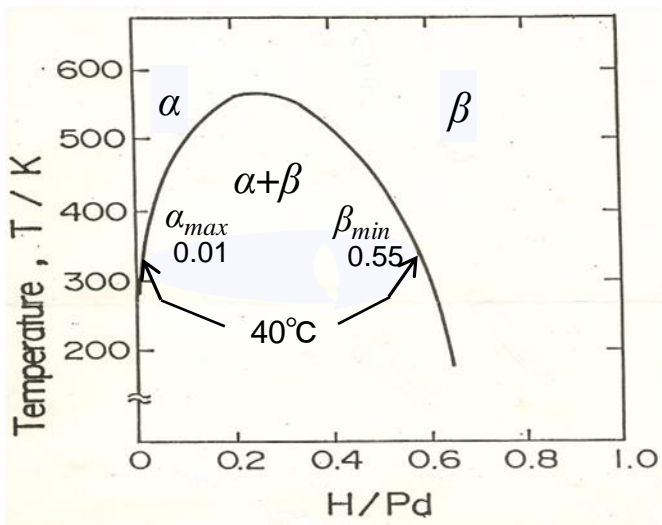


Fig. 4 Temperature composition diagram of Pd-H system.

of equilibrium pressure and composition at a given temperature. It indicates phase boundary conditions, i.e., pressure and composition for single phase, two phase coexistence and stoichiometric compound. The equivalent hydrogen pressure p_{H_2} of two phase coexistence region at 40°C was estimated as 0.05×10^5 Pa from the literature [5] where the isotherm represents the data at selected temperatures. Thus, these characteristic values [α_{max} , β_{min} of phase transition and equivalent hydrogen pressure p_{H_2} of two phase coexistence] are consistent with those of the Pd-H isotherm obtained by the gas equilibrium method.

2.3 Calculation of thermodynamic parameters of the β phase

For the comparison of thermodynamic parameters over β_{min} with those obtained by electrochemical method, the following procedure was undertaken.

As the first step, the chemical potential of the single β phase lattice defect free assumes dependence on X_H (H/Pd ratio). There has been reported that the chemical potentials at particular compositions were estimated through the thermodynamic calculation. Following these procedures the compounds with vacancies can be applicable incorporating a particular lattice structure. When the ratio of such imperfect lattice vs. lattice defect free is arranged to β_{min} , further change of the ratio may estimate the chemical potential of a matter with any amount of defects at a given

electrode.

Figure 5 shows the p_{H_2} (the hydrogen pressure equilibrated with that in the Pd matrix) vs. H/Pd ratio assuming the Nernst Eq. The two phase coexistence pressure is determined as 0.05×10^5 Pa, as indicated in Fig. 5. When the state is turned into the single β phase, the hydrogen pressure again begins to increase until a final pressure of 16×10^5 Pa has been reached.

A pT diagram imposed by the Pd-H binary phase diagram represents phase behavior for variation

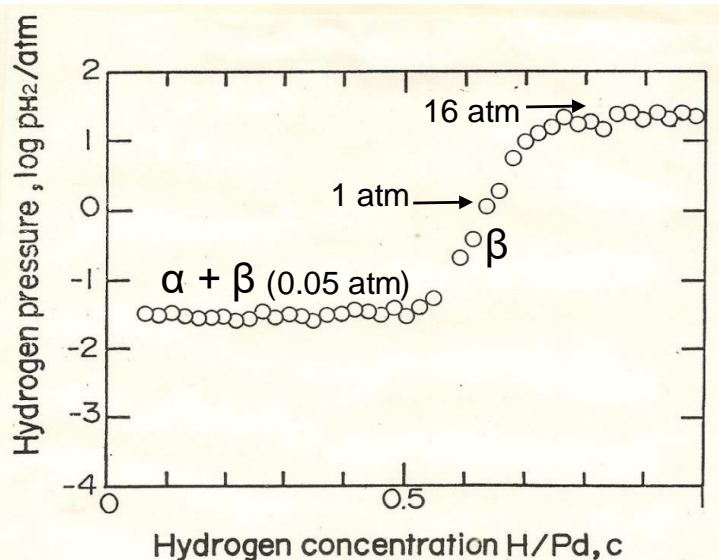


Fig. 5 Equivalent H pressure vs. H/Pd ratio at 40°C ; the $\alpha + \beta$ coexistence phase pressure is 0.05×10^5 Pa.

whole X_H . Here, we prepare the lattice structure possessing defects with a given non-stoichiometric compound as a base compound.

The second step is to convert the calculated chemical potentials to the equivalent electrode potentials. Then the electrode potentials estimated will be compared with the experimental data, which validates this procedure. At the same time, the most suitable base compound is also evaluated.

As for Pd hydride, possible covalent compound is derived through the followings:

The difference between Pd and H electronegativity is negligibly small,

Valence Pd: 2+, 4+; H: 1+,

The difference between Pd and H atomic radii is large.

It is noted that a single solid solution with a wide range of composition (e.g., Ag-Au binary system) is not anticipated but two phase coexistence phase diagram.

2.3.1 Base compounds for the β phase thermodynamic parameters

Thermodynamic parameters are calculated using statistic thermodynamics method under quasi-chemical approach. The following at first describes how we search base compounds considering so far known experimental data compiled in the literatures.

For the Pd-H system, we determined the structures of a base compound reviewing many candidates considering the consistency with hitherto experimental reports. The composition of base compound is H/Pd ratio = 0.6 possessing f.c.c structure. To construct the lattice the following conditions are required.

- the number of Pd atoms 1, hydrogen atoms 0.6 in the unit cell:

For [Pd: H = 1: 0.6] hypothetical lattice structure composing 500 Pd and 300 H atoms is introduced as schematically shown below.

- In an interstitial hydrogen compound assuming 100 % occupation at octahedral sites f.c.c unit cell contains regularly Pd 4 and H 4 atoms, respectively. To visualize the lattice structure possessing 500 Pd and 300 H atoms the number of unit cell is calculate as: 500 atoms equals 4(for one unit cell) multiplied by 125(for cell number), therefore 500 Pd and 300 H atoms are distributed in 3D space: 5 unit cells constitute x, y, z coordinates in the Cartesian coordinate system and then the volume contains 5x5x5 (=125) unit

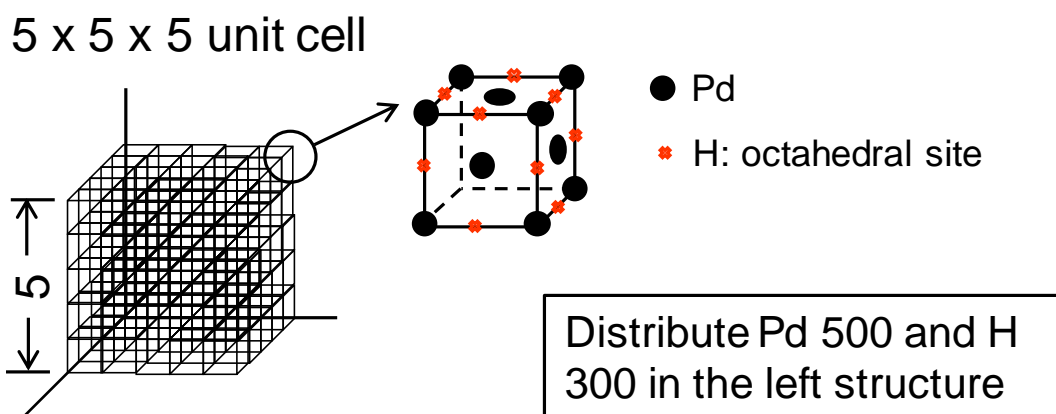


Fig. 6 Schematic of a base compound consisting of Pd 500 and H 300 atoms.

cells, as shown in Fig. 6.

- the other candidate base compounds are listed as:
 - (1) Pd₃H₄ and Pd₂H
 - (2) compound occluding vacancy, and superlattice

2.3.2 pcT diagram for the Pd-H binary system

For unambiguous Pd-H phase over β_{\min} it is necessary that the comparison between the calculated chemical potentials and experimental data has been performed taking into account a chemical equilibrium of the relevant compounds.

(Thermodynamic calculation for a binary system)

The standard $\Delta_f G^0$ free energy of formation of the binary Pd-H system at the absolute temperature T is defined as

$$G^0 = RT \left\{ \left(X_{\text{Pd}} \right) \left(X_{\text{H}} \right) \right\} \quad (3)$$

where the system is Pd/H₂/PdH_X; and $X_{\text{H}} = \text{H/Pd}$ ratio and $X_{\text{Pd}} = (1-\text{H/Pd})$ ratio). The above Eq. (3) is obtained from the Gibbs-Duhem relation under constant temperature shown as

$$\ln a_{\text{Pd}} = \frac{\Delta_f G^0}{RT} \quad (4)$$

where a_{Pd} is the activity of Pd, and f_{H_2} is the fugacity of hydrogen.

(The relation of $\Delta_f G^0$ and $\mu_{\text{H}} - X_{\text{H}}$)

Accompanied with the above Eq. (3), the following chemical equilibrium could exert an effect on the free energy calculation through possible crystal structures. For example Pd_{1-x}H_{0.6} containing defects consists of vacancy of Pd plus octahedral sites occupation and that plus tetrahedral sites occupation (see Fig. 7).

To reflect such structural defects in the calculation of free energy we define PF (Partition function) according to Fowler and Guggenheim [6],

$$\text{PF} = \sum_{\Omega} e^{-\frac{E}{kT}} \quad (5)$$

where k is the Boltzmann constant, N_{Pd} and g_{Pd} are the number and microcanonical partition function of Pd, and same notation for H. Here, E means the potential energy of the given grandcanonical ensemble, and Ω is the summation of the number for all distinguishable arrangements corresponding to E . As for an approximation, E can be replaced by the summation of interaction energies between nearest neighbor atoms in

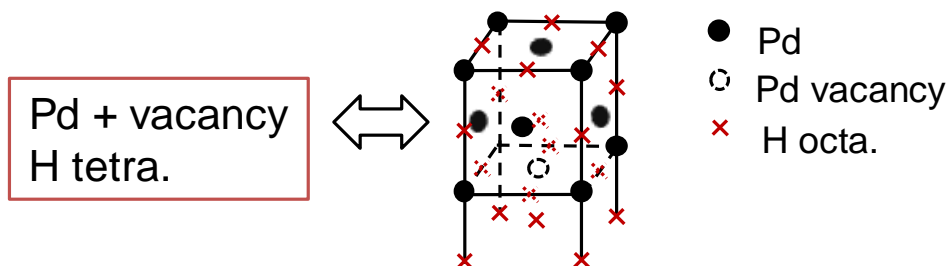


Fig. 7 Schematic of a possible arrangement of Pd vacancy and octahedral (tetrahedral) H.

the system, as expressed by the following Eq. (6):

$$E = \epsilon_{\text{HH}}^i + \epsilon_{\text{PdH}}^i + \epsilon_{\text{PdPd}}^i \quad (6)$$

where i indicates 1st, 2nd and 3rd nearest neighbor atoms.

Thus, the Helmholtz energy F is expressed as

$$F = -kT \ln(\Omega) = -kT \{ N_{\text{Pd}} \ln(\Omega_{\text{Pd}}) + N_{\text{H}} \ln(\Omega_{\text{H}}) \} - kT \ln(\Omega) + E_{\text{eq}} \quad (7)$$

The free energy of Eq. (7) is differentiated with N_{H} to give the chemical potential of H: μ_{H} in $\text{Pd}_{1-x}\text{H}_{0.6}$ as follows:

$$\mu_{\text{H}} = \left(\frac{\partial F}{\partial N_{\text{H}}} \right)_{T,p,N_{\text{Pd}}} = \left(\frac{\partial E}{\partial N_{\text{H}}} \right)_{T,p,N_{\text{Pd}}} + P \left(\frac{\partial V}{\partial N_{\text{H}}} \right)_{T,p,N_{\text{Pd}}} \quad (8)$$

where the condition that the volume of the system is constant and the activity coefficient is unity holds. Thus, Eq. (8) gives μ_{H} as a function of X_{H} .

3. Summary

We summarize our study as follows:

1. For the Pd-H binary phase diagram, the characteristic values: α_{max} , β_{min} of phase transition and equivalent hydrogen pressure p_{H_2} of two phase coexistence estimated from the electrochemical experiment were consistent with those of the Pd-H isotherm obtained by the gas equilibrium method.
2. In H/Pd ratio $> \beta_{\text{min}}$, a base compound without lattice defects was determined for further thermodynamic calculation.
3. We presented a possible method to understand the Pd-H binary system over β_{min} .

References

- [1] H. Numata: Proc. JCF19, pp. 148 (2019)
- [2] T.B. Flanagan and W.A. Oates: " Hydrogen in Intermetallic compounds I", edited by L. Schlapbach, in Topics in Appl. Phys. Vol. 63 (Springer-Verlag, Berlin, 1988) pp.49
- [3] H. Numata and I. Ohno: *Fusion Technol.*, **38**, pp.206 (2000)
- [4] H. Züchner and H.G. Schöneich: *J. Less-Common Met.*, **101**, pp.363 (1984)
- [5] E. Wicke and H. Brodowsky: "*Hydrogen in Metals II*", pp.73, J. Völkl and G. Alefeld, eds., Springer-Verlag, Berlin (1979)
- [6] R.H. Fowler and E.A. Guggenheim: Statistical Thermodynamics, The Cambridge University Press, London, 1965, pp. 42 and 576

A theoretical study on the possible change of the phonon dispersion relation due to the nuclear reaction in two-dimensional lattice III

Ken-ichi TSUCHIYA

*Department of Chemical Science and Engineering,
National Institute of Technology, Tokyo College,
1220-2 Kunugida, Hachioji, Tokyo 193-0997, Japan*

E-mail: tsuchiya@tokyo-ct.ac.jp

Abstract

The nuclear reactions in solids may change the phonon dispersion relation, because this relation sensitively depends on the lattice structures. In our previous, we have discussed the changes in phonon dispersion relations caused by changes in the lattice structure due to the DD reactions. At a first step, complete uniform nuclear reactions were considered for simplicity. However, local reactions are more realistic. In JCF20, we showed the method how to detect the local change of lattice defects due to the nuclear reactions by introducing the theory of local modes described in the text book of C. Kittel.

In this study, we show the method how to detect the local change of lattice defect by generalized theory of local modes. This theory may provide evidences of the nuclear reactions in solids hidden in the old data of phonon dispersion relations.

(**keywords;** phonon dispersion relation, local phonon mode, nuclear reaction in solids)

1 Introduction

It is well known that the relations between the frequency of the lattice vibration and the wave number of the phonon wave propagation are called phonon dispersion relations, which depends on the lattice structure sensitively [1]. This fact suggests that we can detect the structure change of the lattice due to the nuclear reactions in solids.

For example, if we consider the case where deuterons occupy the all stable positions of a two-dimensional simple cubic Pd lattice, the structure change happens as in the sketch drawn in Fig.1. The structural change of the primitive cell directly changes the phonon dispersion relation. Before the reaction, the primitive cell includes one Pd and one deuteron. This means that the type of the dynamical matrix is 6×6 . On the contrary, after the reaction, the primitive cell includes two Pd and one He, and the dynamical matrix of the lattice changes to 9×9 . Therefore, the number of the dispersion branch increases from 6 to 9. If such changes are observed in the measurement of the phonon dispersion relation, they are indirect evidence of nuclear reactions.

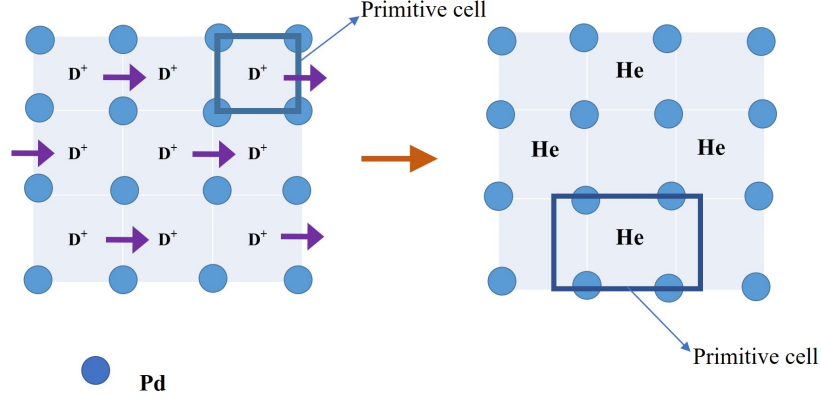


Fig. 1. An example of DD reactions in two-dimensional lattice, where 1/2 deuterons migrate and all deuterons happen to react.

2 Local phonon mode

The structure change by uniform reaction is an oversimplified model, so it is realistic to consider that the nuclear reaction occurs locally rather than uniformly in the lattice. The theory of the lattice vibration including such a change of the local lattice structure is described in some text books of solid state physics as local phonon mode [1]. That book introduces a one-dimensional linear lattice with a substitutional light impurity, which is illustrated in Fig.2.

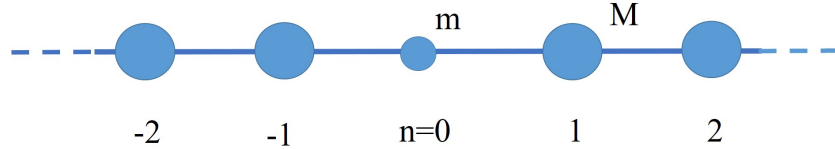


Fig. 2. One-dimensional lattice with a light impurity at the origin ($n=0$). The mass of a light impurity is m and the mass of a host atom is M . The distance between all atoms is assumed to be constant.

The equation of motion for the atom at position n is written as

$$M_n \frac{d^2 u_n}{dt^2} = C (-2u_n + u_{n-1} + u_{n+1}) \quad , \quad (1)$$

where u_n and M_n mean the amplitude and the mass of the atom at position n . There is only one light impurity at the origin, so M_n is M except for $M_0 = m$. Strictly, the force constants should differ depending on the distance from the origin, but here, all of them are assumed to be C . The following solution is obtained from the

simultaneous equations of motion for the atom at position n and $n + 1$ as

$$u_n = U e^{iqna} e^{-i\omega t} e^{-|n|\alpha} , \quad (2)$$

where q , ω and a mean wavenumber, angular frequency and lattice constant, respectively. In order for $e^{-|n|\alpha}$ in Eq.(2) to be a damping factor, the constant α must be a positive real number. If such α exists, then this solution represents a local phonon mode created by a light impurity at $n = 0$, whose influences decrease as $|n|$ increases. We can easily find the positive real α for the case of the zone boundary of $k = \frac{\pi}{a}$ as

$$\alpha = \log \left(\frac{M}{m} - 1 \right) , \quad (3)$$

where $M > m$.

In the proceedings of JCF20 [3], we discussed the local phonon mode of deuteron storage Pd lattice and showed a new method how to detect the structural change due to the nuclear reaction in the lattice. In this study, we correct some mistakes in the previous work and extend it not only to two-dimensional but also to three-dimensional cubic lattice. The sketch of the two-dimensional lattice including a deuteron at the origin is shown in Fig.3. Actually, the Pd lattice has an fcc structure, but in this study, we regard it as a simple cubic lattice with lattice constant a . The lattice points of this lattice are defined as

$$\mathbf{R}_{pq} = a(p\hat{\mathbf{x}} + q\hat{\mathbf{y}}) \quad (p, q = \dots, -1, 0, 1, \dots) , \quad (4)$$

where the characters $\hat{\mathbf{x}}$ and $\hat{\mathbf{y}}$ mean unit vectors that are orthogonal to each other.

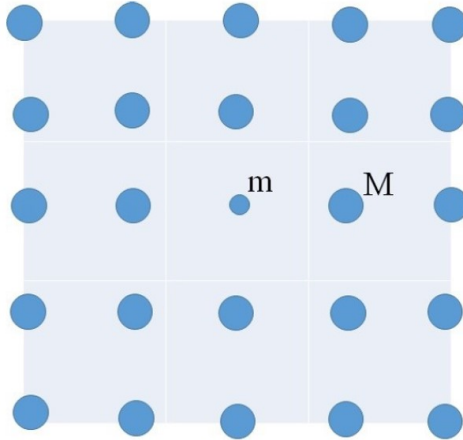


Fig. 3. Two-dimensional lattice with a light impurity at the origin. The mass of a light impurity is m and the mass of a host atom is M .

Here we briefly introduce an equation of motion in the nearest neighbor approximation for two-dimensional model illustrated in Fig.3 again. It is written as

$$M_{pq} \frac{d^2 \mathbf{u}_{pq}}{dt^2} = C(-4\mathbf{u}_{pq} + \mathbf{u}_{p+1,q} + \mathbf{u}_{p,q+1} + \mathbf{u}_{p-1,q} + \mathbf{u}_{p,q-1}), \quad (5)$$

where M_{pq} and \mathbf{u}_{pq} mean mass and displacement vector of the atom with equilibrium position $\mathbf{R}_{p,q}$, respectively. As a solution of this equation, we assume

$$\mathbf{u}_{pq} = \mathbf{U} e^{i\mathbf{k} \cdot \mathbf{R}_{pq}} e^{-i\omega t} e^{-|\mathbf{R}_{pq}| \alpha / a}, \quad (6)$$

where \mathbf{k} means wave number vector of the phonon wave. The constant vector \mathbf{U} is determined by the initial condition at the origin. This solution is similar to the one-dimensional case in Eq.(2). If the constant α exists a positive real number, it is a solution of the local phonon mode. We can easily obtain the following equation when $\mathbf{k} = \frac{\pi}{a} \hat{\mathbf{x}}$:

$$\cosh \alpha = e^{(-\sqrt{2}+1)\alpha} + 2M \left(\frac{1}{m} - \frac{1}{M} \right). \quad (7)$$

This equation has a positive real solution for α when $2M \left(\frac{1}{m} - \frac{1}{M} \right) > 0$ is satisfied.

Lastly, we show the case of three-dimensional simple cubic lattice. The lattice points are defined as

$$\mathbf{R}_{pqr} = a(p\hat{\mathbf{x}} + q\hat{\mathbf{y}} + r\hat{\mathbf{z}}) \quad (p, q, z = \dots, -1, 0, 1, \dots), \quad (8)$$

where the characters $\hat{\mathbf{x}}$, $\hat{\mathbf{y}}$ and $\hat{\mathbf{z}}$ mean unit vectors that are orthogonal to each other. The equation of motion for this case is written as

$$M_{pqr} \frac{d^2 \mathbf{u}_{pqr}}{dt^2} = C(-6\mathbf{u}_{pqr} + \mathbf{u}_{p+1,q,r} + \mathbf{u}_{p,q+1,r} + \mathbf{u}_{p-1,q,r} + \mathbf{u}_{p,q-1,r} + \mathbf{u}_{p,q,r+1} + \mathbf{u}_{p,q,r-1}), \quad (9)$$

where M_{pqr} and \mathbf{u}_{pqr} mean mass and displacement vector of the atom with equilibrium position $\mathbf{R}_{p,q,r}$, respectively. Here, following solution is assumed as in the cases of one and two-dimensional problems. It is written as

$$\mathbf{u}_{pqr} = \mathbf{U} e^{i\mathbf{k} \cdot \mathbf{R}_{pqr}} e^{-i\omega t} e^{-|\mathbf{R}_{pqr}| \alpha / a}, \quad (10)$$

where \mathbf{k} means wave number vector of the phonon wave. The constant vector \mathbf{U} is determined by the initial condition at the origin.

When we consider the wave with $\mathbf{k} = k\hat{\mathbf{x}}$ and substitute Eq.(10) into Eq.(9), the

equation

$$\begin{aligned}
-\omega^2 M_{pqr} e^{-\sqrt{p^2+q^2+r^2}\alpha} = & C \left(-6e^{-\sqrt{p^2+q^2+r^2}\alpha} + e^{ika} e^{-\sqrt{(p+1)^2+q^2+r^2}\alpha} \right. \\
& + e^{-\sqrt{p^2+(q+1)^2+r^2}\alpha} + e^{-ika} e^{-\sqrt{(p-1)^2+q^2+r^2}\alpha} + e^{-\sqrt{p^2+(q-1)^2+r^2}\alpha} \\
& \left. + e^{-\sqrt{p^2+q^2+(r+1)^2}\alpha} + e^{-\sqrt{p^2+q^2+(r-1)^2}\alpha} \right) \quad (11)
\end{aligned}$$

is obtained. For the cases of $(p,q,r)=(0,0,0)$ and $(1,0,0)$, Eq.(11) gives

$$\omega^2 = -\frac{C}{m} (-6 + e^{ika} e^{-\alpha} + e^{-\alpha} + e^{-ika} e^{-\alpha} + e^{-\alpha} + e^{-\alpha} + e^{-\alpha}) \quad (12)$$

and

$$\omega^2 = -\frac{C}{M} (-6 + e^{ika} e^{-\alpha} + e^{(-\sqrt{2}+1)\alpha} + e^{-ika} e^{\alpha} + e^{(-\sqrt{2}+1)\alpha} + e^{(-\sqrt{2}+1)\alpha} + e^{(-\sqrt{2}+1)\alpha}) . \quad (13)$$

Since the frequencies ω in Eq.(12) and Eq.(13) must be the same one, we obtain

$$\frac{1}{m} (-3 + e^{-\alpha}) = \frac{1}{M} (-3 - \cosh \alpha + 2e^{(-\sqrt{2}+1)\alpha}) , \quad (14)$$

where the zone boundary of $k = \frac{\pi}{a}$ is assumed. This equation is transformed into

$$\cosh \alpha = 2e^{(-\sqrt{2}+1)\alpha} + 3M \left(\frac{1}{m} - \frac{1}{M} \right) - \frac{M}{m} e^{-\alpha} . \quad (15)$$

As well as Eq.(3) and Eq.(7), there must exist a positive real α that satisfies Eq.(15).

3 Results and Discussions

In JCF20 [3], we discussed the local phonon mode including a substitutional light impurity in the two-dimensional simple cubic host lattice, whose mass ratio between heavy and light atom is $M/m = 3/2$. In that study, we found a positive real α , however the mass ratio was too small for the deuteron storage Pd. In this study, $M/m = 50$ is assumed in the calculation of Eq.(7), because the mass of Pd and D is 106 and 2, respectively. The calculation for three-dimensional model has also done by using Eq.(15).

Seeing the results plotted in Fig.4, the positive real α 's have been found both for two and three-dimensional cases. This suggests that local phonon modes can appear at the zone boundary in these lattices. If such a situation occurs, it will be possible to detect the nuclear reaction in solids by observing the phonon dispersion relation.

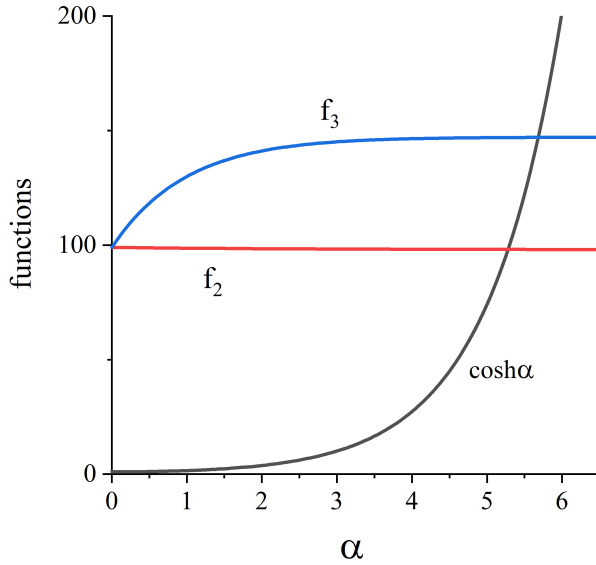


Fig. 4. Plots of the functions f_2 and f_3 , which denote the right hand sides of Eq.(7) and Eq.(15), respectively. The intersections with $\cosh \alpha$ correspond to the solutions of each equation. The mass ratio between heavy and light atom is assumed to be $M/m = 50$, because the mass ratio between Pd and D is about 50.

4 Conclusions

In this study, we have derived the Eq.(7) and Eq.(15) and shown the existence of positive real α for local phonon mode at zone boundary in wavenumber space. The conditions for the calculations are described as following.

(i) Only one substitutional light impurity exists at the origin of the simple cubic lattice. (ii) The mass ratio of heavy and light atom is assumed $M/m = 50$, because the masses of Pd and D are 106 and 2, respectively. (iii) The three-dimensional Pd lattice has fcc structure, however we use simple cubic lattice for simplicity. (iv) The force constants should vary depending on the position in the lattice, but we regard it as a constant.

Within these conditions, we have found positive real α 's as illustrated in Fig.4. They can work as constants in local phonon modes. Therefore, we may have chances to detect nuclear reactions in solids by observing the change of the phonon dispersion relation. In near future, we will have calculations for fcc Pd lattice including some deuterons.

Acknowledgements

I would like to express my gratitude to Dr. Hiroshi Yamada (Prof. Emeritus of Iwate Univ.) and Dr. Sigeji Fujita (Prof. Emeritus of SUNY at Buffalo) for their long-term encouragements to our study. I would also like to thank my grandson Kazushi Kurosawa for his nice smile. The progress of our research is sensitively influenced by his smile.

References

- [1]C. Kittel, “ Introduction to Solid State Physics ” , section 5 Phonon and Lattice vibrations.
- [2]K. Tsuchiya, “ A theoretical study on the possible change of the phonon dispersion relation due to the nuclear reaction in two-dimensional lattice ” , proceedings of JCF19, p77
- [3]K. Tsuchiya, “ A theoretical study on the possible change of the phonon dispersion relation due to the nuclear reaction in two-dimensional lattice II ” , proceedings of JCF20, p97

Cold Fusion Phenomenon in the Composite CF Materials

– Mixed Hydrogen Isotopes, Alloys, Ceramics, and Polymers –

Hideo Kozima*

Cold Fusion Research Laboratory <http://www.kozima-cfml.com/>

597-16Yatsu, Aoi, Shizuoka, 421-1202 Japan

*Corresponding author: hjrfq930@ybb.ne.jp

Abstract

Using the TNCF (trapped neutron catalyzed fusion) and ND (neutron drop) models, which were successful to give a unified explanation of various kinds of experimental data sets obtained in a great variety of CF materials hitherto, we explained various features of the cold fusion phenomenon (CFP) observed in the composite (multi-component) CF materials, CF materials composed of host elements (alloys, ceramics, and polymers) and hydrogen isotopes (H or/and D). We take up in this paper following CF materials: (1) Alloys, (2) Ceramics, and (3) Polymers including XLPE and biological systems in addition to (4) the case where used a mixture of hydrogen isotopes, H and D.

Despite of the rather complex host materials of various compositions and structures in the composite CF materials, we could give a consistent explanation of the specific experimental data obtained in them. We have proposed a tentative criterion for a minor element added to a major element (Pd or Ni) to make the alloy to be a composite CF material. Because of the importance of the composite CF materials used frequently in recent works with many interesting results especially on the improved qualitative reproducibility and the elevated amount of excess heat generation, it is useful to understand the physics of the nuclear reactions occurring there. The fundamental problems related to the premises of our models in relation to the composite CF materials will be discussed in another paper presented in this Conference.

Contents

1. Introduction
2. Brief Review of the Fundamental Works in Relation to the Composite CF Materials
3. Effects of Chemical and Physical Conditions on the CF Materials
4. Experimental Data in the Composite CF Materials – Alloys, Ceramics and Polymers
–
5. Conclusion

Appendices

Appendix A1. History of the Acceptance of the TNCF Model

Appendix A2. Diffusivity of Hydrogen Isotopes in Mo, Nb and Ta [Voelkl 1978, Tanabe 1992]

Appendix A3. Diffusivity of Hydrogen Isotopes in Ni, Pd and Cu [Voelkl 1978]

Appendix A4. Crystal Structures and Characteristics of Ceramics containing Hydrogen Isotopes; TiC, VC, ZrB₂, ZrC, ZrN, LaB₆ [Kageyama 2020, Kobayashi 2020]

Appendix A5. Experiments at the Elevated Temperature by Romodanov et al. [Romodanov 1993, 1998a, 1998b, 1998c]

Appendix A6. Experiments with Pd_xNi_{0.35-x}Zr_{0.65}, CuNi_y and others at the Elevated Temperature by Kitamura et al. [Kitamura 2014 – 2018]

Appendix A7. Experimental Data on the Hydrogen in Ternary Alloys [Smith 1948, Wicke 1978]

References

1. Introduction

In the papers presented until JCF19 (December 2018), we took up mainly the “simple” cold fusion materials (CF materials) composed of a simple host element and a hydrogen isotope and analyzed experimental data sets including various events in the cold fusion phenomenon (CFP) with the inductive logic using phenomenological approach. The reason of such an approach with the inductive logic is justified as experimental results obtained in various CF materials are effects of the same cause satisfying the common necessary conditions: One of the necessary conditions should be the formation of the superlattice of host elements and hydrogen isotopes. This is the reason of applicability of the meta-analysis as discussed in a recent paper [Kozima 2019a].

We investigate the experimental data obtained in the composite and the compound CF materials using the phenomenological approach used for the CF materials with simple host elements and show our approach is effective also to the rather complex systems.

1.1 Composite and Compound CF materials

The two kinds of CF materials listed below had been left out of our detailed investigation because their complex structure perplexed us. They are (1) the composite materials including alloys, ceramics and polymers and (2) the compound materials including various kinds of interfaces between two CF materials, between a CF material

and its substrate, or between a CF material and its environment (cf. [Kozima 2021a (Introduction)]).

It should be noticed that the interfaces have been inevitable parts of any CF material and they are classified into four types: the solid-solid, solid-liquid, solid-gas and solid-plasma interfaces. The second type has been investigated most extensively in the electrochemistry [Bockris 1970a, 1970b, 2000, Horiuti 1951, 1970, Kita 1971, 1973] but other types are also important in the CFP. It is, however, probable that the characteristics of the solid-liquid interface investigated thoroughly in the electrochemistry are common, at least partially, to other interfaces and are very important in our research on the CFP in the composite and compound CF materials. This problem will be investigated specifically in the forthcoming paper [Kozima 2021c].

In the investigation of the CFP in the group (2) listed above (the compound CF materials), all interfaces belonging to the four types may influence the CFP in these CF materials. The first group (the composite CF materials) is taken up in this paper and the second group (the compound CF materials) will be investigated in another paper presented in this Conference [Kozima 2021a].

It is possible to say that these materials (1) and (2) pointed out above have been investigated by many researchers from rather the application point of view to find out effective candidates for application than the scientific one to clarify the mechanism realizing the CFP.

The CFP is, in our opinion, realized in materials (CF materials) where are formed a superlattice of host elements and hydrogen isotopes (H or D) [Kozima 2006, 2021b]. The hydrogen isotopes for the formation of the superlattice are supplied from outside through the interfaces around the host material to feed protons/deuterons by chemical reactions at around solid electrodes in the electrolytic system (cf. e.g. [Bockris 1970a, 1970b, 2000, Horiuti 1970]) including the so-called “*hydrogen electrode reaction (HER)*” [Horiuti 1951, Kita 1971, 1973] where the catalytic action plays an essential role, which will be discussed in detail in another paper [Kozima 2021c].

In the case of the CFP in the composite CF materials, the supply of the protons/deuterons to the host CF material noticed in the above paragraph seems to have close relation with the “*active sites*” of catalysis and the “*supported catalysis*” defined as follows:

“A heterogeneous catalyst has ***active sites***, which are the atoms or crystal faces where the reaction actually occurs. Depending on the mechanism, the active site may be either a planar exposed metal surface, a crystal edge with imperfect metal valence or a complicated combination of the two.” [Wikipedia Catalysis]

“Heterogeneous catalysts are typically "*supported*," which means that the catalyst is dispersed on a second material that enhances the effectiveness or minimizes their cost.”
[Wikipedia Catalysis]

In this paper, we will introduce many examples of the CFP in the composite CF materials from experimental data sets in the CFP and suggest the role of the *active sites* and the *supported catalysis*.

Some features of the CFP related to the HER at the interfaces will be discussed in another paper on the CFP in the compound CF materials presented at this Conference [Kozima 2021a].

1.2 Necessary Conditions for the Cold Fusion Phenomenon (CFP)

The necessary conditions for the CFP are expressed as follows: Formation of CF materials = Realization of the superlattice of host elements and hydrogen isotopes (PdD, NiH, etc.) \leftarrow Occlusion of H/D in the host materials \leftarrow Hydrogen electrode reaction ($2\text{H}^+ + 2\text{e}^- \rightleftharpoons \text{H}_2$) at the interface of the host material = A kind of catalysis.

Main features of these flow are taken up in several papers presented by us:

- (1) Explanation of essential features of the CFP by a phenomenological approach i.e. the TNCF model and the Neutron Drop model [Kozima 1998, 2006, 2021b (Introduction)].
- (2) Explanation of various phases of the CFP by the TNCF and the TN models in the phenomenological approach [Kozima 1998, 2006, 2019b].
- (3) General investigation of the effects of the catalytic action on the CFP will be given elsewhere [Kozima 2021c]

There are several kinds of CF materials which we did not take up specifically until now. They include as pointed out above two kinds of materials; (1) the *composite materials* including alloys, ceramics, and polymers and (2) the *compound materials* with interfaces between several parts (materials supported by substrates, multi-layered materials, etc.) composing the system . The materials in the second group are (a) CF materials surrounded by liquids and gases, (b) those supported by substrates, (c) and those have multilayered structure.

In this paper, we discuss the CFP in the CF materials in the group (1) and the CFP in the group (2) will be discussed in another paper presented in this Conference [Kozima 2021a].

1.3 Short History of Our Research on the CFP

In the analyses presented until JCF19 (December 2018), we took up whole experimental data sets as tabulated in Table 1.1 below. We have employed in the inductive logic using the phenomenological approach using a model named the TNCF (trapped neutron catalyzed fusion) model to investigate the various events in the CFP observed in a variety of materials as results of the same cause satisfying the necessary conditions such as the formation of the superlattice of host elements and hydrogen isotopes (protons or deuterons) on the basic assumption of applicability of the meta-analysis [Kozima 2019a].

It should be emphasized that the partner of host elements for the superlattice is either protons or deuterons. The necessary and sufficient condition for the CFP is the formation of the neutron bands containing the trapped neutrons (neutron Bloch waves) in them. The meta-analysis has shown that the trapped neutron induces the CFP independent of the species of the hydrogen isotope in the CF material if the superlattice is formed.

Table 1.1. Systems and Obtained Evidence of the CFP: Host solids, agents, experimental methods, direct and indirect evidence, cumulative and dissipative observables are tabulated. Q and NT express excess energy and the nuclear transmutation, respectively. The direct evidence of nuclear reactions in the CFP is the dependences of reaction products on their energy (ϵ) and position (\mathbf{r}), the decrease of decay constants of radioactive nuclides, the decrease of fission threshold energy of compound nuclei.

Host solids	C, Pd, Ti, Ni, Au, Pt, KCl + LiCl, ReBa ₂ Cu ₃ O ₇ , Na _x WO ₃ , KD ₂ PO ₄ , TGS (triglycine sulfate), SrCe _a Y _b Nb _c O _d , XLPE (cross linked polyethylene), Biological Systems (microbial cultures) Pd _x Ni _{0.35-x} Zr _{0.65} ,
Agents	$n, d, p, {}^6_3\text{Li}, {}^{10}_3\text{B}, {}^{12}_6\text{C}, {}^{39}_{19}\text{K}, {}^{85}_{37}\text{Rb}, {}^{87}_{37}\text{Rb}$
Experiments	Electrolysis, Liquid contact, Gas discharge, Gas contact
Direct evidence of nuclear reaction	Gamma ray spectrum $\gamma(\epsilon)$, Neutron energy spectrum $n(\epsilon)$, Space distribution of NT products NT(\mathbf{r}), Stabilization of unstable nuclei (Decrease of decay constants), Lowering of fission threshold energy
Indirect evidence of nuclear reaction	Excess energy Q , Number of neutrons N_n , Amounts of tritium atom N_t , Helium-4 atom* N_{He4} , NT products (NT _D , NT _F , NT _A), X-ray spectrum X(ϵ)
Cumulative observables	NT(\mathbf{r}), Amount of tritium atom N_t , Amount of helium 4* N_{He4} ,
Dissipative	Excess energy Q , Neutron energy spectrum $n(\epsilon)$, Number of

observables	neutrons N_n , Gamma ray spectrum $\gamma(\varepsilon)$, X-ray spectrum $X(\varepsilon)$,
-------------	---

(In the rows of “Direct evidence” and “Indirect evidence,” observables relevant to discussions given in this paper are printed in red.)

On the other hand, the investigation of the events taken up in this and the next papers [Kozima 2021a] is rather deductive than inductive used in the research in the former works (cf. [Kozima 2019a]). The case studies, so to speak, of experimental data here depend on individual conditions in the experiments asking appropriate explanation for their relationship with the necessary conditions developed in the inductive research based on the meta-analysis of a lot of positive experimental data. Especially important in this paper is the chemical characteristics of such host transition elements as Ti, Ni, Pd, Pt, etc. showing subtle but magical catalytic action at interfaces with their environment. The “supports” noticed in the heterogeneous catalysis [Wikipedia Catalysis] may have a close relation with the CFP in the composite CF materials taken up in this paper. An extensive investigation of this problem will be given in another paper [Kozima 2021c] but a brief glimpse of possible influence of the supports will be discussed in this paper.

The physical applicability of our models, the original TNCF and the Neutron Drop models [Kozima 2006], is explained briefly in another paper presented at this Conference [Kozima 2021a]. The subtle problem of the catalysis in relation to the generation of the necessary conditions for the CFP will be investigated extensively elsewhere.

1.4 Nuclear Reactions in Free Space and in the CF Materials

It should be noticed the fundamental difference of nuclear reactions generating nuclear transmutations in the CF materials from that in free space, first.

1.4.1 Nuclear reactions in free space

Reactions in free space supposed by Fleischmann et al. to be responsible to their experimental results are written down as follows [Fleischmann 1989, Kozima 2019c]:



The branching ratios of these reactions have been determined in the nuclear physics as $1 : 1 : 10^{-7}$ down to low energies of a few keV.

For the convenience of our discussion in this paper, we cite nuclear reactions between light nuclei. Reactions in free space related to the TNCF model. [Kozima 1997]

$$n + p = d (1.3 \text{ keV}) + \gamma (2.2 \text{ MeV}). \quad (1.4)$$

$$n + d = t (6.98 \text{ keV}) + \gamma (6.25 \text{ MeV}). \quad (1.5)$$

$$n + {}^6_3\text{Li} = t (2.7 \text{ MeV}) + {}^4_2\text{He} (2.1 \text{ MeV}), \quad (1.6)$$

$$t + d = {}^4_2\text{He} (3.5 \text{ MeV}) + n (14.1 \text{ MeV}), \quad (1.7)$$

$$n + d = n + p + n, \quad (1.8)$$

$$\gamma + d = p + n. \quad (1.9)$$

Unified Explanation of the CFP by the Phenomenological Theory using models – the TNCF model and the Neutron Drop Model – is given by us in which the gamma in Eqs. (1.4) and (1.5) in free space should be read as φ 's (phonons excited by the reaction in contact with trapped neutrons) as explained below. [Kozima 1994, 1997, 1998, 2000, 2006, 2019a, 2019b]

1.4.2 Nuclear reactions in CF materials

The phenomenological theory using the trapped neutron catalyzed fusion model (TNCF model) [Kozima 1994] has shown its effectiveness to give a unified consistent explanation of the experimental data sets with full of variety in the kinds of the CF materials and in the observed physical quantities [Kozima 1998, 2006]. The trapped neutrons with a density n_n , one of the key premises of the model [Kozima 1994, 1998] has been extended to the neutrons in the neutron energy bands formed by the super-nuclear interaction between neutrons in lattice nuclei in the superlattice made of host elements and hydrogen isotopes [Kozima 2006]. The name “the trapped neutron” will be used throughout this paper to call the neutrons in the original meaning in the early papers [Kozima 1994, 1998] and the neutrons in the neutron energy bands in the recent papers [Kozima 2006, 2019b]. The trapped neutrons in the neutron bands and the itinerant protons/deuterons form the *cf-matter* containing the trapped neutrons and the neutron drops ${}^A_Z\Delta$, composed of Z protons and $(A - Z)$ neutrons, in the CF material where the superlattice is formed [Kozima 2005, 2006 (Sec. 2.4.2)].

The brief explanation of the TNCF model is given in the books [Kozima 1998, 2006] and papers [Kozima 2005, 2021b (Appendix A2)].

According to the discussions for the phenomenological approach given in these books and papers, we have assumed that the gammas in the reactions (1.4) and (1.5) in free space should be read as φ 's (phonons excited in the CF materials by the fusion reactions in contact with trapped neutrons) in the CF material:

$$n + p = d + \varphi's + Q, \quad (1.4')$$

$$n + d = t + \varphi's + Q', \quad (1.5')$$

where $Q = 2.2$ MeV and $Q' = 6.25$ MeV.

It is interesting to notice the liberated energies Q_{n-p} and Q_{n-d} by and the fusion cross sections σ_{n-p} and σ_{n-d} for the reactions (1.4) and (1.5). The liberated energies are $Q_{n-p} = 2.2$ MeV and $Q_{n-d} = 6.25$ MeV, respectively. And the fusion cross sections for the reactions σ_{n-p} and σ_{n-d} in free space are given as 3.22×10^{-1} and 5.5×10^{-4} barns, respectively.

$$\sigma_{n-p} = 3.22 \times 10^{-1} \text{ barns}, \quad (1.10)$$

$$\sigma_{n-d} = 5.5 \times 10^{-4} \text{ barns}. \quad (1.11)$$

These values will be used in the discussion of the experiments by Fleischmann et al. [Fleischmann 1989] given in Sec. 2.4.1.

1.5 Fundamental Problems related to the Formation of the CF Materials

In this investigation, we must take care of the subtle effect of the catalytic nature of the key host elements such as Pd, Ni and Ti on the formation of the CF materials especially at its first stage of adsorption of protons/deuterons on the interface. This factor of the key elements has been investigated in the electrochemistry for long but not carefully in the cold fusion experiments yet and its detailed consideration will be given in near future [Kozima 2021c].

1.6 Characteristics of the Nuclear Reactions in the CFP

“A remarkable characteristic of the nuclear reactions in the CFP is the fact that there are observed no gamma radiations accompanied to the nuclear reactions producing transmuted nuclei in contrast to the case in free space where are observed always any radiation such as gamma, beta and alphas with energies liberated by the nuclear reaction [Kozima 1998, 2006, 2017]. Furthermore, there is another remarkable characteristic of the nuclear transmutations in the CFP that the generation of new elements A_ZX with large shifts of the mass number A and the proton number Z from those of elements pre-existed in the CF materials. It is also noticed that the observed distribution of A_ZX over the proton number Z is in accordance with the abundances of elements in the universe [Kozima 2006, 2012b, Suess 1956, Trimble 1975].” [Kozima 2019d (Table 2.1)]

(1) Relations between Observed Values of Physical Quantities. [Kozima 1998 (p. 150), 2006 (p. 76)]

$$N_Q \approx N_t \approx 10^7 N_n. \quad (1.13)$$

(2) Surface nature of nuclear reactions in the CFP [Kozima 1998 (Sec. 12.16), 2006 (Sec. 2.2.1.), 2011a]

Summary of the analyses of the experimental data by the TNCF model is given in Appendix A1. Recognition of the value of the phenomenological approach using the TNCF model is traced historically in Appendix A2. It is interesting to notice that very few of CF researchers expressed their favor to the phenomenological approach as seen in Appendix A2.

1.7 Outline of This Paper

In this paper, we explain various features of the cold fusion phenomenon (CFP) observed in the composite (multi-component) CF materials, i.e. CF materials composed of host elements (alloys and ceramics, etc.) and hydrogen isotopes (H or/and D). In our phenomenological approach, we used the TNCF (trapped neutron catalyzed fusion) and ND (neutron drop) models, which have been successful to give a unified explanation of various kinds of experimental data sets obtained in a great variety of CF materials hitherto, are applied to deduce explanation of the specific experimental data obtained in these composite CF materials with various compositions and structures. We take up in this paper following CF materials: (1) Alloys, (2) ceramics, and (3) polymers including XLPE and biological systems. The characteristics of the CFP observed in these composite CF materials have been explained successfully by our model as we have done for the various experimental data obtained in rather simple host materials as published hitherto.

Several examples of the composite CF materials taken up in this paper are (a) Pd cathodes with an electrolytic solution 0.1 M LiOD in 99.5% D₂O + 0.5% H₂O solutions [Fleischmann 1989], (b) Stainless steel cathode Fe_{1-x-y}Cr_xNi_y [Dufour 1993], (c) Pd-Rh alloys, PdRh_xCo_yB ($x=5\%$, $y=3\%$), PdRh_xCr_y ($x=5\%$, $y=5\%$) [Claytor 1998], (d) Ceramic cathode TiC, VC, ZrB, ZrC, ZrN, LaB in glow discharges [Romodanov 1998b], (e) Stainless steel cathode Fe₇₁Cr₁₈Ni₁₀Ti₁ in glow discharges [Romodanov 1998c], (f) Nickel alloy Ni_{7.6}Cr_{20.6}Fe_{70.4}Mn_{1.4} in gas contact experiments [Campari 2004b], (g) Constantan Cu₅₅Ni₄₄Mn₁ [Celani 2012]. (h) Pd-Ni alloys Pd_xNi_{0.35-x}Zr_{0.65} [Kitamura 2018].

Various features of the experimental results obtained in these composite CF materials have been explained from our point of view briefly summarized in the beginning of this abstract.

2. Brief Review of the Fundamental Works in Relation to the Composite CF Materials

2.1 Superlattice of the Host Element and the Hydrogen Isotope

The formation of the superlattice XH/XD of a host element X and a hydrogen isotope H/D had been investigated as a process in complexity and out of our control resulting in the qualitative reproducibility, a characteristic of the CFP [Kozima 2013]. The specific attention about the effect of the minor element A_ZX added to a host element Ni or Pd on the CFP will be discussed in another paper presented in this Conference [Kozima 2021b].

2.2 TNCF and Neutron Drop Models for the Cold Fusion Phenomenon

To give a unified explanation for the very many experimental data sets obtained in various systems with variety of components of host elements and either protium and/or deuterium, we proposed a phenomenological approach based on a model (TNCF model) [Kozima 1994, 1998, 2006, 2021a]. Fortunately, we could give a unified qualitative, even sometimes semi-quantitative, explanation for the whole data obtained in this field. Details have been presented in the papers and books cited above and references given there.

2.3 Effects of Background Neutrons

It should be emphasized that the experimental data on the effects of thermal neutrons on the realization of the CFP, even if we described them in our papers and books already.

We can have no CFP without background neutrons [Jones 1994, Forsly 1998, Kozima 1998]. We can cite a convincing sentence by S. Jones describing this fact as follows: “We invite those with evidence for neutron production to accept our invitation to test their system **in the deep-underground neutron detection facility in Provo Canyon to confirm results**. Gamma and x-ray spectrometers are also available on request.” ([Jones 1994 (p. 26-13)] [Kozima 1998 (Sec. 8.1)])

On the contrary, there are many evidence showing a positive effect of thermal neutrons on the CFP [Shani 1989, Yuhimchuk 1992, Celani 1992, Stella 1993, Oya 1996, Lipson 1996] [Kozima 1998 (Sec. 8.2)].

2.4 The CFP in the CF Materials with Composite Host Elements

The analyses of many experimental results using the TNCF model had been published in many papers and the results were compiled in our two books published in 1998 [Kozima 1998] and 2006 [Kozima 2006].

Several splendid ones of very many experimental results would be referred as follows [Fleischmann 1989, Jones 1989, Packham 1989, Morrey 1990, Srinivasan 1990, McKubre 1993, Ohmori 2016] which had been analyzed and presented in our books and papers. Detailed discussion on the peculiarity of the composite CF materials will be given

in Section 4 from our present point of view.

2.4.1. On the Mixed Hydrogen Isotopes in Electrolytic Solution

There are several experiments where used solvent including both light and heavy waters for the electrolyte. We introduce here only two experiments by Fleischmann et al. [Fleischmann 1989] and Swartz et al. [Swartz 2003, 2019] which are interesting from our point of view.

2.4.1.1 Experiments by Fleischmann et al. [Fleischmann 1989]

We want to add a word on the experiment by Fleischmann et al. [Fleischmann 1989] where they used an electrolytic solution, 0.1 M LiOD in a solvent of mixed light and heavy water (99.5% D₂O + 0.5% H₂O), as explained in their sentence cited below:

“In the work reported here D⁺ was compressed galvanostatically into sheet, rod and cube samples of Pd from 0.1 M LiOD in 99.5% D₂O + 0.5% H₂O solutions. Electrode potentials were measured with respect to a Pd-D reference electrode charged to the α-β phase equilibrium. We report here experiments of several kinds:” [Fleischmann 1989 (p. 302)]

Why did they add “0.5% H₂O” to the electrolytic solution? This fact is not considered seriously hitherto but the addition of H₂O may be closely related to the large difference about three orders of magnitudes of the fusion cross sections of the above reactions (1.4) and (1.5), $\sigma_{n-p} = 3.22 \times 10^{-1}$ and $\sigma_{n-d} = 5.5 \times 10^{-4}$ barns, respectively. The reaction (1.4) will heat the CF material in this case PdD_x/PdH₂ to suffice necessary conditions for the CFP related to the temperature effect [Kozima 2020].

From our point of view, the PdD_x system forms an alloy stable for large ranges of deuteron contents x and the CFP in this system is explained by the self-organization of the superlattice PdD in the open, non-equilibrium condition [Kozima 2013].

If this speculation is correct, we may be able to depict a following explanation: It is probable that the process of occlusion of hydrogen isotopes through the solid-liquid interface depends on the species of the isotopes as we know from knowledge of electrochemistry. However, we may assume that the amounts of deuterons and protons included in the CF material are around $n_d : n_p = 99.5 : 0.5$ in ratio, close to the ratio of D₂O : H₂O in the solution.

Then, we can anticipate that the addition of 0.5% H₂O to the electrolytic solution do not influence much on the formation of the neutron energy bands (and therefore the generation of the cf-matter) but influence strongly on the reaction between the trapped

neutron (neutrons in the neutron band) and hydrogen isotopes *at disordered situation* of the protons by the following speculation.

In the formation of the super-nuclear interaction between two neutrons in different lattice nuclei mediated by interstitial protons/deuterons, the effects of the different species of the interstitial hydrogen isotopes are averaged out. While the interaction between a neutron Bloch wave and a proton/deuteron as a two-body collision directly reflects the disordered situation of the latter, the position and the difference of species. A neutron Bloch wave encounters with protons more often than with deuterons in this case.

Neglecting this factor, we can estimate the large effect of the addition of 0.5 % H₂O in the solvent on the system as follows.

Let us estimate the numbers of the two-body *n – p* and *n – d* collisions simply as two body collisions between free particles (neglecting the enhancement of the *n – p* interaction due to the disordered situation of the protons) generating excess energies $Q_{n-p} = 2.2$ MeV and $Q_{n-d} = 6.25$ MeV, respectively. Using the absorption cross-section determined in the Nuclear Physics, we obtain the ratio of excess heat generations by *n-d* and *n-p* reactions,

$$\begin{aligned} \sigma_{n-d} n_d Q_{n-d} : \sigma_{n-p} n_p Q_{n-p} &\approx 5.5 \times 10^{-4} \times 99.5 \times 6.25 : 3.22 \times 10^{-1} \times 0.5 \times 2.2 \\ &= 5.47 \times 6.25 : 37.2 \times 2.2 \\ &= 34.2 : 81.8. \end{aligned}$$

This ratio shows that the contribution of the excess heat generation by the *n – p* reaction is almost three times larger than that by the *n – d* reaction for the elevation of the sample to induce the temperature effect on the nuclear reactions between the trapped neutrons and the deuterons resulting in the excess heat generation in the system [Kozima 2013 (Sec. 3.1), 2020].

2.4.1.2 Experiments by Swartz et al. [Swartz 2003, 2019]

The solvent used by Swartz et al. are opposite to that used by Fleischmann et al. They used solvents composed of light water containing small amount of heavy water up to 3.7 % with Ni cathode and Pt anode.

The characteristic of their experiments is the effect of the heavy water added to the light water solvent on the excess energy evolution. Their results are qualitatively explained as follows:

“Heavy water (D₂O) yields significant increases in the excess heat observed for nickel light water systems for all input electrical power levels examined (250 to 1500 milliwatts).”

[Swartz 2003 (p. 335, Abstract)]

“These results indicate a loss of deuterium (more precisely, “deuterons”) from ordinary

water when excess heat is observed in an aqueous Ni CF/LANR system (Ni/ordinaryH₂O/Pt) using a very large cathodic area.” [Swartz 2019 (p. 169, Abstract)]

From our point of view, the NiH_x system forms an alloy stable for large ranges of hydrogen contents x and the CFP in this system is explained by the self-organization of the superlattice NiH in the open, non-equilibrium condition [Kozima 2013]. From this point of view, the experimental results obtained by Swartz et al. are explained as follows.

Fundamentally, the NiH superstructure is generated by self-organization when there are formed NiH_{1-x}D_x ($x < 0.04$) alloys by the diffusion of H and D from the solid-liquid interface on the Ni surface. The super-nuclear interaction between neutrons in lattice Ni nuclei results in the neutron bands and the neutrons in the bands (the trapped neutrons) make nuclear interactions with disordered nuclei including protons and deuterons (cf. Sec. 1.4). There should be other nuclear interactions of the trapped neutron with disordered nuclei, but we write down only those with a proton (at disordered position) and a deuteron:

$$n + p = d + \varphi's + Q, \quad (1.4')$$

$$n + d = t + \varphi's + Q', \quad (1.5')$$

where $Q = 2.2$ MeV and $Q' = 6.25$ MeV.

The deuterons are fundamentally exotic nuclei in the superlattice NiH and the interaction (1.5') occurs more frequently than (1.4'). This is the reason Swartz et al. observed much excess heat with more deuterons [Swartz 2003] and loss of deuterium when excess heat is observed [Swartz 2019].

2.4.2 Cold Fusion Phenomenon in the Composite CF Materials

The experimental data sets performed with the composite CF materials, alloys, ceramics and polymers, have been piled up in these almost 30 years and show various characteristics difficult to give quantitative explanation due mainly to the complicated structure of their samples. We introduce them qualitatively in Section 4 after summarization of fundamental natures of the nuclear reactions in the CF materials.

3. Chemical and Physical Conditions on the CF Materials

It is our regret that we did not considered the chemical conditions in the CFP even if we touched slightly on them in relation to the Pd-D-Li and Ni-H-K combinations as favorable ones for the realization of the CFP [Kozima 2004].

In the reality of the CFP, the chemical conditions are very important for the realization of the necessary conditions for the nuclear reactions especially in the earlier stages of the

superlattice formation as the absorption and occlusion of hydrogen isotopes depend strongly on the catalytic action at interfaces [Kita 1971, 1973, Wikipedia Catalysis].

We give a brief investigation of this problem in Section 3.1 leaving detailed treatments on this problem to the following paper [Kozima 2021c].

3.1 Effects of Electrolyte in the Electrolytic Experiments

In this subsection, we cite sentences showing the complex process of hydrogen absorption into the metal cathode investigated in the electrochemistry for more than 50 years and investigated from a new point of view in relation to the CFP after the discovery by Fleischmann et al. in 1989 [Fleischmann 1989].

In the early days of the research on the CFP, the effects of electrolytes and impurities in electrolytic experiments had been investigated [McBreen 1990]. We cite their explanation to touch the chemical flavor in them.

“The absorption of hydrogen and deuterium in Pd, at potentials positive to hydrogen evolution, was studied by cyclic voltammetry. Results in 0.1 M NaOH, LiOH and LiOD were compared. In LiOH hydrogen ingress into Pd is faster than in NaOH. However, hydrogen egress is inhibited. In LiOD all processes are slower than those in LiOH.” [McBreen 1990 (p. 279, Abstract)]

It was shown that addition of a very small quantity of cyanide into the electrolytic solution had resulted in several major effects on the behavior of the electrolysis. The subtlety of the effect of cyanide is best understood by the original sentences.

“Addition of 10^{-3} M CN^- to these electrolytes resulted in several major effects. The formation of the oxide and the ingress of hydrogen and deuterium were inhibited. Egress of hydrogen and deuterium from Pd was essentially completely inhibited until the adsorbed cyanide was displaced by oxide at positive potentials. Hydrogen permeation measurements through Pd membranes were made in 0.1 M NaOH and in 0.1 M NaOH + 10^{-3} M NaCN. Cyanide adsorption decreased the permeation rate and had large effects on the permeation decay transients.” [McBreen 1990 (p. 279, Abstract)]

Ulmann et al. had shown the large effects of contamination of a Pd cathode on the electrolysis. In this case, we cite the original explanation for the complicated electrochemical situation in their experiment.

“One of the typical characteristics of the hydrogen evolution reaction is its extreme sensitivity to various impurities present in the solution. - - - We showed recently [3] that the contamination of a palladium cathode, polarized in LiOD + D_2O solution, with lead and more so with zinc leads to the buildup of very large over voltages for D_2 evolution.

In the present communication we describe the results of surface analyses for a series of Pd electrodes used as cathodes in the D₂O electrolysis cells run for up to 34 days."

[Ulmann 1990 (p. 257, Abstract)]

[3] J. Augustynski, M. Ulmann and J. Liu, *Chimia*, **43**, p. 355 (1989). [Augustynski 1989]

Furthermore, we cite sentences on the complex processes of hydrogen absorption into the cathode metal by electrolysis from the paper by L. Schlapbach [Schlapbach 1991]..

"We then ask how hydrogen reacts at the interface with the metal, whether and how hydrogen diffuses into the metal and forms a solid solution, a metal hydride or other types of 'hydrogen-metal-alloys'." [Schlapbach 1991 (p. 409, Introduction)]

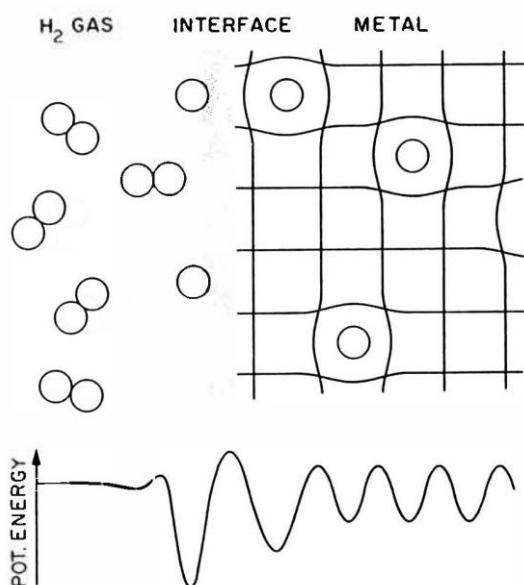


Fig. 3.1. Simplified model of the dissociation of molecular hydrogen at an interface and of the solution of hydrogen atoms in the bulk, on interstitial sites." [Schlapbach 1991 (p. 410, Fig. 1)]

*"There is experimental and theoretical evidence that chemisorbed H does not necessarily occupy sites on top of the first metal atom layer, but also **sites between and underneath top surface metal atoms**. Subsurface H was observed together with a strong surface reconstruction (surface hydride formation)."* [Schlapbach 1991 (p. 415)]

3.2 Temperature Effects (cf. Appendix A2)

It should be remembered that the temperature of the sample has decisive influence on the occurrence of the CFP as several experimental data had shown it clearly.

We determined a quantitative measure of the temperature effect on the CFP in the paper published in 2008 [Kozima 2008].

“1) If the temperature of the experimental system is lower than a critical temperature T_c (from the experiment, we may take it higher than 60 °C; $T_c \geq 60$ °C), there are no cold fusion reactions.

2) Increasing the temperature higher than T_c ($T_c < 90$ °C as confirmed by experiments), the cold fusion reactions start to occur and produce excess energy inducing more reactions as we see in the occurrence of many pulses.

This means that the critical temperature T_c in this case is in between 60 and 90 °C (60 °C $\leq T_c \leq 90$ °C).

3) We may assume that higher temperature is more favorable for the CFP if other conditions are the same. Then, when the temperature of the sample increases due to CF reactions generating more excess energy than dissipating energy from the system and the shape of the tubular cathode is favorable of the positive feedback of the CFP, there may occur a positive feedback which increases the temperature of the system, thus inducing more CF reactions.” [Kozima 2008]

The larger increase of the diffusivity in NiH than in PdH(D) may be responsible to the more often occurrence of nuclear transmutations in NiH than in PdD tabulated in figures in our books ([Kozima 1998 (Figs. 11.2 and 11.3) and 2006 (Figs. 2.22 and 2.3)]

Heating CF material by chemical reactions (crystallization, chemical reaction, etc.) results in the elevation of the temperature of the sample and accordingly in acceleration of nuclear reactions in the CFP. This effect seems to be observed in the recent experiments by Kitamura et al. [Kitamura 2018] as pointed in our recent paper [Kozima 2020].

3.3 Effects of Chemistry at Interfaces and the Qualitative Reproducibility

It is inevitable to have some kinds of interfaces surrounding the CF material (necessarily solid) where we observe the CFP. The interfaces are divided into four; (1) solid-solid, (2) solid-liquid, (3) solid-gas, and (4) solid-plasma interfaces. The chemistry of atomic processes at the solid-liquid interface have been extensively investigated for more than 70 years in the electrochemistry and many interesting characteristics of chemical reactions, especially the HER (hydrogen electrode reaction) [Bockris 1970a, 1970b, 2000, Horiuti 1951, 1970].

Especially interesting is the dependence of catalytic reactions on the lattice plane facing to the interface [Kita 1971, 1973]. It had been well known fact that the catalytic reaction is subtle about the existence of minute additives for long and the data given by

Kita et al. added a concrete evidence to it.

This knowledge obtained in the electrochemistry on the solid-liquid interface may have common characteristics for the chemistry of atomic reactions at other interfaces; solid-solid, solid-gas and solid-plasma interfaces. Then, the subtleness of the catalytic action depending on the polycrystalline structure of the solid at the interfaces, which is not controllable macroscopically, gives rise to the qualitative reproducibility of the CFP depending strongly on the inclusion of hydrogen isotopes through the interfaces surrounding the CF material.

We have now two causes of the qualitative reproducibility, one pointed out before the *self-organization of the superlattice* in the CF material by a process of complexity, and another pointed out above the catalytic action depending on *the polycrystalline structure of the CF material*.

Now, it is possible to say that the nature of the CFP explained by our phenomenological approach shows the qualitative reproducibility is a nature of this research field and should not be rejected by the lack of the quantitative reproducibility existing only in physics where works only linear interactions in it. The problem of the reproducibility of the events in the CFP had been one of tumbling blocks for acceptance of this field by the established science community for more than 30 years without correct knowledge of the science of the CFP.

4. Experimental Data in the Composite CF Materials – Alloys, Ceramics and Polymers (XLPE and Biological Systems)

There are many experimental data obtained in the CF materials with the composite structure, that is alloys, ceramics and polymers composed of several kinds of host elements.

4.1 Alloys.

In the early days of the research on the CFP, many researchers have taken up alloys as CF materials guided perhaps by their properties of large occlusion and/or of large diffusivity of hydrogen isotopes in them. In the period when there have been no guiding principles to choose host materials other than their properties in relation to the hydrogen isotopes noticed above, the above mentioned standard of the choice is a reasonable one and revealed several characteristics for the realization of the nuclear reactions in the CF materials at around room temperature. Some features of these characteristics have been introduced in our papers and books [Kozima 1998 (Sec. 6.1e,), 2006 (Section 2.2.2)].

In these more than 30 years after the discovery of the CFP in 1989, there have accumulated experimental data performed in composite CF materials. We would like to classify tentatively these CF materials into two groups; (1) Alloys and ceramics containing at least one element which is known as a host element of a CF material showing the CFP, and (2) Alloys and ceramics composed of several elements which have not been known as a host element of a CF material by now.

The first group, let us name them as **Type I alloys and ceramics**, includes Stainless Steel ($\text{Fe}_{71}\text{Cr}_{18}\text{Ni}_{10}\text{Ti}_1$), Pd alloys used by Claytor et al. (such as PdRh_x and PdCu_x), Constantan ($\text{Cu}_{55}\text{Ni}_{44}\text{Mn}_1$) used by Celani et al., Ni alloys used by Campari et al. ($\text{Ni}_{7.6}\text{Cr}_{20.6}\text{Fe}_{70.4}\text{Mn}_{1.4}$), Ni alloys used by Iwamura et al. ($\text{Ni}_x\text{Cu}_y\text{Ca}_z$) and Pd/Ni alloys used by Kitamura et al. ($\text{Pd}_x\text{Ni}_{0.35-x}\text{Zr}_{0.65}$). In this type I CF materials, we may be able to include the original CF materials composed of single elements Ti, Ni, Pd, Pt, Au and others.

The second group, let us name them as **Type II alloys and ceramics**, includes ceramics used by Romodanov et al. (such as VC, ZrB, ZrC, ZrN, LaB) and those used by Mizuno et al. (such as SrCeO_3 and $\text{Sr}_{1.0}\text{Ce}_{0.9}\text{Y}_{0.08}\text{Nb}_{0.02}\text{O}_{2.97}$). In this type II CF materials, we may be able to include the graphite which had shown a specific CFP of various nuclear transmutations [Kozima 2012a, 2017 (Sec. 2.1.1)].

The classification of the CF materials into two types, Type I and Type II, will be investigated in our forthcoming paper in relation to the characteristics of the hydrogen diffusivity in them [Kozima 2021d].

Alloys and ceramics cultivated for the CF materials are heat-resisting in general and the CFP in them have been observed in the higher temperature region up to 1000 °C (up to 3000 °C in the case of graphite) utilizing the temperature effect for the super-nuclear interaction in the CF material [Kozima 2008, 2013 (Sec. 3.1)].

Experiments on alloys and ceramics performed at elevated temperatures are discussed in Appendix A2 in relation to the temperature dependence of diffusivity of H/D in these CF materials.

It should be noticed that the physical properties of transition metal alloys have been investigated for more than 70 years in relation to the occlusion and super-diffusivity of hydrogen isotopes in them. We listed several data on them in Appendix A7 from books by D.P. Smith [Smith 1948] and E. Wicke and H. Brodowsky [Wicke 1978].

4.1.1 Stainless Steel by Sparking in Hydrogen Isotopes [Dufour 1993]

Dufour et al. have measured excess heat generation in stainless steel occluding

hydrogen isotopes with the discharge experiment [Dufour 1993]. It is well known that SS is composed of Cr-Fe-Ni with following compositions:

$^{A}_{24}\text{Cr}$ ($A = 50, 52, 53, 54$)

$^{A}_{26}\text{Fe}$ ($A = 54, 56, 57, 58$)

$^{A}_{28}\text{Ni}$ ($A = 58, 60, 61, 62, 64$)

As we have shown in our book [Kozima 2006 (p. 99)], there is a possibility to occur the CFP in the stainless steel if the temperature is high enough to make the hydrogen isotopes can permeate through it. It was reported that Cr exhibits extremely low solubility for hydrogen in room temperature even though the existence of a hexagonal monohydride CrH and a cubic dihydride CrH₂ was reported [Shavely 1949]. However, $^{53}_{24}\text{Cr}$ (9.55 %) and $^{57}_{26}\text{Fe}$ (2.19 %), and $^{54}_{24}\text{Cr}$ (2.38 %) and $^{58}_{26}\text{Fe}$ (0.33 %) can absorb a deuteron ($\Delta A = 2$), and a proton ($\Delta A = 1$), respectively to produce stable Mn, and Co isotopes. Therefore, the stainless steels Fe_{1-x-y}Cr_xNi_y, widely used in technology, may be responsible for CFP at high temperatures where hydrogen isotopes can permeate through them. This is the reason Dufour [Dufour 1993] could obtain positive experimental data of CFP in the stainless steel with D₂ and H₂ in discharge experiments [Kozima 2006 (p. 99)].

4.1.2 Ceramics and Stainless Steel in Discharge Experiments [Romodanov 1998]

Romodanov et al. had performed elaborate experiments on the CFP with the solid-plasma interfaces in the discharge with various cathodes including several metals, ceramics, and alloys [Romodanov 1998a, 1998b, 1998c]. A part of their data sets had been introduced in our books [Kozima 1998 (Sec. 6.4e), 2006 (p. 99)]. Experiments with ceramics will be treated in Sec. 4.2.

Ceramics and Alloys

Ceramics; TiC, VC, ZrB, ZrC, ZrN, LaB [Romodanov 1998b].

Metals and Alloys; Fe, Alloy SS, Ti, Nb [Romodanov 1998c] (SS; Fe-Cr-Ni-Ti (71-18-10-1)).

In the glow discharge experiments, they observed tritium generation in several ceramics. The significant tritium generation rate is obtained in borides, carbides and nitrides of titanium, vanadium, zirconium and lanthanum by glow discharge. For samples of ZrB₂, the tritium generation rate reached $(3.6 - 3.9) \times 10^7$ atom/s.

In another experiment with ceramics heated by a resistor heater, they observed emission of tritium, also.

They had resistive heater to heat up the samples up to $T = 670\text{K} - 1200\text{K}$ (900 and

1100 – 1200 K for SS) and made them contact with H₂ , D₂, H₂ + D₂ at P = (5 – 60)·10³ Pa (for 0.1 – 50 h). [Romodanov 1998c]. Their data was discussed by us using the TNCF model [Kozima 2006 (p. 99)].

4.1.3 Pd Alloys [Claytor 1998]

Claytor et al. in the Los Alamos National Laboratory had made experiments on the various types of Pd alloys. We summarize their experiments on the following Pd alloys in this paper and will give more extensive review of their papers on various types of CF materials in another paper to be presented at this Conference [Kozima 2021a (Appendix A3)].

The experimental data we take up in this section is on the following CF materials: PdRh_xCo_yB (x=5%, y=3%), PdRh_x (x =10, 5, 0.5, 0.1%), PdCu_x (x=1, 10%), PdFe_x (x = 10%), PdRh_xCr_y (x=5%, y=5%), PdCr_x (1.1%), PdNi_x (1.1%)” [Claytor 1998 (p. 90)]

They observed production of tritium in several alloys and investigated effects of minor elements in the CF materials on the production rate of tritium as shown in Table 4.1..

Table 4-1. Palladium alloys and highest tritium rates observed during the plasma experiments (a part of Table 1 in [Claytor 1998]).

alloy composition	alloy type	Number of runs	highest tritium rate, nCi/h	significance
PdRh (10%)	melt spun	1	-0.00073	1
PdRh(5%)	melt spun	1	-0.0024	1
PdRh (0.5%)	rolled alloy	1	-0.00017	0
PdRh (0.1%)	homogenized, rolled alloy	1	+0.0048	2

This experimental results on the impurity dependence of the tritium production are very interesting in relation to the analysis of the data by Fleischmann et al. [Fleischmann 1989] given in Sec. 2.4.1. As we have given justification of our model to the composite CF materials [Kozima 2021b], the addition of some minor elements (*CF active elements*) to the host material (Pd in this case) may not give fatal influence for the generation of the cf-matter including neutrons and deuterons. (This situation has similarity to the case of Fleischmann et al. where a small amount of H₂O added to D₂O will not influence much for the generation of the cf-matter).

The reasoning of this speculation may be described as follows in the case of the host

alloy Pd_{1-x}X_x when the element X is a CF active one:

(1) The first effect appears in the formation of the cf-matter: In the super-nuclear interaction in an alloy Pd_{1-x}X_xD ($x < 10\%$), the nuclear interactions Pd-*d* and X-*d* between an interstitial deuteron and the surrounding lattice nuclei Pd or X are summed up and finally the resulting super-nuclear interaction between neutrons in different lattice nuclei does not suffer much from the addition of foreign element X when its concentration is small. (cf. the similar reasoning in the case of Pd + (99.5 % D₂O and 0.5 % H₂O) in Sec. 2.4.1).

(2) The second effect appears in the interaction between the trapped neutron and other nuclei: The nuclear reactions between a trapped neutron (a neutron in a neutron energy band) and nucleus ^A_ZX in disordered sites such as written down below suffer directly by the addition of foreign nuclei which the trapped neutron sees as disordered nuclei:

$$n + {}^A_ZX = {}^{A+1}_ZX^* = {}^{A+1}_ZX + \varphi's, \quad (4.1)$$

$$= {}^{A+1-a}_{Z-b}X' + {}^a_bX'' + \varphi's, \quad (4.2)$$

including the tritium generating reaction

$$n + d = t + \varphi's. \quad (1.5')$$

On the other hand, the addition of a CF nonadditive

General Tendency: When the concentration of the foreign element X is small, the effect (1) does not influence the cf-matter formation and the effect (2) is observed which increases with the concentration of X.

Dependence on the Species of the Minor Element.

When the concentration of X (Rh) increases, the effects (1) give the deterioration of the cf-matter and the nuclear reactions between the trapped neutron and other nuclei (including deuterons) decrease in the case of PdRh_x ($x=10, 5, 0.5, 0.1\%$). This story gives explanation of the data given in Table 1.

In the case of PdCu_x ($x=1, 10\%$) and PdRh_xCo_yB ($x=5\%, y=3\%$) alloys, on the other hand, the effect (1) by X (Cu, Co) is small and X intensifies the effect (2) and the reaction (1.5'). This is an explanation of the fact observed in these alloys [Claytor 1998 (pp. 90 – 91)].

This may be the cause of the events observed by Claytor et al. [Claytor 1998] described in the paragraph cited above (with emphases marked by red).

4.1.4 CF Active and CF Inactive Elements [Claytor 1998]

From the experimental data obtained by Claytor et al. [Claytor 1998], we must care about the species of the minor elements in the composite CF materials to extend the phenomenological approach to apply them due to the following reason.

(1) It is revealed by Claytor et al. [Claytor 1998] that addition of minor elements to a host element (Pd, for instance) causes the increase of tritium generation by some element (B and Cu, for instance) and its decrease by some others (Li, Be, and Hf, for instance).

(2) On the other hand, there are several evidence that iron-group elements are active in the HER (hydrogen electrode reaction) [Kita 1973] and UPD (underpotential deposition) [Akiyama 1986, Fukushima 1993, Nakano 1998, Bockris 2000 (Sec. 7.12.11)].

Considering the experimental data given above (1) and (2), we may be able to define tentatively (a) CF active (or constructive) elements and (b) CF inactive (or destructive) elements as follows according to the inductive logic [Kozima 2019a]:

(a) *CF active elements*; elements in 3d and 4d transition metals.

(b) *CF inactive elements*; other elements than those in the group (a).

Then, we may be able to use the analogy of the electron bands in the (In, Ga)N alloy to the neutron bands in the CF materials composed of Pd (or Ni) and *CF active elements* as discussed in our paper presented at this Conference [Kozima 2021b (Appendix A6-2)].

Fortunately, according to the above criterion, the TNCF model is applicable to these CF materials including those used in recent works by Celani et al. (Constantan $\text{Cu}_{55}\text{Ni}_{44}\text{Mn}_1$) and Kitamura et al. ($\text{Pd}_x\text{Ni}_{0.35-x}\text{Zr}_{0.65}$).

4.1.5 Ni Alloys $\text{Ni}_x\text{Cu}_y\text{Ca}_z$ and $\text{Ni}_x\text{Cu}_y\text{Y}_z$ [Iwamura 2020a, 2020b]

Iwamura et al. had performed extensive experiments with a specific CF materials composed of the so-called the Pd complexes (Pd/CaO/Pd) and (Pd/MgO/Pd) through which permeated the D_2 gas (cf. [Kozima 2021a (Sec. 4.4.5)]). Recently, they made an interesting experiments of excess heat and elemental distributions on the “nano-sized multilayer metal composite” samples composed of Ni, Cu, CaO or Y_2O_3 shown in Fig. 4.1 (In the figure caption, elements of the layers are colored corresponding to that in the figure).

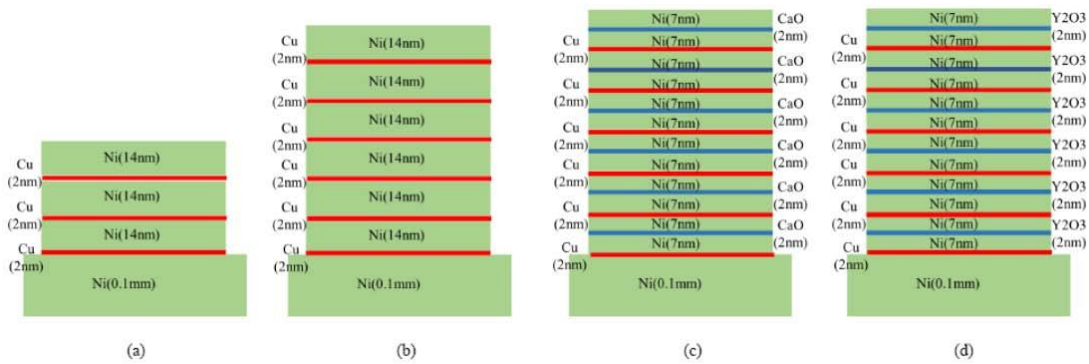


Fig. 4.1. Structures of nano-sized multilayer metal composite samples; (a) example #1: 3 layers of Cu (2 nm) and Ni (14 nm), (b) Example #2: 6 layers of Cu (2 nm) and Ni (14 nm), (c) Example #3: 6 layers of CaO (2 nm), Cu (2 nm) and Ni (14 nm), (d) Example #4: 6 layers of Y₂O₃ (2 nm), Cu (2 nm) and Ni (14 nm). [Iwamura 2020b (Fig. 4)]

The magnitudes and temporal variations of the excess heat generation in the composite sample with different compositions reveal interesting characteristics depending on the composition and the temperature of the samples as shown in Fig. 4.2. (In the figure caption, materials of the layers are colored corresponding to the figure.)

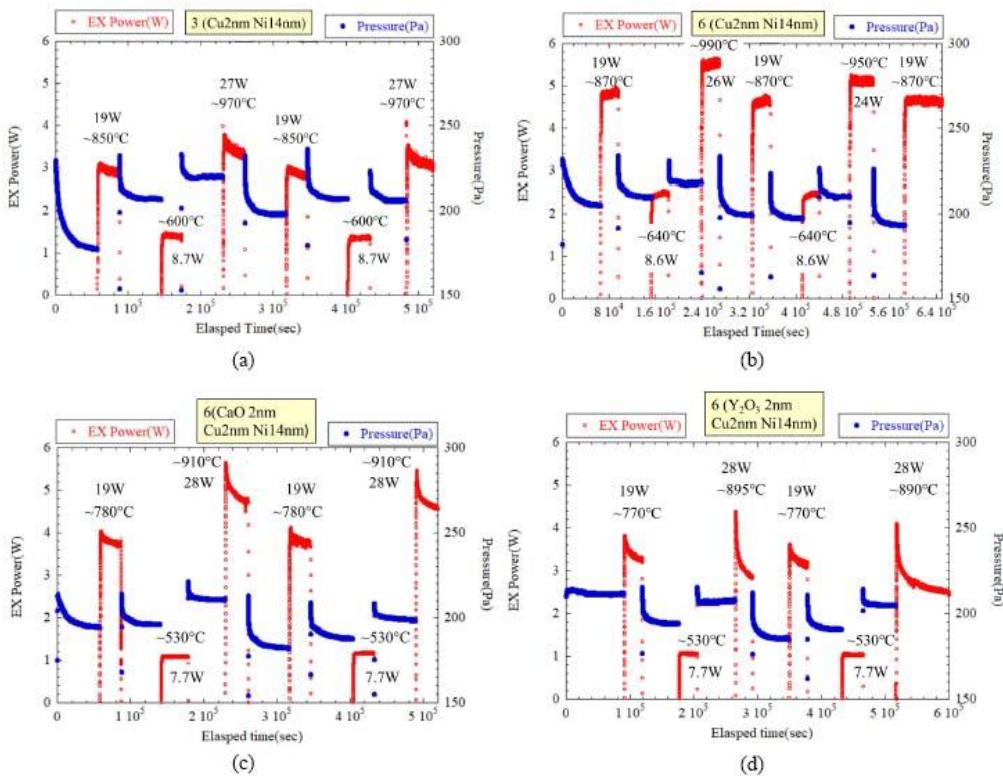


Fig. 4.2. Examples on excess heat generation; (a) example #1: 3 layers of Cu (2 nm) and

Fig. 4.3. An example of TOF–SIMS analysis; (a) structure of the sample before experiment, (b) depth profiles of the after the series of the excess heat generations. [Iwamura 2020b (Fig. 11)]

Then, we can give a story telling us the nuclear reactions and the structure changes occurring in the samples depicted in the Figs. 4.2 and 4.3 as follows.

- (1) The NiH superlattice is formed near the solid-gas interface of the sample.
- (2) The neutron energy bands and therefore the cf-matter including the trapped neutrons are generated where the superlattice is formed.
- (3) The trapped neutrons induce nuclear reactions between protons ($n - p$ reactions) and other nuclei A_ZX 's ($n - {}^A_ZX$ reactions) at disordered sites; main sites may be near the solid-solid interfaces of the layered structure. The difference of the excess heat generation in Figs. 4.2 (a) and (b) may be explained by the number of solid-solid interfaces 3 in (a) and 6 in (b); the excess heat in (a) is almost 60 % of that in (b) while the ratio of the layers is 0.5.
- (4) The main reaction participating in the excess heat generation in the experiments may be the following $n-p$ fusion reaction:



where $Q = 2.2$ MeV and the fusion cross-section is $\sigma_{n-p} = 3.22 \times 10^{-1}$ barns.

- (5) The liberated excess energy by the reaction (4.3) (and if any other) heats up the sample and destroys finally the layer structure of the sample (Fig. 4.3 (a)) into alloys as shown in Fig. 4.3 (b).
- (6) In the case of alloys composed of Ni and Cu (active element), the cf-matter formed by the trapped neutrons and itinerant protons remains without much damage and the reaction (4.3) last long as appeared in Fig. 4. 2 (a) and partially in (b). The increase of the excess power seen in Fig. 4.2 (b) might be the enhancing effect of the active impurity observed by Claytor et al. [Claytor 1998] introduced in Section 4.1.3.
- (7) In the case of other alloys including Ca or Y as minor elements, the cf-matter may be influence by the characteristics of the minor elements. Looking into the data in Fig. 4.2 (c) and (d), we see that Ca is an active element for the CFP in Ni and Y is inactive if we can ignore other factors influencing to the nuclear reactions in the experiments.
- (8) The temperature effect on the CFP [Kozima 2008, 2013 (Sec. 3.1), 2020 (Sec. 2-(3))], the higher the sample temperature the more the nuclear reactions, is clearly shown in the excess heat vs. heater temperature relation as seen in Fig. 4.2 and as shown more clearly in Fig. 4.4 [Iwamura 2020b (Fig. 6)].

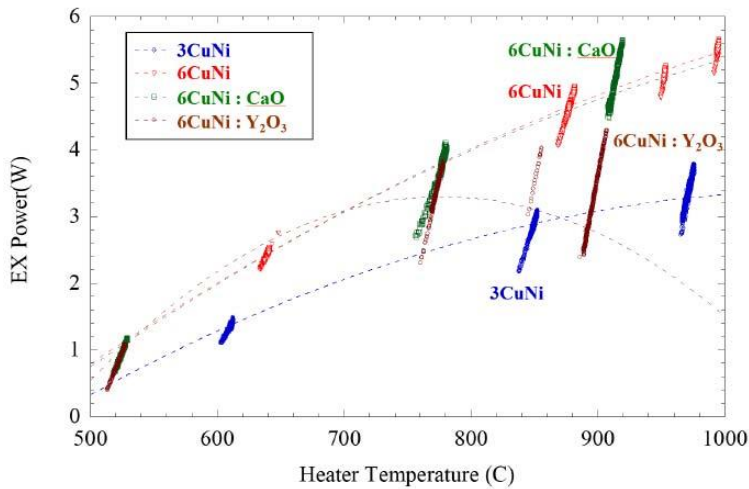


Fig. 4.4. Temperature dependence on excess power for four examples. [Iwamura 2020b (Fig. 6)]

It is interesting to notice that the temporal decreases of the excess heat generation do not appear in Fig. 4.2 (b) at all and in Figs. 4.2 (a), (b) and (c) when the input powers to the sample are less than 9 W in (a) and 8 W in (c) and (d).

4.1.6 Ni Alloys $Ni_xCr_yFe_zMn_{1.4}$ ($x = 7.6$, $y = 20.6$, $z = 70.4$) [Campari 2004a, 2004b]

Campari et al. [Campari 2004a, 2004b] investigated the CFP in the CF materials of the Ni-H system where observed emissions of photons and neutrons along the heat production at high temperature in the range of 400 to 700 K. They performed investigation of surface transformation of the samples where observed the above CF effects. The transformation of the sample had been on the surface, i.e. at most in the first μm . This surface nature of the nuclear transmutation has been almost a common characteristic observed by many researchers we have already notice several times (cf. e.g. [Kozima 1998 (Section 12.16), 2006 (Section 2.2.1.3), 2020 (Section 2.2)]).

4.1.7 Constantan Wires Coated by Sub-micrometric Surface Sponge [Celani 2012 – 2020b]

The extensive investigation of the constantan wire coated by sub-micrometric surface layer has been performed by Celani et al. [Celani 2012 – 2020b]. We will give rather minute introduction to their work in another paper presented in this Conference [Kozima 2021a (Sec. 2.3.2 and Appendix A5)].

We have given a brief explanation of the nuclear transmutation obtained in a multiply nano-coated Ni wire [Kozima 2011b].

The nuclear transmutation of several elements confirmed by the experiment is qualitatively explained assuming the single neutron absorption by elements in the surface layer. The decrease of Ru might be explained by absorption of a single $n-p$ cluster.

4.1.8 Pd/Ni/Zr ($\text{Pd}_x\text{Ni}_{0.35-x}\text{Zr}_{0.65}$) and Cu/Ni (CuNi_y) [Kitamura 2014 – 2018]

Kitamura et al. [Kitamura 2014 – 2018] had performed extensive investigations on the Pd-Ni and Cu-Ni nanocomposite CF materials, Pd/Ni/Zr ($\text{Pd}_x\text{Ni}_{0.35-x}\text{Zr}_{0.65}$) or Cu/Ni (CuNi_y), supported by Zirconia (ZrO_2) or by Silica (SiO_2). These CF materials are composite and compound ones from our classification but have ambiguity about their structures and we take up them in this paper leaving the problem related to the interfaces to another paper.

We give a brief survey of the common characteristics of the works by Kitamura et al. in addition to a brief comment given recently [Kozima 2020] and the detailed introduction to the experimental data obtained by them will be given in Appendix A5.

Several of the characteristics obtained in the works by Kitamura et al. are listed as follows; (1) the excess heat is observed only in the elevated temperature phases of the runs with binary nanocomposite samples, but not with single-element nanoparticles. (2) Excess power from Pd-Ni nanocomposite CF materials at elevated temperature of 200 ~ 300 °C depend strongly on the Pd/Ni ratio, which will be one of the key factors to increase the excess power.

Considering the catalytic action of the electrodes noticed already long ago by the electrochemists [Bockris 1970a, 1970b, 2000, Horiuti 1970, Kita 1971] and the common knowledge listed in the general guidance to the catalysis (e.g. [Wikipedia Catalysis]), these characteristics cited above and others observed by Kitamura et al. show clearly that the CFP observed by them (AHE, the anomalous heat effect, in their terminology) is the nuclear reactions induced by the common mechanisms to the CFP observed hitherto in various CF materials summarized in several reviews (e.g. [Kozima 2019c]) and books (e.g. [Kozima 1998, 2006, Storms 2007]) characterized by the catalytic action of electrocatalysis [Bockris 1970a, 2000].

4.2 Ceramics

There are several works on the CFP in ceramics by Romodanov et al. [Romodanov 1998b] and Mizuno et al. [Mizuno 1996, 1997]. We give a brief introduction of the data in this section and will give an overview on the data obtained in ceramics and others by Romodanov et al [Romodanov 1993, 1998a, 1998b, 1998c] in Appendix A5.

There are several interesting investigations on the new ceramics possible to expect

the CFP in them. A brief survey on these new ceramics is given in Appendix A4.

Romodanov et al. [Romodanov 1993, 1998a, 1998b, 1998c] had performed extensive experiments with CF materials including transition metals, alloys (including SS) and ceramics (including TiC, VC, ZrB₂) in glow discharges with D₂, H₂ and D₂ + H₂ gases.

They observed generation of neutron, tritium and gamma radiation from cathode materials at elevated temperatures up to 1200 °C. They determined the maximum $N_n/N_t|_{\max}$ and minimum $N_n/N_t|_{\min}$ ratios of neutron and tritium generation in transition metal cathodes including Mo, Nb, Ta ranging $N_n/N_t|_{\max} = 8.5 \times 10^{-6}$ to 0.6×10^{-9} , $N_n/N_t|_{\min} = 1.7 \times 10^{-3}$ to 8×10^{-7} [Romodanov 1993].

In the case of ceramics cathode, they observed tritium generation depending on the species of the ceramics [Romodanov 1998b] a part of which had been explained in Sec. 4.1.2. Further explanation of the data by Romodanov et al. is given in Appendix A5.

Mizuno et al. observed excess heat and nuclear transmutations in the CF materials composed of Sr and Ce oxides (SrCeO₃) charged with D₂ gas at elevated temperatures ranging from 200 to 700 °C [Mizuno 1996, 1997].

4.3 Polymers; XLPE and Biological Systems

We have investigated already the CFP in XLPE [Kozima 2007, 2010, 2016a, 2019c] and biotransmutation in the glowing biological cultures [Kozima 1996, 2016b, 2019c] using the TNCF model to give a unified explanation of the observed results.

In biological systems, it should be mentioned a necessity of a microscopic investigation including atomic processes using knowledge developed in electrochemistry (cf. e.g. [Woodbury 1970]) to clarify the mechanism working there for the CFP which will be given in another paper to be published recently [Kozima 2021c].

There are many ceramics which can contain a lot of hydrogen isotopes forming a regular lattice of host elements and hydrogen isotopes like those we met in XLPE and biological systems. We show several examples of them in Appendix A3 as future candidates where we can expect the CFP according to the mechanism working in XLPE and biological systems.

5 Conclusion

The necessary conditions to realize the CFP include two processes governed by the complexity:

(1) *Adsorption of hydrogen isotope atoms (H/D), molecules (H₂/D₂) or ions (H⁺/D⁺) by*

the host material composed of elements X's (A_ZX 's). Adsorption of ions on the electrode is a subtle problem of catalytic nature in the solid-liquid interface investigated extensively in electrochemistry (cf. e.g. [Bockris 1970a, 2000, Quaino 2007, Seo 2012]).

(2) *Generation of the superlattice XH/XD (${}^A_ZX-p/{}^A_ZX-d$)* by the self-organization as a nonlinear process under a nonequilibrium condition belonging to the complexity. [Kozima 2013, 2014] (cf. also Section 1.1 of another paper presented in this Conference [Kozima 2021b]).

In the above two processes to fill the necessary conditions for the CFP in the composite CF material (details should be referred to the cited papers), we must take into our consideration the specific atomic processes in alloys and ceramics different from those in simple host elements like Ni and Pd.

In this paper, we have taken up experimental data sets on several features of the composite CF materials obtained from the early days to recent few years considering recent tendency to concentrate research works on them.

The experimental results obtained in the composite CF materials have shown the same characteristics as those observed in the CF materials with rather simple host materials. This fact suggests us that the cf-matter composed of the trapped neutrons and the neutron drops ${}^A_Z\Delta$ has a common nature and it is possible to investigate the CFP in the composite CF materials using the TNCF and ND models which have shown their usefulness to understand the CFP observed hitherto.

However, there are characteristics of the composite CF materials different from the CF materials composed of simple host materials. Since Claytor et al. [Claytor 1998] had shown twenty years ago, the composite CF materials have shown their ability to realize the CFP until now as we pointed out in this and another paper which is presented in this Conference [Kozima 2021a]:

“Alloys have been discovered that gave much enhanced tritium output over randomly selected materials.” [Claytor 1998 (pp. 92, Conclusion)]

The characteristics of alloys and ceramics responsible to the aptitude for the CFP are listed up as follows from our point of view: (1) Elevated temperature of their operation up to 300 °C ($\text{Pd}_x\text{Ni}_{0.35-x}\text{Zr}_{0.65}$) – 1000 °C (constantan) and more than 1500 °C in the case of ceramics (cf. [Kozima 2013 (Sec. 3.1), 2020]), (2) Distribution of minor elements at disordered sites (cf. [Kozima 2019b (Sec. 3-4)]), (3) Distribution of protons and deuterons at disordered sites (cf. [Kozima 2019b (Sec. 3-4)]), and (4) Interfaces around the CF material (cf. [Kozima 2021a]) which intensify the effects (2) and (3) in this list. The characteristic (4) is extensively discussed in another paper presented at this Conference

[Kozima 2021a].

In the explanations of the CFP obtained in the composite CF materials, we want to emphasize the interesting facts observed by Fleischmann et al. [Fleischmann 1989] and by Claytor et al. [Claytor 1998] as explained in Sec. 2.4.1 and Sec. 4.1.3, respectively.

In these two cases, curious events related to both the formation of the cf-matter and the nuclear reactions between a trapped neutron and nuclei at disordered sites in the CF material have been observed and explained by our model.

The experimental data discussed in this paper have several characteristics depending on the several factors of the sample. One of the factors is the interfaces surrounding the CF material which is investigated in another paper presented in this Conference [Kozima 2021a]. Several of the factors not taken up at present due to the lack of space will be investigated in future.

We will give a justification of our approach to the composite CF materials using the TNCF model in another paper presented at this Conference [Kozima 2021b] where we use an analogy between neutron and electron energy bands.

Acknowledgements

The author would like to express his thanks to Dr. Y. Iwamura and Dr. A. Kitamura for the valuable communications on their experiments analyzed in Sec. 4.1.5 (Iwamura et al.) and Sec. 4.1.8 and Appendix A6 (Kitamura et al.). He is indebted also to Dr. T. Ohmori for valuable discussions on the hydrogen electrode reaction (HER) and the underpotential deposition (UPD).

Appendices

Appendix A1. History of the Acceptance of the TNCF Model

Appendix A2. Diffusivity of hydrogen isotopes in Mo, Nb and Ta [Voelkl 1978, Tanabe 1992].

Appendix A3. Diffusivity of Hydrogen Isotopes in Ni, Pd and Cu [Voelkl 1978]

Appendix A4. Characteristics of Ceramics containing Hydrogen Isotopes [Kageyama 2020, Kobayashi 2020]

Appendix A5. Experiments at the Elevated Temperature by Romodanov et al. [Romodanov 1993, 1998a, 1998b, 1998c]

Appendix A6. Experiments with the $\text{Pd}_x\text{Ni}_{0.35-x}\text{Zr}_{0.65}$, CuNi_y , and others at the Elevated Temperature by Kitamura et al. [Kitamura 2014, 2018]

Appendix A7. Experimental Data on the Hydrogen in Ternary Alloys [Smith 1948, Wicke

1978]

Appendix A1. History of the Acceptance of the TNCF Model

It is interesting to notice the history of the acceptance of a phenomenological approach as a possible trial to the science of the cold fusion phenomenon. There are several researchers who have shown their tolerance for the TNCF model in whom we can count John Dash, Makoto Okamoto and Koji Fusimi and some others who have been a personal acquaintance of the author needless to say the colleagues and co-authors of the present writer (H.K.). We cite some other people who recognized the value of the phenomenological approach in their course of investigation on the CFP.

A1-1 J.O'M. Bockris

It is interesting to notice that Prof. J.O'M. Bockris was only one in the CF researchers expressed explicitly an affirmative comment on the TNCF model showing his genuine scientific spirit and his correct understanding of the model. [Bockris 1999a, 1999b]

“Three points summarize the historical significance of the discovery of LENR:- - -

3 The work must give rise to modifications of the theory of the nucleus. However, new physics is probably not needed. Classical nuclear physicists have maintained an agnostic stance for so long because their knowledge of fusion is concerned with reactions in plasma, and they have paid little attention to the effects of a solid lattice upon nuclear activity within it after injection of H and D at high fugacity, or to the effect of free neutrons in the lattice.” [Bockris 1999a (p. 71)] (Underlines are added at citation)

“An all embracing theory must account for the long (500 hours) delay in a switch on of nuclear effects in electrolysis of D-Pd-LiOD, irreproducibility that is diminished by the use of codeposition of D₂ and Pd on Au, and by use of thin films; internal damage in Pd; burst-like nature of the phenomena in Pd; occurrence in organic and biomaterials. No theory yet published accounts for all these effects. - - - Kozima⁵ has made a detailed case in which neutrons in the ambient enter all substances and are trapped there. These entities then undergo various reactions with Li, H, D, T, etc., and produce the observed effects. Although Kozima's model serves to explain the widespread nature of the effects (he sees neutrons as being “in” everything), his numerical analyses show the required neutron concentration to vary from 10⁴ to 10¹³ cc⁻¹ in D-Pd to achieve consistence, with results and this seems too large a range for consistency. Stress is put in Kozima's model on reaction with Li⁶ but it was shown in 1990 by Appleby and Srinivasan²⁹ at Texas A&M

that there was no difference in the heat evolved in Pd-LiOD in systems containing only Li⁶ and those containing natural Li.” [Bockris 1999b] (Underlined at citation)

[Kozima⁵] 5. Kozima, H. *Discovery of the Cold Fusion Phenomenon*, Ohtake Shuppan, Inc., Tokyo, Japan. [Kozima 1998]

[Srinivasan²⁹] 29. Appleby, A. J. and Srinivasan, S. 1990. *ICCF-1*, Salt Lake City.

In these sentences, Professor Bockris cited the trapped neutron as a probable new idea to explain seemingly contradicting experimental data such as the relations between numbers of tritium, neutron and helium-4 known already at that time. It is interesting to notice his comment on the choice of models in the *Preface* of his book published in 1970: “*They have tried to present, with due admission of the existing imperfections, a simple version of that model which seemed to them at the time of writing to reproduce the facts most consistently. They have for the most part refrained from presenting the detailed pros and cons of competing models in areas in which the theory is still quite mobile.*” [Bockris 1970a (p. vii)] (Underlined at citation)

A1-2 D.R.O. Morrison

Prof. D.R.O. Morrison, a well-known cons against the CFP from the early days of the history of the CF research, has shown his correct understanding of the TNCF model as his explanation of the lack of radiation in the nuclear reaction in the CFP.

[Morrison 2000]

“12. H. Kozima (abs. 044, 045, 046) Trapped Neutron Catalyzed Fusion, TNCF model. *Energy band of neutrons interacts coherently with lattice nuclei.*

e.g.

$n + {}_{46}\text{Pd} \text{ -----} > {}_{13}\text{Al} + {}_{33}\text{As}$ or $\text{-----} > {}_{26}\text{Fe} + {}_{20}\text{Ca}.$ ”

[Morrison 2000 (Appendix 2, Theories at ICCF-8)] (italicized partially at citation).

In this citation, Morrison has shown his correct understanding of the TNCF model as his explanation of the lack of radiation in the nuclear reaction in the CFP as “*Energy band of neutrons interacts coherently with lattice nuclei.*” Almost ten years after the discovery of the CFP, Dr. Morrison as a scientist seemed to arrive at recognition that there is something reflecting truths behind the vast pile of experimental data and became more tolerant about assumptions to explain the facts inconsistent with the framework of the nuclear physics at that time.

A1-3 DOE Report 2004

In the DOE Report 2004 [DOE 2004], there are several positive evaluations for the works in the CFP. We cite only one of them related to the TNCF model.

[DOE 2004]

“(1) H. Kozima *J. Electroanalytical Chemistry* **425** 173 (1997), ISSN: 1572-6657.

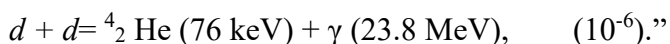
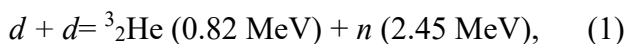
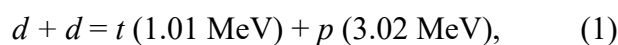
Theory is presented using the ${}^6\text{Li}$ atom in the electrolyte of many experiments to provide a neutron that begins an interesting series of reactions leading to $d + d$ fusion.

(2) H. Kozima *J. Hydrogen Energy* **25** 505 (2000)

Use of his theory to understand Tritium production in others experiments.

(3) H. Kozima *J. Hydrogen Energy* **25** 509 (2000)

This article gives branching ratios:



[DOE 2004 (Summary, Reviewer #4, pp. 7 – 8)] (Italicized partially at citation)

The reviewer #4 has cited three papers from ours published before 2004 as possible candidates for a unified explanation of the contradicting experimental data on the tritium, neutron and helium-4 and of data obtained not only in deuterium but also in protium systems.

A1-4 E. Storms

On the other hands, Dr. E. Storms had shown that he did not understand the nature of the phenomenological approach at all.

[Storms 2007]

“Kozima^{180 – 183} at Shizuoka University (Japan) and Portland State University (US) proposes that solids contain clusters of neutrons. According to his TNCF (Trapped Neutron Catalyzed Fusion) theory, these are stabilized by a unique configuration and are released to cause cold fusion reactions under certain conditions. Two of the many questions not answered are: ‘*Why is the extra mass added by these neutron structures not observed in normal material and why are neutrons not released in a detectable form when the stabilizing solid structure is vaporized?*’ ” [Storms 2007 (p. 135)] (Italicized partly at citation. The references [180] – [183] are those of the references in the original book [Storms 2007])

The “*Two of the many questions not answered*” raised by Storms in this sentence show that he does not understand the meaning of the phenomenological approach at all, to our regret.

A1-5 Conclusion

It should be mentioned again that there are almost no favorable mentions on the TNCF model in the cold fusion community despite a few supporters such as John Dash, Makoto Okamoto, and Koji Husimi needless to say colleagues and co-authors of the present author (H.K.). Only one exception is Prof. J.O’M. Bockris who had shown his genuine scientific spirit and his correct understanding of the model.

In this meaning, there have been a large contrast between true scientists, such open minded people looking for the truth behind the complicated experimental facts as pointed out above, and the “*Voodoo Scientists*” relying only on the second-hand articles (written in such books as [Huizenga 1992, Taubes 1993]) discarding and neglecting experimental facts in “the Medawar zone” [Kozima 1998 (Sec. 16.5, “A Message from the Right Side of the Medawar Zone” by Peter Gluck)]. It is a sad history in modern science to see many people remain as Voodoo Scientists even after about 30 years of piling up of vast positive facts and of sincere theoretical efforts.

In the Voodoo Scientist, there should be Dr. Bob Park who had criticized the CF research enthusiastically for many years not depending on the facts and had written many negative comments on the CFP and finally a book “Voodoo Science” [Park 2000] in which he used the word *voodoo* suggesting the meaning of that word used to define the “Voodoo Scientist” given above.

It is surprising to read *at present* an article appeared in *Physics Today* (Feb. 17, 2021) by Harry Collins, a sociologist of science (by Wikipedia), ignorant of the today’s physics changed drastically in the last half of 20th century by the inclusion of complexity in it.

He said,

“In an area of serious dispute, you can’t tell who is right simply by repeating the experiments because scientists disagree about when replication has been done properly. So, in cases like this, scientists invent theoretical reasons for why it must be this way, or it must be that way. They will argue, and eventually settle by broad agreement, that such an apparatus should or should not see gravity waves. It is more like a social agreement than a transfer of information or a formula.

For example, to debunk Weber's detection claims, scientists had to get others to agree that Weber made mistakes in his statistical analysis and his handling of the data. *And to debunk cold fusion, it had to be agreed that [Stanley] Pons and [Martin] Fleischmann were not the right kind of scientists to be doing the work. In neither case was it enough, at the time, simply to say the results weren't replicated, even though that is how we describe it in retrospect.* In 2015, with the first accepted discovery of gravitational waves, that kind of accusation could not be made to stick, even though some people tried it." (Italicized and colored partially at citation.) [Collins 2021]. (Italicized, boldfaced and colored partially at citation.)

Harry Collins do not entirely understand that the quantitative reproducibility is a specific attribute of the physics governed by the linear dynamics and therefore we must satisfy with the qualitative reproducibility discarding the quantitative one in the physics like the cold fusion phenomenon where events are governed by the nonlinear interaction between particles in the system [Kozima 2013, 2019b].

It is really a very difficult work to do science rightly avoiding many bypaths leading to mistaken results. In the history of the cold fusion research, the most important characteristics in this science may be the complexity of the cold fusion phenomenon destined by the nonlinear interaction between participating particles [Kozima 2013] and the meta-analysis of the data handling due to the characteristics of the CF materials [Kozima 2019a]. If we forget this fact, we will lose the way.

Appendix A2. Diffusivity of hydrogen isotopes in Mo, Nb and Ta. [Voelkl 1978, Tanabe 1992]

Romodanov et al. had measured tritium production in many CF materials including various transition metals Y, Mo, Nb, Er, Ta, and W and ceramics TiC, VC, ZrB, ZrC, ZrN, and LaB at high temperature realized by glow discharges and electric heaters (Appendix A4). We can contemplate the cause of the CFP in those transition metals at higher temperatures up to 1000 – 2000 K considering the diffusivity of hydrogen isotopes in Mo, Nb, Ta and Pd (for comparison) as shown in Figs. A2-1 – A2-4.

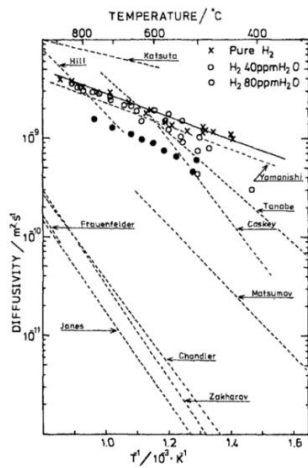


Fig. A2-1. Temperature dependence of the diffusivity for pure H₂, H₂ with 40 and 80 ppm H₂O in Mo. Literature data [8,9,11,16- 22] are also shown for comparison [Tanabe 1992].

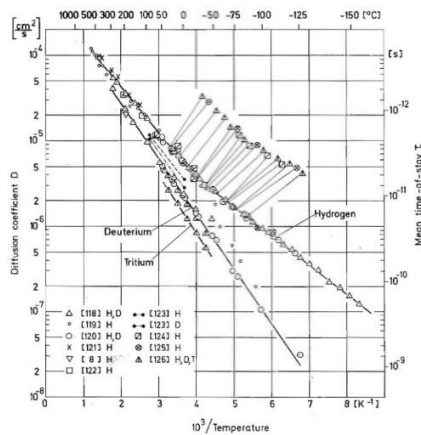


Fig. A2-2. Diffusion coefficient of H, D, and T in Nb. The mean time-of-stay τ is calculated for tetrahedral-tetrahedral jumps. (Numbers in brackets refer to References cited in [Voelkl 1978 (Fig. 12.5)].

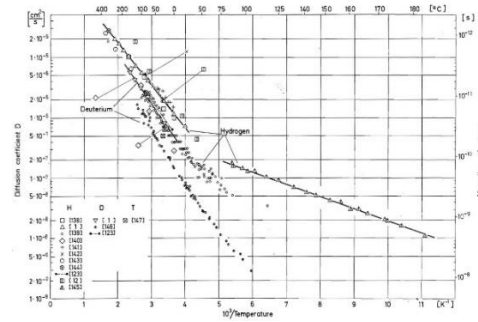


Fig. A2-3. Diffusion coefficient of H, D, and T in Ta. In addition, results with Pd-coated samples [12.123] are shown. Nevertheless, discrepancies in the absolute value (not so much in the slopes) can be note. (Numbers in brackets refer to References cited in [Voelkl 1978]) [Voelkl 1978 (Fig. 12.6)].

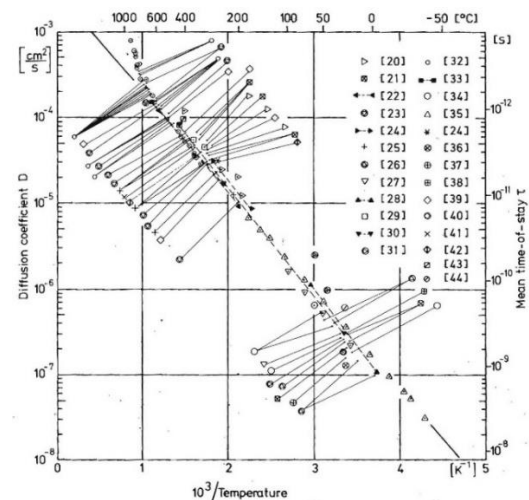


Fig. A2-4. Diffusion coefficients of H in Pd. The right-hand scale for the mean time-of-stay τ refers to octahedral-octahedral jumps. (Numbers in brackets refer to the paper cite in [Voelkl 1978]) [Voelkl 1978 (Fig. 12.2)].

Compare the value of the diffusion coefficients D (cm²/s) in Mo, Nb and Ta with that

in Pd, $D = 2 \times 10^{-5} \text{ cm}^2/\text{s}$ in Pd at 200 C: $D = 1 \times 10^{-9} \text{ cm}^2/\text{s}$ in Mo at 400 C, $5 \times 10^{-5} \text{ cm}^2/\text{s}$ in Nb at 200 C, and $2 \times 10^{-5} \text{ cm}^2/\text{s}$ in Ta at 200 C. We can see the necessity of high temperature for Mo to realize the CFP compared with Pd which have been used very often in the experiments in the CFP. The durability of Pd over Nb and Ta is advantageous for the experiments and the latter two have not used often hitherto.

Appendix A3. Diffusivity of Hydrogen Isotopes in Pd, Ni and Cu [Voelkl 1978]

As the data shown below (Fig. A3-1 – A3-4), the diffusion coefficients of hydrogen isotopes in Pd, Ni, and Cu have similar values in the elevated temperature region above 800 °C. It is interesting to notice that they have almost the same values in Ni and Cu around the room temperature (300 °C).

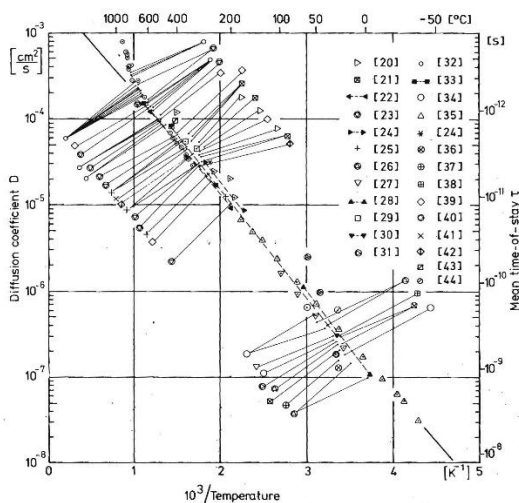


Fig. A3-1. Diffusion coefficients of H in Pd. The right-hand scale for the mean time-of-stay τ refers to octahedral-octahedral jumps. (Numbers in brackets refer to References of the original paper) [Voelkl 1978 (Fig. 12.2)]

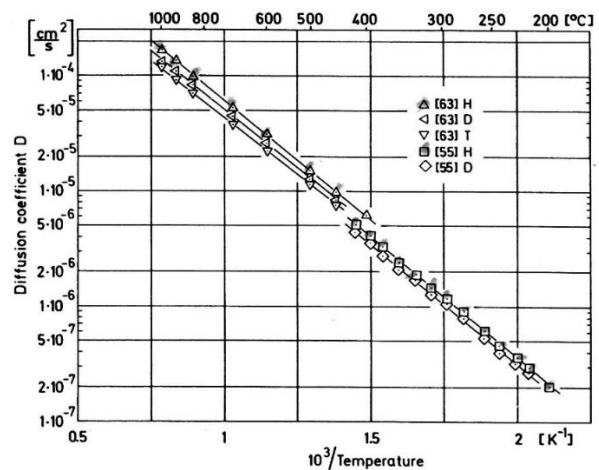


Fig. A3-2. Diffusion coefficient of isotopes of hydrogen in Ni (Numbers in brackets refer to References) [Voelkl 1978 (Fig. 12.17)].

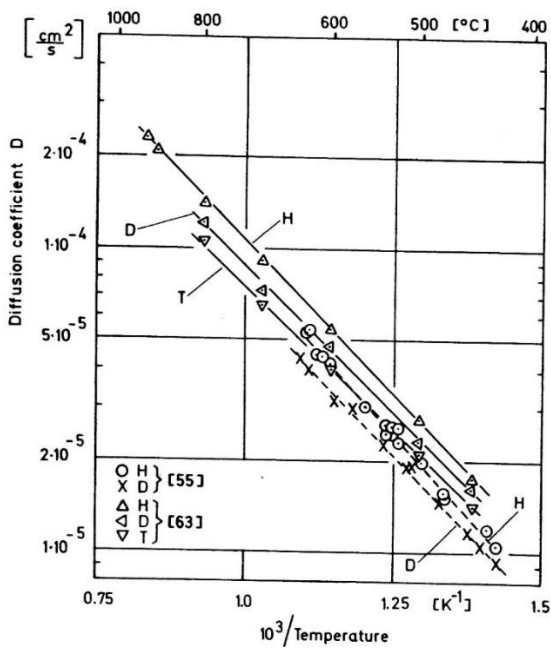


Fig. A3-3. Diffusion coefficient of isotopes of hydrogen in Cu (Numbers in brackets refer to References in the original paper) [Voelkl 1978 (Fig. 12.18)].

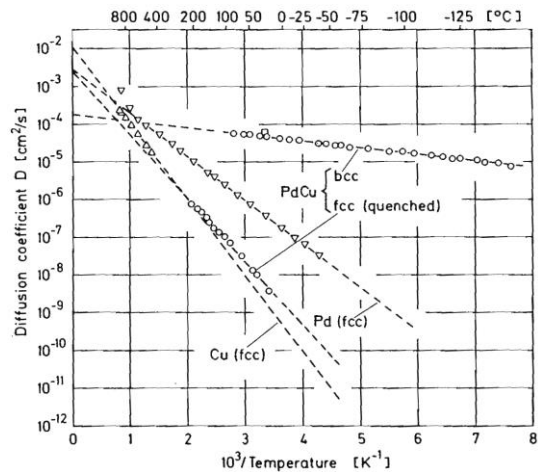


Fig. A3-4. Diffusion coefficient D for Pd, Cu [12.63] and Pd_{0.47}Cu_{0.53} (bcc) [12.179] and Pd_{0.47}Cu_{0.53} (fcc) [12.180]; \square = Piper [12.174] [Voelkl 1978, (Fig. 12.21), numbers in square bracket [] are references in the original paper] [Voelkl 1978 (Fig. 12.21)]

Appendix A4. Crystal Structures and Characteristics of Ceramics; TiC, VC, ZrB₂, ZrC, ZrN, LaB₆ [Kageyama 2020, Kobayashi 2020]

There are several CF experiments on the ceramics such as by Romodanov et al. [Romodanov 1998b] and Mizuno et al. [Mizuno 1996, 1997a]. We want to point out further possibility to observe the CFP in ceramics which have not observed it until now.

There are a few ceramics which can contain a lot of hydrogen isotopes as shown by many researchers (e.g. [Kageyama 2020, Kobayashi 2020]). Considering our knowledge about the CFP in XLPE [Kozima 2016a, 2019c] and biological systems [Kozima 2016b, 2019c], we must pay attention to them for the CF materials even if they did not show the nuclear reactions in them yet. We show some examples of their structure in Figs. A3-1 – A3-4 [Kageyama 2020, Kobayashi 2020] which remind us the structure we know in the XLPE and biological systems where the CFP had been observed.

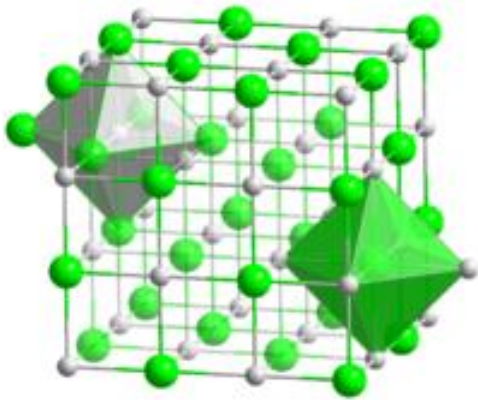


Fig. A4-1. Zirconium nitride ZrN

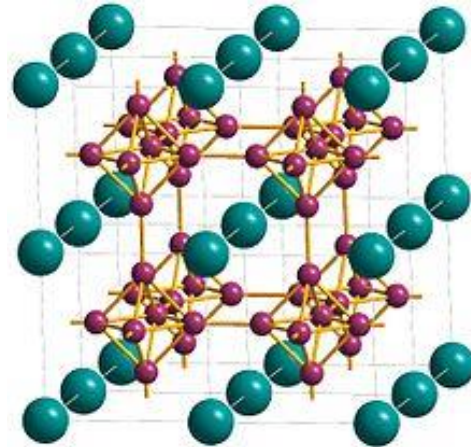


Fig. A4-3. Lanthanum hexaboride LaB₆

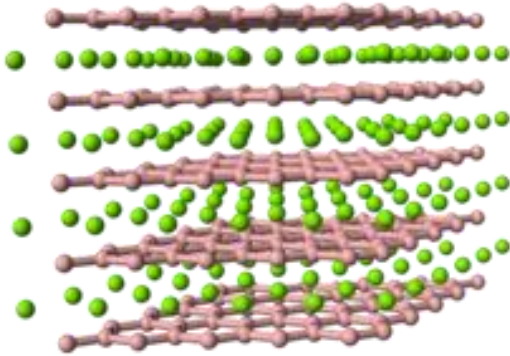


Fig. A4-2. Zirconium Diboride ZrB₂

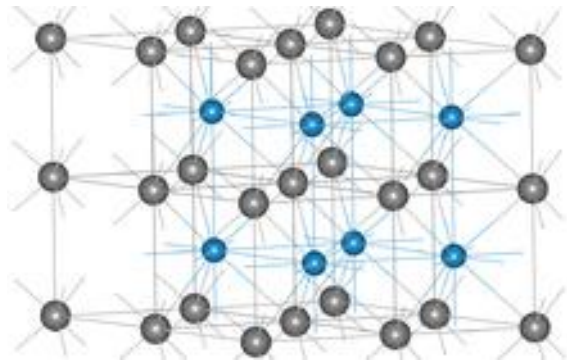


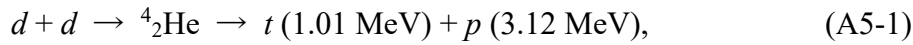
Fig. A4-4. α -WC structure, carbon atoms are gray.

Appendix A5. Experiments at the Elevated Temperature by Romodanov et al. [Romodanov 1993, 1998a, 1998b, 1998c]

In the three papers by Romodanov et al. [Romodanov 1993, 1998a, 1998b, 1998c], they observed tritium from three kinds of CF materials; (1) Transition metals Y, Mo, Nb, Er, Ta, and W [Romodanov 1993], (2) H/D transfusion through V, Nb, Ta and Mo, (3) ceramics TiC, VC, ZrB₂, ZrC, ZrN, and LaB₆ [Romodanov 1998b], and (4) transition metals Fe, Ti, Nb and an alloy Fe-Cr-Ni-Ti (71-18-10-1) [Romodanov 1998c]. In the cases (1) (2) and (3), the glow discharges with large currents were used to heat the samples, and in the case (4) electric heater was used instead.

It is apparent that the purpose of the experiments (1) and (2) is detection of the nuclear products by the $d-d$ fusion reactions in these CF materials using the accelerated deuteron

onto the targets where are occluded enough deuterium. However, the acceleration of deuteron by the glow discharge was insufficient to realize the expected nuclear reactions.



We must understand the effect of the glow discharge in these experiments (1) – (2) is to heat these CF materials up to around 1000 K and to feed deuterium into them which are difficult to absorb and occlude hydrogen isotopes in lower temperatures than 300 K.

In all experiments performed at the elevated temperature more than 1000 K, sometimes up to 2100 K, they observed generation of tritium, an event characteristic of the CFP. These experiments show clearly the elevated temperature is favorable for the CFP. The large amount of the observed tritium is explained by the reaction (A4) written down below in consistent with other various events in the CFP as shown in our works [3, 4, 5]:



where $\varphi's$ expresses phonons excited by the freed excess energy of ${}^3_1\text{H}^*$ [3, 4] replacing the gamma in the reaction in free space written down as follows:



The necessity of high temperatures for the Mo (and for ceramics) is discussed in Appendix A1 using the data of diffusivity in Mo compared to that in Pd. Unfortunately, we have no data of diffusivity in ceramics which may be comparable to or smaller than that of Mo at around room temperature.

“Table 2

Ratio of neutron and tritium fluxes when irradiating a number of materials by deuterium ions.” [Romodanov 1993 (p. 313, Table 2)]

Table 2

Ratio of neutron and tritium fluxes when irradiating a number of materials by deuterium ions

Material	Process parameters			Background, pulse/100 s	Reduced activity in view of background, Bc/ml	Ratio of deuterium activities after and before experiments	Tritium atom flux, atom/s	Nuclear interaction coefficient, atom/ion	Neutron-to-tritium flux ratio	
	E, eV	T, K	τ , h						min	max
D ₂	-	-	-	240	130	-	-	-	-	-
Y	40	1170	80	210	290	2.2	$1.2 \cdot 10^5$	$4.1 \cdot 10^{-15}$	$8.5 \cdot 10^{-6}$	$1.7 \cdot 10^{-3}$
Y	80	1270	23	250	$1.2 \cdot 10^3$	9.2	$4.5 \cdot 10^6$	$1.6 \cdot 10^{-12}$	$2.2 \cdot 10^{-7}$	$4.4 \cdot 10^{-5}$
Mo	125	1470	10	150	$6 \cdot 10^3$	46	$4.5 \cdot 10^6$	$9.2 \cdot 10^{-12}$	$2.2 \cdot 10^{-7}$	$4.4 \cdot 10^{-5}$
Mo	100	970	10	170	$1.6 \cdot 10^3$	12.3	$1.8 \cdot 10^7$	$5.9 \cdot 10^{-12}$	$5.5 \cdot 10^{-8}$	$1.1 \cdot 10^{-5}$
Nb	75	1170	162	230	$4.7 \cdot 10^4$	$3.6 \cdot 10^2$	10^7	$3.8 \cdot 10^{-13}$	10^{-7}	$2 \cdot 10^{-5}$
Nb	80	1170	60	700	$3 \cdot 10^6$	$2.3 \cdot 10^4$	$1.7 \cdot 10^9$	$6.8 \cdot 10^{-11}$	$0.6 \cdot 10^{-9}$	$1.8 \cdot 10^{-7}$
Nb	100	1670	8	240	$5.5 \cdot 10^4$	$4.2 \cdot 10^2$	$0.9 \cdot 10^9$	$1.2 \cdot 10^{-10}$	$1.1 \cdot 10^{-9}$	$2.2 \cdot 10^{-7}$
Er	50	1070	140	460	$1.2 \cdot 10^3$	9.6	$3.1 \cdot 10^5$	$9.9 \cdot 10^{-15}$	$3.2 \cdot 10^{-6}$	$6.4 \cdot 10^{-4}$
Er	70	1270	6	530	$8.9 \cdot 10^2$	6.8	$1.5 \cdot 10^7$	$3.2 \cdot 10^{-12}$	$6.7 \cdot 10^{-8}$	$1.3 \cdot 10^{-5}$
Ta	70	1570	110	350	$3.1 \cdot 10^3$	23.5	$9.6 \cdot 10^5$	$3.6 \cdot 10^{-14}$	$1.1 \cdot 10^{-6}$	$2.1 \cdot 10^{-4}$
Ta	90	1670	5	180	$1.6 \cdot 10^3$	12.3	$3.4 \cdot 10^7$	$7.3 \cdot 10^{-12}$	$2.9 \cdot 10^{-8}$	$5.9 \cdot 10^{-6}$
W	70	1500	115	600	$8.5 \cdot 10^5$	$6.5 \cdot 10^3$	$2.5 \cdot 10^8$	$9.1 \cdot 10^{-12}$	$4 \cdot 10^{-9}$	$8 \cdot 10^{-7}$
W	110	1670	10	760	$1.3 \cdot 10^4$	10^2	$1.7 \cdot 10^8$	$2.5 \cdot 10^{-11}$	$5.8 \cdot 10^{-9}$	$1.2 \cdot 10^{-6}$

“The tritium generation rate has increased by four orders of magnitude, while increasing the specific power by a factor of four, and it has reached the value of 10^9 atom/s when the neutron-to-tritium yield ratio is in the range from 10^{-7} to 10^{-9} .” [Romodanov 1993 (p. 307)]

The data telling that the neutron-to-tritium yield ratio is in the range from 10^{-7} to 10^{-9} is consistent with the theoretical prediction of $N_n/N_t \approx 10^{-7}$ by the TNCF model cited in Eq. (1.1).

“- - deuterium transfusion through sample in plasma for V, Nb, Ta has not rendered the appreciable influence on tritium generation rate. For samples from molybdenum single crystal and polycrystal the deuterium transfusion resulted in increase of tritium generation rate in two times, in comparison with stationary conditions.” [Romodanov 1998a (p. 585)]

“It is shown, that the heaviest rate of tritium generation, of materials TiC, VC, ZrB₂, ZrC, ZrN, and LaB₆, was observed at bombardment by deuterium ions from plasma of glow

discharge for ZrB₂ and made $3.6 \times 10^7 - 3.9 \times 10^7$ atoms/s, at efficiency $2.5 \times 10^{-12} - 2.9 \times 10^{-12}$ (? Exponents -12 is ambiguous) atom/ion, that is comparable with results for metal targets.” [Romodanov 1998b (p. 590)]

Translation of the sentence in the above paragraph.

“ - - - At bombardment of materials TiC, VC, ZrB₂, ZrC, ZrN, and LaB₆ by deuterium ions from plasma of glow discharge, the heaviest rate of tritium generation was observed for ZrB.”

“4. Conclusion

4.1 The significant tritium generation rate, is fixed at radiation by ions deuterium of samples from borides, carbides and nitrides of titanium, vanadium, zirconium, and lanthanum from plasma powerful of glow discharge. For samples of ZrB₂, the tritium generation rate reached $(3.6 - 3.9) \times 10^7$ atom/s.

- - -

4.3 The most proof of materials, at radiation in plasma of glow discharge, were ZrB₂ and ZrN, and the least proof samples of LaB₆.” [Romodanov 1998b]

“The research is conducted on samples of iron, and its alloys as well as on samples of titanium and niobium at interaction, basically, with ordinary hydrogen. It is established, hydrogen that the short-term bursts of tritium generation, arising at interaction of isotopes in which is immersed, previously heated up metal sample, relate to output tritium, early activated, owing of effects isotopes.” [Romodanov 1998c (Abstract)]

Appendix A6. Experiments with Pd_xNi_{0.35-x}Zr_{0.65}, CuNi_y, and others at the Elevated Temperature by Kitamura et al. [Kitamura 2014 – 2018]

Kitamura et al. have developed the so-called “nano-composite samples of Pd-Ni alloys” on some stable solid materials such as silica (SiO₂) and zirconia (ZrO₂) and have worked out elaborate experiments on the large amount of excess heat when the materials were in contact with protium or deuterium gas in rather higher temperature above about 200 °C [Kitamura 2014, 2015, 2016, 2017, 2018]. It should be mentioned that their work was stimulated by the work developed by Celani et al. since 2011 as introduced in the Appendix 4 in another paper presented at this Conference [Kozima 2021a].

We review works by Kitamura et al. below according to the material used in the experiments.

We can characterize the experimental systems taken up by Kitamura et al. by two

properties; (1) The composite CF materials and (2) the solid-solid interface between the CF material and the supporter. In this paper, we will concentrate our investigation on the first characteristic leaving the second to another papers [Kozima 2021a, 2021b, 2021c]. The first characteristic has close relation to the *supported catalysis* explained in Introduction of this paper [Wikipedia Catalysis].

A6-1. Silica based samples [Kitamura 2016, 2018]

“Abstract

Hydrogen isotope absorption characteristics of nanoparticles supported by silica, Pd/SiO₂ (“PSf1”) and Cu₁Ni₁₀/SiO₂ (“CNS3”), have been examined. Large absorption energy (1.3 ± 0.3 eV/Pd) with large apparent loading ratio ($LM = 2.6$) was observed in the initial phase of the D-PSf1#1 run with D₂ at room temperature, which could be ascribed to reduction of PdO and hydrogen absorption by Pd nanoparticles. To reduce the NiO in the CNS3 sample, heating up to around 200 °C was necessary. The excess heat was observed in the elevated temperature phases of the runs with CNS3, while no excess heat was observed with PSf1. Taking also into account the experimental results obtained previously for other samples, we can conclude that the excess heat is observed only in the elevated temperature phases of the runs with binary nanocomposite samples, but not with single-element nanoparticles. In the HCNS3#2 run, the excess heat amounts to 200 eV/Ni or more than 0.9 keV/H without detectable dose rate of hard radiations, which cannot be explained by any chemical process.” [Kitamura 2016]

A6-2. Zirconia based samples [Kitamura 2015, 2017, 2018]

“Abstract

Hydrogen isotope absorption characteristics of Ni-based nano-composites supported by zirconia, Pd_{0.044}Ni_{0.31}/ZrO₂ (“PNZt”) and Cu_{0.044}Ni_{0.31}/ZrO₂ (“CNZt”), have been examined. Large absorption/adsorption (sorption) energy of $(1.6\pm 0.2)\times 10^1$ eV/atom-Pd or (2.3 ± 0.9) eV/atom-D in the initial phase of the #1 run with D₂ at room temperature was observed. If Ni is taken into account as the absorbent element, a rather plausible value of 2.0 ± 0.3 eV/atom-M (M stands for both Pd and Ni), yet one-order-of-magnitude larger than the conventional absorption energy of 0.2 eV/H, is obtained. This means that Pd atoms act as a catalyzer for deuterium absorption of Ni. The large sorption energy was repeatable with about $(6\sim 9)\times 10^{-1}$ eV/atom-M in D-PNZt#2 through H-PNZt#4 runs. In

the elevated temperature (200 ~ 300 °C) phases, on the other hand, excess temperature of 15 ~ 16 °C corresponding to conservatively evaluated excess power of 11 ~ 12 W (or 1.3 ~ 1.5 W/g-Ni) was recorded repeatedly in both PNZt and CNZt sample runs with both H and D.” [Kitamura 2015 (p. 1 (Abstract))]

$\text{Pd}_{0.044}\text{Ni}_{0.31}/\text{ZrO}_2$ (“PNZt”) and $\text{Cu}_{0.044}\text{Ni}_{0.31}/\text{ZrO}_2$ (“CNZt”), have been examined. - - This means that Pd atoms act as a catalyzer for deuterium absorption of Ni. This is a typical case of the *supporter* for the catalysis [Wikipedia Catalysis].

“Abstract

Anomalous heat effect by interaction of hydrogen isotope gas and nanoparticles supported by zirconia, $\text{Pd}_1\text{Ni}_{10}/\text{ZrO}_2$ (“PNZ6” and “PNZ6r”) and $\text{Pd}_1\text{Ni}_7/\text{ZrO}_2$ (“PNZ7k”), has been examined. Excess power of 3 ~ 24 W from PNZ6 at elevated temperature of 200 ~ 300 °C continued for several weeks. The PNZ6 and PNZ6r samples with Pd/Ni=1/10 generated much higher excess power than PNZ7k with Pd/Ni=1/7. The Pd/Ni ratio is one of the key factors to increase the excess power. The maximum phase-averaged sorption energy, $\eta_{\text{av},j}$, exceeded 270 keV/D, and the integrated excess energy, E_a , reached 1 keV/Pd·Ni. It is impossible to attribute the excess energy to any chemical reaction; it is possibly due to some unidentified radiation-free nuclear process.

Index Terms – Zirconia supported nanoparticles, Pd·Ni/ZrO₂, hydrogen isotope gas, absorption and desorption, excess power, sorption energy of 270 keV/D. I” [Kitamura 2017 (p. 14, Abstract)]

Anomalous heat effect by interaction of hydrogen isotope gas and nanoparticles supported by zirconia, $\text{Pd}_1\text{Ni}_{10}/\text{ZrO}_2$ (“PNZ6” and “PNZ6r”) and $\text{Pd}_1\text{Ni}_7/\text{ZrO}_2$ (“PNZ7k”), has been examined. Excess power of 3 ~ 24 W from PNZ6 at elevated temperature of 200 ~ 300 °C continued for several weeks. The PNZ6 and PNZ6r samples with Pd/Ni=1/10 generated much higher excess power than PNZ7k with Pd/Ni=1/7. The Pd-Ni alloy shows a typical example of the *supported catalysis* [Wikipedia Catalysis].

A6-3. Review of the work from the viewpoint of the TNCF model [Kozima 2020]

The data finally compiled in the paper published in International J. Hydrogen Energy [Kitamura 2018] was briefly reviewed by us [Kozima 2020] and the essential result is cited below.

It should be noted that the occurrence of the exothermic reactions accompanied with

the crystallization of component elements in Pd-Ni alloys well-known in metallurgy of Pd alloys (cf. [Mizumoto 1989]).

“In the electroless plating of Pd-Ni-P alloys from ethylenediamine complex solutions containing sodium hypophosphite as a reducing agent, the generation of heat due to the crystallizations of palladium and palladium phosphides were observed at around 300°C. Another generation of heat was observed also at around 400°C due to the crystallization of Ni₃P₁. We found several broad peaks of the heat generation between the two peaks of the heat generations due to the Pd-P deposit and Ni-P deposit. Figure 5 shows the relation between the phosphor content in the deposit of Pd-Ni-P plating and amount of heat generation (determined by the peak of heat generation in the D_{sc} curve).” [Mizumoto 1989 (p. 68, Translated into English by H.K. The Fig. 5 in the above sentence is cited below as Fig. A6-1)

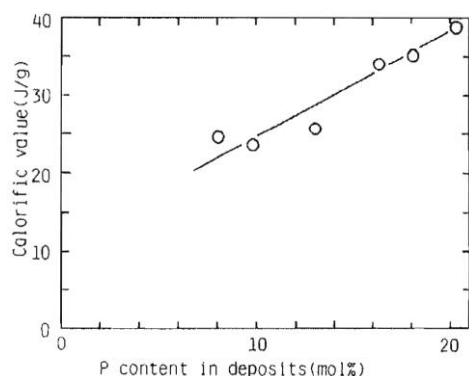


Fig. A6-1. Relation between P content in electroless Pd-Ni-P films and calories of exothermic reaction. ([Mizumoto 1989 (Fig. 5)])

It is probable to occur similar exothermic reaction in the hydrides/deuterides used in the experiments reported in the paper [Kitamura 2018]. Then, it is possible that there occurs a mutual acceleration of the positive feedback of the energy to the nuclear reactions in the CFP [Kozima 2013] and of the energy to the exothermic crystallization of component elements. The exothermic crystallization depends definitively on the composition of the CF material and therefore the process should be very complicated. If this mutual acceleration occurs, the CFP in the CF materials composed of Pd-Ni alloys works very effective to realize nuclear reactions between neutrons and nuclei at disordered position and then the structure of the CF material deteriorates rapidly to terminate the reactions by destruction of the optimum structure for the CFP [Kozima 2013]. So, it is desirable to check the occurrence of the crystallization in the sample after the experiments.

Appendix A7. Experimental Data on the Hydrogen in Ternary Alloys [Smith 1948, Wicke 1978]

In the discussion of the CFP in the composite CF materials, we used mainly the data obtained in the cold fusion research especially in Section 4. In the phenomenological approach to the physics of the CFP, we have used not only the data of nuclear reactions but also the occlusion and super-diffusion of hydrogen isotopes in transition metals. In this point, we could not use enough data of physics of hydrogen in metal alloys in this paper. In this Appendix, we cite two tables showing the essential properties of ternary alloys including hydrogen isotopes from the book by D.P. Smith [Smith 1948] and E. Wicke and H. Brodowsky [Wicke 1978] which will be taken up in our future works.

A7-1. Occlusive Characteristics of Ternary Alloys $A_xB_yH_z$ [Smith 1948]

The occlusive characteristics of transition metals and alloys had been exclusively investigated by D.P. Smith by 1948 and summarized in his book [Smith 1948]. Following tables show the occlusion characteristics of transition metals in Table A7-1 and those of ternary alloys in Table 17-2.

“2.1 In regard to their behavior toward hydrogen, the solid metals fall into three classes, as may most readily be seen from the eighteen-group arrangement of the elements shown in our Table 1.” [Smith 1948 (p. 2)]

Table A7-1. Periodic System & Occlusion. [Smith 1948 (p. 7, Table I)]

TABLE I. PERIODIC SYSTEM & OCCLUSION.

LEGEND FOR C-METALS (⊕ EXOTHERMIC OCCLUDER; ⊖ ENDOTHERMIC OCCLUDER; X NON-OCCLUDER; ⊗ EVIDENCE INDECISIVE; △ UNINVESTIGATED,

H																	He																
Li	<table border="1" style="display: inline-table; border-collapse: collapse;"> <tr><td>La</td><td>Ce</td><td>Pr</td><td>Nd</td><td>Sa</td></tr> <tr><td>⊕</td><td>⊕</td><td>⊕</td><td>⊕</td><td>⊕</td></tr> </table>					La	Ce	Pr	Nd	Sa	⊕	⊕	⊕	⊕	⊕												Be	NON-METALS					Ne
La	Ce	Pr	Nd	Sa																													
⊕	⊕	⊕	⊕	⊕																													
Na	★ RARE EARTH METALS																Mg	Al		Si	P	S	Cl	Ar									
K	Ca	Sc	Ti	V	Cr	Mn	Fe	Co	Ni	Cu	Zn	Ga	Ge	As	Se	Br	Kr																
Rb	Sr	Y	Zr	Cb	Mo	Ma	Ru	Rh	Pd	Ag	Cd	In	Sn	Sb	Te	I	X																
Cs	Ba	★	Hf	Ta	W	Re	Os	Ir	Pt	Au	Hg	Tl	Pb	Bi	Po	85	Rn																
87	Ra	△	Th	Pa	U																												
1	2	3	4	5	6	7	8	9	10	11	12	13	14	15	16	17	18																
A-METALS		C-METALS									B-METALS																						

Table A7-2. Occlusion characteristics of binary alloys [Smith 1948 (p. 213)]

System	Types	System	Types
(Fe-W)	Endo—non	Pd-Ag	Exo—endo
Fe-Cr	Endo—endo	Pd-Pr	Exo—endo
Fe-Ni	Endo—endo	Fe-V	Exo—endo
Fe-Mo	Endo—endo	(Pd-Cu)	Exo—endo
(Fe-Mn)	Endo—anom	(Pd-Ni)	Exo—endo
Pd-Au	Exo—non	(Ce-Mg)	Exo—endo
Pd-B	Exo—non	(Ce-La)	Exo—exo
(Ce-Mn)	Exo—anom		

“In the accompanying table are displayed most of the binary alloy systems upon which the literature accords any information regarding occlusion of hydrogen(see, however, 6.6.b; 6.10b; 6.15.d). Those placed in parentheses have been too little investigated to warrant detailed discussion. The remainder have been taken up in foregoing sections. Systems are arranged according to the occlusive types of their components, whether absorbing *endo(thermically)*, *exo(thermically)*, or *anom(alously)*, or whether *practically non(occluding)*.

The table makes it apparent that no system composed of two exothermically occluding metals has been studied with an approach to adequacy and that the combination of an endothermic with a nonoccluding metal is represented only by one study of a rather

preliminary character. Chromium and molybdenum are both classed here as endothermically occluding, this being certainly the case for Cr above 300° C, while evidence as to Mo is conflicting.

With regard to diffusion in ternary and other hydrogen alloys, reference may be made to the series of papers by Baukloh and his fellow-workers from 1933 to 1938, cited in our General Bibliography. [Smith 1948 (p. 213)] (Italicized partially at citation).

A7-2. Diffusion data of H, D, and T in Pd and Pd alloys [Wicke 1978]

E. Wicke and H. Brodowsky collected diffusion data of H, D, and T in Pd and Pd alloys [Wicke 1978]. From Table A7-3, we can obtain characteristics of ternary Pd alloys useful for the investigation of the CFP in the composite CF materials used frequently in nowadays.

Table A7-3. Diffusion data of H, D, and T in Pd and Pd alloys at $n \rightarrow 0$, obtained by electrochemical and radiochemical time-lag methods [Wicke 1978 (Table 3.4)].

System	X_i [at %]	$D \cdot 10^7$ [cm ² s ⁻¹] (25 °C)			$D_0 \cdot 10^3$ [cm ² s ⁻¹]			A_E [kcal g-atom ⁻¹]			Remarks	Ref.
		H	D	T	H	D	T	H	D	T		
Pd	0	1.3										[3.181]
		1.2										[3.182]
Pd/Ag	10	5.4	6.0	4.8	5.3	2.7	7.2	5.45	4.9	5.7		[3.189, 195]
	20	5.2	3.5*	4.2	4.3	2.3*	6.3	5.35	5.2*	5.7		[3.185, 189, 195]
	30	4.1	5.3	3.7	3.4	1.6	5.6	5.35	4.75	5.7*		
	40	1.8	1.7*	1.9	2.3	1.1*	6.5	5.6	5.2*	6.2		
	50	0.23*	0.51*	0.28	1.9*	2.5*	2.7	6.7*	6.4*	6.8		[3.184, 185, 189]
	60	0.020*	0.041*	0.033	1.1*	1.3*	4.7	7.8*	7.5*	8.4		
Ag	100	0.0035*	0.0046*	0.0012	1.0*	3.0*	7.0	8.8*	9.3*	10.6		[3.192]
Pd/Au	18.8	(7 ± 3) · 10 ⁻⁵										Evaporated thin Ag films
	26.5	3.5										D values are valid for 37 °C;
	35.1	1.7										prehistory of the foils is
	44.7	0.27			0.6			7.3				unknown
	55.7	0.037										
Pd/Cu	5	0.0074		4.3			4.6			5.5		[3.190]
	10			3.1			2.8			5.4		
	15			3.0			3.3			5.5		
	20			2.3			2.8			5.6		
	25			2.3			3.0			5.6		
	30			4.9			6.1			5.6		[3.190]
Pd/Ni	7			3.8			4.8			5.6		
	10			3.4			4.3			5.6		
	15			2.6			3.9			5.7		
	20			2.3			3.4			5.7		
	26			1.6			3.9			6.0		
	30			3.1			4.7			5.7		
Pd/V	2			3.1			4.7			5.7		
	4			1.4			2.5			5.8		[3.190]
	6			1.3			2.8			5.9		
	10			0.5			3.4			6.6		
Pd/Rh	10	1.1			10.4			6.8			Prehistory of the foils is unknown	[3.191]

* Foils have not been annealed

The references such as [3.181] in the Table are the original ones. [Wicke 1978 (Table 3.4)]

Acknowledgement

The author would like to express his thanks to Dr. A. Kitamura, Dr. H. Yamada, Dr. K. Kaki and Dr. F. Celani for valuable communications with them on the experimental results investigated in this paper.

References

- [Akiyama 1986] T. Akiyama, H. Fukushima, K. Higashi, "Mechanism of Abnormal Type Alloy Deposition," *ISIJ International*, **72**, 918 – 923 (1986), ISSN: 0021-1575 (in Japanese).
- [Augustynski 1989] J. Augustynski, M. Ulmann and J. Liu, *Chimia*, **43**, p. 355 (1989). ISSN: 0009-4293.
- [Bockris 1970a] J.O'M. Bockris and A.K.N. Reddy, *Modern Electrochemistry – An Introduction to an Interdisciplinary Area –*, Plenum Press, New York, 1970, Library of Congress Catalog Card Number 6819518.
- [Bockris 1970b] J. O'M. Bockris and A.R. Despić, "The Mechanism of Deposition and Dissolution of Metals," in *The Mechanism of Deposition and Dissolution of Metals, in Physical Chemistry – An Advanced Treatise –*, Vol. **IXB**/Electrochemistry, Chapter 7, Ed. Henry Eyring, Academic Press, N.Y and London, 1970, Library of Congress Catalog Card Number: 66-29951.
- [Bockris 1999a] J. O'M. Bockris, "Early Contributions from Workers at Texas A&M University to (so-called) Low Energy Nuclear Reactions," *J. New Energy*, **4**, No 2, pp. 40 – 72 (1999), ISSN 1086-8259.
- [Bockris 1999b] J.O'M. Bockris and E.F. Mallove, "Is the Occurrence of Cold Nuclear Reactions Widespread Throughout Nature?" *Infinite Energy*, **27**, pp. 1 – 5 (1999), ISSN 1081-6372.
- [Bockris 2000] J.O'M. Bockris, A.K.N. Reddy, M.E. Gamboa-Aldeco, *Modern Electrochemistry*, 2nd edition, Volume 2A, *Fundamentals of Electrode Processes*, Kluwer Academic/Plenum Publishers, 2000, ISBN 978-0-306-47605-1.
- [Campari 2004a] E. Campari, G. Fasano, S. Focardi, G. Lorusso, V. Gabbani et al., "Photon and particle emission, heat production and surface transformation in Ni-H system," *Proc. ICCF11*, pp. 405 – 413 (2004), ISBN 981-256-640-6.
- [Campari 2004b] E. Campari, S. Focardi, V. Gabbani, V. Montalbano, F. Piantelli and S. Veronesi, "Surface Analysis of Hydrogen loaded Nickel Alloys," *Proc. ICCF11*, pp. 414 – 420 (2004), ISBN 981-256-640-6.

- [Celani 1992] F. Celani, A. Spallone, L. Libaratori, F. Groce, A. Storelli et al., "Search for Enhancement of Neutron Emission from Neutron-Irradiated, Deuterated High-Temperature Superconductors in a Very Low Background Environment", *Fusion Technol.*, **22**, pp. 181 – 186 (1992), ISSN 0748-1896.
- [Celani 2012] F. Celani, O.M. Calamai, A. Spallone, A. Nuvoli *et al.*, "Development of a High Temperature Hybrid CMNS Reactor," *J. Condensed Matter Nucl. Sci.*, **6**, pp. 24–33 (2012), ISSN 2227-3123.
- [Celani 2020a] F. Celani, C. Lorenzetti, G. Vassallo *et al.*, "First Evaluation of Coated Constantan Wires Incorporating Capuchin Knots to Increase Anomalous Heat and Reduce Input Power at High Temperatures," *J. Condensed Matter Nucl. Sci.*, **30**, pp. 25–35 (2020), ISSN 2227-3123.
- [Celani 2020b] F. Celani, C. Lorenzetti, G. Vassallo, E. Purchi, S. Fiorilla et al., "Progress toward an Understanding of LENR-AHE Effects in Coated Constantan Wires in D₂ Atmosphere: DC/AC Voltage Stimulation," *J. Condensed Matter Nucl. Sci.*, **33**, pp. 46 – 73 (2020), ISSN 2227-3123.
- [Claytor 1991] T.N. Claytor, D.G. Tuggle and H.O. Menlove, "Tritium Generation and Neutron Measurements in Pd-Si under High Deuterium Gas Pressure," *Proc. ICCF2*, pp. 395 – 408 (1991), ISBN 88-7794-045-X.
- [Claytor 1998] T. N. Claytor, M. J. Schwab, D. J. Thoma, D. F. Teter and D. G. Tuggle, "Tritium Production from Palladium Alloys," *Proc. ICCF7*, pp. 88 - 93 (1998), ENECO Inc., Salt Lake City, Utah 84108, USA.
- [Collins 2021] H. Collins, "On Acquiring and Using Scientific Knowledge," *Physics Today*, 6.4.20210217a (2021).
<https://physicstoday.scitation.org/doi/10.1063/PT.6.4.20210217a/full/>
- [DOE 2004] "Report of the Review of Low Energy Nuclear Reactions."
http://www.science.doe.gov/Sub/Newsroom/News_Releases/DOE-SC/2004/low_energy/CF_Final_120104.pdf.
- This report is posted at the *New Energy Times* website:
<http://newenergytimes.com/v2/government/DOE2004/7Papers.shtml>
- [Dufour 1993] J. Dufour, "Cold Fusion by Sparking in Hydrogen Isotopes," *Fusion Technology*, **24**, pp. 205 – 228 (1993), ISSN 0748-1896.
- [Fleischmann 1989] M. Fleischmann, S. Pons and M. Hawkins, "Electrochemically induced Nuclear Fusion of Deuterium," *J. Electroanal. Chem.*, **261**, pp. 301 – 308 (1989), ISSN 1572-6657.

- [Forsly 1998] L. Forsly, R. August, J. Jorne, J. Khim, F. Mis and G. Phillips, “Analyzing Nuclear Ash from the Electrocatalytic Reduction of Radioactivity in Uranium and Thorium,” *Proc. ICCF7*, pp. 128 – 132 (1998), ENECO Inc.
- [Fukushima 1993] H. Fukushima, M. Yano, T. Ishikawa and R. Kammel, “Electrodeposition Behavior of Zn-Iron-group Metal Alloys from Sulfate and Chloride Baths,” *ISIJ International*, **33**, No. 9, pp. 1009-1015 (1993), ISSN: 1883-2954.
- [Horiuti 1951] J. Horiuti, T. Keii, K. Hirota, “Mechanism of Hydrogen Electrode of Mercury, ‘Electrochemical Mechanism’,” *J. Res. Inst. Catalysis, Hokkaido Univ., Vol. 2*, No.1, pp. 1 – 72 (1951), ISSN 0034-530X.
- [Horiuti 1970] J. Horiuti, “Gas Evolution Reactions,” pp. 543 – 610, in *The Mechanism of Deposition and Dissolution of Metals*, in *Physical Chemistry – An Advanced Treatise* – , Vol. **IXB**/Electrochemistry, Chapter 6, Ed. Henry Eyring, Academic Press, N.Y and London, 1970, Library of Congress Catalog Card Number: 66-29951.
- [Huizenga 1992] J.R. Huizenga, *Cold Fusion – The Scientific Fiasco of the Century*, University of Rochester Press, 1992, ISBN 1-878822-07-1.
- [Iwamura 2020a] Y. Iwamura, “Heat generation experiments using nano-sized metal composite and hydrogen gas,” in *Cold Fusion: Advances in Condensed Matter Nuclear Science*, Ed. J.-P. Biberian, pp. 157 – 165, Elsevier, 2020, ISBN-10: 0128159448.
- [Iwamura 2020b] Y. Iwamura, T. Itoh, J. Kasagi, S. Murakami and M. Saito, “Excess Energy Generation using a Nano-sized Multilayer Metal Composite and Hydrogen Gas”, *J. Condensed Matter Nucl. Sci.*, **33**, pp. 1–13, (2020), ISSN 2227-3123.
- [Jones 1989] S.E. Jones, E.P. Palmer, J.B. Czirr, D.L. Decker, G.L. Jensen et al., “Observation of Cold Nuclear Fusion in Condensed Matter,” *Nature*, **338**, 737 – 740 (1989), ISSN 0028-0836.
- [Jones 1994] Jones et al., “Search for Neutron, Gamma and X-ray Emission s from Pd/LiOD Electrolytic Cells: A Null Result” *Proc. ICCF4*, Vol. **3**, pp. 26-1 – 26-14 (1994).
- [Kageyama 2020] H. Kageyama, “Commonplace Ceramics Can Absorb a Large Amount of Hydrogen!”
http://www.spring8.or.jp/en/news/publications/press_release/2012/120416
- [Kita 1971] H. Kita, “Catalytic activity and the reaction mechanism on the hydrogen electrode reactions” *Nihon Kagaku Zasshi* **92**, pp. 99 – 114 (1971) (in Japanese).
- [Kita 1973] H. Kita and T. Kurisu, “Electroanalysis by *d*- and *sp*- Metals,” *J. Res. Inst. Catalysis, Hokkaido Univ.*, **21**, No.3, pp. 200 – 246 (1973), . ISSN 0034-530X
- [Kitamura 2014] A. Kitamura, A. Takahashi, R. Seto, Y. Fujita, A. Taniike and Y. Furuyama, “Comparison of Some Ni-based Nano-composite Samples with Respect to

- Excess Heat Evolution under Exposure to Hydrogen Isotope Gases,” *Proc. JCF15*, pp. 1 – 16 (2014), ISSN 2187-2260.
- [Kitamura 2015] A. Kitamura, E. F. Marano, A. Takahashi, R. Seto et al., “Heat Evolution from Zirconia-supported Ni-based Nanocomposite Samples under Exposure to Hydrogen Isotope Gas,” *Proc. JCF16*, pp. 1 – 19 (2015), ISSN 2187-2260.
- [Kitamura 2016] A. Kitamura, A. Takahashi, K. Takahashi, R. Seto, T. Hatano et al., “Heat Evolution from Silica-supported Nano-composite Samples under Exposure to Hydrogen Isotope Gas,” *Proc. JCF17*, pp. 1 – 14 (2016), ISSN 2187-2260.
- [Kitamura 2017] A. Kitamura, A. Takahashi, K. Takahashi, R. Seto, T. Hatano et al., “Comparison of Excess Heat Evolution from Zirconia-supported Pd-Ni Nanocomposite Samples with Different Pd/Ni Ratio under Exposure to Hydrogen Isotope Gases,” *Proc. JCF18*, pp. 14 – 31 (2017), ISSN 2187-2260.
- [Kitamura 2018] A. Kitamura et al., “Excess Heat Evolution from Nanocomposite Samples under Exposure to Hydrogen Isotope Gases” *Int. J. of Hydrogen Energy*, **43**. Issue 33, pp. 16187 – 16200 (2018).
- [Kobayashi 2020] Y. Kobayashi, O.J. Hernandez, T. Sakaguchi, et al., "An Oxyhydride of BaTiO₃ Exhibiting Hydride Exchange and Electric Conductivity," *Nature Materials*, **11**, pp.507–511(2012), <http://dx.doi.org/10.1038/nmat3302>.
- [Kozima 1994] H. Kozima, “Trapped Neutron Catalyzed Fusion of Deuterons and Protons in Inhomogeneous Solids,” *Transactions of Fusion Technology*, **26**, No. **4T**, Part 2 FUSTE8 (4), pp. 508 – 515 (1994), ISSN 0748-1896.
- [Kozima 1996] H. Kozima, K. Hiroe, M. Nomura and M. Ohta, “Elemental Transmutation in Biological and Chemical Systems,” *Cold Fusion*, **16**, pp. 30 – 32 (1996). ISSN 1074-5610.
- [Kozima 1997] H. Kozima, K. Kaki and M. Ohta, "The Physics of the Cold Fusion Phenomenon," *Cold Fusion*, **22**, pp. 58 – 78 (1997).
- [Kozima 1998] H. Kozima, *Discovery of the Cold Fusion Phenomenon – Development of Solid State-Nuclear Physics and the Energy Crisis in the 21st Century* –, Ohtake Shuppan Inc., 1998, ISBN 4-87186-044-2. The “References” in this book is posted at the CFRL (Cold Fusion Research Laboratory) Website:
<http://www.kozima-cfrl.com/Books/bookse/bookee.html>
- [Kozima 2000] H. Kozima. “Neutron Drop: Condensation of Neutrons in Metal Hydrides and Deuterides”, *Fusion, Technol.*, **37**, pp. 253 - 258 (2000), ISSN 0748-1896.
- [Kozima 2004] H. Kozima, “Quantum Physics of Cold Fusion Phenomenon,” *Developments in Quantum Physics Research – 2004*, pp. 167 – 196, Ed. V. Krasnoholovets, Nova Science Publishers, Inc., New York, 2004. ISBN 1-59454-003-9.

- [Kozima 2005] H. Kozima, “CF-Matter and the Cold Fusion Phenomenon,” *Proc. ICCF10*, pp. 919 – 928 (2005), ISBN 981-256-564-7.
- [Kozima 2006] H. Kozima, *The Science of the Cold Fusion Phenomenon, – In Search of the Physics and Chemistry behind Complex Experimental Data Sets –*, 1st Edition, Elsevier, Amsterdam, 2006, ISBN-13: 978-0-08045-110-7, ISBN-10: 0-080-45110-1.
- [Kozima 2007] H. Kozima, “An Explanation of Nuclear Transmutation in XLPE (Crosslinked Polyethylene) Films with and without Water Trees,” *Proc. JCF8*, pp. 44 – 50 (2008), ISSN 2187-2260.
- [Kozima 2008] H. Kozima, W.-S. Zhang, and J. Dash, “Precision Measurement of Excess Energy in Electrolytic System Pd/D/H₂SO₄ and Inverse-Power Distribution of Energy Pulses vs. Excess Energy,” *Proc. ICCF13*, pp. 348 – 358 (2008), ISBN 978-5-93271-428-7.
- [Kozima 2010] H. Kozima and H. Date, “Nuclear Transmutations in Polyethylene (XLPE) Films and Water Tree Generation in Them” *Proc. ICCF14*, pp. 618 – 622 (2010), ISBN 978-0-578-06694-3.
- [Kozima 2011a] H. Kozima, “Localization of Nuclear Reactions in the Cold Fusion Phenomenon,” *Proc. JCF11*, pp. 59 –69 (2011), ISSN 2187-2260.
- [Kozima 2011b] H. Kozima and F. Celani, “Brief Explanation of Experimental Data Set on Excess Heat and Nuclear Transmutation in Multiply Nanocoated Ni Wire,” *Proc. JCF11*, pp. 53 – 58 (2011), ISSN 2187-2260.
- [Kozima 2012a] H. Kozima and M. Tada, “The Cold Fusion Phenomenon in Hydrogen-Graphites,” *Proc. JCF12*, pp. 77 – 92 (2012), ISSN 2187-2260.
- [Kozima 2012b] H. Kozima, “Cold Fusion Phenomenon in Open, Non-equilibrium, Multi-component Systems,” *Reports of CFRL (Cold Fusion Research Laboratory)*, **12-1**, pp. 1 – 14 (2012). <http://www.kozima-cfrl.com/Papers/paperr/paperr.html>
- [Kozima 2013] H. Kozima, “Cold Fusion Phenomenon in Open, Nonequilibrium, Multi-component Systems – Self-organization of Optimum Structure,” *Proc. JCF13*, **13-19**, pp. 134 - 157 (2013), ISSN 2187-2260.
- [Kozima 2014] H. Kozima, “Nuclear Transmutations (NTs) in Cold Fusion Phenomenon (CFP) and Nuclear Physics,” *Proc. JCF14*:**14-15**, pp. 168 - 202 (2014). ISSN 2187-2260.
- [Kozima 2016a] H. Kozima, “Nuclear Transmutations in Polyethylene (XLPE) Films and Water Tree Generation in Them (2),” *Proc. JCF16*, **16-17**, pp. 210 – 215 (2016), ISSN 2187-2260.
- [Kozima 2016b] H. Kozima, “Biotransmutation as a Cold Fusion Phenomenon,” *Proc. JCF16*, **16-18**, 216 - 239 (2016), ISSN 2187-2260.

- [Kozima 2017] H. Kozima, T. Ohmori and M. Ohta, “Nuclear Transmutations in Critical and Supra-critical Electrolysis with Graphite, Pd, W, Re, Pt and Au Cathodes Analyzed by the TNCF Model,” *Proc. JCF17*, **17-12**, pp. 89-147 (2017), ISSN 2187-2260.
- [Kozima 2019a] H. Kozima, “Inductive Logic and Meta-analysis in the Cold Fusion Phenomenon,” *Proc. JCF19*, **19-14**, pp. 85 - 111 (2019), ISSN 2187-2260.
- [Kozima 2019b] H. Kozima, “Development of the Solid State-Nuclear Physics,” *Proc. JCF19*, **19-15**, pp. 112 – 147 (2019), ISSN 2187-2260.
- [Kozima 2019c] H. Kozima, “Nuclear Transmutations and Stabilization of Unstable Nuclei in the Cold Fusion Phenomenon” *Proc. ICAMRWT (International Conference on the Application of Microorganisms for the Radioactive Waste Treatment)*, (May 18, 2018, Pukyung National University, Busan, Korea) as a special issue of the *J. CMNS (Condensed Matter Nuclear Science)*, **28**, pp. 28 – 49 (2019), ISSN 2227-3123.
- [Kozima 2019d] H. Kozima and H. Yamada, “Characteristics of the Nuclear Reactions in the Cold Fusion Phenomenon,” *Proc. of JCF19*, **19-13**, pp. 165 - 191 (2019), ISSN 2187-2260.
- [Kozima 2020] H. Kozima, “The “anomalous heat effect” is a normal event in the cold fusion phenomenon – On the paper “Excess heat evolution from nanocomposite samples under exposure to hydrogen isotope gases” by Kitamura et al. published in the *Int. J. Hydrogen Energy* **43**, pp. 16187 – 16200 (2018) –,“ *Int. J. Hydrogen Energy*, **45** (38), pp. 19577 – 19582 (2020), ISSN 2187-2260.
- [Kozima 2021a] H. Kozima, “Cold Fusion Phenomenon in the Compound CF Materials – Effects of Interface,” *Proc. JCF21*, **21-3** (2021), ISSN 2187-2260 (to be published).
- [Kozima 2021b] H. Kozima, “Neutron Energy Bands in the Composite and Compound CF Materials – Speculation on the Bases of the TNCF Model –,” *Proc. JCF21*, **21-4** (2021), ISSN 2187-2260, (to be published).
- [Kozima 2021c] H. Kozima and T. Ohmori, “Nuclear Force between Lattice Nuclei and Interstitial Hydrogen and HER and UPD,” (to be published).
- [Kozima 2021d] H. Kozima, “Overview on the Solid State-Nuclear Physics – Super-diffusion of Hydrogen, HER and UPD, and CFP in Transition Metals and Alloys –,” (to be published).
- [Lipson 1996] A.G. Lipson, V.A. Kuznetsov, D.M. Sakov and E.I. Saunin, “Cold Fusion and Electrophysical Processes in Ferroelectric Deuterated Crystal. Influence of Thermal Neutron Background Level, D-H Substitution and Crystal Mass,” *Proc. ICCF6*, pp. 512 – 518 (1996), NEDO and Institute of Applied Energy, Tokyo, Japan, 1998.

- [McBreen 1990] J. McBreen, "Absorption of Electrolytic Hydrogen and Deuterium by Pd: The Effect of Cyanide Adsorption," *J. Electroanal. Chem.*, **287**, pp. 279 ~ 291 (1990), ISSN 1572-6657.
- [McKubre 1993] M.C.H. McKubre, S. Crouch-Baker, Riley, S.I. Smedley and F.L. Tanzella, "Excess Power Observed in Electrochemical Studies of the D/Pd System," *Proc. ICCF3*, pp. 5 – 19 (1993), ISBN 4-946443-12-6.
- [Mizumoto 1989] S. Mizumoto, H. Nawafune, T. Okada and M. Haga, "Electroless Pd-Ni-P Alloy Plating and Properties of the Deposit," *J. Surf. Finish. Soc. Jpn.*, **40**, No.5, pp. 680 – 684 (1989), ISSN 0915-1869 (in Japanese).
- [Mizuno 1996] T. Mizuno, T. Akimoto, K. Azumi et al., "Anomalous Heat Evolution from a Solid-state Electrolyte under Alternating Current in High-temperature D₂ Gas," *Fusion Technology*, **29**, pp. 385 – 389 (1996), ISSN 0748-1896.
- [Mizuno 1997] T. Mizuno, K. Inoda, T. Akimoto, K. Azumi, M. Kitaichi et al., "Anomalous γ Peak Evolution from SrCeO₃ Solid State Electrolyte Charged in D₂ Gas," *Intern. J. Hydrogen Energy*, **22**-1, pp. 23 – 25 (1997), ISSN 0360-3199.
- [Morrey 1990] J.R. Morrey, M.R. Caffee, H. Farrar, IV, N.J. Hoffman, et al., "Measurements of Helium in Electrolyzed Palladium," *Fusion Technol.*, **18**, pp. 659 – 668 (1990), ISSN 0748-1896.
- [Morrison 2000] D.R.O. Morrison, "Status of Cold Fusion and Report on 8th International Cold Fusion Conference," *Cold Fusion Updates*, No. **13**, pp. 1 – 33 (2000).
- [Nakano 1998] H. Nakano, T. Akiyama and H. Fukushima, "Underpotential Deposition of Zn with Iron-group Metals," *J. Surf. Finish. Soc. Jpn*, **49**, No. 11, pp. 1209 – 1220 (1998), ISSN: 0915-1869 (in Japanese).
- [Ohmori 2016] T. Ohmori, "Anomalous Reactions Induced by Light and Heavy Water Electrolysis", in *New Topics in Electrochemistry Research*, Ed. M. Nunez, pp. 47 – 84, Nova Science Publisher, 2016, ISBN: 1-60021-015-5.
- [Oya 1996] Y. Oya, H. Ogawa, T. Ono, M. Aida and M. Okamoto, "Hydrogen Isotope Effect Induced by Neutron Irradiation in Pd-LiOD (H) Electrolysis," *Proc. ICCF6*, pp. 370 – 376 (1996), NEDO and Institute of Applied Energy, Tokyo, Japan, 1998.
- [Packham 1989] N.J.C. Packham, K.L. Wolf, J.C. Wass, R.C. Kainthla and J.O.'M. Bockris, "Production of Tritium from D₂O Electrolysis at a Palladium Cathode," *J. Electroanal. Chem.*, **270**. 451 – 458 (1989). ISSN: 1572-6657.
- [Park 2000] R.L. Park, *Voodoo Science – The Road from Foolishness to Fraud* – Oxford University Press, 2000, ISBN 0-19-513515-6.

- [Quaino 2007] P.M. Quaino, M.R. Gennero de Chialvo, A.C. Chialvo, "Hydrogen Electrode Reaction: A Complete Kinetic Description," *Electrochimica Acta*, **52**, pp. 7396–7403 (2007), ISSN 0013-4686.
- [Reifenschweiler 1995] O. Reifenschweiler, "Some Experiments on the Decrease of the Radioactivity of Tritium Sorbed by Titanium Particle," *Proc. ICCF5*, pp. 163 – 172 (1995), International Conference on Cold Fusion 5, Valbonne France.
- [Romodanov 1993] V.A. Romodanov, V.I. Savin, Y.B. Skuratnik and Y. Timofeev, "Nuclear Fusion in Condensed Matter," *Proc. ICCF3*, pp. 307 – 319 (1993), ISBN 4-946443-12-6.
- [Romodanov 1998a] V.A. Romodanov, V.I. Savin and Y.B. Skuratnik, "Tritium Generations at Transfusion of Hydrogen Isotopes through Targets in Plasma of Powerful Glow Discharge," *Proc. ICCF6*, pp. 585 – 589 (1998), NEDO and Institute of Applied Energy, Tokyo, Japan, 1998.
- [Romodanov 1998b] V.A. Romodanov, V.I. Savin and Y.B. Skuratnik, "Nuclear Reactions at Effect of Ions Deuterium on Ceramic Materials from Plasmas of Glow Discharge," *Proc. ICCF6*, pp. 590 – 594 (1998), NEDO and Institute of Applied Energy, Tokyo, Japan, 1998.
- [Romodanov 1998c] V.A. Romodanov, V.I. Savin, Y.B. Skuratnik and V.N. Majorov, "Tritium Generation in Metals at Thermal Activation," *Proc. ICCF7*, pp. 319 – 324 (1998).
- [Schlapbach 1991] L. Schlapbach, "Hydrogen and its Isotopes in and on Metals," *Proc. ICCF2*, pp. 409 – 418 (1991), ISBN 88-7794-045-X.
- [Seo 2012] M. Seo, "Underpotential Deposition and Metallic Corrosion Reaction," *Corrosion Engineering of Japan*, **61**, No.9, pp. 341 – 348 (2012), ISSN: 1884-1155 (in Japanese).
- [Shani 1989] G. Shani, C. Cohen, A. Grayevsky and S. Brokman, "Evidence for a Background Neutron Enhanced Fusion in Deuterium Absorbed Palladium," *Solid State Comm.* **72**, 53 – 57 (1989), ISSN 0038-1098.
- [Shavely 1949] C.A. Shavely and D.A. Vaughan, "Unit Cell Dimension of Face-centered Cubic Chromium Hydride and Space Groups of Two Chromium Hydrides," *J. Am. Chem. Soc.* **71**, 313 – 314 (1949).
- [Smith 1948] D.P. Smith, *Hydrogen in Metals*, Univ. Chicago Press, 1948, ASIN B0007G3GOO.
- [Srinivasan 1990] M. Srinivasan, A. Shyam, T. C. Kaushik, R. K. Rout, L. V. Kulkarni et al., "Observation of Tritium in Gas/Plasma Loaded Titanium Samples," *AIP Conference Proceedings 228* pp. 1 – 21 (1990). Brigham Young Univ., Provo, UT: American Institute of Physics, New York.

- [Stella 1993] B. Stella, M. Corradi, F. Ferrarotto, V. Malone, F. Celani and A. Spallone, “Evidence for Stimulated Emission of Neutrons in Deuterated Palladium,” *Frontiers of Cold Fusion (Proc. ICCF3)*, pp. 437 – 440 (1993), ISSN 0915-8502.
- [Storms 2007] E. Storms, *The Science of Low Energy Nuclear Reactions*, World Scientific Publishing, 2007. ISBN-10 981-270-620-8.
- [Suess 1956] H.E. Suess and H.C. Urey, “Abundances of the Elements,” *Rev. Mod. Phys.* **28**, pp. 53 – 74 (1956), ISSN 0034-6861.
- [Swartz 2002] M.R. Swartz, G.M. Verner and A.H. Frank, “The Impact of Heavy Water (D₂O) on Nickel Light Water Cold Fusion Systems,” *Proc. ICCF9*, pp. 335 – 342 (2003), ISBN 7-302-06489-X/O•292.
- [Swartz 2019] M.R. Swartz, B. Ahern, C. Haldemann and A. Weinberg, “Excess Heat is Linked to Deuterium Loss in an Aqueous Nickel LANR System,” *J. Condensed Matter Nucl. Sci.*, **29**, pp. 169–176 (2019), ISSN 2227-3123.
- [Tanabe 1992] T. Tanabe, Y. Yamanishi and S. Imoto, “Hydrogen permeation and diffusion in molybdenum,” *Journal of Nuclear Materials* **191-194**, pp. 439-443 (1992).
- [Taubes 1993] G. Taubes, *Bad Science – The Short Life and Weird Times of Cold Fusion* –, Random House, New York, 1993. ISBN 0-394-58456-2.
- [Trimble 1975] V. Trimble, “The Origin and Abundances of the Chemical Elements,” *Rev. Mod. Phys.*, **47**, No. 4, pp. 877 – 975 (1975).
- [Ulmann 1990] M. Ulmann, J. Liu, J. Augstynski, F. Meli and L. Schlapbac, “Surface and Electrochemical Characterization of Pd Cathodes after Prolonged Charging in LiOD + D₂O Solutions,” *J. Electroanal. Chem.*, **286**, pp. 257 – 264 (1990), ISSN: 1572-6657.
- [Voelkl 1978] J. Voelkl and G. Alefeld, “Diffusion of Hydrogen in Metals,” G. Alefeld and J. Voelkl Ed., *Hydrogen in Metals I*, Springer, Berlin, 1978, pp. 321 – 348 (1978), ISBN 978-3-662-30846-2.
- [Wicke 1978] E. Wicke and H. Brodowsky, “Hydrogen in Palladium and Palladium Alloys,” in J. Voelkl and G. Alefeld Ed., *Hydrogen in Metals, II*, Springer, 1978, pp. 73 – 155, ISBN 0-387-08883-0.
- [Wikipedia Catalysis] <https://en.wikipedia.org/wiki/Catalysis>
- [Woodbury 1970] J.W. Woodbury, S.H. White, M.C. Mackey, W.L. Hardy and D.B. Chang, Chapter 11 “Bioelectrochemistry,” pp. 903 – 983, in *The Mechanism of Deposition and Dissolution of Metals, in Physical Chemistry – An Advanced Treatise* –, Vol. **IXB**/Electrochemistry, Ed. Henry Eyring, Academic Press, N.Y and London, 1970, Library of Congress Catalog Card Number: 66-29951.

[Yamaguchi 1993] E. Yamaguchi and T. Nishioka, "Direct Evidence for Nuclear Fusion Reactions in Deuterated Palladium," *Proc. ICCF3*, pp. 179 – 188 (1993), ISBN 4-946443-12-6.

[Yuhimchuk 1992] A.A. Yuhimchuk, V.I. Tichonov, S.K. Grischechkin, et al., "Registration of Neutron Emission in Thermocycle of Vanadium Deuterides," (in Russian) *Kholodnyi Yadernyi Sintez*, p. 57, ed. R. N. Kuz'min, *Sbornik Nauchnykh Trudov* (Kariningrad) 1992. (cf. [Kozima 1998 (Sec. 8.2)])

Cold Fusion Phenomenon in the Compound CF Materials

– Effects of Interfaces –

Hideo Kozima*

Cold Fusion Research Laboratory <http://www.kozima-cfml.com/>

597-16Yatsu, Aoi, Shizuoka, 421-1202 Japan

*Corresponding author: hjrfq930@ybb.ne.jp

Abstract

Using our TNCF model composed in a phenomenological approach, we investigated the cold fusion phenomenon (CFP) observed in the compound (combined) CF materials, the CF materials composed of host elements (Pd, Ni, C, etc.) and hydrogen isotopes (H and/or D) with solid-solid, solid-liquid, solid-gas and solid-plasma interfaces. The CF materials are surrounded by an environment composed of a gas, a liquid or by plasma according to the experimental condition to feed a hydrogen isotope into it. A CF material, therefore, has inevitably an interface dividing itself from the environment. Sometimes, a CF material has a solid-solid interface between a substrate or solid-solid interfaces between layers intentionally imposed to it.

In this paper, we use the TNCF and ND models, which we have used successfully to give a unified explanation of various kinds of experimental data sets obtained in a great variety of CF materials hitherto, to investigate and deduce explanations of the specific experimental data obtained in these compound CF materials with various structures. Some characteristics and specific features of the CFP observed in these compound CF materials have been explained for the first time. In the investigation, we noticed especially the important effect of the interfaces on the CFP.

The interfaces are classified into four types which have specific influences on the CFP respectively, solid-solid, solid-liquid, solid-gas and solid-plasma interfaces. The physics and chemistry of the atomic processes in the solid-liquid interface have been investigated intensively in electrochemistry for many years. The characteristics of the catalytic action found in the solid-liquid interfaces must have common characteristics to those in other interfaces and we must give more attention to them in the investigation of the CFP in the compound CF materials. It is regrettable that we have almost ignored its importance until now even if there were some electrochemists who had given their attention to this phase of the CFP in the early days in this field.

The fundamental problems related to the premises of our models in relation to the existence of the interfaces in the compound CF materials will be developed in another paper presented in this Conference.

Contents

1. Introduction
2. Brief Review of the Fundamental Works in Relation to the Compound CF Materials
3. Effects of Catalytic Action on the CFP
4. Experimental Data in the Compound CF Materials – Size and Interface Effects
5. Conclusion

Appendices

- A1. Experimental Data Sets Analyzed by the TNCF Model [Kozima 1998, 2006]
- A2. Nuclear Reactions at Interfaces – 1. Experiments by Srinivasan et al. [Srinivasan 1990]
- A3. Nuclear Reactions at Interfaces – 2. Experiments by Claytor et al. [Claytor 1991a, 1991b, 1993, 1996, 1998, Tuggle 1994]
- A4. Experiments by Celani et al. on Coated Constantan Wires at the Elevated Temperature [Celani 2010 – 2020b]
- A5. Science and Philosophy – A Dialogue with Plato – [Plato Phaedo]

1. Introduction

In our long history of the investigation of the CFP, we have postponed until now the investigation of the CFP in two kinds of CF materials, (1) the composite materials and (2) the compound materials. The CF materials (1) and (2) have rather complicated structure than those investigated in our works presented until 2019. Recently, there have been many works on these CF materials (1) and (2) from a rather application-oriented point of view than on the CF materials with simple host elements investigated in the early stages of this field where were more works from the science-oriented point of view. About the relation between the two points of view, we will give a short discussion in Appendix A7 in this paper.

In the experiments with application-oriented point of view, it is apt to occur the experimental conditions are not necessarily determined with scientific rigor but altered easily to find out better results in the assumed object. This is another reason we had to leave these experimental data outside of our investigation until now. After successful establishment of our phenomenological approach to the CFP, we now take up experimental data in the composite and compound CF materials and investigate them by our models taking into our consideration the characteristics of their structure, especially the nature of interfaces which had been investigated in the electrochemistry for more than

a half century.

It should be noticed, as we have noticed in another paper presented at this Conference [Kozima 2021a], that the interfaces have been inevitable parts of any CF material and they are classified into four types: the solid-solid, solid-liquid, solid-gas and solid-plasma interfaces. The second type has been investigated most extensively in the electrochemistry [Bockris 1970a, 1970b, Horiuti 1951, 1970, Kita 1971, 1973] but other types are also important in the CFP. It is, however, probable that the characteristics of the solid-liquid interface investigated in the electrochemistry are common, at least partially, to other interfaces, solid-solid, solid-gas and solid-plasma interfaces, and are very important in our research on the CFP in the compound CF materials. This problem will be investigated specifically in the forthcoming paper [Kozima 2021c].

In this paper, we investigate characteristics of the experimental data obtained in the compound CF materials and explain them on the TNCF model leaving the composite CF materials to another paper presented in this Conference [Kozima 2021a]. The investigation of the applicability of our models, the original TNCF model and the Neutron Drop model, to the composite CF materials is given in another paper presented at this Conference [Kozima 2021b].

It should be mentioned at first that the characteristic of our investigation of the events in the CFP in the composite and compound CF materials is rather deductive than inductive which was used in the research hitherto (e.g. [Kozima 1998, 2019a, 2019b]).

It is also necessary to notice the effects of catalytic action on the CFP which we had to postpone taking it into our consideration hitherto. The elaborate investigations of the hydrogen electrode reaction (HER) (e.g. [Kita 1971, 1973, Horiuti 1976]) have shown complex but interesting features of the reaction $2\text{H}^+ + 2\text{e}^- \rightleftharpoons 2\text{H}$ on the transition metal electrode.

The effects of the solid-solid, solid-liquid, solid-gas and solid-plasma interfaces on the CFP must be investigated more seriously even if the interesting phenomena in relation to the second interface had been investigated in the electrochemistry (cf. e.g. [Bockris 1970a, 1970b, Horiuti 1970]). It is very interesting to notice several correspondences between the HER and the CFP (cf. [Kita 1971, 1973, Horiuti 1976]) and to investigate the relation between them from our point of view. Several features of the relation between HER and CFP in addition to the general effects of the chemical reactions at interfaces on the CFP will be investigated elsewhere [Kozima 2021c].

We point out here its importance in relation to the processes for the realization of the CFP:

- (1) *Adsorption of hydrogen isotopes H/D on the surface of a host material* including appropriate elements X. ← In the solid-liquid interface, there is a catalytic action of the hydrogen electrode reaction ($2\text{H}^+ + 2\text{e}^- \rightleftharpoons \text{H}_2$) on the host material = A kind of catalysis.
- (2) *Absorption and occlusion of the hydrogen isotopes* into the material to form the CF material where the proton/deuteron wavefunctions extend from the interstitial site out over the neighboring lattice points. ← Super-diffusion of hydrogen isotopes in the host material.
- (3) *Formation of the superlattice* of XH/XD by the self-organization as a process of complexity in non-equilibrium condition.
- (4) *Generation of the neutron energy bands* by the super-nuclear interaction among neutrons in different lattice nuclei mediated by the interstitial protons/deuterons.
- (5) Accumulation of neutrons in the neutron bands (the *trapped neutrons*) and formation of the *cf-matter* containing the trapped neutrons and the neutron drops ${}^A_Z\Delta$, composed of Z protons and $(A - Z)$ neutrons, in the CF material where the superlattice is formed [Kozima 2006 (Sec. 2.4.2)].
- (6) *Realization of nuclear reactions* between the trapped neutrons (neutrons in the neutron bands) or the neutron drops and nuclei at disordered sites on and in the CF material.

Let us review the nuclear reactions related to the CFP. Reactions supposed by Fleischmann et al. [Fleischmann 1989, Kozima 2019c]



The branching ratios of these reactions have been determined in the nuclear physics as $1 : 1 : 10^{-7}$ down to low energies of a few keV. The gamma in Eq. (1.3) in free space should be read as ϕ 's (phonons excited by the reaction in contact with trapped neutrons) in the CF materials.

Unified Explanation of the CFP by the Phenomenological Models – the TNCF model and the Neutron Drop Model [Kozima 1994, 1997, 1998, 2000, 2006, 2019a, 2019b]

The phenomenological approach using the trapped neutron catalyzed fusion model (TNCF model) has shown its effectiveness to give a unified consistent explanation of the experimental data sets with full of variety in the kinds of the CF materials and in the

observed physical quantities [Kozima 1994, 1998, 2006]. The *trapped neutrons* with a density n_n , one of the key premises of the model [Kozima 1994] has been extended to the neutrons in the neutron energy bands formed by the super-nuclear interaction between neutrons in lattice nuclei in the superlattice made of host elements and hydrogen isotopes.

The name “*the trapped neutron*” will be used throughout this paper to call neutrons in the original meaning in the early papers [Kozima 1994, 1998] and neutrons in the neutron energy bands in the recent papers [Kozima 2006, 2019b]. The brief explanation of the TNCF model is given in another paper presented in this Conference [Kozima 2021b (Appendix A2)].

For the convenience of our discussion in this paper, we cite nuclear reactions between light nuclei.

Reactions in free space related to the TNCF model [Kozima 1997]:

$$n + p = d (1.3 \text{ keV}) + \gamma (2.2 \text{ MeV}). \quad (1.4)$$

$$n + d = t (6.98 \text{ keV}) + \gamma (6.25 \text{ MeV}). \quad (1.5)$$

$$n + {}^6_3\text{Li} = t (2.7 \text{ MeV}) + {}^4_2\text{He} (2.1 \text{ MeV}), \quad (1.6)$$

$$t + d = {}^4_2\text{He} (3.5 \text{ MeV}) + n (14.1 \text{ MeV}), \quad (1.7)$$

$$n + d = n + p + n, \quad (1.8)$$

$$\gamma + d = p + n. \quad (1.9)$$

The gammas in the reactions (1.4) and (1.5) in free space should be read as φ 's (phonons excited in the CF materials by the fusion reactions in contact with trapped neutrons).

The fusion cross sections for the reactions (1.4) and (1.5) σ_{n-p} and σ_{n-d} in free space are given as 3.22×10^{-1} and 5.5×10^{-4} barns, respectively.

$$\sigma_{n-p} = 3.22 \times 10^{-1} \text{ barns}, \quad (1.10)$$

$$\sigma_{n-d} = 5.5 \times 10^{-4} \text{ barns}. \quad (1.11)$$

In this investigation, we must take into our consideration the subtle effect of the catalytic nature of the key elements such as Pd, Ni and Ti on the formation of the CF materials. The effects of the electrodes on the hydrogen reactions at their surface region have been extensively investigated in electrochemistry as the hydrogen electrode reaction (e.g. [Kita 1971, 1973]), On the other hand, this factor of the key elements has not investigated carefully in the cold fusion experiments and its detailed consideration will be given in near future. We will give our attention on the catalytic action of host elements including the properties of the hydrogen electrode reaction (HER) in the CFP in this paper and give an extensive consideration on the effects of the catalytic action on the CFP in

another work [Kozima 2021c].

Perhaps it is redundant to give a word on the electrons in the CF materials. We assume the electric neutrality of the system is fulfilled automatically even if we did not refer it at all explicitly in our description of the experimental data thitherto. It is possible that the state of electrons in the CF material influence the CFP in some way, but we did not care about them. We might take them into our consideration if we need it to do so in future.

2. Brief Review of the Fundamental Works in Relation to the Compound CF Materials

In this section, we give a brief review of our treatment of the CF materials [Kozima 1998, 2006], especially putting emphasis on the compound materials formed unintentionally or artificially in the experiments. It should be noticed that there are always interfaces around a CF material in our experiments the existence of which we could ignore as far as the cf-matter is formed by any means that is the direct object of our investigation in relation to the CFP. There are, however, various effects related to the existence of the interfaces which we will take up in this paper and investigate them from our point of view.

In this Section, we point out the characteristics of the effects induced by the interface and leave detailed discussions to Section 4.

2.1 The CFP in the CF materials with interfaces

In this subsection, we cite works related to the compound characteristics involved in the work not taken up in our analyses given before.

In the early times of the CF research, Srinivasan et al. made extensive investigation on the solid-gas/plasma system with Ti and D₂ and detected generation of tritium concentrated in highly localized spots (fraction of a millimeter or less in size) near the surface of the Ti sample each containing typically about 10¹² to 10¹⁴ atoms (2 to 200 kBq) of tritium [Srinivasan 1990]. They also determined the ratio of neutron/tritium production as low as in the range of 10⁻⁸ to 10⁻⁹. Analysis of the data obtained by Srinivasan et al. [Srinivasan 1990] is given in Section 4 and in Appendix A2.

At almost the same time, Bockris et al. [Bockris 1990] observed a massive production of tritium at a Pd electrode. They also determined the ratio of neutron/tritium production as low as $\sim 10^{-8}$ in accordance to the result obtained by Srinivasan et al. [Srinivasan 1990]. Analysis of the data obtained by Bockris et a. is given in Section 4.

The investigation of the tritium generation with various metals had been investigated by Romodanov et al. [Romodanov 1993] (cf. Appendix A4 in [Kozima 2021a]) in the glow discharge experiment with deuterium gas and obtained very small neutron/tritium

ratios like those obtained by Srinivasan et al. [Srinivasan 1990] and Claytor et al. [Claytor 1991b] (cf. Appendix A3).

Nuclear reactions in the CF material have been investigated by Szpak et al. [Szpak 1991, 2011] with a specific CF material devised by them, the codeposited PdD on the Cu substrate. There are two problems in the experiments by Szpak et al., one is the problem of the interfaces with the Cu substrate and with the electrolyte solution of the codeposited PdD and the second is the structure of the PdD_x. The former will be taken up in Section 4 and the latter in another paper [Kozima 2021a].

In the early days of the CF research, Claytor et al. in the Los Alamos National Laboratory had given extensive investigation on the CFP in various CF materials including composite and compound systems. A part of their works had been introduced in our book already [Kozima 1998 (Sec. 6.4c)]. Their results on the Pd alloys [Claytor 1998] was introduced in another paper presented at this Conference [Kozima 2021a (Section 4.1.3)] and experiments on various types of compound CF materials will be summarized in Section 4.5 and in Appendix A3.

It should be noticed a comment by M. McKubre, an excellent electrochemist, on the effect of some unknown elements on the CFP. He had written as follows:

“This observation raises the interesting possibility that one or more species, other than deuterium, are required to be present in the cathode to observe excess power, species which are not present initially and are thus required to diffuse into the cathode, presumably from the electrolyte. Analyses of used cathodes have revealed the presence of several light elements in the near-surface region (to a depth of several microns); in particular, lithium.” [McKubre 1993 (p. 18)]

This comment may be related to the reaction (1.6) which produces a triton with an energy $\varepsilon = 2.7$ MeV and then a neutron by the reaction (1.7):



The cross section σ_{t-d} of the reaction (1.7) depends strongly on the energy ε of the triton and is given as 3.0×10^{-6} b ($\varepsilon = 6.98$ keV) and 1.4×10^{-1} b ($\varepsilon = 2.7$ MeV).

$$\sigma_{t-d} = 3.0 \times 10^{-6} \text{ b } (\varepsilon = 6.98 \text{ keV}), \quad (1.12)$$

$$= 1.4 \times 10^{-1} \text{ b } (\varepsilon = 2.7 \text{ MeV}). \quad (1.13)$$

The reaction (1.6) and then (1.7) works to heat and feed neutrons to the CF material, in this case PdD_x, to prepare the necessary conditions for the CFP.

It is interesting to notice that Campari et al. has confirmed the surface nature of the nuclear transmutation in CF materials made of alloys [Campari 2004]. Their conclusion had declared it clearly as follows:

“To correctly compare the components of the alloy, we note that the changes are essentially on the surface, i.e., at most in the first μm . This fact is confirmed by the elemental analysis performed in the central region showed in Fig. 5c, which is identical to an analysis of the *blank*.” [Campari 2004 (p. 417)]

It will be not useless to cite the results of our phenomenological approach on the relation of the “Relations between Observed Values of Physical Quantities” and the surface nature of the nuclear reactions.

According to the theoretical investigation, relations between observed values of physical quantities [Kozima 1998 (p. 150), 2006 (p. 76)]

$$N_Q \approx N_t \approx 10^7 N_n. \quad (1.13)$$

In the above relations, N_x is the observed number of observable x where N_Q is defined as $Q \text{ (MeV)}/5 \text{ MeV}$ for the observed value of excess energy.

Surface nature of nuclear reactions in the CFP had been noticed already in our works cf. e.g. [Kozima 1998 (Sec. 12.16), 2006 (Sec. 2.2.1.), 2011a].

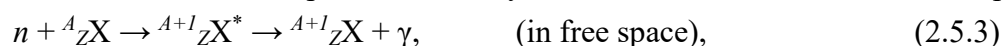
Summary of the analyses of the experimental data by the TNCF model is given in Appendix A1. Recognition of the value of the phenomenological approach using the TNCF model is traced historically in another paper presented in this Conference [Kozima 2021a (Appendix A1)]. It is interesting to notice that very few of CF researchers expressed their favor to the phenomenological approach as seen there.

2.2 Nuclear Reactions between the Trapped Neutrons and Host Elements at Boundaries and Surfaces

Interaction of the neutron Bloch wave and Elements occurs effectively at disordered positions in the CF materials.

Gamma ray spectrum have not usually observed in the CFP experiments. This fact is explained in our TNCF model as follows; in the CF materials, there formed the superlattice of the host element and the hydrogen isotope where the nuclei of the host element and the protons/deuterons of the hydrogen isotope are interacting with the strong nuclear force. Therefore, the transmuted nuclei by the neutron-host nucleus interaction decay not by gamma radiation as in the free space but by phonon emission (dissipation of energy to lattice) as we sometimes written down as follows.

The familiar neutron absorption reaction by a nucleus ${}^A_Z\text{X}$ known in the nuclear physics



is replaced by a reaction written down as follows,



where ϕ 's represents phonons generated in the reaction in the CF material.

2.3 Recognition of the importance of surface states

It has been long recognized the importance of the surface state of the sample on the CFP as we cite several papers on this problem in this Subsection.

2.3.1 Experimental data by Castagna et al. [Castagna 2012]

“The reproducibility of anomalous excess heat production during electro-chemical deuterium permeation of Pd cathodes has been recently observed¹ to be strongly correlated with the palladium surface properties (easy loading at low current, crystal grain distribution, crystallographic orientation, and surface morphology). The understanding of the physical mechanism that is responsible for such observed correlation is very challenging and it is complicated further by the fact that the different features are not, in principle, independent each from the other. In this work, the experimental results concerning the correlation of the excess heat production with the cathode surface properties are reviewed and some possible connections of the observed effects with the deuterium kinetics inside the palladium and the electromagnetic interactions at the metal/electrolyte interface are discussed.” [Castagna 2012 (p. 444, Abstract)]

[1] [Violante 2008]

“The cathode’s surface morphology seems to be a crucial parameter in controlling the anomalous excess heat reproducibility. Different mechanisms can be imagined explaining the experimentally observed dependence of the excess heat results on the cathode surface status. - - - This mechanism (the correlation between the surface morphology and the excess heat production) should be considered when the electrochemical kinetics at the cathode is considered, in the case of nano-structured cathode surfaces.” [Castagna 2012 (pp. 449 – 450, Conclusions)]

2.3.2 Experimental Data Sets by Celani et al. [Celani 2010 – 2020b]

Celani et al. have worked on the coated Constantan wires with the solid-gas and solid-solid interfaces mainly in H_2 gas for more than 10 years with a definite object to cultivate CF materials with low costs applicable for a new energy source [Celani 2010 – 2020b].

Their investigation in these works has been one of the main objects of science in modern world as we analyzed it before [Kozima 2017]. We investigate their works in detail in Subsection 4.4.7 and Appendix A4 and give only a brief introduction to them in this Subsection.

They used Ni instead of Pd for its low cost and its congeniality with H₂. They effectively used the CF materials based on the Constantan (Cu₅₅Ni₄₄Mn₁) which are the alloys composed of an element Ni which has been known as a CF material itself and another Cu which is an active element from our classification described in another paper presented in this Conference [Kozima 2021a (Sec. 4.1.4)]. In their experiment, they confirmed one of the necessary conditions, “nonequilibrium condition” for the realization of the CFP. Furthermore, they confirmed another characteristic of the CFP, the temperature effect for the occurrence of nuclear reactions using operating temperatures from 500 °C up to 900°C (e.g. [Kozima 2013 (Sec. 3.1), 2020]). It is interesting that they realized multi-layer samples in Pd experiments; the Pd wire was covered by sub-micrometric layers of several elements, Pd included. There are porous and very thin layers (like a *sponge*) *spontaneously developed* there and work effectively to realize the “anomalous heat effect” (AHE) according to their terminology which is the excess heat generation, an event in the CFP as we had shown in relation to the experimental data by Kitamura et al. [Kozima 2020] (cf. Appendix A4).

They have given the details of shapes and components of the CF materials in their experiments and we can use them to analyze the physics of the nuclear reactions occurring in them. We have given a brief explanation [Kozima 2011a] of the nuclear transmutations observed in a CF material in addition to the excess heat in one of their experiments [Celani 2010].

We cite several paragraphs below to show their intention of the experiments and variety of their CF materials [Celani 2010 – 2020b] leaving extensive introduction of their work to Appendix A4:

“Ni (under suggestion of Enel) was studied because low cost and, claimed (by F. Piantelli and recently also by S. Focardi-A. Rossi), working even with H₂. General approach of experiment was to use, as much as possible, the same overall materials, coatings (nano-materials, multilayer, two main kinds of materials) and measurement procedures as previously adopted for Pd wires by us.” [Celani 2010 (p.1)].

“The active volume (i.e., the thickness of sub-micrometric one): the thickness of active section is of the order of 10 – 30 μm. The main drawback in using wires with reduced

thickness is the tendency of the wire to break, in particular when the diameter is below 100 microns ($\Phi \leq 100 \mu\text{m}$).” [Celani 2019 (p. 1 Introduction and Motivation)]

“The hunted effect appears also to be increased substantially by depositing segments of the wire with a series of elements: Fe, Sr (via thermal decomposition of their nitrates) properly mixed with a solution of KMnO_4 (all diluted in acidic heavy-water solution).” [Celani 2019 (p. 1 Introduction and Motivation)]

2.4 Materials on/in Substrates

There have been used several CF materials deposited or codeposited on substrates of Cu and Si and other metals. The extensive experiments by Miley et al. [Miley 1996a, 1996b] are classified to this case where Pd and/or Ni thin films were deposited on a polystyrene or glass bead. Their works are extensively explained in another paper presented at this Conference [Kozima 2021b (Appendix A10)]. Recently, Kitamura et al. [Kitamura 2018] developed the CF material composed of Pd-Ni alloys on the stable solid materials such as silica (SiO_2) and zirconia (ZrO_2) which are investigated in another paper presented at this Conference [Kozima 2021a (Appendix A6)].

2.4.1 Codeposited PdD Films on Cu Foil [Szpak 1991]

Szpak et al. used a specific CF material, the codeposited PdD_x films on the Cu foil, to obtain effective positive results for the CFP.

“Two types of working electrodes were constructed. The first, Fig. 1, illustrates the arrangement for excess enthalpy measurements. Here, a copper foil, ca 4.0 cm² in area and 0.02 cm thick, attached to a glass tube, served as the cathode. - - -The codeposition occurred from a solution of 0.05 M PdCl_2 (Aldrich) and 0.3 M LiCl (Mallinckrodt) dissolved in a 99.9% pure D_2O (Merck) under potentiostatic control (AMEL model 553). [Szpak 1991 (p. 255)]

Further explanation of the data obtained by Szpak et al. is given in Sec. 4.4.3.

2.4.2 Pd/Si Stacks [Claytor 1991a, 1991b]

Claytor et al. had measured the tritium and neutron productions in palladium and silicon stacks when pulsed with a high electric current.

“ Evidence has been found for tritium and neutron production in palladium and silicon stacks when pulsed with a high electric current. These palladium-silicon stacks consist of alternating layers of pressed palladium and silicon powder. A pulsed high electric current is thought to promote non-equilibrium conditions important for tritium and

neutron production.” [Claytor 1991a] (Confer Appendix A3 for farther explanations on the palladium and silicon stacks.)

2.5 Thin films [Miley 1994, 1996a, 1996b] (Appendix A4)

Miley et al. had given elaborate experiments on the Pd, Ti, and Pd/Ti thin films on plastic and glass beads measuring very interesting results of nuclear transmutations with various new elements with large differences of the nucleon A and proton Z numbers from those existed in the system before experiments [Miley 1994, 1996a, 1996b]. Our preliminary analyses of their results had been given already in our papers and books (cf. e.g. [Kozima 1998 (Sec. 11.11h), 2006 (Sec. 2.5.3, Appendix C6)]. Their remarkable and extensive experimental data are summarized and analyzed in another paper presented at this Conference [Kozima 2021b (Appendix A10)].

3. Effects of Catalytic Action on the Cold Fusion Phenomenon

It has been known well that the catalytic action has tremendous effects on the chemical reactions. And it is also well known that the electrolysis is a chemical reaction, and the catalysis is working in its process giving decisive influences on the process in various manner. The hydrogen electrode reaction (HER) is the most important catalytic action influencing the electrolytic process of hydrogen desorption, absorption, and occlusion into the CF materials even if the HER itself is not well understood in the electrochemistry, yet. The investigation of the HER itself will be investigated thoroughly in relation to the CFP in another paper [Kozima 2021c].

Anyway, the HER has been remarked as an important factor for the realization of the CFP from the early days of this field.

3.1 Catalytic Action

We give summary of a fundamental characteristics of the catalytic action in this section to understand the experimental data obtained in the compound CF materials using properties of the relevant catalytic action as shown in the later sections. Main sources of the explanation are from Wikipedia [Wikipedia Catalysis].

3.1.1. Heterogeneous catalysis

“Heterogeneous catalysts act in a different phase than the reactants. Most heterogeneous catalysts are solids that act on substrates in a liquid or gaseous reaction mixture. Important heterogeneous catalysts include zeolites, alumina, higher-order oxides, graphitic carbon, transition metal oxides, metals such as Raney nickel for hydrogenation,

and vanadium(V) oxide for oxidation of sulfur dioxide into sulfur trioxide by the so-called contact process.” [Wikipedia Catalysis (p. 5)]

3.1.2. Active sites

*“A heterogeneous catalyst has **active sites**, which are the atoms or crystal faces where the reaction actually occurs. Depending on the mechanism, the active site may be either a planar exposed metal surface, a crystal edge with imperfect metal valence or a complicated combination of the two. Thus, not only most of the volume, but also most of the surface of a heterogeneous catalyst may be catalytically inactive. Finding out the nature of the active site requires technically challenging research. Thus, empirical research for finding out new metal combinations for catalysis continues.” [Wikipedia Catalysis (pp. 5 – 6)]*

3.1.3. Cooperative catalysis

“1. Cooperative catalysis: two or more catalysts cooperate in a catalysis.” [Wikipedia Catalysis (pp. 6)]

3.1.4. Supported catalysis.

Supported catalysis; a catalyst is supported by supports.

“Heterogeneous catalysts are typically “supported,” which means that the catalyst is dispersed on a second material that enhances the effectiveness or minimizes their cost. Supports prevent or reduce agglomeration and sintering small catalyst particles, exposing more surface area, thus catalysts have a higher specific activity (per gram) on a support. Sometimes the support is merely a surface on which the catalyst is spread to increase the surface area. More often, the support and the catalyst interact, affecting the catalytic reaction. Supports can also be used in nanoparticle synthesis by providing sites for individual molecules of catalyst to chemically bind. Supports are porous materials with a high surface area, most commonly alumina, zeolites or various kinds of activated carbon. Specialized supports include silicon dioxide, titanium dioxide, calcium carbonate, and barium sulfate.” [Wikipedia Catalysis (p. 6)]

3.2 Effects of Electrolyte and Interfaces on the CFP

In the early days of the research on the CFP, the effects of electrolytes and impurities in electrolytic experiments had been investigated often.

“The absorption of hydrogen and deuterium in Pd, at potentials positive to hydrogen evolution, was studied by cyclic voltammetry. Results in 0.1 M NaOH, LiOH and LiOD

were compared. In LiOH hydrogen ingress into Pd is faster than in NaOH. However, hydrogen egress is inhibited. In LiOD all processes are slower than those in LiOH.” [McBreen 1990 (p. 279, Abstract)]

It was shown that addition of a very small quantity of cyanide into the electrolytic solution had resulted in several major effects on the behavior of the electrolysis.

“Addition of 10^{-3} M CN^- to these electrolytes resulted in several major effects. The formation of the oxide and the ingress of hydrogen and deuterium were inhibited. Egress of hydrogen and deuterium from Pd was essentially completely inhibited until the adsorbed cyanide was displaced by oxide at positive potentials. Hydrogen permeation measurements through Pd membranes were made in 0.1 M NaOH and in 0.1 M NaOH + 10^{-3} M NaCN. Cyanide adsorption decreased the permeation rate and had large effects on the permeation decay transients.” [McBreen 1990 (p. 279, Abstract)]

Ulmann et al. had shown the large effects of contamination of a Pd cathode on the electrolysis.

“One of the typical characteristics of the hydrogen evolution reaction is its extreme sensitivity to various impurities present in the solution. - - - We showed recently [3] that the contamination of a palladium cathode, polarized in LiOD + D_2O solution, with lead and more so with zinc leads to the buildup of very large over voltages for D_2 evolution. In the present communication, we describe the results of surface analyses for a series of Pd electrodes used as cathodes in the D_2O electrolysis cells run for up to 34 days.” [Ulmann 1990 (p. 257, Abstract)]

[3] J. Augustynski, M. Ulmann and J. Liu, *Chimia*, **43**, p. 355 (1989).

Recently, Celani et al. had shown the characteristic catalytic effect of a solid-solid interface (an interface between a porous, thin film and a CF material (Pd wire)) on the absorption of hydrogen isotopes into the CF material [Celani 2010] (cf. Appendix A4).

“The Pd wire was covered by a sub-micrometric layer of several elements, Pd included. Because the spontaneous developing of such porous and very thin layer (like a sponge) the characteristics of D_2 absorption changed dramatically and the loading time was reduced of several order of magnitude (from hours to minutes) even, and specially, at low current density of electrolysis (about 10-20 mA/cm²).” [Celani 2010 (p. 10, Origin of new INFN-LNF procedure.)]

4. Experimental Data in the Compound CF Materials – Size and Boundary Effects

It is necessary to give a conventional comment on the ubiquitous existence of the

interfaces in the experimental system even if we have almost ignored it in our investigation of the CFP thitherto [Kozima 1998, 2006, 2019b]. We have taken up for the first time the specific characteristics related to the composite structure in another paper [Kozima 2021a] and to the compound structure in this paper. The effects of the size and the boundary layer are briefly taken up in this section leaving several investigations to Appendices.

4.1 Explanation of the Experimental Data obtained in the Compound CF Materials where are Size and Interface Effect exist

We give brief explanations on the physics of the CFP occurring in the CF materials due to the existence of the interfaces.

4.1.1 Neutron-Nucleus interaction due to the disordered arrangement of nuclei at interface regions

It is a common knowledge that the electron Bloch wave is not scattered by atoms in a regular array. We cite a sentence to confirm the fact below not minding tedious citation. “(iv) Electrons are scattered by disturbances in the lattice periodicity; these processes can be treated by perturbation theory. Static imperfections cause elastic scattering, and thermal vibrations scatter with the emission or absorption of a phonon.” [Klemens 1960]

Similarly, the neutron Bloch wave does not interact with lattice nuclei at their regular site. Therefore, the nuclear reactions induced (or catalyzed) by the trapped neutron in the form of the Bloch wave occur when there are nuclei displaced from the regular site at around interfaces or by the thermal disturbance. This is a cause of the temperature effect on the CFP taken up recently in relation to the experiment by Kitamura et al. [Kitamura 2018, Kozima 2013 (Sec. 3.1), 2020].

4.1.2 Increase of the density of the trapped neutrons by the flow of neutrons from A to B components through the boundary layer

There is an effect of the compound structure on the increase of the neutron density (cf. [Kozima 2021b (Appendix A8)]).

4.2 Size Effects

It is possible to consider the positive size-effect on the H/D occlusion into the CF material with a host element X to make easy the formation of the superlattice of XH/XD by the self-organization (cf. e.g. [Kozima 2013]).

(a) **Microscopic particles**

Self-organization is easier in small-size samples as discussed above [Kozima 2013]. There are several experimental examples showing this fact [Reifenschweiler 1994, 1995, 1996, Arata 1996, Kitamura 2009]

In the cases of compound materials (artificially fabricated), we can expect some effects of the interfaces in the system as we investigate individually them below. [Yamaguchi 1993, 1998, Miley 1996a, 1996b, Iwamura 2006a, 2006b, Kitamura 2018, Celani 2012 – 2020b]

(b) **Thin Films**

There are also several CF materials composed of thin films which show interesting positive effects on the CFP even if their analyses are difficult due to the complex structure [Miley 1994, 1996a, 1996b, Mizuno 1997, Kitamura 2018]. They will be investigated below.

4.2.1 Pt/Ceramics/Pt multi-layers where observed absorption of a neutron by $^{196}_{78}\text{Pt}$
[Mizuno 1997]

Mizuno et al, observed gamma ray spectra from Pd/Ceramics/Pt sandwich structure (Ceramics = $\text{Sr}_{1.0}\text{Ce}_{0.9}\text{Y}_{0.08}\text{Nb}_{0.02}\text{O}_{2.97}$) finding a new peak

“ Abstract-

A proton conductor, the solid state electrolyte, made from an oxide of strontium, cerium, niobium and yttrium can be charged in a hot D_2 gas atmosphere. Anomalous radioisotopes were detected in all samples charged with an alternating current with voltages ranging from 5 to 45 V, at temperatures ranging from 400 to 700 °C. No radioisotopes were detected from the sample treated in a H_2 gas atmosphere. The radioisotopes may be induced from a catalytic reaction between the metal and oxide interface to deuterium atoms.” [Mizuno 1997 (p. 23, Abstract)]

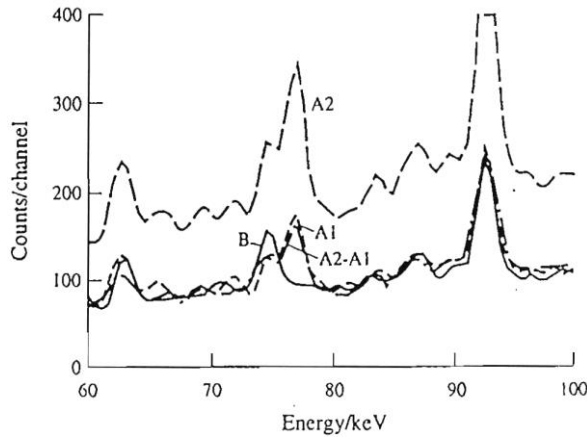


Fig. 4.1. Gamma ray spectra (B) before the electrolysis, (A1) after electrolysis accumulated from 0 to 24 h and (A2) accumulated from 0 to 48 h. The spectrum (A2 – A1) is the subtraction of (A1) from (A2). Gamma ray spectra were obtained by a 4 inches Ge (Li) detector in four shielded containers of 20 cm and 5 mm thick of Pb outer and Cu inner shields. A multichannel analyzer of 8000 channels was made to coincide to 0 – 4000 keV energy range. A gaussian window was fitted to calculation of the spectrum analysis. [Mizuno 1997 (Fig. 3)]

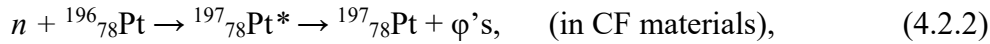
“A clear peak is shown in Fig. 3 (A1) and (A2) at 77 keV. The peak was obtained after electrolysis in a deuterium gas atmosphere. It was not observed with hydrogen gas. - - -. We performed the electrolysis with the same sample in deuterium gas followed by hydrogen gas: the ^{197}Pt peak was only observed with deuterium gas.” [Mizuno 1997 (p. 24)]

In the case of the experiment shown in Fig. 4.1, the Pt film on the proton conductor $\text{Sr}_{1.0}\text{Ce}_{0.9}\text{Y}_{0.08}\text{Nb}_{0.02}\text{O}_{2.97}$ is said to be very thin [Mizuno 1997]. It is then possible that the situation in the CF materials in this experiment is fairly different from the ordinary CF materials; in the ordinary CF materials, the connection between the host nuclei and the hydrogen isotope is very strong and the transmuted nucleus $^{197}_{78}\text{Pt}^*$ decay with the formula (A4.1) below, however in the CF material of the experiment [Mizuno 1997] the connection is not so strong and the transmuted nucleus $^{197}_{78}\text{Pt}^*$ was possible to decay with the formula (4.2.1) in addition to that with (4.2.2) below.

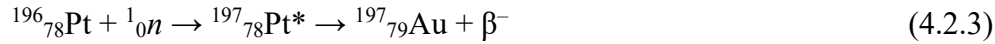
Because $^{197}_{78}\text{Pt}$ nuclei do not exist in nature and can be generated by the following reaction realized by the existence of the trapped neutron:



which is replaced by a reaction in the CF material written down as follows,



Then, the ${}^{197}_{78}\text{Pt}$ reacts with a trapped neutron to produce ${}^{197}_{79}\text{Au}$ by the following reaction:



4.3 Effects of Interfaces on the CFP

The surfaces of the CF materials are inevitably boundaries between the materials and the environments. In the case of the electrolytic systems, especially, the surfaces of the CF materials form intervening boundaries of the materials and the electrolytic liquids. There have been observed nuclear reactions between the trapped neutrons and elements in the boundary layers unintentionally formed on the surfaces. A theoretical explanation of the experimental data on the surface layers in the electrolytic systems had been given in our paper based on the TNCF model [Kozima 2003].

4.3.1 Importance of the Lattice Plane at the Interface

As we know from the research of the hydrogen electrode reaction (HER) [Kita 1971, 1973], the reaction activity of the electrode depends on the lattice plane of the electrode.

In the case of Pt, the adsorption rate depends strongly on the lattice plane. In the case of Ni, the activity of the electrode increases in the order of (100), (110) and (111) plane [Kita 1971] (cf. also Appendix A2).

“The adsorption rate of the lattice planes in Pt decreases from the maximum value for the lattice plane (110) to those of the lattice planes (100) and (111) gradually.” [Kita 1971 (p. 109)]

“In the case of the hydrogen electrode reaction (HER) in Ni, the reaction rates have a saturation current the value of which increases in order of (110), (100) and (111). In the current region where the Tafel law is applicable, the reaction rate from the plane (111) is overwhelming and the contribution from other planes is negligible.” [Kita 1971 (p. 113)]

Unfortunately, we have no data of the dependence of the activity on the lattice plane in the case of Ti. However, it is probable to assume that there is a similar dependence of the activity of the Ti electrode on the lattice plane of the electrode surface.

Then, we may be able to assume that there are differences of the super-lattice formation below the surface layer of the Ti electrode depending on the lattice plane facing to the interface (the solid-gas and solid-plasma interfaces in the experiments by

Srinivasan et al.). In the near-surface region under a surface where the most active lattice plane is facing the interface, the super-lattice TiD composed of the Ti and D sublattices is formed effectively and therefore the neutron energy bands are formed there to realize the CFP, the $n - d$ fusion reaction in this case.

This is the most probable cause of the localization of the tritium atoms observed by Srinivasan et al. [Srinivasan 1990]. A semi-quantitative analysis of the data obtained in the discharge experiment is given in Appendix A2.

We can illustrate several data below for the illustration of the importance of the surface layers for the occurrence of the CFP noticed from the early times of investigation without full explanations on their decisive roles on the nuclear reactions.

It should be noticed that the supposed importance of the surface layers had been felt by researchers from the early days of the CF research as we see in the sentences cited below:

“Even though the preparation and D₂ gas absorption methods evolved during this series, apparently most of the samples emitted excess neutrons. In contrast, a few very early samples from Ref. 1 contained unique materials, unknown surface contamination, and unknown bottle gas purity but gave some large bursts on successive LN (liquid nitrogen) cycles [1]. Such dramatic results are not easily reproduced. (Ref.1 [Menlove 1990c])”
[Menlove 1990b (p. 297)]

“ - - tritium is invariably concentrated in highly localized spots (fraction of a millimeter or less in size) each containing typically about 10¹² to 10¹⁴ atoms (2 to 200 K Bq) of tritium. - - - it is tempting to speculate that in these titanium samples perhaps some kind of a cascade reaction or micronuclear explosion probably occurs in specific sites in the near surface region resulting in 10¹⁰ to 10¹² fusion reactions during each event.”
[Srinivasan 1990 (p. 2)]

“In spite of the electrochemical approach taken by Fleischmann and Pons, most of the research hitherto has concentrated upon manifesting nuclear effects (neutron emission, tritium formation) and there has been little [1, 2] investigation of the situation of the surface chemistry of the palladium electrode, the mechanism by which molecular deuterium is formed or that by which adsorbed D diffuses inside the palladium, - and what its fugacity there would be. [1, 2] [McBreen 1990, Ulmann 1990]” [Bockris 1991 (p. 337, Introduction)]

“This observation raises the interesting possibility that one or more species, other than deuterium, are required to be present in the cathode to observe excess power, species which are not present initially and are thus required to diffuse into the cathode, presumably from the electrolyte. Analyses of used cathodes have revealed the presence of several light elements in the near-surface region (to a depth of several microns); in particular, lithium.” [McKubre 1993 (p. 18)]

4.3.2 Effects of Catalytic Action at Interfaces

We must notice the characteristics of the catalytic action as explained in an Encyclopedia as follows:

*“A heterogeneous catalyst has **active sites**, which are the atoms or crystal faces where the reaction actually occurs. Depending on the mechanism, the active site may be either a planar exposed metal surface, a crystal edge with imperfect metal valence or a complicated combination of the two. Thus, not only most of the volume, but also most of the surface of a heterogeneous catalyst **may be catalytically inactive**. Finding out the nature of the active site requires technically challenging research. Thus, empirical research for finding out new metal combinations for catalysis continues.” [Wikipedia Catalysis (p. 8)]*

Such Effects of the catalytic actions cited above had been noticed in relation to the CFP by several electrochemists, especially by Bockris et al. [Bockris 1990] and McKubre et al. [McKubre 1993]. They have expressed their expectation on the effects qualitatively putting their major interest in the first stage of the H/D occlusion in the CF materials. One or other characteristics of the catalysis seems to have close relation with the effective occlusion of hydrogen isotopes in the host material as suggested by Bockris et al. [Bockris 1990] and McKubre et al. [McKubre 1993] (cf. (1), (2) and (3) below).

The active sites may be formed by the dendrite formation [Bockris 1990] or by the one or more species in the cathode [McKubre 1993] as seen in the following sentences:

(1) On the dendrite formation as a catalytic site by Bockris et al.

“The rate of production of tritium was $c. 10^{10}$ atoms $cm^{-2} sec^{-1}$. The branching ratio of tritium to neutrons was $\sim 10^8$. A theoretical dendrite enhanced fusion model is suggested. Growing gas layer breakdown occurs at sufficiently high surface potential dendrite tips and correspondingly fusion reactions occur. The model gives quantitative consistence

with experiment, especially the sporadic nature and the observed branching ratio.”
[Bockris 1990 (p. 137, Abstract)]

(2) On the formation of active sites on the cathode by McKubre et al.

“As a possible solution to this problem, we have observed that the addition of small amounts (typically 200 ppm) of non-classical additives, such as aluminium or silicon (in metallic and oxide form, respectively), to the electrolyte, results in the ability to maintain high loadings for longer periods, without impeding the initial attainment of high loadings. In this context, it should be mentioned that, in cells which utilize glass components, silicon-containing species will accumulate in basic electrolytes over extended time periods.” [McKubre 1993 (p. 6)]

“This observation raises the interesting possibility that one or more species, other than deuterium, are required to be present in the cathode to observe excess power; species which are not present initially and are thus required to diffuse into the cathode, presumably from the electrolyte. Analyses of used cathodes have revealed the presence of several light elements in the near-surface region (to a depth of several microns); in particular, lithium.” [McKubre 1993 (p. 18)]

This comment by McKubre et al. may have connection with the work by Okamoto et al. [Okamoto 1994] described below in Sec. 4.3.4.

(3) Speculations on the mechanism of the CFP by Bockris et al. [Bockris 1991, 1993, 1994, 1995]

It will be helpful to read several expressions by Bockris et al. on the nature of the CFP prior to the investigation of their works in detail given in Section 4.4.2.

“If the obtained results are compared with previously published data for deuterium evolution on Pd^[2] it is then obvious that Pd deposition took place with simultaneous deuterium evolution at high overpotentials. Also, within the first 40-50 hours of electrolysis a highly dendritic layer of Pd was visible at the electrode and was approximately 2-3 mm thick.” [Bockris 1993 (p. 235, 3.2 Tritium produced on Pd co-deposited with deuterium)]

[2] [Bockris 1991]

“However, a successful theory must be consistent with the following:

- 1. The sporadicity of observation of the effects,*
- 2. Switch-on is dependent upon impurities in the solution, or the metal,*
- 3. Switch-on does not occur for times of the order of 100 hours of electrolysis.”* [Bockris

1994 (p. 79)]

“In experiments carried out recently in which hydrogen was electrolyzed from water in contact with a palladium electrode, the concentration and depth of impurities were measured as a function of electrolysis time. It was found that after 3 weeks, two different sets of impurities could be observed, one set within 50Å of the surface and another set different chemical spaces, about 1μ inside the metal.” [Bockris 1995 (p. 67)]

“The concentration of platinum found in the palladium, for example, rose to a maximum at about 8-11 Å from the surface and decreased exponentially so that by 50Å from the surface no further platinum could be seen. Similar concentration profiles were observed for silicon and zinc.” [Bockris 1995 (p. 67)]

4.3.3 Localization of Tritium Generation observed by Srinivasan et al. [Srinivasan 1990]

The experimental data obtained by Srinivasan et al. [Srinivasan 1990] shows a peculiar accumulation of generated tritium atoms at localized spots near surface region of the titanium sample as described in their Abstract:

“ - - tritium is invariably concentrated in highly localized spots (fraction of a millimeter or less in size) each containing typically about 10^{12} to 10^{14} atoms (2 to 200 K Bq) of tritium. - - - it is tempting to speculate that in these titanium samples perhaps some kind of a cascade reaction or micronuclear explosion probably occurs in specific sites in the near surface region resulting in 10^{10} to 10^{12} fusion reactions during each event.” [Srinivasan 1990 (p. 2)]

[Srinivasan 1990]

“One of the most interesting findings to emerge out of the autoradiographic imaging of deuterated Ti samples from different experiments is the fact that tritium is invariably concentrated in highly localized spots (fraction of a millimeter or less in size) each containing typically about 10^{12} to 10^{14} atoms (2 to 200 kBq) of tritium. If this is viewed in the light of the observations of other groups notably, the Los Alamos work, that neutrons are produced in bunches of 30 to 300 within time spans of microseconds and also that the neutron-to-tritium yield ratio is in the range of 10^{-8} to 10^{-9} , it is tempting to speculate that in these titanium samples perhaps some kind of a cascade reaction or micronuclear explosion probably occurs in specific sites in the near surface region resulting in 10^{10} to 10^{12} fusion reactions during each event. This intriguing possibility warrants further

experimental study.” [Srinivasan 1990 (pp. 1 – 2)]

Analysis of the data obtained by Srinivasan et al. [Srinivasan 1990] is given in Appendix A2.

It is possible to identify the “specific sites in the near surface region” imagined in this paper with the localized superlattice of Ti at the lattice points and D at the interstices, in this case, self-organized by the process of complexity evolution of the cf-matter in the surface region [Kozima 2012]

It should be noticed that the lattice planes (110), (100) and (111) have the specific role for the hydrogen electrode reaction (HER) in Pt (cf. Sec. 4.3.1 and [Kita 1971, Horiuti 1976]) and accordingly for the absorption of deuteron to form the superlattice TiD₂ under the surface region. This situation might have close relation to the experimental data by Iwamura et al. [Iwamura 2000, 2006a, 2006b] where in addition to the HER noticed above the cooperative catalysis is taking a part in the nuclear transmutations observed there (cf. Section 4.4.5).

4.3.4 Nuclear Transmutations at the Surface Region of Pd Cathode [Okamoto 1994]

Distribution of minor elements in the Pd cathode used in a Pd/LiOD + D₂O/Pt system was determined by Okamoto et al. [Okamoto 1994] as shown in Fig. 4.2 (cf. also [Kozima 2006 (Sec. 2.5.1)]). The explanation of the distribution of minor elements observed by Okamoto et al. was given in the book [Kozima 2006 (Sec. 2.5.1)] on the TNCF model.

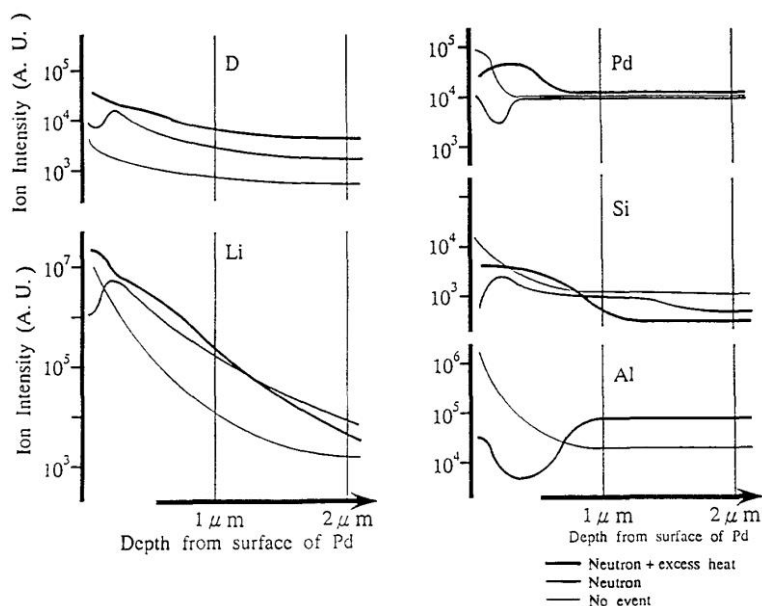


Fig. 4.2 Examples of Depth Profiles for Each Element [Okamoto 1994 (Fig. 1)]

“The examples of the depth profiles of D, Li, Pd, Si, and Al are illustrated in Fig.1. The profiles with bold line represent the depth profiles of each elements obtained from the Pd sample with the nuclear effect of neutron emission and excess heat generation, the medium line for Pd sample with only neutron emission, and the chain-line for Pd sample with no nuclear effect. The curves shown in these figures are normalized to the secondary ion intensity of Pd obtained in each analysis run to carry out the discussion on the concentrations on the same elements. Evidently from the figures, (1) the depth profiles of the elements with no nuclear effects are monotonous as expected from the electrochemical point of view. (2) While the depth profiles with some nuclear effects have some of irregular structures, especially in the surface within 2 μm for every element. The depth profiles of lithium and deuterium are very similar in each. This fact indicates that there is a very strong chemical relation between the lithium behavior and the deuterium behavior as discussed in the previous paper.” [Okamoto 1994 (p. 14-2)]

4.4 Effects of Artificial Boundaries

There are many boundaries established intentionally with some purposes to establish favorable conditions for the nuclear reactions in the CFP. Despite of the purposes assumed in the experiments; the boundary layers have common effects on the mechanism of the nuclear reactions from our point of view as explained below.

4.4.1 Experimental Results related to the Existence of Boundaries – Data by Yamaguchi et al.

Yamaguchi et al. [Yamaguchi 1993, 1998] had investigated the relation between the excess heat Q_{ex} and the ^4He production N_{He} to confirm the presumption assumed by Fleischmann et al. [Fleischmann 1989]. Their elaborate and precise experiments denied the presumed production of Q_{ex} and N_{He} without further investigation of causes of the CFP. In their experimental data, we can see interesting effects of the supported catalysis and interfaces as shown below.

The detection of the ^4He in a Pd-D system by Yamaguchi et al. has been one of the reliable experimental data (cf. e.g. [Kozima 2016 (Sec. 3.1)]) and it is interesting to investigate the meaning of the data as a whole. Schematic diagram of the measuring apparatus in the experiment by Yamaguchi et al. [Yamaguchi 1993] is shown in Fig. 4.3.

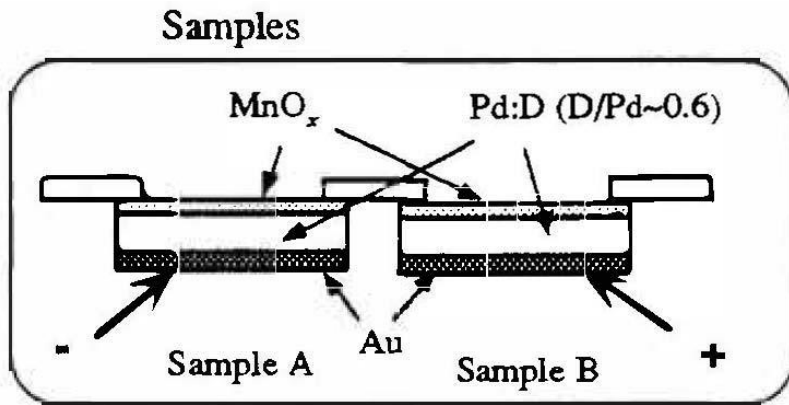


Fig. 4.3. Schematic diagram of the measuring apparatus (Sample part). [Yamaguchi 1993 (Fig. 1)]

“One side of these Pd:D surfaces is covered with a thick Au-film that prevents leakage of D atoms from that side, and the other side of the surface is covered with an oxide (MnO_x , SiO_x , or AlO_x) that provides a surface barrier to out-diffusing D atoms. A layer of D atoms therefore accumulates in the Pd near the Pd/oxide interface.” [Yamaguchi 1993 (p. 181)]

The experimental results of mass spectroscopy at nominal mass 4 for released gases are shown in Fig. 4.4.

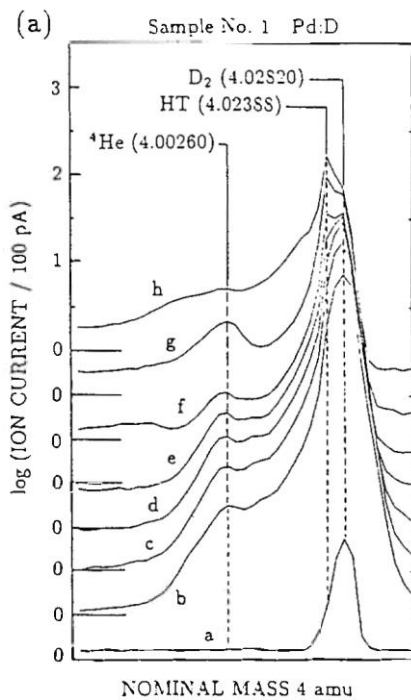
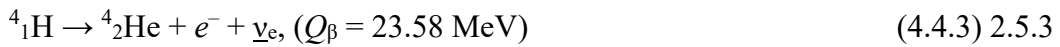


Fig. 4.4. The experimental results of mass spectroscopy at nominal mass 4 for released gases from (a) sample No. 1 where each spectrum was taken at every 72 min, for sample

No. 1, 28 min. for No. 2 and 3, and 55 min. for No. 4. [Yamaguchi 1993 (Fig. 3 (a))].

“In the final stages of ${}^4\text{He}$ production, a peak attributable to HT appears and increases with the time. Since there is also no background T in this system, this experiment also gives definite evidence for T production.” [Yamaguchi 1993 (p. 184)]

In the free space, the reactions (1) between a neutron n and a deuteron d or ${}^2_1\text{H}$ and (2) between a neutron n and a triton t or ${}^3_1\text{H}$ are written down as follows.



The cross sections for these reactions (4.4.1) and (4.4.2) are known as $\sigma_{n-d} = 0.519 \text{ mb}$ and $\sigma_{n-t} < 0.006 \text{ mb}$, respectively. Therefore, the experimental data shown in Fig. 4.4 is difficult to explain with the reactions depicted in Eqs. (4.4.1) and (4.4.2).

[How fast the beta decay of ${}^4_1\text{H}$ (3) occurs?]

However, the situation in the CF material differs very much from that of free space. The tritons generated in the reaction (4.4.1) displace the deuterons in interstitials in the CF material. They interact with lattice nuclei by the nuclear force as we assume in our model. Also, the trapped neutrons (the neutron Bloch waves in the neutron conduction band) interact strongly with disordered nuclei out of the ordered array of deuterons. The deuterons at around and in boundary regions are then responsible to the reaction (4.4.3') below displacing the 4.4.1) in the free space:



where φ 's represents phonons excited by the dissipated energy from the excited state of triton ${}^3_1\text{H}^*$ interacting with surrounding deuterons by the nuclear force. The triton generated thusly plays in this case as a disordered nucleus for the neutron Bloch wave and the reaction between them will be written down as follows with the cross-section unknown yet.



The interaction of an interstitial triton with neutrons in lattice nuclei is also expected to share a part of forces participating in the self-organization of the superlattice.

The tritons generated by the reaction (4.4.3') in the region where the density of the disordered deuteron is high will remain in the sample by the oxide barrier on the surface. On the other hand, the helium ${}^4_2\text{He}$ generated by the reaction (4.4.4) leaks out through the

MnO_x layer almost freely from the sample. The temperature of the sample will be elevated gradually by the liberated energy of the reactions (4.4.3). The tritons accumulated in the sample become more diffusible with temperature to escape from the sample. This may explain the experimental result that “In the final stages of ⁴He production, a peak attributable to HT appears and increases with the time.”

Speculation:

The same consideration is applicable to the protium system in addition to the deuterium system discussed above. In this case, the equation corresponding to Eq. (4.4.3') is the following Eq. (4.4.5),



In the experiment performed in Yamaguchi's work [Yamaguchi 1993], the deuterons generated in this reaction remain in the sample and the next reaction corresponding to Eq. (4.4.4) will be the Eq. (4.4.6),



The tritons generated in this reaction are fundamentally confined in the sample in this experiment not observed outside.

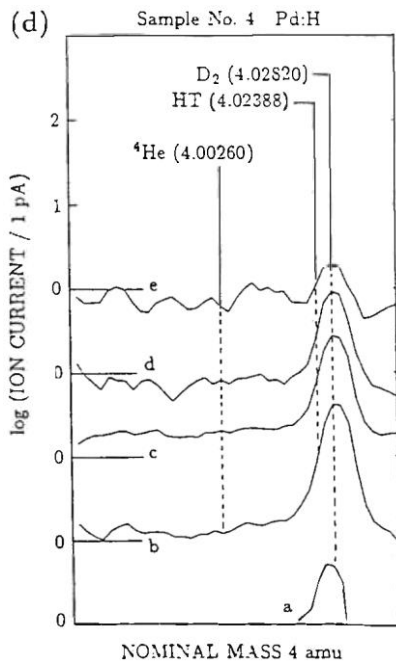


Fig. 4.5. The experimental results of mass spectroscopy at nominal mass 4 for released gases from (a) sample No. 1 where each spectrum was taken at every 72 min, for sample No. 1, 28 min. for No. 2 and 3, and 55 min. for No. 4. [Yamaguchi 1993 (Fig. 3 (d))].

Looking into the Fig. 4.5 ([Yamaguchi 1993 (Fig. 3 (d)), we notice the swelling of the point corresponding to HT (4.02388) in the curve a despite the authors' explanation cited below.

“The time-resolved mass spectra for experiment No. 4 (Pd:H), shown in Fig. 3(d), show only a single small peak at 4.02820 amu. This peak is due to D₂ contamination from the H₂ bottle or the inner wall of the chamber, or both. We can therefore conclude that Pd:H systems exhibit (neither) ⁴He production nor T production. This figure also shows that there is no background ⁴He in these experiments.” [Yamaguchi 1993 (p. 184)].

[Yamaguchi 1998]

The experiments in [Yamaguchi 1998] is a little different from that of [Yamaguchi 1993] in the sample geometry: the largest difference is the interchange of MnO_x layer by that of SiO₂ on the opposite side of PdD(H) to the Au coated side in 1998 experiments. By this difference of MnO_x layer, tritons produced by the $n + d$ fusion reaction (2.5.3) might dissipate, and the reaction (2.5.4) becomes ineffective to produce ⁴He in the 1998 experiment.

The difference of MnO_x in 1993 and SiO₂ in 1998 experiments may have a decisive effect on the physics of the CFP in each experiment if we notice the subtle effects of active site on the catalysis [Wikipedia Catalysis]. Thus, the null result reported in 1998 by Yamaguchi et al. [Yamaguchi 1998] is interesting but does not have direct correlation with the data obtained in 1993 [Yamaguchi 1993] as we see in the following sentences cited from the 1998 paper.

“Abstract

We report a recent progress on the experimental studies of excess power and the search for nuclear products from Pd:D/Au (Pd:H/Au) or SiO₂/Pd:D/Au (SiO₂/Pd:H/Au) heterostructures by the 'in-vacuo' method. The excess power generation correlated to the sample distortion was observed with 100 % reproducibility. The peak excess power was estimated as much as 8 W with the input being 0.1 W. The total amount of excess power was at most 39 kJ, indicating that the energy generated was of the order of 1 eV per D (H) atom. Nevertheless, none of the nuclear products was detected clearly. This result suggests that the highly reproducible excess power observed in the present experiment is correlated to the structural phase transition at the Pd surface. We discuss the origin of the anomalous heat generation within the condensed matter physics.” [Yamaguchi 1998 (Abstract)] (underlined at citation).

“A thin SiO₂ film with the thickness of 100 Å was then deposited on the other side of the surface for some samples.” [Yamaguchi 1998 (p. 421)]

“This plastic deformation always occurred within 10 seconds when the sample exhibited the maximal excess power. In both cases for **Pd:D/Au (No. 67)** and **Pd:H/Au (No.68)**, the sample was set on the Mo holder under the condition of free external force, i. e., the holder give no external stress to the sample.” [Yamaguchi 1998 (p. 422)]

“Therefore, we have to conclude that the observed ⁴He peak as shown in Ref. 4 may be an artifact due to ⁴He adsorbed at the sample surfaces. However, since the resolution of the mass spectrometer used in the present experiment is less than half of that used in the experiment in [4], future investigation must be needed to draw a definite conclusion for ⁴He production.” [Yamaguchi 1998 (p. 422)]

[4] E. Yamaguchi and T. Nishioka; *Proc. ICCF-3*, Nagoya, October 1992, p.179. [Yamaguchi 1993].

4.4.2 Experimental data by Bockris et al. [Bockris 1990]

To confirm the nuclear origin of the excess heat observed by many including the pioneering work by Fleischmann et al. [Fleischmann 1989], experiments had been performed to detect existence and amount of tritium in the experimental systems. One of the early reliable data confirmed the production of tritium was obtained in Texas A&M group [Packham 1989]. They obtained the data of neutron and helium isotopes also. They had shown the ratio of neutron and tritium amounts N_n/N_t is very small as $\approx 10^{-9}$ compared with the value ≈ 1 expected from the presupposed $d-d$ fusion reactions. The data of ⁴He was also expressed as $N_{He}/N_t \approx 10^{-14}$ where N_{He} is the number of ⁴He generated in the system when tritium number is N_t .

[Bockris 1990] (Section 4.3.2)

“The rate of production of tritium was *c.* 10^{10} atoms $cm^{-2} sec^{-1}$. The branching ratio of tritium to neutrons was $\sim 10^8$. A theoretical dendrite enhanced fusion model is suggested. Growing gas layer breakdown occurs at sufficiently high surface potential dendrite tips and correspondingly fusion reactions occur. The model gives quantitative consistence with experiment, especially the sporadic nature and the observed branching ratio.”

[Bockris 1990 (p. 137, Abstract)]

[Bockris 1993]

“An account is given of the massive production of tritium at a Pd electrode. Production continued for ~ 750 hours after which time it was arbitrarily curtailed. - - - Helium production was found to accompany that of T. The He was analyzed by thermal expulsion and mass spectroscopy. No ^3He was found but ^4He was measured in nine specimens out of ten examined.” [Bockris 1993 (Abstract)]

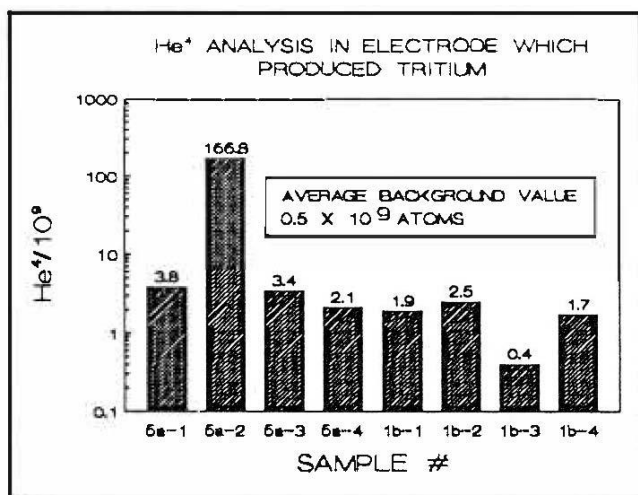


Figure 4.6. He⁴ analysis in electrode which produced tritium. [Bockris 1993 (p. 234, Fig. 5)]

“All samples, with and without thermal treatment showed positive findings of He⁴. The data in Fig. 5. represent the amounts of He⁴ released by the specimens that exceeded the average amount released or desorbed during the analysis of the Rockwell control specimens. Excess of He⁴ was observed in 9 out of the 10 electrolyzed palladium samples from electrode which produced tritium.” [Bockris 1993 (p. 233)]

Then, the ratio reduces very small as 10^{-14} ,

$$N_{\text{He4}}/N_{\text{t}}|_{\text{ex}} \sim 10^{-14}$$

On the other hand, we have a theoretical value based on the TNCF model [Kozima 2006 (p. 59)],

$$N_{\text{He4}}/N_{\text{t}}|_{\text{th}} \sim 5 \times 10^{-7}.$$

This is an opposite case of the experiment by Yamaguchi et al. [Yamaguchi 1993] where tritium was kept in the CF material by the MgO substrate but in this case, it escaped freely from the CF material and the chance to transmute into ^4He by the following reaction is very scare [Kozima 2021a].



4.4.3 Experiment by Szpak et al. [Szpak 1991]

There are two problems in the experiments by Szpak et al. [Szpak 1991, 2011], one is the problem of the interfaces with the Cu substrate and with the electrolyte solution of the codeposited PdD and the second is the structure of the PdD_x. The latter will be taken up in another paper [Kozima 2021a].

“This note reports on an alternative experimental approach to produce conditions favorable to the observation of this extraordinary behavior by exploiting the Pd/D codeposition. The approach, because an ever expanding electrode surface is created, assures the existence of non–steady state conditions as well as simplifies the cell geometry by eliminating the need for uniform current distribution on the cathode and, more importantly, eliminates long charging times effectively.” [Szpak 1991 (p. 255, Introduction)]

“Two types of working electrodes were constructed. The first, Fig. 1, illustrates the arrangement for excess enthalpy measurements. Here, a copper foil, ca 4.0 cm² in area and 0.02 cm thick, attached to a glass tube, served as the cathode. - - -The codeposition occurred from a solution of 0.05 M PdCl₂ (Aldrich) and 0.3 M LiCl (Mallinckrodt) dissolved in a 99.9% pure D₂O (Merck) under potentiostatic control (AMEL model 553).” [Szpak 1991a (p. 255)]

4.4.4 Experimental data by Miley et al. [Miley 1996a, 1996b]

Detailed description of the extensive experimental data sets on the nuclear transmutations in the multi-layered cathodes by Miley et al. [Miley 1996a, 1996b] will be given in another paper presented at this Conference [Kozima 2021b (Appendix A10)]. In this subsection, we will give a rather simple description of their work as an introduction to it.

We would like to give a comment here on the opinion “multi-body reactions” expressed by Miley et al. [Miley 1996a] as follows:

“The present results not only confront that disbelief, but add a new dimension to the issue by reporting copious light and heavy element reaction products that seem to imply multi-body reactions due to the formation of heavier elements such as Cu and Ag from Ni. Further, a reaction which does not emit intense high-energy gammas is required by the experimental results.” [Miley 1996a (p. 36)]

This opinion on the necessity of multi-body reactions is a natural conclusion deduced from the experimental facts the authors obtained in their elaborate experiments presented in their work [Miley 1996a, 1996b]. Our answer to this problem is given by the reactions where participates the neutron drops ${}^A_Z\Delta$ composed of Z protons and $(A - Z)$ neutrons [Kozima 2006 (Sec. 3.7.6)]. The reactions between a neutron drop and a nucleus A_ZX proceed as follows:

$${}^A_Z\Delta + {}^{A'}_{Z'}X \rightarrow {}^{A-a}_{Z-z}\Delta + {}^{A'+a}_{Z'+z}X^{**} \rightarrow {}^{A-a}_{Z-z}\Delta + {}^{A'+a-a'}_{Z'+z-z'}X'' + a'_{z'}X'''. \quad (2.5.9)$$

(4.4.7)

$${}^{A'}_{Z'}\Delta + {}^{A+1}_Z X^* \rightarrow {}^{A'}_{Z'}\Delta^* + {}^{A+1}_Z X \rightarrow {}^{A'}_{Z'}\Delta + \varphi's + {}^{A+1}_Z X, \quad (2.5.10) \quad (4.4.8)$$

$${}^{A'}_{Z'}\delta + {}^A_Z X \rightarrow {}^{A+A'}_{Z+Z'} X^* \rightarrow {}^{A+A'}_{Z+Z'} X + \varphi's, \quad (2.5.11) \quad (4.4.9)$$

$${}^A_Z\Delta \rightarrow {}^A_Z X + \varphi's, \quad (2.5.12) \quad (4.4.10)$$

The φ 's in these equations represents phonons generated in the reactions where participated neutrons in the cf-matter. The last equation expresses the case where a neutron drop ${}^A_Z\Delta$ transmutes directly into a nucleus ${}^A_Z X$ by an assistance of the phonons designated as φ 's.

4.4.5 Experimental data by Iwamura et al. [Iwamura 2006a, 2006b]

Iwamura et al. performed experiments with a specific CF materials composed of the so-called the Pd complexes (Pd/CaO/Pd) and (Pd/MgO/Pd) through which permeated the D_2 gas as shown in Fig. 4.7 [Iwamura 2000 – 2006].

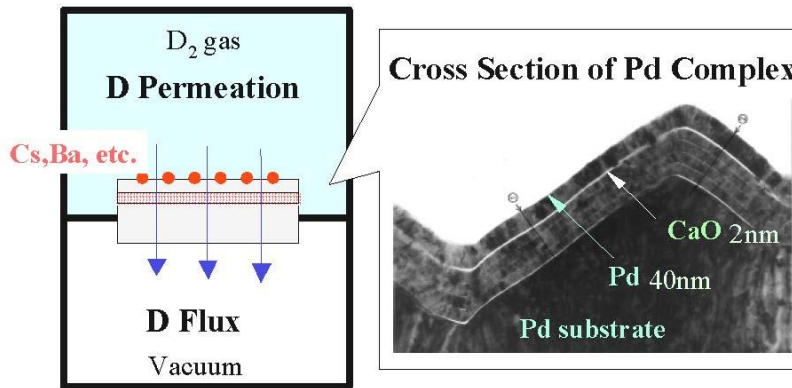


Fig. 4.7. Schematic of Iwamura's experimental method. [Iwamura 2006a (Fig. 1), 2006b (Fig. 1)]

They observed emergence of new elements, Mg, Si, S, F, Al, and increase of ${}^{33}S/{}^{32}S$ ratio of one order larger than that of natural abundance [Iwamura 2000]. Furthermore, they observed nuclear transmutations of Cs into Pr, Ba into Sm and Sr into Mo when Cs, Ba and Sr are deposited on the surface of Pd layer through the solid-gas interface

[Iwamura 2002, 2003, 2006a, 2006b]. These experimental data on the nuclear transmutation had been analyzed and explained by the TNCF model [Kozima 2011b].

“In this paper, we describe the following recent progress and results:

- 1) Transmutations of Ba into Sm,*
- 2) Confirmation of Pr by XRF (X-Ray Fluorescence spectrometry) at SPring-8,*
- 3) Some experiments relating to the role of CaO layer in the Pd complex.” [Iwamura 2006a (p. 341)]*

“The next topic is the role of CaO layer in Pd complex. - - -. If we could assume that Cs transmutation occurred in the near surface region up to 10 nm, direct electronic effect on the region by CaO layer in 40nm depth might be difficult.” [Iwamura 2006a (p. 347)]

“When we replaced CaO with MgO, we did not obtain any positive results. It means that MgO cannot work instead of CaO.” [Iwamura 2006a (p. 348)]

The events observed by Iwamura et al. about the effect of substrate CaO and MgO on the CFP are understandable from the TNCF model point of view. There are surely the superlattice of Pd-D around the surface of the sample where the nuclear transmutations occurred. In the process of the formation of the superlattice, it should be participated the catalytic actions at the solid-solid interface, (1) the microscopic grain boundaries of Pd and the oxide facing to it, e.g., <100>, <110>, and <111> planes, and (2) the effect of Ca or Mg on the HER at the interface (the cooperative catalysis, cf. Sec. 3.1)].

The superlattice has a large thickness compared to the lattice distance of about a few Å or few tens of 10^{-1} nm. Let us take the thickness of the superlattice as 1000 Å or 100 nm, then the substrate of CaO below 40 nm is possible to take part a role in the transmutation at the surface of the Pd foil. It is the problem of the nonlocal nature of the superlattice participating in the CFP.

Farther more, the difference of the CaO and the MgO substrates on the CFP may have its origin in the difference of the interactions between Ca-Pd and Mg-Pd in the solid-solid interfaces. This phase of the relation between the host element and the substrate will be investigated in another paper to be presented at this Conference [Kozima 2021b].

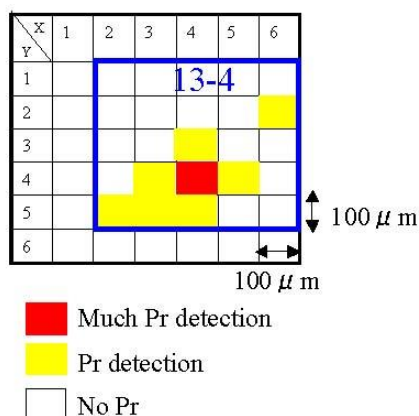


Fig. 4.8 Surface Distribution of Pr for SP-24 using 500-micron and 100-micron x-ray beams; (b) Mapping of Pr by 100-micron beam at point 13 -4 of SP-24 corresponding to XRF spectra [Iwamura 2006a (Fig. 10(b))]

The distribution of Pr obtained by Iwamura et al. [Iwamura 2006a] is shown in Fig. 4.8. The localization of the detected Pr nucleus may have a close relation to the characteristics of the hydrogen electrode reaction (HER) and the under-potential deposition (UPD) described briefly in Appendix A2. The deposition of Cs, Ba and Sr (CS in this case) on the surface of Pd seems not necessarily have a cause to localize the deposited element. Then, we must consider another cause for the observed localization of the transmuted Pr atoms.

Here, we again meet with the catalytic nature of the deposition of D atoms on the Pd layer. The Pd layer is necessarily composed of polycrystalline structure and the Pd-D superlattices formed at around the near subsurface region are localized under the favorable crystallite as shown in Sec. 4.31.

4.4.6 Experimental data by Arata et al. [Arata 1996]

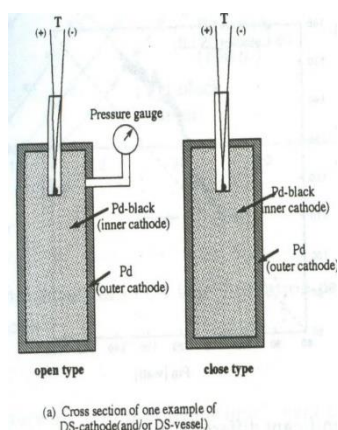


Fig. 4.9. The closed cell system with OS-cathode. Note: This diagram is author's (Arata's) 'Closed Cell' system. Left side (is shown here) shows the DS-cathodes, the open and the closed types. The open type cathode can detect inner pressure, up to about 900 atmosphere which is limited by only pressure gage. On the contrary, the closed type cathode will be rising some thousand atmospheres [atm]. [Arata 1996 (a part of Fig. 2)]

4.4.7 Experiments by Celani et al. [Celani 2010 – 2020b]

Celani et al. have given extensive works on the nano-coated Ni alloy wires according to their philosophy to realize the CFP with economically accessible techniques since 2010 [Celani 2010 – 2020b] as introduced briefly in Subsection 2.3.2. Their works will be reviewed in Appendix A4 while an analysis of the nuclear transmutation [Kozima 2011a] and an introductory comment on their CF material is given in this Section.

We have shown that the anomalous heat effects (AHE) they observed is fundamentally a kind of the CFP by giving a consistent explanation of the nuclear transmutation observed in their CF material [Kozima 2011a] (cf. also [Kozima 2020]).

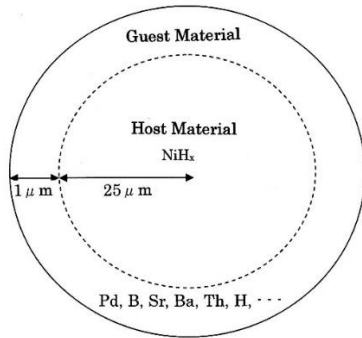


Fig. 4.10. Schematic cross section of the multiply nanocoated Ni wire. [Kozima 2011b (Fig. 1)]

“The Ni wire nanocoated, after several loading-deloaded and thermal high temperatures cycles, at very high temperatures (900°C) and under electromigration current of the order of 40-45 kA/cm², showed an excess power, in respect to a similar “virgin” wire with the same applied power (148W), of about 26W.” [Kozima 2011a (p. 55)]

“Experimental data of excess heat generation and nuclear transmutation obtained in Ni wire multiply nano-coated with Pd and a compound of B, Sr, Ba and Th at up to 900 °C have been analyzed using the TNCF model.” [Kozima 2011a (Abstract)]

The changes of isotope ratios of boron and palladium, $^{10}_5\text{B}/^{11}_5\text{B}$, $^{105}_{46}\text{Pd}$, $^{102}_{46}\text{Pd}$, were explained fairly well by the TNCF model with the parameter $n_n = 10^9 \text{ cm}^{-3} \sim 10^{11} \text{ cm}^{-3}$ in accordance with the values $n_n = 10^8 \text{ cm}^{-3} \sim 10^{11} \text{ cm}^{-3}$ determined for many experimental data [Kozima 1998 (Tables 11.2 and 11.3)]. Using the determined value n_n , we compared the excess energy measured in the experiment and that expected from the model with a reasonable accordance.

The schematic figure given in Fig. 4.9 shows a cross section of the multiply nanocoated Ni wire where observed various product elements by the nuclear transmutation in the CFP. This schematic figure clearly shows the CF materials used by Celani et al. have characteristics of the composite and compound materials and we must care about the characteristics of the electrodes [Bockris 1970a] having catalytic actions [Bockris 1970a, 1970b, Horiuti 1970, Kita 1971] (cf. Appendix A4-1). It is not easy to take into our account the catalytic action [Wikipedia Catalysis] influencing strongly on the generation of the necessary conditions for the CFP in CF materials, we point out here only its importance on the CFP and leave our consideration on this problem to another paper [Kozima 2021c].

4.5 Multi-layered CF Materials

Experimental data sets obtained by Claytor et al. in the Los Alamos National Laboratory had given remarkable works shedding light on the physics of the CFP in the early days of the CF research even if the CF materials used there were complex and difficult to analyze without a steady standpoint [Kozima 1998 (Sec. 6.4c)] as we have now after almost 30 years of elaborate endeavors. We will give an extensive introduction to the works by Claytor et al. in Appendix A3 giving a short introduction in this Subsection.

4.5.1 Experiments by Claytor et al. [Claytor 1991a, 1991b, 1993, 1996, Tuggle 1994]

Claytor et al. had measured the CFP including excess heat, tritium and neutron productions with four types of cells where are the artificial solid-solid interfaces in addition to the natural solid-gas or solid-plasma interfaces depending on the experimental conditions: (1) those with palladium powder and silicon powder, (2) those with palladium foil and silicon powder, (3) those with palladium foil and silicon wafers and (4) one with palladium foil and silicon powder [Claytor 1991a, 1991b, 1993, 1996, Tuggle 1994].

They applied the samples a pulse (typically a unipolar square pulse) of a high electric current to promote non-equilibrium conditions for them. The pulse was a voltage of 200

to 2500 V with a width of at least 150 μs at a repetition rate of 100 pulses per second and at voltages typically 1200 to 2500 V. The currents were up to 5 A. The application of the high current pulse to the sample may result in the elevation of the temperature of the sample favorable for the CFP from our point of view in addition to the intended promotion of non-equilibrium conditions.

They could improve the (qualitative) reproducibility. The tritium production of cells had correlated with the current density in the pulse and the cell type. They have measured an anomalously low value for neutrons detected to tritium produced ($< 4 \times 10^{-9}$). This result is not inconsistent with the theoretical prediction, $N_n/N_t = 10^{-6}$, based on the TNCF model [Kozima 1998 (Sec. 11.1), 2006 (Sec. 3.3.1)].

Detailed analyses of their data sets are given in Appendix A3.

4.5.2 Experiments by Miley et al. [Miley 1996a, 1996b]

In the extensive experiments with the so-called the Patterson Power Cell [Miley 1996a, 1996b], Miley et al. detected very many new elements with a large change of the proton Z and nucleon A numbers from those of the elements existed prior to the experiment. We have given a brief explanation of the result using our phenomenological model as results of the nuclear transmutation [Kozima 2006 (Sec. 2.5.3, Appendix C6)].

A detailed analyses of the data by Miley et al. with our models are given in another paper presented at this Conference [Kozima 2021b (Appendix A10)].

5 Conclusion

As is summarized in another paper presented in this Conference [Kozima 2021b (Section 1.1)], the necessary conditions to realize the CFP include two processes governed by the complexity:

(1) *Adsorption of hydrogen isotope atoms (H/D), molecules (H_2/D_2) or ions (H^+/D^+) by the host material composed of elements X 's (A_ZX 's).* Adsorption of ions on the electrode is a subtle problem of catalytic nature investigated extensively in electrochemistry (cf. e.g. [Bockris 1970a, Quaino 2007, Seo 2012]).

(2) *Generation of the superlattice X_1H_1/X_1D_1 (${}^A_ZX\text{-p}/{}^A_ZX\text{-d}$) by the self-organization as a nonlinear process under a nonequilibrium condition belonging to the complexity.* [Kozima 2013, 2016 (Sec. 3.8)]

The CF materials have inevitably the interfaces between a gas or a liquid containing hydrogen isotopes surrounding them and sometimes interfaces between a solid substrate artificially set in. In our investigations given hitherto until 2019, we had not taken this fact in our consideration avoiding the difficulty related to the catalytic nature of the

electrodics [Bockris 1970a, 1970b].

In this paper, we have investigated several interesting effects on the CFP induced by the existence of the interfaces but leaving general investigation of the effect of the interface on the CFP to another paper [Kozima 2021c].

As J.O'M. Bockris noticed already in his book on the electrochemistry [Bockris 1970a (Section 1.7)], the chemical reaction occurring at electrodes is a catalytic one as he called it *electroodic reaction* and the electrode as *electrocatalyst*:

*“Now, an electrode, too, acts as the site or substrate for the **electroodic** reaction. Further, it survives unchanged during the process of the reaction.* Hence, an electrode is a catalyst for **charge-transfer reactions**; it is a charge-transfer catalyst, or an **electrocatalyst**.*

** Except, of course, when it grows or dissolves (electrodeposition or dissolution) or when it “feeds on itself” (corrosion).” [Bockris 1970a (p. 1141, Chapter 10)]*

Therefore, as the catalysis is a subtle reaction depending sensitively on the minor changes of the structure and composition of the catalyst at the interfaces, the electrocatalysis gives the qualitative reproducibility to the process of the proton/deuteron absorption into the CF material. We have considered already the qualitative reproducibility due to the complexity in the process of the self-organization of the superlattice composed of the host elements and the hydrogen isotopes [Kozima 2013]. In addition to this cause of the qualitative reproducibility of the CFP, we have another cause, the electrocatalytic nature of the H/D inclusion at the interfaces of the CF materials as explained above.

The experimental data of the Yamaguchi et al. [Yamaguchi 1993] have given us a possibility of the participation of the nuclear interaction where participate the triton in the CF materials as discussed in Section 4.4.1. As is well known in the nuclear physics that the cross-section for the $n - t$ fusion reaction is negligibly small in free space. This is a new phase of the nuclear interaction between the lattice nuclei and the interstitial protons/deuterons which has been the key factor to realize the cold fusion phenomenon through the formation of the neutron energy bands.

Finally, we want to give a word on the negative data where no evidence of the nuclear reactions observed. In this paper, we did not take into our account any negative data with the same reason expressed already in the *DOE Report* published in 1989 [DOE 1989] where are following words applicable to any discussion related to the evaluation of negative data. We cite the sentence from our book [Kozima 1998]:

“A scientific spirit in the Report is sparkling in the following sentence added as a comment (believed to be written by N.F. Ramsey).

“- - - as a result, it is difficult convincingly to resolve all cold fusion claims since, for

example, any good experiment that fails to find cold fusion can be discounted as merely not working for unknown reasons. Likewise, the failure of a theory to account for cold fusion can be discounted on the grounds that the correct explanation and theory has not been provided. Consequently, with the many contradictory existing claims it is not possible at this time to state categorically that all the claims for cold fusion have been convincingly either proved or disproved - - -." [DOE 1989]"

Acknowledgement

The author would like to express his thanks to Dr. F. Celani for communications on the works by his group since 2010 to 2020 analyzed in this paper.

Appendices

Appendix A1. Experimental Data Sets Analyzed hitherto by the TNCF Model [Kozima 1998, 2006]

Appendix A2. Nuclear Reactions at Interfaces – 1. Experiments by Srinivasan et al. [Srinivasan 1990]

Appendix A3. Nuclear Reactions between the Trapped Neutrons and Host Elements at Interfaces 2 – Experiments by Claytor et al. [Claytor 1991a, 1991b, 1993, 1996, Tuggle 1994]

Appendix A4. Experiments by Celani et al. with Coated Constantan Wires at Elevated Temperature [Celani 2013, 2020a, 2020b]

Appendix A5. Science and Philosophy – A Dialogue with Plato –

Appendix A1. Experimental Data Sets Analyzed hitherto by the TNCF Model [Kozima 1998, 2006]

The results of the theoretical analyses of experimental data sets obtained by 1989 were tabulated in Tables 11.2 and 11.3 in a book *The Discovery of the Cold Fusion Phenomenon* [Kozima 1998]. The contents of the tables have already shown several characteristics of the CFP in these early stages of the research.

One of characteristics interesting from the contents of this paper will be the detection of tritium confined only in deuterium systems.

Table A1-1. Pd/D(H)/Li Systems. Neutron density n_n and relations between the numbers N_x of the event x obtained by theoretical analysis of experimental data on the TNCF model ($N_Q \equiv Q$ (MeV)/5 MeV). Typical value of the surface vs. volume ratio S/V (cm^{-1}) of the sample is tabulated, also. [Kozima 1998 (Table 11.2)]

Authors	System	S/V cm^{-1}	Measured Quantities	n_n cm^{-3}	Other Results (Remarks)
Fleischmann et al. ¹⁾	Pd/D/Li	6 ~40	Q, t, n $N_t/N_n \sim 4 \times 10^7$ $N_Q/N_t \sim 0.25$	$\sim 10^9$	($Q=10\text{W}/\text{cm}^3$) $N_t/N_n \sim 10^6$ $N_Q/N_t = 1.0$
Morrey et al. ¹⁻⁴⁾	Pd/D/Li	20	$Q, {}^4\text{He}$ ${}^4\text{He}$ in $t \leq 25\mu\text{m}$	4.8×10^8	$N_Q/N_{\text{He}} \sim 5.4$ (If 3% ${}^4\text{He}$ in Pd)
Roulette ^{1''')}	Pd/D/Li	63	Q	$\sim 10^{12}$	
Storins ⁴⁾	Pd/D/Li	9	$t(1.8 \times 10^2 \text{Bq}/\text{ml})$	2.2×10^7	($\tau=250\text{h}$)
Storms ⁴⁾	Pd/D/Li	22	Q ($Q_{\text{max}}=7\text{W}$)	5.5×10^{10}	($\tau=120\text{h}$)
Takahashi et al. ⁵⁾	Pd/D/Li	2.7	t, n $N_t/N_n \sim 6.7 \times 10^4$	3×10^5	$N_t/N_n \sim$ 5.3×10^5
Miles et al. ^{18')}	Pd/D/Li	5	$Q, {}^4\text{He}$ ($N_Q/N_{\text{He}}=1 \sim 10$)	$\sim 10^{10}$	$N_Q/N_{\text{He}} \sim 5$
Okamoto et al. ^{12')}	Pd/D/Li	23	Q, NT_D $l_0 \sim 1 \mu\text{m}$	$\sim 10^{10}$	$N_Q/N_{NT} \sim 1.4$ (${}^{27}\text{Al} \rightarrow {}^{28}\text{Si}$)
Oya ¹²⁻⁵⁾	Pd/D/Li	41	Q, γ spectrum	3.0×10^9	(with ${}^{252}\text{Cf}$)
Arata. et al. ¹⁴⁾	Pd/D/Li	7.5 $\times 10^4$	$Q, {}^4\text{He}$ ($10^{20} \sim 10^{21}$ cm^{-3}) $N_Q/N_{\text{He}} \sim 6$	$\sim 10^{12}$	(Assume t channeling in Pd wall)
McKubre ³⁾	Pd/D/Li	125	Q (& Formula)	$\sim 10^{10}$	Qualit.explan.
Passell ^{3''')}	Pd/D/Li	400	NT_D	1.1×10^9	$N_{NT}/N_Q=2$
Cravens ^{24''')}	Pd/H/Li	4000	Q ($Q_{\text{out}}/Q_{\text{in}}=3.8$)	8.5×10^9	(If PdD exists)
Bockris ⁴³⁾	Pd/D/Li	5.3	$t, {}^4\text{He}; N_t/N_{\text{He}} \sim 240$	3.2×10^6	$N_t/N_{\text{He}} \sim 8$
Lipson ¹⁵⁻⁴⁾	Pd/D/Na	200	γ ($E_\gamma=6.25\text{MeV}$)	4×10^5	If effic. =1%
Will ⁴⁵⁾	Pd/D ₂ SO ₄	21	$t(1.8 \times 10^5/\text{cm}^2\text{s})$	3.5×10^7	(If $l_0 \sim 10\mu\text{m}$)
Cellucci et al. ^{51''')}	Pd/D/Li	40	$Q, {}^4\text{He}$ $N_Q/N_{\text{He}}=1 \sim 5$	2.2×10^9	(If $Q=5\text{W}$) $N_Q/N_{\text{He}}=1$
Celani ^{32''')}	Pd/D/Li	400	Q ($Q_{\text{max}}=7\text{W}$)	1.0×10^{12}	(If 200% output)
Ota ⁵³⁾	Pd/D/Li	10	Q (113%)	3.5×10^{10}	($\tau=220\text{h}$)
Gozzi ^{51''')}	Pd/D/Li	14	$Q, t, {}^4\text{He}$	$\sim 10^{11}$	($\tau \sim 10^3\text{h}$)
Bush ^{27')}	Ag/PdD/Li	2000	Q ($Q_{\text{max}}=6\text{W}$)	1.1×10^9	($\tau=54\text{d}$, Film)
Mizuno 26-4)	Pd/D/Li (If Cr in Pd)	3.4	Q, NT_D $l \leq 2 \mu\text{m}$	2.6×10^8	$\tau=30\text{d}$, Pd $1\text{cm} \phi \times 10\text{cm}$
Iwamura ¹⁷⁾	PdD _x	20	n (400/s), t	3.9×10^8	$4.4 \times 10^6\text{t/s}$
Itoh ^{17')}	PdD _x	13.3	n (22/m), t	8.7×10^7	$7.3 \times 10^{10}\text{t/s}$
Itoh ^{17''')}	PdD _x	13.3	n ($2.1 \times 10^3/\text{s}$)	3.9×10^8	
Iwamura 17''')	PdD _x	20	Q (4 W) NT_F (Ti, Cr etc.)	3.3×10^{10}	($NT_F?$ unexplained)
Miley ⁶⁵⁾	Pd/H/Li	150	NT_F (Ni, Zn, ...)	4.5×10^{12}	
Dash ⁵⁹⁾	Pd/D, H ₂ SO ₄	57	Q, NT_D	$\sim 10^{12}$	Pt \rightarrow Au
Kozima ²⁰³⁾	Pd/D, H/Li	200	n ($2.5 \times 10^{-4}/\text{s}$)	2.5×10^2	Effic. =0.44%

Table A1-2. Ni/H/K Systems + α . Neutron density n_n and relations between the numbers N_x of the event x obtained by theoretical analysis of experimental data on the TNCF model ($N_Q \equiv Q$ (MeV)/5 MeV). Typical value of the surface vs. volume ratio S/V (cm^{-1}) of the sample is tabulated, also. [Kozima 1998 (Table 11.3)]

Authors	System	S/V cm^{-1}	Measured Quantities	n_n cm^{-3}	Other Results (Remarks)
Jones ²⁾	Ti/D/Li	8.1	n (2.45 MeV)	3.1×10^{11}	
Mills ²⁵⁾	Ni/H/K	160	Q (0.13 W)	3.4×10^{10}	
Bush ^{27')}	Ni/H/K	~ 160	NT_D (Ca)	5.3×10^{10}	$N_Q/N_{NT} \sim 3.5$ ($^{40}\text{K}\tau=0$)
	Ni/H/Na	~ 160	NT_D (Mg)	5.3×10^{11}	
Bush ^{27'')}	Ni/H/Rb	$\sim 10^4$	NT_D (Sr)	1.6×10^7	$N_Q/N_{NT} \sim 3$
Savva- timova ^{34''}	Pd/D ₂	100	NT_D (Ag)	9×10^{10}	
Alekseev ^{44')}	Mo/D ₂	4.1	t ($\sim 10^7$ /s)	1.8×10^7	(If MoD)
Romodanov ^{44'''}	TiC/D	4.1	t ($\sim 10^8$ /s)	$\sim 10^6$	(D/Ti \sim 0.5 assumed)
Reifenschweiler ^{38')}	TiT _{0.0035}	7×10^5	β decay reduction	1.1×10^9	($T=0\sim 450^\circ\text{C}$)
Dufour ⁷⁾	Pd,SS/D ₂ Pd,SS/H ₂	48	Q, t, n	9.2×10^{11} 4.0×10^9	(D(H)/Pd \sim 1 is assumed)
Claytor ⁹⁾	Pd/D ₂	400	t (12.5 nCi/h)	1.6×10^{13}	(If D/Pd \sim 0.5)
Srinivasan ¹⁶⁾	Ti/D ₂	1500	t ($t/d \sim 10^{-5}$)	1.9×10^8	(Aged plate)
De Ninno ^{6')}	Ti/D ₂	440	n, t	1.2×10^6	(D/Ti=1,1w)
Focardi ²³⁾	Ni/H ₂	8.2	Q	3.0×10^{12}	(If $N_p=10^{21}$)
Oriani ⁵²⁾	SrCeO ₃ /D ₂	22	$Q \sim 0.7\text{W}$	4.0×10^{10}	$V=0.31\text{cm}^3$
Notoya ^{35''}	Ni/D,H/K	3.4 $\times 10^4$	Q (0.9 W), t	2.4×10^{13}	(If 1/2 t is in liquid)
Notoya ³⁵⁻⁴⁾	Ni/D,H/K	same	NT_D (Ca)	1.4×10^9	(Sintered Ni)
Yamada ⁵⁴⁾	Pd/D ₂	185	n, NT_D (C)	2.0×10^{12}	
Cuevas ⁵⁵⁾	TiD _{1.5}	134	n (102 n/s)	5.4×10^{11}	
Niedra ⁵⁶⁾	Ni/H/K	80	Q (11.4 W)	1.4×10^9	5km \times 0.5mm ϕ
Ohmori ^{22''}	Au/H/K	200	Q, NT_F (Fe)	$\sim 10^{11}$	(Au plate)
Li ⁵⁷⁾	Pd/D ₂	185	Q	1.6×10^{12}	(Pd wire)
Qiao ^{57')}	Pd/H ₂	185	NT_F (Zn)	3.8×10^{10}	(40%NT in 1y)
Bressani ^{58')}	Ti/D ₂	$\leq 10^3?$	n (ϵ)	$10^5 - 10^6$	(Ti shaving)
Miley ^{65')}	Ni/H/Li	50	NT_D (Fe,Cr,...)	1.7×10^{12}	

Appendix A2. Nuclear Reactions at Interfaces – 1. Experiments by Srinivasan et al. [Srinivasan 1990]

A2-1. Hydrogen Electrode Reaction (HER) and Under-potential Deposition (UPD) in Electrochemistry

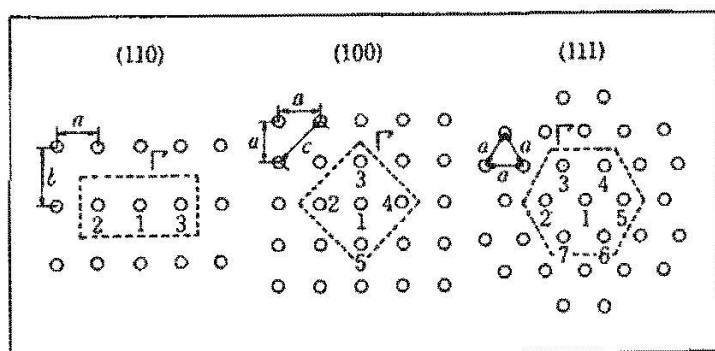
There has been a long history of experimental investigation of atomic processes in the solid-liquid interfaces elaborated by electrochemists (e.g. [Bockris 1970a, 1970b, 2000,

Horiuti 1970]). The interesting features of the dissociation of hydrogen molecules and deposition of metals at and on the electrodes are divided into two categories; the hydrogen electrode reaction (HER) [Kita 1971, 1973] (cf. Sec. 4.3.1) and the under-potential deposition (UPD) [Ohmori 1988, 1993, Nakano 1998, Bockris 2000] the relation of which will be investigated in another paper [Kozima 2021c].

In this subsection A2-1, we will give a brief discussion on a relation of the HER and the CFP in relation to the localized nuclear transmutation observed in the CFP.

As was discussed in the text (cf. Sec. 4.3.1), the localization of the nuclear reactions at around the surface region is explained by a result of the hydrogen-electrode reaction (HER) [Horiuti 1951, Kita 1971, 1973] depending on the distribution of polycrystalline grains at the Ti surface. Brief explanation of the HER results obtained by Kita [Kita 1971] was given in Section 4.3.1.

Kita had shown that the adsorption rate of deuterium on the lattice plane decreases from the (110) to (100) and (111) in Pt (cf. Fig. A2-1) reaching the minimum there [Kita 1971 (p. 109)].



$$a = 3.9158/\sqrt{2} \text{ \AA}, \quad b = 3.9158 \text{ \AA}, \quad c = 3.9158\sqrt{3/2} \text{ \AA}$$

Fig. A2-1. Atomic arrangements in the lattice planes (110), (100) and (111) in Pt crystal. [Kita 1971 (Fig. 9)]

Furthermore, he analyzed the rate of the Ni HER and concluded that the saturation current at the crystal plane increases from (110) to (100) and (111). In the current region where the Tafel law is applicable, the saturation current is governed by the contribution from the crystal plane (111) [Kita 1971 (p. 113)].

It is impossible to overemphasize the importance of the effect of the lattice structure in the CF materials on the occurrence of the CFP depending on the catalytic action in the interfaces noticed by electrochemistry as cited above. We will discuss this problem further

in the paper presented recently [Kozima 2021c].

For the illustration of the ubiquitous presence of the polycrystalline structure in materials, we cite here an example of a polycrystalline structure of Pd films deposited on a substrate of sapphire (Al_2O_3) [Salcedo 2011]. It is shown that the films a thickness of 10 nm are composed of grains with sizes of 130 – 504 nm depending on the evaporation temperature of 473, 523 and 573 K.

Furthermore, we can cite a polycrystalline structure of Si thin films for an illustration of possible variety of deposited thin films [MKS p-s-t-f]. Polycrystalline silicon (polysilicon) thin films are produced using a process known as chemical vapor deposition or CVD. Depending on the thin film process (i.e., polysilicon, silicon dioxide, silicon nitride, etc.) and the nature of the CVD process (i.e., thermal low pressure, high pressure CVD, or plasma enhanced CVD) the deposition temperature can range between 300°C and 800°C.

Polycrystalline silicon films on a silicon substrate are composed of domains of small (typically about 0.1 μm) microcrystals of silicon, commonly called grains, separated by grain boundaries as shown by a transmission electron micrograph (TEM) cross-section in Fig. A2-2. [MKS p-s-t-f (p. 2)]

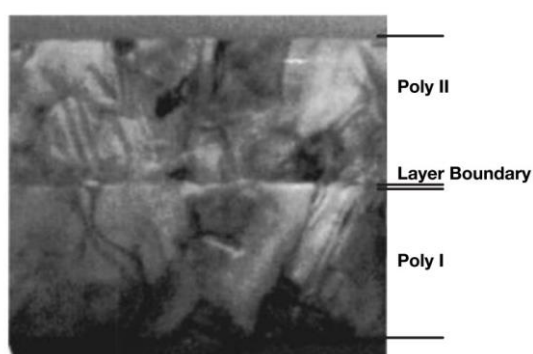


Fig. A2-2. Cross-sectional TEM of polycrystalline silicon thin film (Reproduced by permission of the Electrochemical Society) [MKS p-s-t-f (p. 3, Fig. 1)].

It is a common knowledge that solids (and films as illustrated above) are composed of microscopic crystallites (grains) and are polycrystals except they are crystalized to be a single crystal by specific techniques or natural conditions favorable for it. Therefore, we must consider the CF materials in almost all experiments for the CFP are composed of host materials with the polycrystalline structure.

A2-2 Experimental Data of Tritium Detection Localized at around Surface Region by Srinivasan et al. [Srinivasan 1990]

Srinivasan et al. extensively investigated evolution of tritium in the solid-gas/plasma interface on Ti samples with several variations of the gas loading procedure including induction heating of single machined titanium targets as well as use of a plasma focus device for deuteriding its central titanium electrode [Srinivasan 1990]. Their interesting results are summarized as follows: (1) Tritium is invariably concentrated in highly localized spots (fraction of a millimeter or less in size) each containing typically about 10^{12} to 10^{14} atoms (2 to 200 K Bq) of tritium. (2) Neutrons are produced in bunches of 30 to 300 within time spans of microseconds and the neutron-to-tritium yield ratio is in the range of 10^{-8} to 10^{-9} . [Srinivasan 1990 (p. 1, Abstract)]

Considering the data obtained by Kita on the HER, we may assume that the adsorption and absorption of hydrogen isotopes on and into the Ti (or further CF materials in general) depend strongly on the crystal plane facing to the interface.

We therefore analyze the experimental data by Srinivasan et al. [Srinivasan 1990] along the line described above. Then, the localization of the tritium in highly localized spots near the surface may be explained by the distribution of the superlattice TiD resulted from the difference of the absorption rate on the crystal plane of the microscopic single crystals distributed over the polycrystalline Ti solid facing to the interface.

In this appendix, we apply the TNCF model to calculate the adjustable parameter n_n of the model to show the semi-quantitative applicability to the tritium production in the titanium.

According to the TNCF model, the number N_t of triton ${}^3_1\text{H}$ ($= t$) generated in a time τ and in a volume V by the reaction (A2-1) between the trapped thermal neutrons and deuterons in the CF material is given by the equation (A2-2) [Kozima 1998, 2006]:

$$n + d = t + \phi's, \quad (\text{A2-1})$$

$$N_t = 0.35 n_n v_n n_d V \sigma_{n-d} \tau. \quad (\text{A2-2})$$

In the equation (A2-1), $\phi's$ express phonons instead of the photon expected in the reaction in vacuum according to our model. In the equation (A2-2), $0.35 n_n v_n$ is the flow density of the trapped thermal neutrons per unit area and time, n_d is the density of the deuteron in the volume V where the reaction occurs. σ_{n-d} ($= 5.5 \times 10^{-4}$ barns) is the cross section of the reaction (A2-1) assumed the same to that in vacuum.

To calculate the value n_n using the equation (A2-2), we use the data obtained in the discharge experiment *V.B Tritium levels on Titanium Electrode* in [Srinivasan 1990 (p. 10)].

“Following the first experiment with a Ti anode (TA1), an attempt was made to look for the presence of tritium activity on the tip of the electrode through autoradiography on the same day (4th January 1990) as the plasma focus shots. Unfortunately, this gave no results, and the experiment was considered a failure and hence plasma focus shots with titanium electrodes were discontinued. However, five weeks later (on 9th February 1990) when the anode was scanned using a newly received NaI detector, the titanium anode TA1 was found to contain a surprisingly large activity of more than 10 MBq (10^{16} atoms) of tritium.” [Srinivasan 1990]

In the general explanation of the experiment, they had given following data for the tritium generation: “Tritium is invariably concentrated in highly localized spots (fraction of a millimeter or less in size) each containing typically about 10^{12} to 10^{14} atoms (2 to 200 K Bq) of tritium.” From this explanation, we use the value of V in Eq. (A2-2) to be $1 \times 10^{-6} \text{ m}^3$ ($V = 10^{-6} \text{ m}^3$). The depth $10^{-6} \text{ m} = 1 \text{ }\mu\text{m}$ use here is taken rather arbitrarily considering general tendency observed in several experiments showing localization of the transmutation products (e.g. [Okamoto 1994, Bockris 1995]). In the above experiment where observed 10^{16} tritium atoms after five weeks ($= 3.02 \times 10^6 \text{ sec}$), we obtain the following value for n_n after inserting necessary values given below in Eq. (A2-2),

$$n_n = 6.8 \times 10^{14} \text{ cm}^{-3}. \quad (\text{A2-3})$$

The values used in the calculation of n_n are given as follows: $n_d = 2 \times 6.71 \times 10^{22} \text{ cm}^{-3}$ assuming TiD_2 , $v_n = 2.2 \times 10^5 \text{ cm/s}$, $\sigma_{n-d} = 5.5 \times 10^{-4} \text{ barns}$.

The value $n_n = 6.8 \times 10^{14} \text{ cm}^{-3}$ (A2-3) is compared with values calculated by various experimental data sets and tabulated in Tables A1-1 and A1-2 (Tables 11.2 and 11.3 [Kozima 1998], and Tables 2.2 and 2.3 [Kozima 2006]). The values of n_n tabulated in the above books are in the range $n_n = 10^6 - 10^{12} \text{ cm}^{-3}$ and the above value obtained for the data by Srinivasan et al. is the largest ever obtained. Considering the arbitrarily assumed values for the parameters in the calculation for the Eq. (A2-2), it will be allowable to say that the applicability of our model is again confirmed by the experimental data seemingly impossible to understand from the common sense of the science.

[Srinivasan 1990]

“If this is viewed in the light of the observations of other groups notably, the Los Alamos work, that neutrons are produced in bunches of 30 to 300 within time spans of microseconds and also that the neutron-to-tritium yield ratio is in the range of 10^{-8} to 10^{-9} , it is tempting to speculate that in these titanium samples perhaps some kind of a cascade reaction or micronuclear explosion probably occurs in specific sites in the near surface region resulting in 10^{10} to 10^{12} fusion reactions during each event. This intriguing

possibility warrants further experimental study.” [Srinivasan 1990 (pp. 1 – 2, Abstract)]

“The presence of tritium was established through direct counting of the radiation (β and Ti K X-rays) emanating from the sample surface. Furthermore, in all the “successful” titanium samples (except the vacuum coated thin film type “aged” deuterium targets) the tritium is found to be lodged in highly localized sites, a fraction of an mm or less in size, as seen through autoradiographic imaging.” [Srinivasan 1990 (p. 19)]

Appendix A3. Nuclear Reactions at Interfaces 2 – Experiments by Claytor et al. [Claytor 1991a, 1991b, 1993, 1996, 1998, Tuggle 1994] –

The researchers in the Los Alamos National Laboratory extended the CF materials with the solid-gas interfaces from the Ti and Pd in pressurized D₂ gas, where they measured the neutron emission [Menlove 1990a, 1990b, 1990c, 1991], to the more complex CF materials with the solid-gas and solid-solid interfaces including Pd alloys and Pd-Si wafers where they observed emissions of neutron N_n and tritium N_t with such a very low ratio of N_n/N_t as 10^{-9} [Claytor 1991a, 1991b, 1993, 1998, Tuggle 1994]. The extremely small ratio of N_n/N_t as 10^{-9} had been observed in other experiments (e.g. [Srinivasan 1990, Romodanov 1993, Kozima 1998 (Tables 11.2, 11.3), 2006 (Tables 2.2, 2.3)]) and is in accordance with the theoretical prediction of about 10^{-6} by the TNCF model [Kozima 1998 (Sec. 11.1b), 2006 (Sec. 3.3.1)].

A short introduction of the experiment by Claytor et al. was given in Section 4.5 leaving more extensive treatment of their experimental data in this Appendix A3.

A3-1. Pd/Si Wafers in D₂ Gas [Claytor 1991a, 1991b]

Pd/Si + D₂, Pd Powder and Foils, Tritium and Neutron measurements

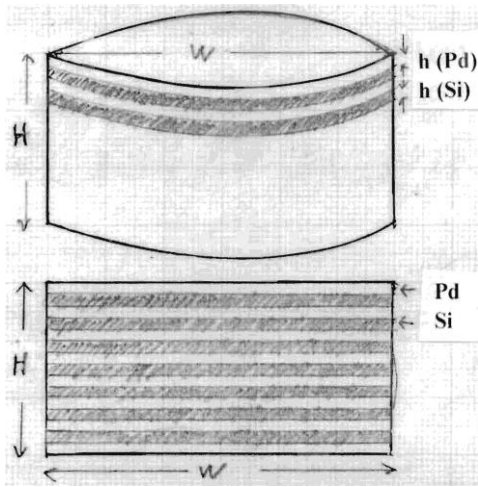


Fig. A3.1. A schematic structure of a cell made of Pd disks and Si powder depicted according to the explanation given in the paper [Claytor 1991b (p. 396)]. $h(\text{Pd}) = 0.48 - 1.16$ mm, $h(\text{Si}) = 0.76 - 2.13$ mm, $H = 1.0 - 2.4$ cm, and $W = 3.05$ cm (Pd) and 3.17 cm (Si). The dimensions given in this figure are those of the Pd and Si layers before pressing. Layers of alternating palladium disks and silicon powder were then pressed into a ceramic form at a pressure of 11.2 MPa resulting in densities of 26% and 68% of theoretical density for the palladium and silicon, respectively. [Claytor 1991b]

[Claytor 1991a]

“Abstract

Evidence has been found for tritium and neutron production in palladium and silicon stacks when pulsed with a high electric current. These palladium-silicon stacks consist of alternating layers of pressed palladium and silicon powder. A pulsed high electric current is thought to promote non-equilibrium conditions important for tritium and neutron production. More than 2000 hours of neutron counting time has been accumulated in an underground, low background, environment with high efficiency counters (21%). Neutron emission has occurred as infrequent bursts or as low-level emission lasting for up to 20 hours. In eight of 30 cells, excess tritium greater than 3 sigmas has been observed. In each of these measurements, with the powder system, the ratio of tritium detected to total integrated total neutrons inferred has been anomalously high. Recent cells have shown reproducible tritium generation at a level of about 0.5 nCi/hr. Several hydrogen and air control cells have been run with no anomalous excess tritium or neutron emission above background. A significant amount of the total palladium inventory (18%) has been checked for tritium contamination by three independent means.” [Claytor 1991a]

[Claytor 1991b]

“This paper summarizes some of the methods applicable for low level tritium detection needed in the search for anomalous fusion in metal hydrides. It is also intended to further detail our tritium and neutron results that have been obtained with the Pd-Si-D system, originally presented at earlier workshops^{1,2}.” [Claytor 1991b (p. 395, Introduction)]
(Cf. Section 3.5.1 for the Pd-Si-D system in the above sentence.)

“While this experiment is rather different from the “standard” electrolytic cell or the Ti gas hydride experiment, similarities exist in that non-equilibrium conditions are sought and the tritium generation levels are low and neutron emission is extremely weak.”
[Claytor 1991b (p. 395, Introduction)]

“In some cells, Sb doped silicon wafers (0.01 ohm-cm in resistivity by 0.5 mm thick disks, 3.07 cm dia.) obtained from Monsanto were used. Between the silicon wafers would be placed the 220 μm thick palladium foil. Because of surface roughness, the plates would only touch over a small fraction of their surface area.” [Claytor 1991b (pp. 396)]

*“Four types of cells have been made: (1) those with palladium **powder** and silicon powder, (2) those with palladium **foil** and silicon powder, (3) those with palladium **foil** and silicon wafers and (4) one with palladium **foil** and silicon powder. A typical cell, made with powders, might contain 12 to 21 grams of palladium in eight layers (one to two grams per layer) and 6 to 8 grams of silicon distributed between seven layers. Silicon layers are typically 0.76 to 2.15 mm thick by 3.17 cm in dia. while the palladium layers vary from 1.16 to 0.48 mm thick by 3.05 cm in dia. for different type cells. The palladium powder was pressed (11.2 MPa, 2000 psi) into disk form and then oxidized, in air, at 350 C for 2 hours (weight gain of 0.37%). Layers of alternating palladium disks and silicon powder were then pressed into a ceramic form at a pressure of 11.2 MPa resulting in densities of 26% and 68% of theoretical density for the palladium and silicon, respectively.”* [Claytor 1991b (p. 397)]

“Neutron detection

Our previous experiments^{1,2} have indicated that there is an anomalously low value for neutrons detected to tritium produced ($< 4 \times 10^{-9}$). Because we have attained a reproducible but small tritium generation rate, we have been striving to make the neutron sensitivity equivalent to that of the tritium detection apparatus. We anticipate that our improved neutron sensitivity illustrated in Figure 6 will make it possible to detect a neutron signal that is unambiguously above zero.” [Claytor 1991b (p. 403 – 404)]

This data of low neutron emission compared to that of tritium ($N_n/N_t < 10^{-9}$) is consistent with the theoretical prediction by the TNCF model cited above as Eq. (1.1).

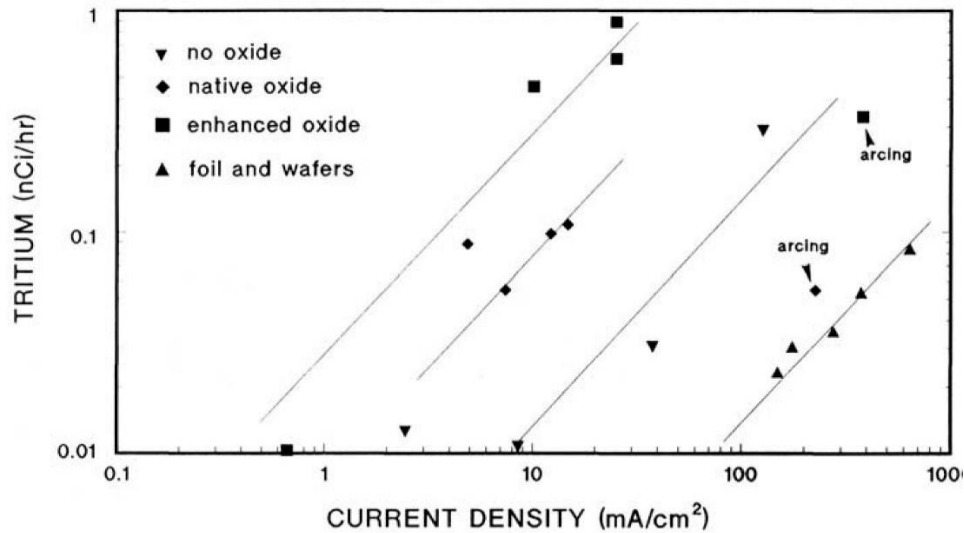


Fig. A3-2. Tritium production of cells correlated with current density and cell type. [Claytor 1991b (Fig. 8)]

The data shown in Fig. A3-1 give us some interesting features of the tritium production in the experiments.

(1) The tritium production increases according to the current density that elevates the temperature of the sample. A rough estimation shows that the temperature of the sample (the 8 layer Pd powder) increases up to 4.35 to 54.4 K in a second by the electric current of $V = 200 - 2500$ V and $I \leq 5$ A, i.e., $W = IV \leq 10^3 - 1.25 \times 10^4$ J/s if we ignore the loss of energy. Thus, it is possible to say that the higher temperature of the sample is favorable for the tritium production.

(2) Pd powders generate more tritium than Pd foil.

(3) Oxidation is favorable to produce tritium.

The characteristics (2) and (3) seem to tell us the importance of the surface condition for the tritium production, or rather the surface nature of tritium preproduction.

“After the cell had been filled, it was placed in the neutron counter and a voltage of 200 to 2500 V generated by a Velonex model 360 pulse generator was applied to the cell. In typical operation, a unipolar, square pulse with a width of at least 150 μ s at a repetition rate of 100 pulses per second was used at voltages as high as possible before breakdown occurred, typically 1200 to 2500 V. Currents of up to 5 A were used in some experiments.

A minimum of 100 hours of pulsing was used; however, in some cases the experiment was terminated earlier than 100 hours because of sudden electrical breakdown of the cell.”
 [Claytor 1991b (p. 400)]

Temperature estimation (High temperature experiments)

$V = 200 - 2500 \text{ V}, I \leq 5 \text{ A},$

$W = IV \leq 10^3 - 1.25 \times 10^4 \text{ J/s} .$

12 – 21 grams Pd in 8 layers:

Thermal capacity (specific heat) at 25°C, 25.98 J/mol K (0.0583 Cal/g K)

Pd (1 mol) = 106.42 g.

12 – 21 g (Pd) = 0.113 – 0.197 mol (Pd).

25.98 J to 1 mol Pd = 1 K (25.98 J mol)

$10^3 \text{ J to } 0.113 \text{ mol Pd} = x \text{ K (} 113 \text{ J mol) } 1.25 \times 10^4$

$25.98/1 = 113/x, \quad x = 113/25.98 = 4.35 \text{ K (} 4.35 \times 12.5 = 54.4 \text{ K)}$

Without loss of energy fed to the 8 layer Pd powder, the temperature of the sample increases up to 4.35 to 54.4 K in a second by the current of $V = 200 - 2500 \text{ V}$ and $I \leq 5 \text{ A}$, i.e., $W = IV \leq 10^3 - 1.25 \times 10^4 \text{ J/s}$.

Table A3-1. Summary of neutron data for three tunnel locations and a comparison of tritium generation rates with the neutron output. [Claytor 1991b (Table 1)]

Cell No's	Location	Conditions	Excess Tritium	Hours	Totals/hr	Reals/hr (Singles)	Total Reals/hr
17-24.5	Center Tunnel 1	Foreground (current applied) tritium producing cells only	374 ±20	810.6	707.9	0.441	0.635
		Background (no current) and non tritium producing cells		8293	700.3	0.434	0.604
24.5-29	Hall Tunnel 1	Foreground (current applied)	39 ±10	837.5	713.9	0.607	0.99
		Background (no current)		958.8	712.9	0.541	0.735
		Background (no current) and dummy cells		1560	710.8	0.576	0.799
30-35	Center Tunnel 2	Foreground (current applied)	65 ±16	878.8	638.1	0.084	0.109
		Background and dummy cells		343	637.2	0.122	0.146

“Conclusion

A reproducible method of tritium generation has been demonstrated. The tritium output scales with the current applied to various configurations of the cells. The tritium yield is found to depend strongly on the type of palladium metal used (powder or foil) and it may be expected that other parameters that have not been investigated thoroughly will have similar effects. Various tests for tritium contamination confirm that there is little chance of initial tritium contamination in the powder, foil, or other materials used in this study. The tritium and neutron results are self-consistent, and consistent with other reports. However, more sensitive neutron measurements are required to give a definitive neutron emission result.” [Claytor 1991b (p. 406)]

A3-2 Pd foil, Pd powder and silicon wafer [Claytor 1993]

“An increase in the tritium level was detected in deuterium when various configurations of palladium foil or powder and silicon wafers or powder *were* subject to a high pulsed current.” [Claytor 1993 (p. 217, Abstract)]

“Cells 41, 42 and 46 were constructed with palladium and silicon powder. A typical cell, made with powders, might contain 12 to 21 grams of palladium in eight layers and 6 to 8 grams of silicon distributed between seven layers.” [Claytor 1993 (p. 219)]

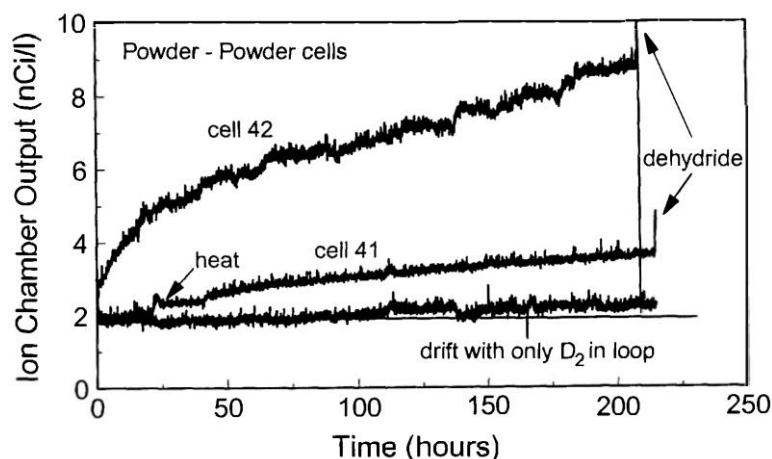


Fig. A3-3. Comparison of background, hot control cell and active powder cell. [Claytor 1993 (p. 223, Fig. 3)]

“Figure A3-4 shows the tritium generation rate for cell 42 as a function of time. Two features are evident, *the initial rate of tritium evolution can be as much as 10 times the average rate and the rate at long times increased slightly perhaps due to the increased*

pulsing current. The nonlinear slope is directly observable in Figure A3-3. The slope for the control cell, by comparison, appears to be approaching an asymptote typical of a source of tritium diffusing out of the wall of the vessel.” [Claytor 1993 (pp. 223 – 224)]

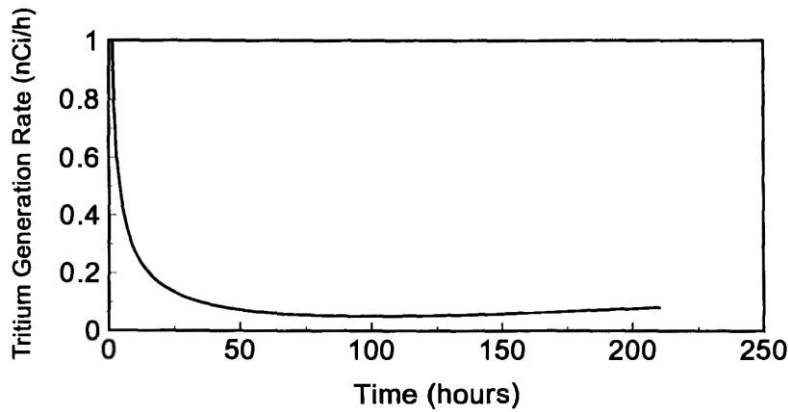


Fig. A3-4. Tritium generation rate from cell 42. [Claytor 1993 (p. 223, Fig. 4)]

The time-dependent decrease of the tritium generation rate shown in Fig. A3-4 reminds us the decrease of excess power in Ni/Cu/CaO and Ni/Cu/Y₂O₃ alloys [Iwamura 2020, Kozima 2021a (Sec. 4.1.5)]. In the sample cell #42, the heating by the electric pulls transformed the multilayer of Pd and Si into an alloy of Pd_xSi_y ($x = 12 - 21$, $y = 6 - 8$) and the minor element Si worked as an inactive element decreasing the tritium generating reaction



where $\varphi's$ represents phonons carrying away the liberated energy in the reaction (A3-1) instead of the photon with an energy 6.25 MeV emitted in free space. The rapid decrease in 10 to 20 hours may be due to the destruction of the cf-matter generated by the self-organization of the superlattice PdD by the reaction (A3-1). The gradual increase after about 120 hours may be due to the recovery of the cf-matter by the reconstruction the superlattice PdD near surface regions of the sample.

They conclude the difference of tritium production due to the sample.

“The foil is less productive than the powder because of smaller surface area and the fact that the surface barrier is largely absent. In the powder cells, the rapid decline in tritium production at the start of the experiment may be due to the depletion of the favored oxygen sites at the interface. The only purpose of the silicon is to provide a non ohmic heat source near the palladium surface.” [Claytor 1993 (pp. 227 – 228)]

“Conclusion

- - it appears that the tritium is produced during the dehydriding of palladium deuteride with a surface impurity layer. The layer in the case of the powder and the foil may be an oxide or a monolayer of adsorbed CO. Other impurity layers such as metals may be much more effective. The main effect of the current is to dehydride the palladium by heating. Only a small area near the surface is important to this process. - - -. The only purpose of the silicon is to provide a non-ohmic heat source near the palladium surface. - - . More robust partially permeable surface modifiers are available, and microfabrication of the palladium would allow rapid hydride-dehydride cycles.” [Claytor 1993 (p. 227)]

Let us investigate the relation between the theoretical ratio $N_t/N_n|_{th}$ obtained in our TNCF model [Kozima 2006 (Sec. 3.2.2.2)] and the experimental ratio $N_t/N_n|_{ex}$ obtained by Srinivasan et al. [Srinivasan 1990] and Claytor et al. [Claytor 1991b].

In our model, the neutron and the triton observed in the experiment are generated by the following reactions:



with the cross section σ_{t-d} of the reaction (3.8) is $3.0 \times 10^{-6} \text{ b}$ ($\varepsilon = 6.98 \text{ keV}$) and $1.4 \times 10^{-1} \text{ b}$ ($\varepsilon = 2.7 \text{ MeV}$).

$$\begin{aligned} \sigma_{t-d} &= 3.0 \times 10^{-6} \text{ b} (\varepsilon = 6.98 \text{ keV}) \\ &= 1.4 \times 10^{-1} \text{ b} (\varepsilon = 2.7 \text{ MeV}) \end{aligned}$$

In the reaction (3.4), the number of deuterons responsible to the $n + d$ fusion reaction is that at displaced sites but not all deuterons in the superlattice PdD. In the reaction (3.8), on the other hand, the number of deuterons responsible to the reaction $t + d$ is just deuterons in the superlattice PdD.

The number n_n determined by the triton generated by the reaction (3.4), then, should be multiplied by the ratio of deuteron number in the superlattice vs. the number of disordered deuteron (let us take it to be 10^2 for instance). The number of n_n should be two orders of magnitude higher than that determined by the density of deuterons assumed as PdD.

The ratio N_n/N_t does not change by this factor change and given by the following equations:

For a case of D/Pd ratio = 1, we obtain a relation N_n/N_t from equation (3.18) [Kozima 2006 (Sec. 3.2.2.2)],

$$\begin{aligned} N_n/N_t &= 2.0 \times 10^{-11} \quad (\varepsilon = 6.98 \text{ keV}), & (a) \\ &= 9.5 \times 10^{-7} \quad (\varepsilon = 2.7 \text{ MeV}). & (3.22) \end{aligned}$$

The value 2.0×10^{-11} should be compared with the experimental value 10^{-8} to 10^{-9} determined by Srinivasan et al. (cf. [Srinivasan 1990 (pp. 1 – 2)] and Appendix A2). It is interesting to notice that Claytor et al. [Claytor 1991b] measured the ratio as “*an anomalously low value for neutrons detected to tritium produced ($< 4 \times 10^{-9}$).*” [Claytor 1991b (p. 405)]

It is interesting to ask, “What is the factor that influence the value in (a) or (3.22)?”

A3-3 Tritium Evolution from Various Morphologies of palladium [Tuggle 1994]

In the experiments presented in 1994, Tuggle et al. tried new samples to produce tritium effectively with use of less amount of palladium [Tuggle 1994]. They used various novel morphologies of palladium in experiments performed in an underground laboratory at BYU. These include (a) ten experiments with Pd-Si Cells, 29 experiments with (b) Solid Wire Cells and (c) Powder Wire, and (d) 4 experiments with Plasma Cells. They carefully checked the contamination of tritium and observed unambiguously the production of tritium. Unfortunately, the system used in their experiment is too complicated to deduce a quantitative conclusion by our analysis as described by them, too.

“In addition, we have observed rates of tritium production (>5 nCi/h) that far exceed most of our previous results. Unfortunately, the methods that we currently use to obtain the tritium are poorly understood and consequently there are numerous variables that need to be investigated before the new methods are as reliable and repeatable as our previous techniques. For instance, it seems that surface and/or bulk impurities play a major role in the successful generation of any tritium. In those samples with total impurity concentrations of >400 ppm essentially no tritium has been generated by our gas loading and electrical simulation methods.” [Tuggle 1994 (Abstract)]

A3-4 Tritium Production from Palladium at Plasma Loading [Claytor 1996]

An experimental confirmation of tritium generation from PdD_x samples was performed by Claytor et al. [Claytor 1996] confirming the experimental result by Romodanov et al. [Romodanov 1993] (cf. [Kozima 2021a, Appendix A5]).

“In contrast to electrochemical hydrogen or deuterium loading of palladium, this method (plasma loading method) yields a reproducible tritium generation rate when various electrical and physical conditions are met. Small diameter wires (100 – 250 microns) have been used with gas pressures above 200 torr at voltages and currents of about 2000

V at 3-5 A.” [Claytor 1996 (p. 111, Abstract)]

They did not measure the sample temperature which should be very high up to 1000 K (supposed from the data by Romodanov et al. [Romodanov 1993]). Then, their data has shown the temperature effect for the nuclear reactions in the CFP which is discussed in relation to the experiment by Fleischmann et al. (cf. [Kozima 2021a (Sec. 2.4.1)]) and extensively discussed in Appendix A4 (in relation to the experiments by Celani et al. [Celani 2020b]) and in our papers [Kozima 2020, 2021a (Appendix A6)] (in relation to the experiments by Kitamura et al. [Kitamura 2018]).

A3-5 Tritium Production from Palladium Alloys [Claytor 1998]

As we have given the discussion of the experimental result obtained in Pd/Rh/Co and Pd/Cu alloys by Claytor et al. [Claytor 1998] in another paper presented this Conference [Kozima 2021a (Secs. 4.1.3 and 4.1.4)], they had shown the active and inactive actions of the minor component in the alloys on the CFP.

“Note that the Rhodium series of alloys gives a negative slope at high concentrations and a positive slope at lower concentrations. This same effect was found before in technical grade palladium, in that increasing the number of impurities in the palladium is likely to suppress the tritium output. However, it appears that the copper and boron alloys at higher concentrations produced higher tritium output rates. More data should be collected in these two alloy systems to confirm these interesting results.” [Claytor 1998 (pp. 90 – 91)]

Discussion on the experimental results obtained by Claytor et al. [Claytor 1998] has been given in another paper [Kozima 2021a (Secs. 4.1.3 and 4.1.4)].

A4. Experiments by Celani et al. on the Coated Constantan Wires at Elevated Temperature [Celani 2010 – 2020b]

In this Appendix A4, we introduce the important papers of the extensive and elaborate experiments by Celani et al. on the coated Constantan ($\text{Cu}_{55}\text{Ni}_{44}\text{Mn}_1$) wires mainly in H_2 gas at a higher temperature range up to 1000 °C since 2010 until now selecting their papers from the first to the recent ones [Celani 2010, 2012, 2013, 2020a, 2020b].

We have given several examples of the analyses of the CFP observed in composite and compound CF materials already in our papers and books published before 2020 (e.g. [Kozima 1998, 2006, 2011a, 2019b, 2020]) and in the papers presented in this Conference [Kozima 2021a, 2021b]. The key elements for the CFP in the composite and compound CF materials are the effects of minor elements in the host element, the effects of solid-solid and solid-gas interfaces, and the elevated temperature on the nuclear reactions in the

sample. In this appendix, we will analyze the experimental data obtained by Celani et al. with the coated Constantan wires.

The chronology of their experiments with Constantan wires is given in Table A4-1 copied from their recent paper [Celani 2020b]. The first paper referred in the Table as [1] is the paper [Celani 2012] in the References in this paper. The paper [Celani 2010] referred in this paper is the paper presented at 9th International Workshop held in Siena-Italy; Sept. 17 – 19, 2010.

The CF materials used in their experiments are based on the Constantan ($\text{Cu}_{55}\text{Ni}_{44}\text{Mn}_1$) and include the solid-solid and solid-gas interfaces. It is difficult, therefore, to give quantitative analysis for all experimental data obtained in their CF materials with various compositions and structures given in their papers. We must satisfy ourselves by the qualitative understanding of their main experimental results in the framework of our phenomenological approach. As is explained in their recent paper [Celani 2020b (Abstract)], the paper summarizes and gives some deeper details of the presentation at the 22nd International Conference on Condensed Matter Nuclear Science (ICCF22) and gives a report on the experimental study of LENR phenomena in Constantan ($\text{Cu}_{55}\text{Ni}_{44}\text{Mn}_1$) from its inception in 2011 to the most recent experiments. Therefore, we depend largely on this paper [Celani 2020a] to introduce the works by Celani et al. in this Appendix.

At first, it is better to give a word on their terminology AHE. They use the words “the anomalous heat effects (AHE)” to express the detection of the excess heat inexplicable by ordinary (known) physical and chemical sources. Therefore, the AHE is used for the generation of the excess heat in the traditional terminology in this field of the CF research. For example, in the experiment #2 in the Table 2 [Celani 2020b], P_{win} is 60.6 W and AHE is +8.7 W. This means in the ordinary terminology, the input power in the experiment #2 is 60.6 W and the excess heat is 8.7 W.

Table A4-1. Chronology of experiments with Constantan wires [Celani 2020b (Table 1)]. (References in the table are original ones and not given in this Appendix A4.)

Year	Main achievement	Reference
2011	Beginning of experiments with oxidized wires, of Nickel–Copper alloys in pure H ₂ , D ₂ or H ₂ /Ar, D ₂ /Ar mixture atmosphere, first measures of AHE in Constantan	[1]
2013	Reproducibility of AHE occurrence enhanced after coating the wires with low work function materials (SrO) and inserting the wires in sheaths of borosilicate glass fibers	[1,2,4]
2015	AHE occurrence associated with Fe impurities on Constantan wires Further improvements in reproducibility after adding Fe, Mn and K to the low work function main coating of the wires Observation of thermionic emission from the wires in accordance with Richardson law and related Child–Langmuir law	[4]
2017	AHE magnitude increased through geometrical arrangements to create thermal gradients along the wires Air flow calorimetry introduced for better AHE measures	[6]
2018	AHE occurrence empirically associated with thermionic emission of the wires, a counter electrode is introduced to enhance electron emission and AHE	[6–8]
2019	AHE effects stabilized (from hours to days) through high voltage and alternating current stimuli. Observation of the effect of dielectric barrier discharge on AHE occurrence and magnitude	[9,10]

A4-1. “Motivation and key points of new experiment with Ni in respect to Pd. [Celani 2010]

Their motivation to use Ni and H₂ instead of Pd and D₂ is clearly explained in the papers published in 2010.

“Ni (under suggestion of Enel) was studied because low cost and, claimed (by F. Piantelli and recently also by S. Focardi-A. Rossi), working even with H₂.” [Celani 2010 (p. 1)]

“Ni (under suggestion of Enel) was studied because low cost and, claimed (by F. Piantelli and recently also by S. Focardi-A. Rossi), working even with H₂. General approach of experiment was to use, as much as possible, the same overall materials, coatings (nano-materials, multilayer, two main kinds of materials) and measurement procedures as previously adopted for Pd wires by us” [Celani 2010 (p. 1)].

This shows they are intentionally using the “supported catalysis” mentioned in the explanation of the catalysis in Wikipedia [Wikipedia Catalysis].

There is another good idea to make inclusion of hydrogen isotopes into the CF material easier by use of the catalytic action of thin layers on the interface of the material:

“f) We experienced, since 1998, in electrolytic environments and using innovative electrolytes (like salts of Ca, Sr, Ba) at very low concentration (<0.1mM) and mild acidic

*pH, that sometimes, especially after several cathodic-anodic cycles, the Pd wire was covered by a sub-micrometric layer of several elements, Pd included. Because the spontaneous developing of such porous and very thin layer (like a **sponge**) the characteristics of D₂ absorption changed dramatically and the loading time was reduced of several order of magnitude (from hours to minutes) even, and specially, at low current density of electrolysis (about 10-20 mA/cm²).*” [Celani 2010 (p. 10, Origin of new INFN-LNF procedure.)]

The dramatic reduction of the loading time mentioned above shows another type of the supported catalysis described in the explanation of the catalysis in Wikipedia [Wikipedia Catalysis]. The “porous and very thin layer (like a sponge)” reminds us the zeolites, one of the heterogeneous catalysts in the explanation given in Secs. 3.1.1 and 3.1.4. The porous skin may work as a heterogeneous catalyst like zeolite (cf. Secs. 3.1.1 and 3.1.4).

We will investigate the effect of the porous layer observed by Celani et al. in our following paper [Kozima 2021c] in relation to the works by electrochemists such as the characteristics of the electrocatalysis [Bockris 1970a] and catalytic actions at solid-liquid interfaces [Bockris 1970a, 1970b, Horiuti 1970, Kita 1971]

They have tried to develop new materials and thin layers as the supported catalysis on the surface of CF materials to improve the performance of their activity of the CFP:

*“We adopted the innovative procedure of coating intrinsically active supports (like Pd and now Ni, planned also Ti, with their alloys, under H₂ and/or D₂ gas) with nanomaterials (used mainly as anti-sintering agent) **containing** also Pd at very low dimensions. The nominal dimension of such nanomaterial, in most recent experiments, was 6-9 nm. The active support is a Pd (now Ni) wire thin ($\Phi=50\ \mu\text{m}$) and long (60-90 cm).”* [Celani 2010 (pp. 11 - 12, The new approach to fractal and nano-layer construction.)]

To improve the performance of the CF material based on the Constantan, they used intentionally active sites of the catalyst known already in the chemistry of catalysis [Wikipedia Catalysis] as explained in Sec. 3.1.2.

“The total number of layers, made by (simple) physical-chemical deposition procedures, is quite large (about 50) so that the apparent increase of thickness of main wire is 1-2 μm .” [Celani 2010 (p. 12, The new approach to fractal and nano-layer construction.)]

This multi-layer structure uses the supportive catalysis and active catalysis at solid-solid interfaces effectively [Wikipedia Catalysis].

They could obtain improved excess heat production with CF materials of a new type of construction and at the elevated temperature:

“The largest value of excess power density detected with Ni was as large as 1800W/g of Ni at a wire temperature of about 900°C. In comparison, the best result obtained by us, using Pd-D system, was 400 W/g at 500°C.” [Celani 2010 (pp. 48, Conclusions.)]

This result shows the temperature effect for the CFP we have noted several times before [Kozima 2013, 2020].

The experimental data on the excess heat and the nuclear transmutation in the work [Celani 2010] had been analyzed consistently [Kozima 2011a] using the TNCF model as explained in Sec. 4.4.7.

A4-2. New Nickel-based Alloys [Celani 2014]

Celani et al. developed new CF material $\text{Cu}_{55}\text{Ni}_{44}\text{Mn}_1$ effective to generate the excess heat [Celani 2014]:

“Abstract

Starting in February 2011, we studied the feasibility of new nickel-based alloys that can absorb significant amounts of hydrogen (H_2) and/or deuterium (D_2) and might, in principle, possibly generate anomalous thermal effects at temperatures $>100^\circ\text{C}$. The interest in Ni alloys comes in part because there is the possibility to use H_2 instead of expensive D_2 . Moreover, a cross-comparison of results using H_2 instead of D_2 can be made and could help the understanding of the phenomena involved (and the possible nuclear origin).” [Celani 2014 (p. 56)]

“Based on some theoretical considerations, and thanks also to some sentences in a paper on catalysis not related to LENR studies [1], we decided to explore the possibility of using Ni-Cu alloys (including Constantan) as starting material that could fit our purposes.”

“[1] S. Romanowski et al., Density functional calculations of the hydrogen adsorption on transition metals..., *Langmuir* **15**(18) (1999) 5773–5780.” [Celani 2014 (p. 56 and p. 67)]

There are some ideas on the quality and the temperature of the material to improve the performance of the CF material as explained in their paper:

“E. The possibility, at least in principle, of producing nano-microstructures (and voids) both at the surface and deeper into the bulk, with selective oxidation of Cu in such alloys at high temperatures (650–1050 °C). Both segregation of pure Ni among to CuO_x and the cooling rate are key aspects of the preparation need to be studied in deeper detail, even though we spent a lot of time and money investigating them.” [Celani 2014 (p. 57)]

“(11) A possible explanation was that the active wire’s temperature with Joule heating was larger than that when the power was indirect. The active wire temperature was 350–400°C, 200°C with indirect heating.

(12) If the explanation in 11 is correct, we see that the reaction, above from some temperature threshold, has a positive feedback with increasing temperature. Similar effects were found by our group with first generation wire/experiment, up to May 2012; - - .” [Celani 2014 (p. 62)]

About the oxidation we must refer the paper by Claytor [Claytor 1991b (Fig. 8)]. We have no evidence, however, showing the explicit effect of oxides formed over the surface of the alloy particles in the samples at present. The temperature effect on the CFP has already been observed in many materials and by many researchers [Kozima 2013, 2020].

“Conclusion

It appears that the commercial Constantan alloy, with the surface geometry deeply modified (i.e., skeletonized) and size reduced to < 100 nm, with multiple layers, is a good candidate for anomalous heat production due to: - - - . We observed that such materials exhibit “positive feedback” of anomalous power with increasing temperature.” [Celani 2014]

A4-3. Anomalous Heat Effect (AHE) in Constantan wires [Celani 2020a, 2020b]

In the recent papers, Celani et al. extended their experiments using novel forms of the Constantan wires to enhance the excess heat generation [Celani 2020a, 2020b].

“This paper summarizes, and gives also some deeper details, the presentation held at the 22nd International Conference on Condensed Matter Nuclear Science (ICCF22) and reports the experimental study of LENR phenomena in Constantan ($Cu_{55}Ni_{44}Mn_1$) from its inception in 2011 to the most recent experiments.” [Celani 2020b (p. 1, Abstract)]

They had found an interesting effect of surface layers on the CFP.
 “Improvements in the magnitude and reproducibility of AHE, and improvements in wire preparation and reactor design were reported by the authors in the present and previous papers. The oxidation of the wires by pulses of electrical current in air creates a rough surface featuring a sub-micrometric texture that proves particularly effective at inducing thermal anomalies when temperature exceeds 400°C. This effect appears also to be increased substantially by depositing segments of the wire with a series of elements (such as Fe, Sr, Mn, K, via thermal decomposition of their nitrates applied from a water solution).” [Celani 2020a (p. 25)]

The positive effects of the rough surface made by the oxidation and the deposition of a series of elements (such as Fe, Sr, Mn, K) on the excess heat generation mentioned in the above sentence show again the *active effect of the heterogeneous catalysis* mentioned in Sec. A4-1 above.

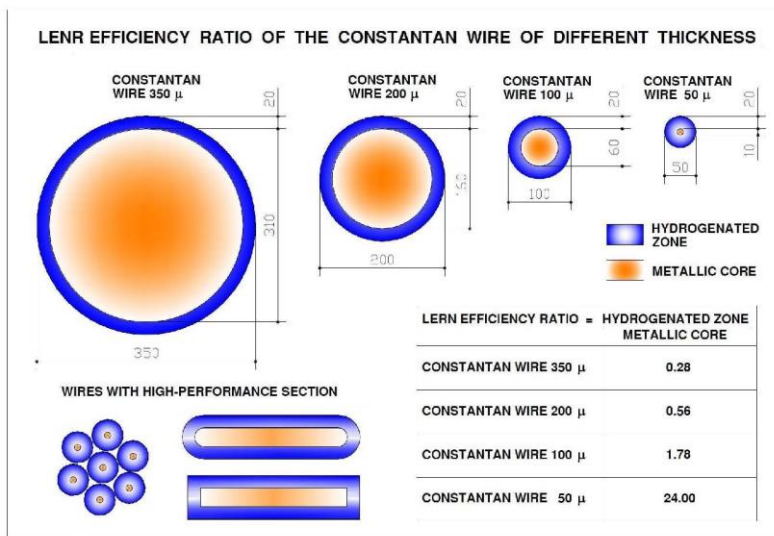


Fig. A4-2. Section of wires of different diameter after oxidation and additional treatments [Celani 2020b (Fig. 2)].

From their explanation in the original figure caption, they observed the formation of a porous oxidized layer that later is reduced by deuterium. The resulting porous skin is

especially prone to enhanced deuterium absorption (blue area). The schematic figures in the Fig. A4-2 are based on measurements taken by Scanning Electron Microscopy. The highly loaded zone (white area) is in the range of 15–25 μm .

We can speculate following physics of the CFP from the data depicted in the Fig. A4-2.

First, as we pointed out in Sec. A4-1, the submicrometric “porous skin” reminds us the zeolites, one of the heterogeneous catalysts in the explanation given in Secs. 3.1.1 and 3.1.4. The porous skin may work as a heterogeneous catalyst like zeolite (cf. Secs. 3.1.1 and 3.1.4).

Second, the highly loaded zone (blue + white area) seems almost the same thickness about 25 – 30 μm (they say that it is in the range of 15 – 25 μm) for all wires with different original thicknesses from 350 – 50 μm . Especially notable is the blue zone with a clear boundary. Then, we may assume the formation of the superlattice of the host elements ($\text{Cu}_{55}\text{Ni}_{44}\text{Mn}_1$) and deuterons in the region (blue + white area) clearly divided from the metallic core (red area). The superlattice prevents diffusion of the deuteron from the solid-gas interface further into the metallic core through the boundary between the superlattice (highly loaded zone) and the metallic core.

This figure reminds us the data by Okamoto et al. [Okamoto 1994] shown in Fig. 4.2. The distributions of D and Pd in the narrow region less than about 0.7 μm are remarkable by the humps overlapped on the smooth curves when there was the CFP (Neutron + excess heat or Neutron). These humps in the Fig. 4.2 may suggest the formation of the superlattice PdD similarly to that speculated to explain the experimental data shown in Fig. A4-2 by Celani et al. [Celani 2020b].

The effect of the knots shown in Fig. A4-2 on the excess heat generation gives us an interesting feature of the Constantan experiments by Celani et al.

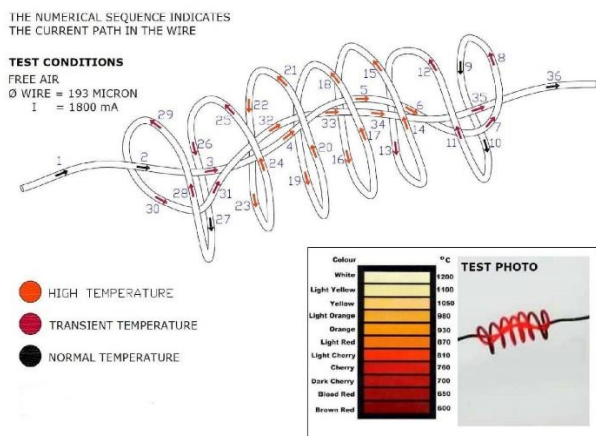
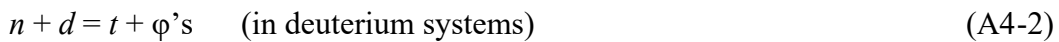


Fig. A4-2. Picture of an eight-loop knot heated in air with a direct current ($I = 1800$ mA). Wire of $200 \mu\text{m}$ diameter. If we estimate the temperature using color, the dark area is likely to be at $<600^\circ\text{C}$, the external spires at about 800°C , while the inmost straight section, may reach 1000°C . [Celani 2020b (Fig. 3)]

One of the effects of the knot may be the elevation of the temperature in the coil which induces the temperature effect on the CFP increasing the excess heat generation by nuclear reactions, in which the main reaction is the following:



with cross sections

$$\sigma_{n-p} = 3.22 \times 10^{-1} \text{ barns}, \quad (1.10)$$

$$\sigma_{n-d} = 5.5 \times 10^{-4} \text{ barns}. \quad (1.11)$$

for the reactions (A4-1) and (A4-2), respectively.

A4-4. Concluding remarks on the work by Celani et al.

In conclusion, we evaluate a chain of the works on the Constantan wire by Celani et al. very high which has pursued intentionally materials and forms of the CF material based on the Constantan for the effective occurrence of the CFP in the composite and compound CF materials.

The characteristics of composite and compound CF materials had been investigated since the beginning of the CF research as reviewed and analyzed in this and another paper presented in this Conference [Kozima 2021a]. The works by Celani et al. developed the characteristics of these materials to their extents as far as possible to obtain the higher qualitative reproducibility and the higher ratio of excess heat/input energy with favorable materials from the economical viewpoint using Ni and H_2 instead of Pd and D_2 .

The intentional use of the supported catalysis induced by the solid-solid interface for the effective inclusion of hydrogen isotopes into CF materials and of higher temperature for the effective occurrence of the CFP by such a geometrical idea of the knot shown in Fig. A4-2 are splendid ideas for the development of application of the CFP for industry.

Appendix A5. Science and Philosophy – A Dialogue with Plato –

In the modern science, the truth behind the phenomena observed in a specific research field are explained by principles established through many repeated checks. The research field is, in other words, determined by the principles governing the phenomena occurring in the field. New phenomena inexplicable by the principles in a research field ask new

principles which generate a new research field containing the new phenomena. Thus, the whole system of the science is constructed as a compound structure as we have now.

The science as a system of knowledge explaining various phenomena in a field is useful, in a word, to apply the knowledge for our use to save our labor and to help our life. This is the main reason the modern science is accepted into our society as a part of its industry and scientists have been useful members. As a result, there had been occurred an episode around the discovery of the CFP by Fleischmann et al. in 1989 which had given large effects on the development of the science of the CFP (e.g. [Kozima 2017]). The motivation of the excellent investigation by Celani et al. introduced in detail in Appendix A4 was guided by the same object as clearly explained by the sentences in their paper cited there.

The science has, however, another face than its application explained briefly in the above sentence. Human beings have inherited various abilities in the process of evolution which have been useful to maintain one's existence on this precious Earth for more than 5 – 2 million years. Does one used the inherited abilities fully positively to maintain one's existence here on the Earth?

We will show a face of the science different from that flourished modern technological society asking Plato, a genius of 2500 years ago. We will know that the science he imagined is useful for a human being as an individual rather than for the society which not necessarily kind for its constituent members. The individuals must seek own satisfaction or happiness themselves reforming the society through it.

As a philosopher Peter Kreeft says that the origin of the Platonic philosophy is composed of Greek myth and Socrates logic:

“In the second lecture, we'll briefly explore Plato's two basic predecessors, or sources, myth and Socrates.” [Kreeft 2018 (p. 3, Lecture I)]

From the myth, Plato induced his principles to explain the phenomena around his society and environment at that time and discussed their meaning using Socrates' logic. His investigation is primitive but fundamental and is useful even now. It gives us a prototype of our investigation of a new scientific field such as the cold fusion phenomenon (cf. [Kozima 2019a]).

Now let us contemplate the Plato's discussion on the nature and society putting weight on the former.

Plato was interested in everything around him not only the relation between human beings but also the relation of human beings and their natural environment. Plato did,

however, not content with the natural science at that time not developed enough to give him satisfaction and he gave up enclosing it in his investigation on the world surrounding him. (In the sentences cited below, we will print the words and phrases in red which we want to emphasize in relation to our contemplation.)

(96A)

“Then I will tell you, said Socrates. When I was young, Cebes, I had a prodigious desire to know that department of philosophy which is called the investigation of nature; to know the causes of things, and why a thing is and is created or destroyed appeared to me to be a lofty profession; and I was always agitating myself with the consideration of questions such as these:--” [Plato Phaedo (96A)]

Plato had interest to have unified world view on the environment around him natural and human altogether.

“Then I heard someone reading, as he said, from a book of Anaxagoras, that mind was the disposer and cause of all, and I was delighted at this notion, which appeared quite admirable, and I said to myself: If mind is the disposer, mind will dispose all for the best, and put each particular in the best place; and I argued that if any one desired to find out the cause of the generation or destruction or existence of anything, he must find out what state of being or doing or suffering was best for that thing, and therefore a man had only to consider the best for himself and others, and then he would also know the worse, since the same science comprehended both. And I rejoiced to think that I had found in Anaxagoras a teacher of the causes of existence such as I desired, - - .” [Plato Phaedo (97C-D)]

“And I thought that I would then go on and ask him about the sun and moon and stars, and that he would explain to me their comparative swiftness, and their returning and various states, active and passive, and how all of them were for the best. For I could not imagine that when he spoke of mind as the disposer of them, he would give any other account of their being as they are, except that this was best; and I thought that when he had explained to me in detail the cause of each and the cause of all, he would go on to explain to me what was best for each and what was good for all.” [Plato Phaedo (98A-B)]

(98B-E)

“What expectations I had formed, and how grievously was I disappointed! As I proceeded,

I found my philosopher altogether forsaking mind or any other principle of order, but having recourse to air, and ether, and water, and other eccentricities.” [Plato Phaedo (98B-E)]

Plato supposed the cause of all should be one and he was delighted to hear that Anaxagoras told that is mind (nous). He had disappointed knowing that Anaxagoras could not use the nous to explain all but explained one event by other events one after another. This is a natural process to proceed the logic into the truth behind apparent phenomena used until the middle of the 20th century but is not the one Plato wanted. We can say that Plato was too early to expect the unified explanation of natural, social, and mental phenomena by the complexity.

The explanation given by Anaxagoras was “scientific” in our modern meaning to pursue the origin of a phenomenon in another entity hidden behind the original phenomenon, e.g., matter into atoms, atoms into fundamental particles, and so on. This is the process the modern science proceeded as we know. However, this process does not give a human being satisfaction if the process has no final answer until the complexity finally has given the negative answer that there is no explanation of the process because the process was traced on the infinitely narrow path negligible and, we must content with the given world as the best solution we have given by the process of evolution.

The sentence (*If mind is -- - and others.*) in the above citation expresses his desire or demand for the cause of phenomena which he had to wait 2500 years until the middle of 20th century when the complexity was discovered (e.g. [Prigogine 1984]).

“And I thought that I had better have recourse to the world of mind (logos) and seek there the truth of existence. I dare say that the simile is not perfect--for I am very far from admitting that he who contemplates existences through the medium of thought, sees them only 'through a glass darkly,' any more than he who considers them in action and operation.

However, this was the method which I adopted: I first assumed some principle which I judged to be the strongest, and then I affirmed as true whatever seemed to agree with this, whether relating to the cause or to anything else; and that which disagreed I regarded as untrue. But I should like to explain my meaning more clearly, as I do not think that you yet understand me.” [Plato Phaedo (100A)]

Plato disappointed with the explanation by the mechanical causes one after another

turned to the explanation by logos abandoning phenomena perceived by human senses. Here, he established a spiritual cathedral towering forever.

“You would say: I will let alone puzzles of division and addition—wiser heads than mine may answer them; inexperienced as I am, and ready to start, as the proverb says, at my own shadow, I cannot afford to give up the sure ground of a principle. And if any one assails you there, you would not mind him, or answer him, until you had seen whether the consequences which follow agree with one another or not, and when you are further required to give an explanation of this principle, you would go on to assume a higher principle, and a higher, until you found a resting-place in the best of the higher; but you would not confuse the principle and the consequences in your reasoning, like the Eristics—at least if you wanted to discover real existence. Not that this confusion signifies to them, who never care or think about the matter at all, for they have the wit to be well pleased with themselves however great may be the turmoil of their ideas. But you, if you are a philosopher, will certainly do as I say.” [Plato P (101D-E)]

The logic recognized by Plato is a standard we must follow even now as explained in the sentences cited above. The situation where Plato was 2500 years ago has changed very much mainly due to the human activity especially in modern 300 years. We are a different world from that Plato was in and contemplated what is happy for human beings. The human beings, however, did not change in these 2500 years and Plato’s contemplation on the human beings is equally true as the time he lived.

Now, we have developed the nonlinear dynamics which has shown *the order from the disorder* answering the question raised by Plato 2500 years ago and giving a unified world view for human beings. We can cite a sentence from the book by Prigogine et al. showing the attainment of human inquiry into the question recognized in the Greek culture:

“Our scientific heritage includes two basic questions to which till now no answer was provided. One is the relation between disorder and order. The famous law of increase of entropy describes the world as evolving from order to disorder; still, biological, or social evolution shows us the complex emerging from the simple. How is this possible? How can structure arise from disorder? Great progress has been realized in this question. We know now that nonequilibrium, the flow of matter and energy, may be a source of order.” [Prigogine 1984 (p. xxix, Introduction)]

We can live now with spiritual satisfaction with Plato knowing the truth behind phenomena surrounding us self-organized in the history of about 5 – 2 million years. We may say the history developed by a God or a Supernatural Existence, or the Nature.

Acknowledgement

The author would like to express his thanks to Dr. F. Celani, Dr. A. Kitamura, Dr. H. Yamada, Dr. M. Ohmori, Dr. K. Kaki and Dr. M. Ohta for valuable communications with them on the experimental results investigated in this paper.

References

- [Arata 1996] Y. Arata, "Achievement of Solid State Plasma Fusion ('Cold Fusion')," *Proc. ICCF6*, pp. 129 – 135 (1996). NEDO and Institute of Applied Energy, Tokyo, Japan, 1998.
- [Augustynski 1989] J. Augustynski, M. Ulmann, and J. Liu, "Electrochemical Measurements on Palladium Cathodes in LiOD/D₂O Solutions related to the 'Cold Fusion Experiments,'" *Chimia*, **43**: p. 355 (1989).
- [Bockris 1970a] J.O'M. Bockris and A.K.N. Reddy, *Modern Electrochemistry – An Introduction to an Interdisciplinary Area –*, Plenum Press, New York, 1970, Library of Congress Catalog Card Number 6819518.
- [Bockris 1970b] J. O'M. Bockris and A.R. Despić, "The Mechanism of Deposition and Dissolution of Metals," in *The Mechanism of Deposition and Dissolution of Metals, in Physical Chemistry – An Advanced Treatise –*, Vol. **IXB**/Electrochemistry, Chapter 7, Ed. Henry Eyring, Academic Press, N.Y and London, 1970, Library of Congress Catalog Card Number: 66-29951.
- [Bockris 1990] J. O'M. Bockris, G.H. Lin, R.C. Kainthla, N.J.C. Packham and O. Velev, "Does Tritium Form at Electrodes by Nuclear Reactions?" *Proc. ICCF1*, pp. 137 – 148 (1990). Published by F.G. Will, The National Cold Fusion Institute, 390 Wakara Way, Salt Lake City, Utah 84108, USA, 1990.
- [Bockris 1991] J. O'M. Bockris, D. Hodko and Z. Minevski, "The Mechanism of Deuterium Evolution on Palladium: Relation to Heat Bursts Provoked by Fluxing Deuterium across the Interface," *Proc. ICCF2*, pp. 337 – 348 (1991), ISBN 88-7794-045-X.
- [Bockris 1993] J. O'M. Bockris, C.-C. Chien, D. Hodko and Z. Minevski, "Tritium and Helium Production in Palladium Electrodes and the Fugacity of Deuterium Therein," *Proc. ICCF3*, pp. 231 – 240 (1993), ISBN 4-946443-12-6.

- [Bockris 1994] J. O'M. Bockris, R. Sundaresan, Z. Minevski and D. Letts, "Triggering of Heat and Sub-Surface Changes in Pd-D System," *Proc. ICCF4*, pp. 267 – 293 (1994),
- [Bockris 1995] J. O'M. Bockris and Z. Minevski, "Two Zones of Impurities" Observed after Prolonged Electrolysis of Deuterium on Palladium," *Infinite Energy*, #5 & #6, pp. 67 – 73 (1995), ISSN 1081-6372.
- [Bockris 2000] J.O'M. Bockris, A.K.N. Reddy, M.E. Gamboa-Aldeco, *Modern Electrochemistry*, 2nd edition, Volume 2A, *Fundamentals of Electrodeics*, Kluwer Academic/Plenum Publishers, 2000, ISBN 978-0-306-47605-1.
- [Campari 2004] E. Campari, S. Focardi, V. Gabbani, V. Montalbano, F. Piantelli and S. Veronesi, "Surface Analysis of Hydrogen loaded Nickel Alloys," *Proc. ICCF11*, pp. 414 – 420 (2004), ISBN 981-256-640-6.
- [Castagna 2012] E. Castagna, S. Lecci, M. Sansovini, F. Sarto and V. Violante, "Correlation Between Surface Properties and Anomalous Effects in F&P Experiments," *J. Condensed Matter Nucl. Sci.* **8**, pp. 49 – 59 (2012), ISSN 2227-3123.
- [Celani 2010] F. Celani, P. Marini, V. Di Stefano, *et al.*, "First measurement on Nano-coated Ni Wire at Very High Temperature under He, Ar, H₂, D₂ Atmosphere and Their Mixtures," Paper presented at 9th International Workshop on Anomalies in Hydrogen/Deuterium Loaded Metals (Certosa di Pontignano, Siena-Italy; Sept. 17 – 19, 2010).
- [Celani 2012] F. Celani, O.M. Calamai, A. Spallone, A. Nuvoli, V. Andreassi *et al.*, "Development of a High Temperature Hybrid CMNS Reactor," *J. Condensed Matter Nucl. Sci. (Proc. ICCF17)* **6**, pp. 24–33 (2012), ISSN 2227-3123.
- [Celani 2013] F. Celani, E. F. Marano, A. Spallone, A. Nuvoli, B. Ortenzi *et al.*, "Experimental Results on Sub-Micro Structured Cu-Ni Alloys under High Temperature Hydrogen/Deuterium Interaction," *Chemistry and Materials Research* **3**, No.3, pp. 27 – 56 (2013), ISSN 2224- 3224.
- [Celani 2014] F. Celani, E.F. Marano, B. Ortenzi, S. Pella, S. Bartalucci, F. Micciulla. *et al.*, "Cu-Ni-Mn alloy wires, with improved submicrometric surfaces, used as LENR device by new transparent, dissipation-type, calorimeter." *J Condensed Matter Nucl Sci* **13**, pp. 56 – 67 (2014), ISSN 2227-3123.
- [Celani 2019] F. Celani, C. Lorenzetti, G. Vassallo, E. Purchi *et al.*, "Unexpected Effects due to Voltage Waveform at Anode, in Gaseous LENR Experiments based on Sub-micrometric Surface Coated Constantan Wires," Terzo Convegno "Assisi Nel Vento", 17-19 Maggio 2019; Domus Laetitia, Assisi (PG)-Italy.
- [Celani 2020a] F. Celani, C. Lorenzetti, G. Vassallo, E. Purchi *et al.*, "First Evaluation of Coated Constantan Wires Incorporating Capuchin Knots to Increase Anomalous Heat and

Reduce Input Power at High Temperatures,” *J. Condensed Matter Nucl. Sci.*, **30**, pp. 25–35 (2020), ISSN 2227-3123.

[Celani 2020b] F. Celani, C. Lorenzetti, G. Vassallo, E. Purchi, S. Fiorilla *et al.*, “Progress toward an Understanding of LENR-AHE Effects in Coated Constantan Wires in D₂ Atmosphere: DC/AC Voltage Stimulation,” *J. Condensed Matter Nucl. Sci.*, **33**, pp. 46 – 73 (2020), ISSN 2227-3123.

[Claytor 1991a] T. N. Claytor, D. G. Tuggle, H. O. Menlove, P. A. Seeger, W. R. Doty and R. K. Rohwer, “Tritium and neutron measurements from deuterated Pd-Si,” *AIP Conference Proceedings* **228**, 467 – 480 (1991); <https://doi.org/10.1063/1.40668>

[Claytor 1991b] T.N. Claytor, D.G. Tuggle and H.O. Menlove, “Tritium Generation and Neutron Measurements in Pd-Si under High Deuterium Gas Pressure,” *Proc. ICCF2*, pp. 395 – 408 (1991), ISBN 88-7794-045-X.

[Claytor 1993] T.N. Claytor, D.G. Tuggle, and S.F. Taylor, “Evolution of Tritium from Deuterided Palladium Subject to High Electrical Currents,” *Proc. ICCF3*, pp. 217 – 229 (1993), ISBN 4-946443-12-6.

[Claytor 1996] T. Claytor, D. Jackson and D. Tuggle, “Tritium Production from a low Voltage Deuterium Discharge on Palladium and Other Metals,” *J. New Energy*, **1**, No. 1, pp. 111 – 118 (1996), ISSN 1086-8259.

[Claytor 1998] T. N. Claytor, M. J. Schwab, D. J. Thoma, D. F. Teter and D. G. Tuggle, “Tritium Production from Palladium Alloys,” *Proc. ICCF7*, pp. 88 - 93 (1998), ENECO Inc., Salt Lake City, Utah 84108, USA.

[DOE 1989] *Cold Fusion Research*, November 1989— A Report of the Energy Research Advisory Board to the United States Department of Energy —, DOE/S-0071 (August, 1989) and DOE/S--0073, DE90, 005611. This report is posted at the *New Energy Times* website; <http://newenergytimes.com/v2/government/DOE/DOE.shtml>

[Fleischmann 1989] M. Fleischmann, S. Pons and M. Hawkins, "Electrochemically induced Nuclear Fusion of Deuterium," *J. Electroanal. Chem.*, **261**, pp. 301 – 308 (1989), ISSN 1572-6657.

[Horiuti 1951] J. Horiuti, T. Keii, K. Hirota, “Mechanism of Hydrogen Electrode of Mercury, ‘Electrochemical Mechanism,” *J. Res. Inst. Catalysis, Hokkaido Univ., Vol. 2*, No.1, pp. 1 – 72 (1951), ISSN 0034-530X.

[Horiuti 1970] J. Horiuti, “Gas Evolution Reactions,” pp. 543 – 610, in *The Mechanism of Deposition and Dissolution of Metals, in Physical Chemistry – An Advanced Treatise* – , Vol. **IXB**/Electrochemistry, Chapter 6, Ed. Henry Eyring, Academic Press, N.Y and London, 1970, Library of Congress Catalog Card Number: 66-29951.

[Horiuti 1976] J. Horiuti and T. Toya, “Adsorption Isotherm and the States of Adsorption”

- J. Res. Inst. Catalysis, Hokkaido Univ.*, **24**, No.3, pp. 159 – 186 (1976), ISSN 0034-530X.
- [Iwamura 2000] Y. Iwamura, T. Itoh and M. Sakano, “Nuclear Products and Their Time Dependence induced by Continuous Diffusion of Deuterium through Multi-layer Palladium containing Low Work Function Material,” *Conference Proceedings*, **70** (*Proc. ICCF8*), pp. 141 – 158 (2000), ISBN 88-7794-256-8.
- [Iwamura 2002] Y. Iwamura, T. Itoh, M. Sakano and S. Sakai, “Observation of Low Energy Nuclear Reactions induce by D₂ Gas Permeation through Pd Complexes,” *Proc. ICCF9*, pp. 141 – 146 (2002), ISBN 7-302-06489-X/O-292.
- [Iwamura 2003] Y. Iwamura, T. Itoh, M. Sakano, S. Sakai and S. Kuribayashi, “Low Energy Nuclear Transmutation in Condensed Matter induce by D₂ Gas Permeation through Pd Complexes: Correlation between Deuterium Flux and Nuclear Products,” *Proc. ICCF10*, pp. 435 – 446 (2003), ISBN 981-256-564-7.
- [Iwamura 2006a] Y. Iwamura, T. Itoh, M. Sakano *et al.*, “Observation of Nuclear Transmutation Reactions Induced by D₂ Gas Permeation through Pd Complexes” *Proc. ICCF11*, pp. 339 – 350 (2006), ISBN 981-256-640-6.
- [Iwamura 2006b] Y. Iwamura, T. Itoh, M. Sakano *et al.*, “Observation of Surface Distribution of Products by X-ray Fluorescence Spectrometry during D₂ Gas Permeation through Pd Complexes” *Proc. ICCF12*, pp. 178 – 187 (2006), ISBN 981-256-901-4.
- [Kita 1971] H. Kita, “Catalytic Activity and the Reaction Mechanism on the Hydrogen Electrode Reactions” *Nihon Kagaku Zasshi*, **92**, pp. 99 – 114 (1971), ISSN: 0369-5387 (in Japanese).
- [Kita 1973] H. Kita and T. Kurisu, “Electroanalysis by *d*- and *sp*- Metals,” *J. Res. Inst. Catalysis, Hokkaido Univ.*, **21**, No.3, pp. 200 – 246 (1973), ISSN 0034-530X.
- [Kitamura 2009] A. Kitamura, T. Yamaguchi, T. Nohmi, Y. Sasaki, Y. Miyashi *et al.*, “CMNS Research Progressing in Kobe University – Deuterium Permeation and Absorption –,” *Proc. JCF9*, pp. 17 – 22 (2009), ISSN 2187-2260.
- [Kitamura 2018] A. Kitamura *et al.*, “Excess Heat Evolution from Nanocomposite Samples under Exposure to Hydrogen Isotope Gases” *Int. J. of Hydrogen Energy*, **43**. Issue 33, pp. 16187 – 16200 (2018), ISSN: 0360-3199.
- [Klemens 1960] P.G. Klemens, “Band Structure of Monovalent Metals and their Alloys,” *Australian Journal of Physics*, **13**, pp. 238 – 246 (1960), ISSN 0004-9506.
- [Kozima 1994] H. Kozima, “Trapped Neutron Catalyzed Fusion of Deuterons and Protons in Inhomogeneous Solids,” *Transactions of Fusion Technology*, **26**, No. **4T**, Part 2 FUSTE8 (4), pp. 508 – 515 (1994), ISSN 0748-1896.
- [Kozima 1997] H. Kozima, K. Kaki and M. Ohta, "The Physics of the Cold Fusion Phenomenon," *Cold Fusion*, **22**, pp. 58 – 78 (1997), ISSN 1074-5610.

[Kozima 1998] H. Kozima, *Discovery of the Cold Fusion Phenomenon – Development of Solid State-Nuclear Physics and the Energy Crisis in the 21st Century* –, Ohtake Shuppan Inc., 1998, ISBN 4-87186-044-2. The “References” in this book is posted at the CFRL (Cold Fusion Research Laboratory) Website:

<http://www.kozima-cfrl.com/Books/bookse/bookse.html>

[Kozima 2000] H. Kozima. “Neutron Drop: Condensation of Neutrons in Metal Hydrides and Deuterides”, *Fusion, Technol.*, **37**, pp. 253 - 258 (2000), ISSN 0748-1896.

[Kozima 2003] H. Kozima, J. Warner, C. Salas-Cano and J. Dash, “TNCF Model Explanation of Cold Fusion Phenomenon in Surface Layers of Cathodes in Electrolytic Experiments,” *J. New Energy*, **7-1**, pp. 81 – 95 (2003), ISSN 1086-8259.

[Kozima 2006] H. Kozima, *The Science of the Cold Fusion Phenomenon, – In Search of the Physics and Chemistry behind Complex Experimental Data Sets* –, 1st Edition, Elsevier, Amsterdam, 2006, ISBN-13: 978-0-08045-110-7, ISBN-10: 0-080-45110-1.

[Kozima 2011a] H. Kozima and F. Celani, “ Brief Explanation of Experimental Data Set on Excess Heat and Nuclear Transmutation in Multiply Nano-coated Ni Wire,” *Proc. JCF11*, **11-10**, pp. 53 – 58 (2011), ISSN 2187-2260.

[Kozima 2011b] H. Kozima, “Localization of Nuclear Reactions in the Cold Fusion Phenomenon,” *Proc. JCF11*, **11-11**, pp. 59 – 69 (2011), ISSN 2187-2260.

[Kozima 2012] H. Kozima, “Cold Fusion Phenomenon in Open, Non-equilibrium, Multi-component Systems,” *Reports of CFRL (Cold Fusion Research Laboratory)*, **12-1**, 1 – 14 (2012): <http://www.kozima-cfrl.com/Papers/paperr/paperr.html>

[Kozima 2013] H. Kozima, “Cold Fusion Phenomenon in Open, Nonequilibrium, Multi-component Systems – Self-organization of Optimum Structure,” *Proc. JCF13*, **13-19**, pp. 134 - 157 (2013), ISSN 2187-2260.

[Kozima 2016] H. Kozima, “From the History of CF Research – A Review of the Typical Papers on the Cold Fusion Phenomenon –,” *Proc. JCF16*, **16-13**, pp. 116 – 157 (2016), ISSN 2187-2260.

[Kozima 2017] H. Kozima, “The Sociology of the Cold Fusion Phenomenon – An Essay –” *Proc. JCF17*, **17-13**, pp. 148-219 (2017), ISSN 2187-2260.

[Kozima 2019a] H. Kozima, “Inductive Logic and Meta-analysis in the Cold Fusion Phenomenon,” *Proc. JCF19*, **19-14**, pp. 85 - 111 (2019), ISSN 2187-2260.

[Kozima 2019b] H. Kozima, “Development of the Solid State-Nuclear Physics,” *Proc. JCF19*, **19-15**, pp. 112 – 147 (2019), ISSN 2187-2260.

[Kozima 2019c] H. Kozima, “On the 30th Anniversary of the Discovery of the Cold Fusion Phenomenon,” *Infinite Energy*, 145, May/June 2019, pp. 28 – 34 (2019), ISSN 1081-6372.

- [Kozima 2020] H. Kozima, “The “anomalous heat effect” is a normal event in the cold fusion phenomenon – On the paper “Excess heat evolution from nanocomposite samples under exposure to hydrogen isotope gases” by Kitamura et al. published in the *Int. J. Hydrogen Energy* 43, pp. 16187 – 16200 (2018) –,“ *Int. J. Hydrogen Energy*, **45** (38), pp. 19577 – 19582 (2020), ISSN 2187-2260.
- [Kozima 2021a] H. Kozima, “Cold Fusion Phenomenon in the Composite CF Materials – Mixed Hydrogen Isotopes, Alloys, Ceramics and Polymers –,” *Proc. JCF21*, **21-2** (2021), ISSN 2187-2260 (to be published).
- [Kozima 2021b] H. Kozima, “Neutron Energy Bands in the Composite and Compound CF Materials – Speculation on the Bases of the TNCF Model –,” *Proc. JCF21*, **21-4** (2021), ISSN 2187-2260 (to be published).
- [Kozima 2021c] H. Kozima and T. Ohmori, “Nuclear Force between Lattice Nuclei and Interstitial Hydrogen and HER and UPD,” (to be published).
- [McBreen 1990] J. McBreen, “Absorption of Electrolytic Hydrogen and Deuterium by Pd: The Effect of Cyanide Adsorption,” *J. Electroanal. Chem.*, **287**, pp. 279 ~ 291 (1990), ISSN 1572-6657.
- [McKubre 1993] M.C.H. McKubre, S. Crouch-Baker, A.M. Riley *et al.*, "Excess Power Observed in Electrochemical Studies of the D/Pd System," *Proc. ICCF3*, pp. 5 – 19 (1993), ISBN 4-946443-12-6.
- [Menlove 1990a] H. O. Menlove, M. M. Fowler, E. Garcia, M. C. Miller, M. A. Paciotti *et al.*, "Measurements of Neutron Emission from Ti and Pd in Pressurized D₂ Gas and D₂O Electrolysis Cells," *Journal of Fusion Energy*, **9(4)**, pp. 495 – 506 (1990).
- [Menlove 1990b] H.O. Menlove, “High Sensitivity Measurements of Neutron Emission from Ti Metal in Pressurized D₂ Gas,” *Proc. ICCF1*, pp. 250 – 251 (1990).
- [Menlove 1990c] H.O. Menlove, M.A. Paciotti, T.N. Claytor, H.R. Maltrud, O.M. Rivera, and D.G. Tuggle, “Reproducible Neutron Emission Measurement from Ti Metal in Pressurized D₂ Gas,” *AIP Conference Proceedings* **228**, pp.287 – 301 (1990).
- [Menlove 1991] H. O. Menlove, M. A. Paciotti, T. N. Claytor, and D. G. Tuggle, “Low-Background Measurements of Neutron Emission from Ti Metal in Pressurized Deuterium Gas,” *Proc. ICCF2*, pp. 385 – 394 (1991), ISBN 88-7794-045-X.
- [Miley 1994] G.H. Miley, H. Hora, E.G. Batyrbekov and R.L. Zich, “Electrolytic Cell with Multilayer Thin-Film Electrodes.” *Trans. Fusion Technol.*, **26(4T)**, pp. 313 – 340 (1994), ISSN 0748-1896.
- [Miley 1996a] G.H. Miley and J.A. Patterson, “Nuclear transmutations in thin-film nickel coatings undergoing electrolysis.” *J. New Energy*, **1(3)**: pp. 5 – 38 (1996), ISSN 1086-8259.

- [Miley 1996b] G.H. Miley, G. Narne, M.J. Williams, J.A. Patterson, J. Nix *et al.*, “Quantitative Observation of Transmutation Products occurring in Thin-film Coated Microspheres during Electrolysis,” *Proc. ICCF6* (1996, Hokkaido, Japan), pp. 629 – 644 (1996), NEDO and Institute of Applied Energy, Tokyo, Japan, 1996.
- [Mizuno 1997] T. Mizuno, K. Inoda, T. Akimoto, K. Azumi, M. Kitaichi *et al.*, “Anomalous γ Peak Evolution from SrCeO₃ Solid State Electrolyte Charged in D₂ Gas,” *Intern. J. Hydrogen Energy*, **22**-1, pp. 23 – 25 (1997), ISSN 0360-3199.
- [MKS p-s-t-f] <https://www.mksinst.com/n/polycrystalline-silicon-thin-films>
- [Nakano 1998] H. Nakano, T. Akiyama and H. Fukushima, “Underpotential Deposition of Zn with Iron-group Metals,” *J. Surf. Finish. Soc. Jpn*, **49**, No. 11, pp. 1209 – 1220 (1998), ISSN: 0915-1869 (in Japanese).
- [Ohmori 1988] T. Ohmori, “Investigation of the Mechanism of the Hydrogen Electrode Reaction on the Surfaces of *sd*- and *d*-Metals and the Variation of the Reaction Mechanism by the upd – Alkaline Metals,” *Doctor Degree Theses*, Hokkaido University, March 1988 (in Japanese).
- [Ohmori 1993] T. Ohmori and M. Enyo, “Excess Heat Evolution During Electrolysis of H₂O with Nickel, Gold, Silver and Tin Cathodes,” *Fusion Technol.*, **24**, No. 1, pp. 293 – 295 (1993), ISSN 0748-1896.
- [Okamoto 1994] M. Okamoto, H. Ogawa, Y. Yoshinaga, T. Kusunoki., and O. Odawara, “Behavior of Key Elements in Pd for the Solid State Nuclear Phenomena Occurred in Heavy Water Electrolysis,” *Proc. ICCF4*, Vol. **3**, pp. 14-1 – 14-8 (1993).
- [Plato Phaedo] *Phaedo* by Plato, translated into English by Benjamin Jowett, CreateSpace Independent Publishing Platform, 2017, ISBN 978-1543-2676-48.
- [Prigogine 1984] I. Prigogine and I. Stengers, *Order out of Chaos – Man’s New Dialogue with Nature*, Bantam Books, Toronto, 1984, ISBN 0-553-34082-4.
- [Quaino 2007] P.M. Quaino, M.R. Gennero de Chialvo, A.C. Chialvo, “Hydrogen Electrode Reaction: A Complete Kinetic Description,” *Electrochimica Acta*, **52**, pp. 7396–7403 (2007), ISSN 0013-4686.
- [Reifenschweiler 1994] O. Reifenschweiler, “Reduced radioactivity of Tritium in Small Titanium Particle,” *Phys. Lett.*, **A184**, pp. 149 – 154 (1994).
- [Reifenschweiler 1995] O. Reifenschweiler, “Some Experiments on the Decrease of the Radioactivity of Tritium Sorbed by Titanium Particle,” *Proc. ICCF5*, pp. 163 – 172 (1995). Published by the International Conference on Cold Fusion 5, IMRA Europe, SA, Centre Scientifique, BP 213, 06904 Sophia Antipolis CEDEX, France.
- [Reifenschweiler 1996] O. Reifenschweiler, “Some Experiments on the Decrease of the Radioactivity of Tritium Sorbed by Titanium Particle,” *Fusion Technol.*, **30**, pp. 261 –

272 (1996), ISSN 0748-1896.

[Romodanov 1993] V.A. Romodanov, V.I. Savin, Y.B. Skuratnik and Y. Timofeev, “Nuclear Fusion in Condensed Matter,” *Proc. ICCF3*, pp. 307 – 319 (1993), ISBN 4-946443-12-6.

[Salcedo 2011] K.L. Salcedo, C.A. Rodríguez, F.A. Perez and H. Riascos, “Morphological Study of Palladium Thin Films Deposited by Sputtering,” *Journal of Physics: Conference Series* **274** 012120, pp. 1 – 6 (2011),
doi:10.1088/1742-6596/274/1/012120.

[Seo 2012] M. Seo, “Underpotential Deposition and Metallic Corrosion Reaction,” *Corrosion Engineering of Japan*, **61**, No.9, pp. 341 – 348 (2012), ISSN: 1884-1155 (in Japanese).

[Srinivasan 1990] M. Srinivasan, A. Shyam, T. C. Kaushik, R. K. Rout, L. V. Kulkarni et al., “Observation of Tritium in Gas/Plasma Loaded Titanium Samples,” *AIP Conference Proceedings* **228**, pp. 1 – 21 (1990). Brigham Young Univ., Provo, UT: American Institute of Physics, New York.

[Szpak 1991] S. Szpak and P.A. Mosier-Boss, “On the Behavior of Pd Deposited in the Presence of Evolving Deuterium,” *J. Electroanal. Chem.*, **302**, pp. 255 – 260 (1991), ISSN 1572-6657.

[Szpak 2011] S. Szpak, *Chemical Aspects of the Pd^NH-H₂O System in its Nuclear Active State*, Prepared for Public Release, July 2020:

<https://www.lenr-canr.org/acrobat/SzpakSchemicalas.pdf>

[Tuggle 1994] D. G. Tuggle, T. N. Claytor and S. F. Taylor, “Tritium Evolution from Various Morphologies of Palladium,” *Proc. ICCF4*, **1**, pp. 7-1 – 7-21 (1994).

[Ulmann 1990] M. Ulmann, J. Liu, J. Augstynski, F. Meli and L. Schlapbac, “Surface and Electrochemical Characterization of Pd Cathodes after Prolonged Charging in LiOD + D₂O Solutions,” *J. Electroanal. Chem.*, **286**, pp. 257 – 264 (1990), ISSN: 1572-6657.

[Violante 2008] V. Violante, F. Sarto, E. Castagna, M. Sansovini, S. Lecci *et al.*, “Material Science on Pd-D System to Study the Occurrence of Excess Power,” *Proc. ICCF14*, pp. 429 – 436 (2008), ISBN 978-0-578-06694-3.

[Violante 2012] V. Violante, F. Sarto, E. Castagna, S. Lecci and M. Sansovini, M. McKubre and F. Tanzella, “The Study of the Fleischman and Pons Effect through the Materials Science Development,” *J. Condensed Matter Nucl. Sci.*, **8**, pp. 60–74 (2012), ISSN 2227-3123.

[Wikipedia Catalysis] <https://en.wikipedia.org/wiki/Catalysis>

[Yamaguchi 1993] E. Yamaguchi and T. Nishioka, “Direct Evidence for Nuclear Fusion Reactions in Deuterated Palladium,” *Proc. ICCF3*, pp. 179 – 188 (1993), ISBN 4-946443-

12-6.

[Yamaguchi 1998] E. Yamaguchi and H. Sugiura, "Excess Heat and Nuclear Products from Pd:D/Au Heterostructures by the '*In-vacuo*' Method," *Proc. ICCF7*, pp. 420 – 424 (1998), ENECO, Inc.

Neutron Energy Bands in the Compound and Composite CF

Materials

– Speculation on the Bases of the TNCF and ND Models –

Hideo Kozima

Cold Fusion Research Laboratory; <http://www.kozima-cfrl.com/>

597-16 Yatsu, Aoi, Shizuoka, 421-1202 Japan

E-mail; hjrfq930@ybb.ne.jp

Abstract

Using a phenomenological approach by the TNCF (trapped neutron catalyzed fusion) and the ND (neutron drop) models, we have given a unified explanation of the complex features of the cold fusion phenomenon (CFP). In the phenomenological approach, the necessary and sufficient condition for the cold fusion phenomenon (CFP) has been established as the formation of the neutron energy bands in the super-lattice of host elements and the hydrogen isotopes realized by the self-organization in complexity.

In this paper, the bases and applicability of the TNCF and the ND models are investigated in the CF materials with rather complicated structures in the compound (multilayered materials and materials on substrates with interfaces) and composite (alloys, ceramics and polymers) structures investigated very often recently. In the investigation we used analogy of the neutron energy bands (neutron bands) to the electron energy bands (electron bands).

The neutron bands in the compound CF materials are investigated with reference to the electron bands in PN junctions. On the other hand, the neutron bands in the composite materials are investigated with reference to the characteristics of the electron bands in alloys at around symmetrical points in the Brillouin zone. The analogy between the electron bands and the neutron bands legitimates qualitatively the use of the concepts of the neutron bands for investigation of the CFP in compound and composite CF materials.

In the investigation of the neutron band in alloys, we noticed two kinds of effects of the minor elements to the CFP, active (or positive) elements including the 3d and 4d transition elements and inactive (negative) elements including other than those in the active ones. The former enhances the nuclear reactions in the CFP and the latter reduces them. Direct evidence of this classification was given by experimental data by Claytor et al. and indirect evidence was given by the HER (hydrogen electrode reaction) and the UPD (underpotential deposition) in the electrochemistry. This problem will be discussed extensively in another paper.

It is shown that the effects of the interfaces of the CF materials on the CFP are essential to induce the nuclear reactions between the neutrons in the bands and nuclei at disordered positions generated by the thermal motion, by the statistical distribution at a finite temperature, and by the specific situation at around interfaces.

Contents

1. Introduction – Phenomenological Approach to the Complex Phenomenon
2. Formation of Neutron Energy Bands in Simple CF Materials
3. Neutron Bloch Waves at Interfaces of the Compound CF Material
4. Neutron Energy Bands in the Compound and Composite CF Materials
5. Conclusion

Appendices

- A1. Meditations of Geniuses
- A2. The Trapped Neutron Catalyzed Fusion (TNCF) Model
- A3. The Neutron Drop (ND) Model
- A4. Valence Neutrons in Exotic Nuclei
- A5. Neutron Energy Bands (Neutron Bands) due to the Super-nuclear Interaction mediated by Interstitials and Halo Neutrons
- A6. Electron Energy Bands (Electron Bands) in Alloys and Neutron Energy Bands (Neutron Bands) in Composite CF Materials (Alloys and Ceramics) – CF Active and CF Inactive Elements
- A7. Electron Energy Bands (Electron Bands) at P/N Junctions in Semiconductors
- A8. Surface States at the Boundary between CF Material and Oxide/Ceramic Substrates
- A9. Neutron Energy Bands (Neutron Bands) in Compound CF Materials – Pd-Ti and Ni-Pd Multilayers
- A10. Nuclear Reactions at Interfaces. Experiments by Miley et al. [Miley 1994, 1996a, 1996b]

1. Introduction – Phenomenological Approach to the Complex Phenomenon

When we engage in contemplation of the truth hidden behind phenomena in the environment surrounding us, it is necessary to use some kinds of logic. In the modern science established in 16th century and lasted exclusively until the middle of 20th century, its main scheme was overwhelmed by the *deductive logic* based on the established

principles in simple linear systems discovered by the *inductive logic* and confirmed by the *deductive logic* thereafter.

It is possible to say in general that our contemplations on the relation with environment have been essentially interlaced with inductive and deductive logics as noticed in the beginning of our civilization born about 2500 years ago. It had been recognized the importance of the *intuition* in the inductive logic as expressed by two geniuses Plato in his letter and A. Einstein in a writing (cf. Appendix A1). We must notice the importance of intuition in the inductive logic to find out a *tentative principle* from our experience in a world and of the alternative use of inductive and deductive logics to proceed our contemplation to find out the *final principle* in a realm of the world as we see in the referred sayings of the geniuses.

In the investigation of the cold fusion phenomenon (CFP) that includes the nonlinear interaction among component particles in a nonequilibrium condition and therefore belongs to complexity, it has been necessary to use the inductive logic to find out fundamental principles for the science of the CFP. We have engaged in the task as practiced in our phenomenological approach to the CFP [Kozima 1998, 2006] unintentionally and explained its meaning definitively in our recent paper [Kozima 2019a].

The CFP observed in the various CF materials have been investigated successfully using our models while we have left the data sets obtained in materials with rather complicated structures such as compound (with interfaces showing outstanding roles) and composite (multi-component host substances). Even if the structures of the CF material differ one from another, we may be able to apply the same approach to analyze the phenomenon having common characteristics as we had shown in our paper [Kozima 2019a] that it is possible to use the inductive logic and meta-analysis for experimental data sets.

In our recent papers, we have investigated the CFP in the compound and composite CF materials rather deductively using the TNCF model [Kozima 2020, 2021a, 2021b]. In the analysis, we had noticed the importance to take into our consideration the characteristics of the hydrogen electrode reaction (HER) and the underpotential deposition (UPD) at interfaces of the composite CF materials. We have presented at this Conference a paper on the composite CF material [Kozima 2021a] and another paper on the effects of the interfaces on the CFP in the compound materials [Kozima 2021b]. We will investigate the general relation of the HER and UPD themselves with the cold fusion phenomenon (CFP) in another paper [Kozima 2021c].

In this paper, we discuss the applicability of the TNCF (trapped neutron catalyzed

fusion) and the ND (neutron drop) models to the composite and compound CF materials used in these papers [Kozima 2021a, 2021b]. The speculative discussion in this paper depends mainly on the knowledge of the electron energy band (electron bands) obtained mainly in the semiconductor physics.

1.1 In the Beginning

It was an accidental coincidence to have similar exclamations by John Dash and by me at the 4th International Conference held five years after the declaration of the discovery of the cold fusion phenomenon by Fleischmann et al. [Fleischmann 1989] as follows:

“A key to open the door to solve the riddles of the Cold Fusion has been neglected by researchers until now is the thermal and cold neutrons existing abundantly everywhere.” [Kozima 1994]

“On the other hand, these elements could have been produced by transmutation if slow neutrons were present.” [Dash 1994]

To investigate the applicability of the TNCF model to composite and compound CF materials, we give first a summary of the structure of the TNCF model.

Fundamental premises and logics of our theory:

(0) Inductive logic and meta-analysis are needed in the analyses of data in the CFP. [Kozima 2019a]

(1) Adsorption of hydrogen isotope atoms (H/D), molecules(H₂/D₂) or ions (H⁺/D⁺) by the host material composed of elements X (^A_ZX).

Adsorption of ions on the electrode is a subtle problem of catalytic nature investigated in electrochemistry (cf. e.g. [Bockris 1970a, 2000, Quaino 2007, Seo 2012]) and we do not discuss it in this paper even if we had touched it before [Kozima 2000].

(2) Absorption of hydrogen isotope ions H⁺/D⁺ (*p/d*) by the hydrogen electrode reaction (HER) into the specific host material where the proton/deuteron wavefunctions are nonlocalized in the interstices but overlap with the lattice nuclei.

[Bockris 1970a, 2000, Kita 1971, 1973, Kozima 2009]

(3) Formation of the CF material composed of the host element X and the hydrogen isotopes H/D where the nuclei ^A_ZX have neutron energy levels at around the evaporation level the neutrons in them have rather extended wavefunctions.

[Kozima 2014a]

(4) Generation of the superlattice XH/XD (^A_ZX-*p*/^A_ZX-*d*) by the self-organization in a non-equilibrium condition as a process in the complexity.

[Kozima 2013, 2014a]

- (5) Formation of neutron energy bands by the super-nuclear interaction (n -(p/d)- n interaction) between neutrons in different lattice nuclei catalyzed by interstitial protons/deuterons.
[Kozima 2006, 2009]
- (6) Supply of initial neutrons into the neutron energy bands (let us call the neutrons in the energy band “trapped neutrons”) with a number density n_n . It may be supplied from outside by environmental background neutrons in the first step.
Null result [Jones 1994, Forsley 1998]
Neutron effects [Shani 1989, Yuhimchuk 1992, Celani 1992, Stella 1993, McKubre 1993 (p. 11), Oya 1996]
- (7) Multiplication of n_n by nuclear reactions between the trapped neutrons and disordered nuclei Y (let us write a displaced host element (X) in bulk or a foreign element X’ at a boundary or at a surface as Y). The nuclear reactions result in the multiplication of n_n .
[Kozima 1998 (Sec. 17.1), 2006 (Sec. 3.7.2.3), 2013 (p. 149), Miley 1996a (p. 21), Iwamura 2006].
- (8) The nuclear reaction of the trapped neutron with the nuclei at disordered sites caused by (a) the thermal motion of host elements, (b) the statistical imbalance of arrangement, (c) the disorder accompanied to the structure change at interfaces. The thermal motion of the nuclei results in the temperature effect of the CFP as summarized in our recent paper [Kozima 2020].
- (9) Then, the positive feedback occurs to increase n_n .
[Kozima 2012b (pp. 10 – 12), 2013 (pp. 149 – 151, Sec. 3.2)]”

The discussions on the experimental data obtained in the composite CF materials [Kozima 2021a] and the compound CF materials [Kozima 2021b] are based on the steps (7) to (9). The discussion in this paper takes up the steps (4) and (5) in the composite and compound CF materials about the electron energy bands investigated in the semiconductor physics. The complicated atomic processes related to the steps (1) and (2) will be taken up in the paper scheduled in near future [Kozima 2021c].

1.2 Development of the TNCF Model

It is helpful to survey the development of our model in relation to the progress of our investigation as tabulated below. Some premises of the model suffered change according to the deepening of our knowledge in the experimental facts and theoretical understanding of the structure of CF materials XH_x/XD_x composed of the host element X and the

hydrogen isotope H/D:

- a. Free quasi-stable neutrons as the *trapped neutrons* in a box surrounded with infinite potential walls [Kozima 1998 (Sec. 11.1, Premise 1)] ← Free electron model of metals (cf. Appendix A2)
- b. *Emission of phonons* by the nuclear reaction between the trapped neutron and a nucleus instead of emission of a photon in free space ← Premise to meet experimental facts (Premise 6).
- c. *Instability parameter* ξ of trapped neutrons [Kozima 1998 (Sec. 17.1)] to meet the experimental fact of the surface nature of nuclear reactions in the CFP (Premise 2).
- d. *Formation of the superlattice* XH/XD by the self-organization in the open, non-equilibrium condition → Qualitative reproducibility of the events in the CFP.
- e. *The super-nuclear interactions among neutrons in different lattice nuclei mediated by interstitial protons/deuterons* → Dissipation of the intermediate nucleus through phonons to explain Premise 6.
- f. *Neutrons in neutron energy bands* which are formed by the super-nuclear interaction → Explanation of the trapped neutron assumed in the Premise 1.
- g. The *accumulation of trapped neutrons* at reflecting walls results in the formation of cf-matter with high-density neutrons containing *neutron drops* ${}^A_Z\Delta$ [Kozima 2006 (Sec. 3.7.2.3)] → Explanation of nuclear transmutations with large changes of A and Z .
- h. The *interaction of neutron Bloch waves (trapped neutrons) and nuclei at disordered sites* → Explanation of the meaning of the instability parameter ξ assumed in Premise 2 [Kozima 2018 (Sec. 4.1.6), 2019b (Sec. 3-2-1)]
- i. The *neutron bands in alloys and at boundaries of two materials* have been investigated in this paper (cf. Sections 3 and 4).

1.2.1 Trapped Neutrons – Neutrons as a free particle trapped in a square well potential –

The *instability parameter* was introduced into the model [Kozima 1998 (Sec. 11.1a)] to adjust it to the experimental facts that the nuclear reactions occur at surface regions with thickness around a few micrometers [Morrey 1990, Okamoto 1994, Qiao 1997].

“If the stability of the trapped neutron is lost by a large perturbation in the surface layer or in volume, the number of trigger reactions (per unit time) between trapped thermal neutrons and a nucleus A_ZM may be calculated by the same formula as the usual collision process in vacuum but an instability parameter ξ ,

$$P_f = 0.35n_n v_n n_M V \sigma_{nM} \xi, \quad (11.1)$$

where $0.35n_nV$ is the flow density of the trapped thermal neutron per unit area and time, n_M is the density of the nucleus, V is the volume where the reaction occurs, σ_{nM} is the cross section of the reaction. The instability parameter ξ as taken into the relation (11.1) expresses an order of the stability of the trapped neutron in the region as explained in premises 2 and 3, and also in the next paragraph.” [Kozima 1998 (p. 145)]

1.2.2 Neutrons in a neutron energy band in a box with a periodical potential array.

The success of the TNCF model to explain consistently various experimental data from excess heat generation to the nuclear transmutation through neutron, tritium, helium emission obtained in various types of the CF materials [Kozima 1998 (Tables 11.2, 11.3)] have given a reality to the existence of neutrons in the materials composed of host elements and hydrogen isotopes. The first mechanisms supposed for the neutrons trapped in the CF materials was the Bragg reflection of the environmental neutrons by the surface alkali-metal layers and by the surface distributions of hydrogen isotopes. [Kozima 1998 (Sec. 11)]

To explain the surface nature of the nuclear transmutations, the idea of the accumulation of neutrons at surface regions was necessitated. For this end, the energy band structure of the neutrons in the CF materials was used. Neglecting differences of isotopic distribution of host elements in the transition metal hydrides and deuterides, the trapped neutrons were identified with the band neutrons; the neutron drops formed at boundary regions by coherent reflection at boundaries could explain the surface nature of the nuclear transmutations of the CFP [Kozima 2006 (Sec. 3.7)].

The neglect of the variety of nucleon numbers of the host elements is justified by the analogy of the electron band in alloys where the band structure is characterized by the preservation of the band character at high symmetry points (such as Γ , L, P) of (In, Ga) N [Popescu 2010] (cf. Appendix A5). If it is possible to infer the same preservation of the band character at high symmetry points, especially at the gamma point, the use of the TNCF model with the free neutron is justified by the behavior of the neutrons in the bottom of the conduction band which behave like the free neutrons.

The same consideration is closely related to the explanation of the CF data in alloys and ceramics that have not been treated in our works due to the complex structure they have [Romodanov 1998a, 19998b, Kitamura 2018]. If we can use the same assumption to verify the use of the free neutron approximation in such complex CF materials as alloys and ceramics, we can understand the experimental data sets in them with the application of the TNCF model [Kozima 2020].

1.2.3 Neutrons in neutron energy bands formed by the super-nuclear interaction between lattice nuclei mediated by interstitials of H/D in the superlattice. [Kozima 2006]

The application of the electron bands in alloys to the case of the neutron bands in compound CF materials is not straight forward due to the following reason related to the nuclear reactions between a neutron and host elements. Neutron captures occur between by lattice nuclei in the CF materials with different A in a simple host element (or with different A and Z in a compound host elements) in the direction to homogenize the host elements.

We can assume that the process considered in the above paragraph is a positive factor to justify the application of the idea obtained in electron bands to the neutron bands. Then, we may apply the idea of the super-nuclear interaction developed in the CF material with a simple host elements to the cases of the CF materials with compound host elements.

The process of the superlattice formation by the self-organization may be influenced largely by the existence of multiple elements in the CF material with compound host elements. The catalytic nature of the electrocics [Bockris 1970a, 1970b, 2000, Horiuti 1970, Kita 1971, 1973] should be taken into our consideration in our forthcoming paper [Kozima 2021c].

It is noticed that the two processes depicted above, the self-organization and the catalytic nature of the electrocics, gives rise to the qualitative reproducibility of the CFP by the nature of complexity of the first [Kozima 2006, 2019b] and the subtle catalytic nature of the second processes [Kozima 2021a, 2021c].

1.3 Some Relations deduced from the TNCF Model and Three Laws found by the Phenomenological Approach

In Appendix A2, we will explain the structure of the trapped neutron catalyzed fusion model (TNCF model). In this subsection, we give several remarkable conclusions deduced from the TNCF model and their relations with experimental data closely related to the assumptions of $d-d$ fusion reactions in the CF materials.

1.3.1 Reactions between two deuterons occluded in the CF materials

The original idea of nuclear fusion reactions between two deuterons occluded in the palladium metal had it origin in the following reactions known in the nuclear physics.



The branching ratios of the reactions (1.3.1.1) to (1.3.1.3) are known to be $1 : 1 : 10^{-7}$ in the low energy region down to a few keV. Despite of the severe criticism on the possibility of the nuclear reactions (1.3.1.1) to (1.3.1.3) in solids without any mechanisms to accelerate deuterons, it is necessary to check the relation in terms of the experimental data.

It is a natural conclusion that the nuclear products of these reactions satisfy following relations between the numbers N_x of observable x .

$$N_t = N_p = N_{32\text{He}} = N_n \approx 10^7 N_{42\text{He}} = 10^7 N_\gamma. \quad (1.3.1.4)$$

Let us define the number N_Q of excess energy generation Q (measured in MeV) as follows to compare with the values N_x given in Eq. (1.3.1.4).

$$N_Q = Q \text{ (MeV)} / 5 \text{ (MeV)}. \quad (1.3.1.5)$$

In this definition, 5 MeV is taken for the sake of convenience from the weighted mean (2.5 MeV) of the excess energies given in the above three reactions (1.3.1.1) – (1.3.1.3).

Then, N_Q has following relations with experimental values of other observables

$$N_t = N_p = N_{32\text{He}} = N_n = 2 N_Q \quad (1.3.1.6)$$

It has well been known that the relations (1.3.1.4) and (1.3.1.6) are in severe contradiction with the corresponding values determined by experiments.

1.3.2 Relations between observables generated by nuclear reactions in the CFP

When there are several observables related to common parameters in a system, we can expect definite relations between observed quantities of these observables. In the TNCF model, there is a single adjustable parameter n_n which is determined by an observed value of an observable, e.g. the number N_t of tritium atoms (or tritons) in the system. If we can observe another observable, e.g. the number N_n of neutrons in the same system simultaneously, we can compare the observed value with the theoretically calculated value using the value n_n determined by N_t .

The theoretical relations between the N_a and N_b for the observables a and b , respectively, have been given as follows [Kozima 2006 (Sec. 3.3.1)]:

$$N_Q = N_t \approx 10^6 N_n, \quad (1.3.2.1)$$

$$N_{\text{He}3} \approx 0, \quad (1.3.2.2)$$

$$N_\gamma \approx 0, \quad (1.3.2.3)$$

$$N_{\text{He}4} \approx m N_Q \quad (m^{-1} = 2 - 4, \text{ in systems with } {}^6_3\text{Li}). \quad (1.3.2.4)$$

The comparison of these relations with the experimental data had been given already in our previous works (e.g. [Kozima 1998 (Tables 11.2 and 11.3), 2006 (Tables 2.2 and 2.3)]).

It is interesting to cite several experimental data related to the above theoretical results about the observed values of the observables from the data discussed in the papers

[Kozima 2021a, 2021b] presented in this Conference.

The data obtained by Yamaguchi et al. [Yamaguchi 1993] gives us more interesting facts than it had shown us superficially. They had given us the experimental result; “In the final stages of ${}^4\text{He}$ production, a peak attributable to HT appears and increases with the time.” This result shows us that the ${}^4_2\text{He}$ they observed was a result of the $n - t$ reaction not of the $d - d$ reaction and the triton was released afterward [Kozima 2021b (Section 4.4.1)].

The experimental data by Srinivasan et al. [Srinivasan 1990] gives us accumulation of tritium in highly localized spots (fraction of a millimeter or less in size) each containing typically about 10^{12} to 10^{14} atoms (2 to 200 K Bq) of tritium. This accumulation was explained by the catalytic nature of the deuteron deposition on the electrode [Kozima 2021b (Appendix A2)]. Furthermore, their data of the small ratio of neutron-to-tritium yield in the range of 10^{-8} to 10^{-9} is explained by the theoretical result (1.3.2.1).

The experimental data obtained by Claytor et al. [Claytor 1991a, 1991b, 1993, 1996] had given us small values of the ratio of numbers of neutron N_n to tritium N_t with such a very low ratio of N_n/N_t as 10^{-9} [Kozima 2021b (Appendix A3)]. This is another example showing the validity of the TNCF model for the explanation of the CFP.

We have further evidence of the small value of the ratio N_n/N_t contradicting the $d - d$ fusion reaction (1.3.1.4). Romodanov et al. [Romodanov 1993] obtained the values

$$N_n/N_t|_{\max} = 8.5 \times 10^{-6} \text{ to } 0.6 \times 10^{-9},$$

$$N_n/N_t|_{\min} = 1.7 \times 10^{-3} \text{ to } 8 \times 10^{-7}$$

in several metals including Mo, Ti and Fe, alloys including SS and ceramics including TiC and ZrB₂. These values of N_n/N_t show again the validity of the TNCF model to the wide range CF materials [Kozima 2021a (Appendix A4)].

1.3.3 Emission of Neutrons with Energies up to about 20 MeV

We can also expect the energies of neutrons generated in the nuclear reactions in the CFP up to 20 MeV [Kozima 1999] exceeding largely the value 2.45 MeV expected by the $d - d$ reaction (1.3.1.2) erroneously assumed by many researchers.

It is well known that the first observation of the energy spectrum of neutrons emitted from cold fusion materials (CF materials) was performed by Jones et al. [Jones 1989] in BYU in the State of Utah, USA. A unified explanation of their data in addition to the data of excess energy observed by Fleischmann et al. was given by us [Kozima 1997, 1998]. Even if they insisted the discovery of the $E_n = 2.45$ MeV neutrons emitted by the reaction Eq. (1.4) of $d-d$ fusion reactions, there remained possibility of higher energy neutrons at channels 230 – 300 ($E_n = 5.8 - 7.5$ MeV) in their data (cf. [Kozima 2006 (Fig. 1.2)]).

The experimental data showing existence of higher energy neutrons than 2.45 MeV had been shown by many researchers including Bressani et al. [Bressani 1991], Takahashi et al. [Takahashi 1991]. We have given discussions on them in our papers and books [Kozima 1999, 2006, 2016 (Sec. 3.3)].

1.3.4 Three Laws found by the Phenomenological Approach

Analyzing experimental data phenomenologically, we found three laws or regularities between observables [Kozima 2012a]. We give here the three laws in enumeration leaving its explanation to the original paper.

- (1) **First Law.** The stability effect for nuclear transmutation products.
- (2) **Second Law.** The inverse power dependence of the frequency on the intensity of the excess heat production.
- (3) **Third Law.** Bifurcation of the intensity of events (neutron emission and excess heat production) in time.

There are two corollaries of the first law:

Corollary 1-1. Production of a nuclide ${}^A_{Z+1}X$ from a nuclide A_ZX in the system.

Corollary 1-2. Decay time shortening of unstable nuclei in the system.

2. Formation of Neutron Energy Bands in Simple CF Materials

The neutron diffraction developed in the solid state physics [Shull 1951, 1956] revealed the wave nature of the neutrons explicitly suggesting existence of the neutron energy bands by analogy to the electron energy bands [Kozima 2006 (Sec. 3.7)]. The idea of the neutron energy bands had taken its quantum mechanical image by the nuclear interaction between interstitial protons/deuterons and neutrons in lattice nuclei suggested by overlapping of the extended proton/deuteron wave functions from the interstitial site and the extended neutron wavefunctions from lattice nuclei [Kozima 1998 (Sec. 12.4), 2009]. The neutrons in different lattice nuclei interact directly with the super-nuclear interaction mediated by interstitial protons/deuterons in the CF materials.

The development of the research of the exotic nuclei with the large excess of the neutron number over the proton number from nuclei with the small mass number A such as ${}^2\text{He}$, ${}^3\text{Li}$ and ${}^4\text{Be}$ to rather large A such as ${}_{11}\text{Na}$, ${}_{13}\text{Al}$ and ${}_{14}\text{Si}$ (cf. Appendix A4) gives reality of our expectation that the host elements like ${}_{28}\text{Ni}$ and ${}_{46}\text{Pd}$ in the CF materials participate in the super-nuclear interaction for the neutron bands in them.

The isolation of halo neutrons in exotic nuclei, as explained in Tables and Figures in

Appendix A4 for nuclei with rather small values of proton numbers known by the time, gives indirect support for the mechanism of the super-nuclear interaction between neutrons in lattice nuclei mediated by interstitial protons/deuterons [Kozima 2006 (Sec. 3.7.2, Fig. 3.3)].

3. Neutron Bloch Waves at Interfaces of the Compound CF Material

The neutron Bloch waves are eigenstates of neutrons in a regular lattice and do not interact with lattice nuclei at absolute zero at all. The neutrons can interact with lattice nuclei that displaced from the equilibrium position by some reason, lattice oscillation or displacement by statistical reason or by surface conditions. The problem at present is the case of interfaces where nuclei of different species or lattice nuclei at displaced sites are. The interfaces of such chemically active metals used as catalytic substances as Ti, Ni, Pd and other alloys are complicated with many characteristics uncovered yet. So, our investigation into their influence on the CFP will be qualitative at present and the quantitative investigation should be left for future.

3.1 Roles of the Boundary Layers in the CF Materials on the CFP

There are almost always boundaries in the CF materials used in the CF experiments. The CF materials are in contact with three kinds of contacting materials, gases (gas and plasma contact systems), liquids (electrolytic systems) and solids (another CF material or substrates).

The boundaries of a CF material work on the CFP in various physical and chemical ways. The physical roles of a boundary include (1) as substrates to make the CF material stable in the severe condition to make the material appropriate for the CFP, (2) as barriers to contain H/D in the CF material, and (3) to induce nuclear reactions between the trapped neutrons and nuclei at disordered sites around the boundaries. The chemical roles of a boundary include (1) chemisorption of active elements on the boundary from environment to make easy completion of the necessary conditions for the CFP, (2) generation of effective molecules by catalysis from molecules in environment. The subtle roles of the chemical reactions at the boundary will be discussed in more detail in the following subsections 4.2 and 4.3.

The physical roles of the boundary layers have been used in many experiments including [Yamaguchi 1993, Miley 1996a, 1996b, Iwamura 2006],

The chemical roles have been noticed already [Kozima 2000] and used in several experiments [Fleischmann 1989, Jones 1989, McKubre 1993, Celani 2020a].

“from 0.1 M LiOD in 99.5% D₂O + 0.5% H₂O solutions.” [Fleischmann 1989 (p. 302)]

“The electrolyte is typically a mixture of ~ 160 g D₂O plus various metal salts in ~ 0.1 g amounts each: FeSO₄ · 7H₂O, NiCl₂ · 6H₂O, PdCl₂, CaCO₃, Li₂SO₄ · H₂O, Na₂SO₄ · 10H₂O, CaH₄(PO₄)₂ · H₂O, TiOSO₄ · H₂SO₄ · 8H₂O, and a very small amount of AuCN. The pH is adjusted to < 3 with HNO₃. All 14 runs reported here began with this basic electrolyte.” [Jones 1989 (p. 738)]

“A PTFE liner was employed in order to prevent the highly corrosive electrolyte, 1 M LiOD + 200 ppm Al, from making contact with the metal cell body.” [McKubre 1993 (p. 7)]

“The oxidation of the wires by pulses of electrical current in air creates a rough surface featuring a sub-micrometric texture that proves particularly effective at inducing thermal anomalies when temperature exceeds 400°C. This effect appears also to be increased substantially by depositing segments of the wire with a series of elements (such as Fe, Sr, Mn, K, - -). Furthermore, an increase of AHE was observed after placing the treated wires inside a sheath made of borosilicate glass (B–Si–Ca; BSC), and even more after impregnating the sheath with the same elements used to coat the wires.” [Celani 2020a (pp. 25 – 26)]

3.2 Chemistry of Boundary Layers of CF Materials

It should not be forgotten that the process of the formation of a CF material is an atomic process working in the formation of a CF material, a structure composed of a host material (e.g. Ni, Pd and other metals which had been used as catalysts) and hydrogen isotopes with interfaces in between them. In the process, it is possible that other materials are sometimes participating with (as substrates or as a component of the CF material).

It is necessary, therefore, to know the chemical state of the interface in the compound CF materials for better understanding of the necessary conditions for the CFP. There have been observed (1) effects of chemical components on the CFP on one hand, and (2) atomic behaviors at the boundary of noble metals working as catalysts on the other. However, we have not enough knowledge yet about the relation between the phenomena pointed out above, it will be helpful to summarize present situations of them for the development of CFP.

We will give summary of the surface effect on the CFP in this section. In the next section, we will introduce subtle effects of transition metal catalysts on the molecules at their boundary. Extensive investigation on the effect of the interfaces between gas, liquid and solid phases where electrochemical characteristics of electrochemicals are taken into

consideration will be given in another paper scheduled to publish recently [Kozima 2021c].

Srinivasan et al. [Srinivasan 1990, 1993] had given extensive investigations on the CFP where were interesting facts related to the electrodischarge [Bockris 1970a, 2000] which we had left for almost 30 years.

“One of the most interesting findings to emerge out of the autoradiographic imaging of deuterated Ti samples from different experiments is the fact that tritium is invariably concentrated in highly localized spots (fraction of a millimeter or less in size) each containing typically about 10¹² to 10¹⁴ atoms (2 to 200 kBq) of tritium. If this is viewed in the light of the observations of other groups notably, the Los Alamos work, that neutrons are produced in bunches of 30 to 300 within time spans of microseconds and also that the neutron-to-tritium yield ratio is in the range of 10⁻⁸ to 10⁻⁹, it is tempting to speculate that in these titanium samples perhaps some kind of a cascade reaction or micronuclear explosion probably occurs in specific sites in the near surface region resulting in 10¹⁰ to 10¹² fusion reactions during each event. This intriguing possibility warrants further experimental study.” [Srinivasan 1990 (pp. 1 – 2)]

“On the whole 15 experiments out of 29 have indicated tritium levels significantly above background values so far. These include K₂CO₃ in 25% D₂O, Li₂CO₃ in 50% D₂O, K₂CO₃ in H₂O as well as Li₂CO₃ in H₂O combinations. Surprisingly, most of the natural lithium carbonate in ordinary-water-cells run so far have generated detectable amounts of tritium whereas some enriched Li₂CO₃ in H₂O cells have not. For other combinations also for every successful case there has been at least one cell with that particular combination which has not yielded tritium. While the maximum amount of tritium generated has been in a K₂CO₃ in 25% D₂O cell (3390 Bq/ml), the second highest (1454 Bq/ml) was with a Li₂CO₃ in H₂O cell.” [Srinivasan 1993 (p. 129)]

The localization of the active region for the tritium generation is discussed in another paper presented at this Conference [Kozima 2021b (Appendix A29)].

To understand the CFP in the multilayered CF materials [Claytor 1991b, Miley 1996a, 1996b], it is necessary to investigate the neutron energy bands at around the solid-solid interface between two CF materials (cf. Appendix A9 for more details). Experimental data by Claytor et al. is analyzed in [Kozima 2021b (Appendix A3)] and by Miley et al. is in Appendix A10 in this paper.

We may contemplate the neutron bands in the compound CF materials using the electron band at the P-N junction of semiconductors (cf. e.g. [Shockley 1950] and Appendix A5).

The difference of the Fermi energies in the adjacent materials A and B causes a flow of neutrons from A with a higher Fermi energy to B with a lower one generating energy corresponding the difference of the Fermi energies of each material. This contributes the excess energy production in the cold fusion phenomenon (CFP) in addition to the nuclear reactions between band neutrons and nuclei at disordered position such as at boundaries of a material and at positions shifted by the thermal motion at finite temperature.

The heterogeneous catalysts, Ni, Pd, Ti, Au, etc., in contact with three kinds of contacting materials, gases (gas contact systems), liquids (electrolytic systems) and solids (substrates for CF materials), may work at least three ways for the CFP. (1) Decomposing H_2/D_2 molecules into $2H/2D$ atoms as catalysts facilitating absorption and occlusion of H/D atoms in the CF materials. (2) Formation of the superlattice of host elements and hydrogen isotopes feeding plenty of the latter generating the neutron bands containing the trapped neutrons. (3) Forming surface/boundary layers at the boundary where are induced nuclear reactions between the trapped neutrons and disordered nuclei.

The tremendous amounts of transmuted nuclei comparable to the fission products of uranium observed by Miley et al. [Miley 1996a, 1996b] are explained by the existence of Ni/polystyrene or Pd/polystyrene boundary in their beads of Patterson Power Cell. Their data sets are introduced and investigated in our paper presented at this Conference [Kozima 2021b (Appendix A4)].

There is an interesting experimental data on the generation of 4_2He and 3_1H by Yamaguchi et al. [Yamaguchi 1993] in Au-Pd- MnO_x compound structure with deuterium. The data shows us an interesting feature of the effect of the interface between MnO_x and PdD_x layers even if it had been accepted as an evidence of the 4_2He generation in the popular CF material, PdD_x as shown in another paper presented at this Conference [Kozima 2021b (Sec. 4.4.1)].

The extensive data sets on the CF materials composed of the alloys based on the constantan and several kinds of substrates in H_2 gas obtained by Celani et al. [Celani 2019, 2020a, 2020b] gives us the CFP in the CF materials with various kinds of interfaces such as gas-solid and solid-solid ones. The data are analyzed in our paper presented at this

Conference [Kozima 2021b (Appendix A5)].

Iwamura et al. had worked on the CF materials so called “Pd Complexes” where D₂ gas was permeated [Iwamura 2006a, 2006b]. The CF material of Pd complex Pd-Pd/CaO-Pd is composed of a following structure Pd (40nm)-CaO/Pd(100nm)-Pd(100μm) with two solid-solid interfaces. There should be subtle catalytic actions in the interfaces suggested by the electrochemistry as pointed out already (e.g. [Bockris 1970a, 1970b, 2000]), and the localization of the nuclear transmutations observed by the authors might be reflecting the catalytic action which we had not pointed out in our former analyses [Kozima 2014b (Sec. 5.2)]. The data by Iwamura et al. are discussed from our present point of view in another paper presented at this Conference [Kozima 2021b (Sec. 4.4.5)].

It should be mentioned on the extensive works with the CF materials including Pd-Ni-Zr, Cu-Ni and other alloys on the zirconia and silica in hydrogen isotopes [Kitamura 2014, 2018]. They observed the excess heat in various experimental conditions which include several types of solid-solid and gas-solid interfaces. We have given a brief comment of on their data [Kozima 2020] and an extensive introduction to their data sets is given in our paper presented at this Conference [Kozima 2021a (Appendix A5)].

3.3 Effects of Transition Metal Catalysts on the Molecules at the Interfaces

We are apt to neglect effects of “the hydrides of the main-group metals” on the CFP regardless of the fact that chemists have noticed its importance as expressed in a review article as follows:

“In the same period little has been made of the hydrides formed by the main-group metals, despite their importance in chemical synthesis, notably as precursors to other metal hydrides and as reducing agents for a wide range of inorganic and organic substrates.” [Aldridge 2001 (p. 3306, Introduction)]

In the investigation of the CFP in the CF materials with interfaces in between, we encounter inevitably with this problem which we do not take into our consideration in this paper. The problem had been taken up partially in our papers presented at this Conference [Kozima 2021a, 2021b] and will be investigated more extensively in the paper published elsewhere [Kozima 2021c]. The specific characteristics of the chemical properties of the host material in the CFP having essential importance in the realization of the nuclear reactions in the CF materials are the hydrogen-electrode reaction [Kita 1971, 1973] and the characteristics of the heterogeneous catalysis (active sites and

supports) [Wikipedia Catalysis, Kozima 2021a, 2021b, 2021c].

Keeping these facts in our mind, we have given only several important properties of the transition metal hydrides seemingly have close relation to the CFP in the above Section 3.2 and give several more below on the papers by Zaera et al. [Zaera 1996], Belkova et al. [Belkova 2016] and Takagi et al. [Takagi 2017].

*“Here we will discuss the results reported to date on **the structure and reactivity of the different types of hydrocarbon moieties** that form on transition metal surfaces. One of the goals of this review is to provide an organometallic guide for **the possible interactions of hydrocarbons with transition metals** with the idea of examining their relation to the corresponding surface chemistry.”* [Zaera 1996 (p. 2651, Introduction)]

“The dihydrogen bond --- an interaction between a transition-metal or main-group hydride ($M-H$) and a protic hydrogen moiety ($H-X$) --- is arguably the most intriguing type of hydrogen bond. It was discovered in the mid-1990s and has been intensively explored since then. Herein, we collate up-to-date experimental and computational studies of the structural, energetic, and spectroscopic parameters and natures of dihydrogen-bonded complexes of the form $M-H\cdots H-X$, as such species are now known for a wide variety of hydrido compounds.” [Belkova 2016 (p. 8545, Abstract)]

It should be noticed the complexity of the interaction of the transition metals and hydrogen atoms as the various metal-hydride complexes are formed on the surfaces of transition metals Re, Tc, Mo, W, Nb, and Ta as shown by Takagi et al. [Takagi 2017]:

“Ninefold coordination of hydrogen is very rare and has been observed in two different hydride complexes comprising rhenium and technetium. Herein, based on a theoretical/experimental approach, we present evidence for the formation of ninefold H-coordination hydride complexes of molybdenum ($[MoH_9]^{3-}$), tungsten ($[WH_9]^{3-}$), niobium ($[NbH_9]^{4-}$) and tantalum ($[TaH_9]^{4-}$) in novel complex transition-metal hydrides, Li_5MoH_{11} , Li_5WH_{11} , Li_6NbH_{11} and Li_6TaH_{11} , respectively.” [Takagi 2017 (p. 1, Abstract)]

[Yvon 1998]

It is interesting to notice new transition metal complexes which take in a lot of hydrogen atoms compared to the host elements. One of their materials are reviewed by Yvon as materials for hydrogen storage as follows:

“Complex transition-metal hydrides provide new opportunities for hydrogen storage. Their hydrogen-to-metal ratios reach values of up to $H/M = 4.5$ ($BaReH_9$) and thus surpass the hydrogen-to-carbon ratios of hydrocarbons (methane: $H/C = 4$); their hydrogen-volume efficiencies exceed that of liquid hydrogen by a factor of up to two (Mg_2FeH_6), their weight efficiencies exceed 5% (Mg_3MnH_7), and their hydrogen dissociation temperatures under 1 bar hydrogen pressure range from ca. 1000 ($NaKReH_9$) to 4000 ($CaMgNiH_4$). Their crystal chemistry is extremely rich and shows a large inventory of transition-metal hydrido complexes that often conform to the 18-electron rule. New synthetic methods are likely to yield further members of this class of materials.” [Yvon 1998 (p. 613, Abstract)]

If the structure of these materials fits to the necessary conditions for the CFP as we formulated before [Kozima 2006] and explained briefly in Sec. 1.2, it may be possible to use these materials for the CF materials to realize the CFP.

3.4 Nuclear Reactions between a Neutron Bloch Waves and Nuclei at Disordered Sites

The neutrons in a neutron band do not interact with lattice nuclei at their regular points as the electrons in an electron band do not with atoms at lattice points. Therefore, the interaction of the trapped neutron with the nuclei in the CF materials occurs when the nuclei exist at disordered sites; (1) nuclei displaced by lattice oscillation at finite temperature, (2) foreign impurity nuclei substituted the host nuclei, (3) foreign impurity nuclei at interstitial positions, (4) nuclei at boundary and surface regions where the array of nuclei is necessarily irregular.

4. Neutron Energy Bands in the Compound and Composite CF Materials

In the development of the phenomenological approach to the CFP based on the inductive logic, we investigated quantum mechanically the bases of the premises of the TNCF model. The neutron energy bands had been a key concept for the realization of the trapped neutrons and the cf-matter; the neutron bands have been realized by the neutrons in lattice nuclei interacting mutually through the super-nuclear interaction mediated by the interstitial hydrogen isotopes (cf. Appendix A4). Extending the experimental data in CF materials with rather simple host elements to those with complicated constituents and structures, we must encounter necessity to justify the applicability of the TNCF model

[Kozima 1998, 2006] to these complicated CF materials [Kozima 2021a, 2021b]. In this chapter, we try to investigate this problem using the TNCF model with reference to the electron bands in semiconductors where the same problem in solid state physics had been investigated for a long time.

It should be noticed that we assume existence of the superlattice in the CF material composing the compound CF material beforehand while it is not necessarily apparent. The investigations of hydrogen isotopes at around the interfaces in the multi-layered metals performed by the Iwate University group guided by Dr. H. Yamada and Dr. S. Narita for more than 10 years have revealed their complex behavior depending on the temperature, loading/deloading processes, species of the component metals and other factors such as coating on the surface [Narita 2008, Hosokawa 2013, Kataoka 2016, Sato 2018, Endo 2020]. We should take these works into our consideration in the detailed investigation of the bases of our phenomenological model for the composite and compound CF materials.

4.1 Neutron energy bands in compound CF materials speculated with reference to the electron energy bands in alloys

We give a model, i.e. the electron energy band in alloys investigated in the solid state physic in Appendix A6 and that around P/N junction in Appendix A7.

It was shown that the preservation of the band character at high symmetry points (such as Γ , L, P) of (In, Ga)N (Appendix A6, [Popescu 2010]). So, we may be able to use the picture of the neutron energy band to the CF materials with alloy host elements when the trapped neutrons (neutrons in the neutron band) are localized at high symmetry points in the k-space. In the cases where the density n_n of the trapped neutrons is not high, this situation is realized as the simple TNCF model has been successful to give consistent explanations for various data sets [Kozima 1998].

In the case of the neutron energy bands at around the solid-solid interface, we can refer to the electron energy bands at P-N junction depicted by Shockley [Shockley 1950] (cf. Appendix A7).

The neutron energy bands in alloys speculated in reference to the electron bands (cf. Appendix 6) may be used to understand the experimental data obtained by Dufour et al. in stainless steel [Dufour 1993] (cf. [Kozima 2021a (Sec. 4.1.1)]), by Celani et al. in constantan [Celani 2019] (cf. [Kozima 2021b (Appendix A4)]), by Kitamura et al. in Pd-Ni-Zr Deposit [Kitamura 2018] (cf. [Kozima 2021a (Appendix A6)]).

4.2 Neutron energy bands at a boundary of two materials

With reference to the electron bands in semiconductor devices, we may speculate the neutron bands at the interface of a CF material and a substrate or another CF material. We give here a glimpse of the neutron band at the interface and their effects on the CFP. More details of this problem are given in Appendix A9.

According to the flow of holes in the right region to the left region in Fig. A7-1 (f), we can assume accumulation of neutrons in the boundary region flowing into there from the higher potential region as shown in Fig. A9-3 (c) making the density n_n very high. Then, there are formed the neutron drops ${}^AZ\Delta$ with large values of A and Z which make the generation of new nuclides corresponding to the natural abundances as shown in Fig. A9-4 observed by Miley et al. [Miley 1996a (p. 635, Fig. 2)] in accordance with the stability law for the nuclear transmutation [Kozima 2006 (Section 2.15), 2012].

4.3 Neutron energy bands in composite CF materials

As illustrated in Appendix A6-1, it is possible to preserve the band character of the quantum states of the electron at high symmetry points (such as Γ , L, P) of (In, Ga)N [Popescu 2010].

If it is possible to infer the same preservation of the band character at high symmetry points, especially at the gamma point, the use of the TNCF model for the behavior of the neutrons in the bottom of the conduction band when their density is not high is justified. This may be the reason that our phenomenological approach had been successful neglecting the variety of nucleon numbers of the host elements (${}^{A}_{28}\text{Ni}$ and ${}^{A}_{46}\text{Pd}$, for example) in our explanation of the CFP in the CF materials based on Pd and Ni.

The same consideration may be applicable to the explanation of the CF data in alloys and ceramics that have not been treated in our works due to the complex structure they have [Romodanov 1993, 1998a, 1998b, Kitamura 2018]. If we can use the same assumption of verification of the use of the free neutron approximation in such complex CF materials as alloys and ceramics, we can understand the experimental data sets in them with the application of the TNCF model [Kozima 2020].

4.4 Formation of exotic nuclei by the absorption of neutrons

Exotic nuclei investigated in free space developed very much in recent years extending its realm to larger values of A and Z . When the environment of the exotic nuclei is extended to the CF materials from the free space, the stability of the formed exotic nuclei increases very much due to the interaction with the interstitial hydrogen isotopes and the investigation of their characteristics should be accelerated. The data of quantum

halo compiled by Jensen et al. are useful to speculate possible existence of exotic nuclei with proton numbers larger than 10 in the CF materials where we can expect stabilization of the exotic nuclei by interaction with the interstitial protons/deuterons.

“The neutron dripline is currently not known with certainty above Ne. Possible halos with low S_n are specified in Table I. The valence neutron in ${}^4_{11}\text{Be}_7$ is an s -state halo, as seen in Fig. 2. The relatively large S_n for ${}^5_{14}\text{B}_9$ indicates that even for the expected s state the halo should not be much extended. In contrast, ${}^6_{19}\text{C}_{13}$ satisfies the halo criterion of Fig. 2 while ${}^6_{17}\text{C}_{11}$ is too small, indicating a dominating $l=2$ component. Other candidates are ${}_{10}{}^{31}\text{Ne}_{21}$ and ${}_{13}{}^{40}\text{Al}_{27}$, in which the neutron bindings are unknown but positive and probably very small.” [Jensen 2004 (p. 235)]

5. Conclusion

Since 1990, we have investigated the CFP observed in the CF materials composed of host elements and hydrogen isotopes either protium or deuterium using a phenomenological approach [Kozima 1990, 1998, 2004, 2005, 2006]. The TNCF model with an adjustable parameter n_n (the density of the trapped neutron) had been useful to give a unified explanation of various experimental data sets in both protium and deuterium systems due to the common nature of the CF material characterized by the superlattice of host elements and hydrogen isotopes in them [Kozima 2019a].

In search of effective CF materials to produce the CFP, the composite and compound materials had been investigated more often recently improving the qualitative reproducibility. The essential mechanism of the CFP in these materials seems common to the rather simple CF materials and then we do not need to change our point of view to analyze the phenomenon. However, it is desirable to investigate the applicability of the phenomenological approach so successful in explanation of the data obtained in rather simple CF materials to the composite and compound materials. This is the main theme of this paper to contemplate the justification of the phenomenological approach to use for the analysis of the CFP obtained in the composite and compound CF materials.

Due to the complex structure of these composite and compound materials, we must use analogy of the electron energy bands developed in the semiconductor physics to the neutron energy bands in the CFP depending on the physical similarity of the two cases.

Applicability of the concept of the neutron energy band to the composite CF materials (alloys and ceramics) might be qualitatively justified by the analogy from the electron bands in semiconductor alloys where the investigation on this problem has been kept deep and a long period. At least in the high-symmetry points of the k -space where the trapped

neutrons stay long time in CF materials where we observe main events in the CFP, we may be able to use the neutron energy band for the investigation of the nuclear reactions in the CF materials. The CFP with generation of new nuclei having large shifts of A and Z (the experiment by Miley et al. [Miley 1996a, 1996b], for instance) may needs special attention for this point different from that mentioned above.

The applicability of the neutron energy band to the compound CF materials (with interfaces between different CF materials) speculated in Appendix A9 seems very promising to give satisfactory explanations for the nuclear transmutations with large changes of A and Z observed by Miley et al. [Miley 1996a, 1996b]. The flow of neutrons from a CF material C_1 to another C_2 through the boundary speculated in Appendix A9 will elevate the density n_n in the C_2 very much to generate the neutron drop ${}^A_Z\Delta$ with large values of A and Z there. According to the nuclear transmutation by the transformation [Kozima 2006 (Sec. 2.5.4)], the neutron drops ${}^A_Z\Delta$ transforms into the transmuted nucleus A_ZX with largely shifted A and Z from the original nuclei in the host material as explained in Appendix A10.

Appendices

Appendix A1. Meditations of Geniuses

Appendix A2. The Trapped Neutron Catalyzed Fusion (TNCF) Model

Appendix A3. The Neutron Drop (ND) Model

Appendix A4. Valence Neutrons in Exotic Nuclei

Appendix A5. Neutron Energy Bands due to the Super-nuclear Interaction mediated by Interstitials and Halo Neutrons

Appendix A6. Electron Energy Bands in Alloys and Neutron Energy Bands in Composite CF Materials (Alloys and Ceramics)

Appendix A7. Electron Energy Bands at P/N Junctions in Semiconductors

Appendix A8. Surface States at the Boundary between CF Material and Oxide/Ceramic

Appendix A9. Neutron Energy Bands in Compound CF Materials – Pd-Ti and Ni-Pd multilayers

Appendix A10. Nuclear Reactions at Interfaces. Experiments by Miley et al. [Miley 1994, 1996a, 1996b]

Appendix A1. Meditations of Geniuses

When we engage in contemplation of the truth behind phenomena in the environment surrounding us, it is necessary to use some kinds of logic. In the modern science

established in 16th century and lasted until the middle of 20th century, its main scheme was overwhelmed by deductive logic based on the established principles discovered by inductive logic and confirmed by deductive logic thereafter.

Contemplation of human has been essentially interlaced with inductive and deductive logics as noticed in the beginning of our civilization born about 25 century ago. It had been recognized the importance of intuition in the inductive logic as expressed in the letter of Plato and in a writing of A. Einstein as cited below. We must notice the importance of intuition in the inductive logic to find out a tentative principle from our experience and the use of inductive and deductive logic alternatively to proceed our contemplation to the final principle as we see in the sayings of the geniuses.

The importance of intuition in the inductive logic had been expressed in the letter of Plato:

“For it does not at all admit of verbal expression like other studies, but, as a result of continued application to the subject itself and communion therewith, it is brought to birth in the soul on a sudden, as light that is kindled [341d] by a leaping spark, and thereafter it nourishes itself.” [Plato 1966 ([341c] – [341d])].

Similar consideration had been expressed by A. Einstein as follows:

“I believe in intuition and inspiration. ... At times I feel certain I am right while not knowing the reason. When the eclipse of 1919 confirmed my intuition, I was not in the least surprised. In fact, I would have been astonished had it turned out otherwise. Imagination is more important than knowledge. For knowledge is limited, whereas imagination embraces the entire world, stimulating progress, giving birth to evolution. It is, strictly speaking, a real factor in scientific research.” [Einstein 1931 (p. 97)]

In addition to these word of wisdom, it is interesting to read a sentence by one of the pioneers of the CFP about his recognition of a positive role of the trapped neutrons who had surely read the book *Discovery of the Cold Fusion Phenomenon* (1998, Ohtake Shuppan, Tokyo, Japan) presented him by the author at the publication of the book.

“Three points summarize the historical significance of the discovery of LENR:- - -

2. The work must give rise to modifications of the theory of the nucleus. However, new physics is probably not needed. Classical nuclear physicists have maintained an agnostic stance for so long because their knowledge of fusion is concerned with reactions in plasma, and they have paid little attention to the effects of a solid lattice upon nuclear

activity within it after injection of H and D at high fugacity, or to the effect of free neutrons in the lattice.” [Bockris 1999 (p. 71)]

Appendix A2. The Trapped Neutron Catalyzed Fusion (TNCF) Model

[Kozima 1998 (Sec. 11, pp.142 – 146)]

For the sake of convenience of readers, we summarize the premises of the trapped neutron catalyzed fusion (TNCF) model in this Appendix A2.

Premises of the TNCF Model [Kozima 1998 (Sec. 11.1a)]

Premise 1. We assume a priori existence of the quasi-stable trapped neutron with a density n_n in pertinent solids, to which the neutron is supplied essentially from the ambient neutron at first and then by breeding processes (explained below) in the sample.

The density n_n is an adjustable parameter in the TNCF model which will be determined by an experimental data set using the supplementary premises which will be explained below concerning reactions of the trapped neutron with other particles in the solids. The quasi-stability of the trapped neutron means that the neutron trapped in the crystal does not decay until a strong perturbation destroys the stability while a free neutron decays with a time constant of 887.4 ± 0.7 s.

Premise 2. The trapped neutron in a solid reacts with another nucleus in the surface layer of the solid, where it suffers a strong perturbation, as if they are in vacuum. We express this property by taking the parameter (the instability parameter) ζ , defined in the relation (A2.1) written down below, as $\zeta = 1$.

We must mention here that the instability parameter ζ in the surface layer is not known at all and it can be, as noticed recently, more than one ($1 > \zeta$) making the determined value of the parameter n_n smaller. This ambiguity is suggested by various anomalous changes of decay character of radioactive isotopes and by unexpected fission products in the surface layer.

Premise 3. The trapped neutron reacts with another perturbing nucleus in volume by a reaction rate given in the relation (11.1) below with a value of the instability parameter $\zeta > 0.01$ due to its stability in the volume (except in special situations such as at very high temperature as 3000 K).

Following premises on the measured quantities of nuclear products and the excess heat are used to calculate reaction rates, for simplicity:

Premise 4. Product nuclei of a reaction lose all their kinetic energy in the sample except they go out without energy loss.

Premise 5. A nuclear product observed outside of the sample has the same energy as its

initial (or original) one.

This means that if an energy spectrum of gamma-ray photon or neutron are observed outside, it reflects directly nuclear reactions in the solid sample. The same is for the distribution of the transmuted nucleus in the sample. Those spectra and the distributions of the transmuted nuclei are the direct information of the individual events of the nuclear reaction in the sample.

Premise 6. The amount of the excess heat is the total liberated energy in nuclear reactions dissipated in the sample except that brought out by nuclear products observed outside.

Premise 7. Tritium and helium measured in a system are accepted as all of them generated in the sample.

The amounts of the excess heat, tritium and helium are accumulated quantities reflecting nuclear reactions in the sample indirectly and are the indirect information of the individual events.

Premises about structure of the sample are expressed as follows:

Premise 8. In electrolytic experiments, the thickness l of the alkali metal layer on the cathode surface (surface layer) will be taken as $l = 1 \mu\text{m}$ (though the experimental evidence show that it is $1 \sim 10 \mu\text{m}$).

Premise 9. The mean free path or path length l_t of the triton with an energy 2.7 MeV generated by $n + {}^6\text{Li}$ fusion reaction will be taken as $l_t = 1 \mu\text{m}$ irrespective of material of the solid. Collision and fusion cross sections of the triton with nuclei in the sample will be taken as the same as those in vacuum.

Premise 10. Efficiency of detectors will be assumed as 100 % except otherwise described, i.e. the observed quantities are the same as those generated in the sample and to be observed by the detector in experiments if there are no description of its efficiency.

A premise will be made to calculate the number of events N_Q producing the excess heat Q ;

Premise 11. In the calculation of the number of an event (a nuclear reaction) N_Q producing the excess heat Q , the average energy liberated in the reactions is assumed as 5 MeV unless the reaction is identified: $N_Q = \text{Excess heat } Q \text{ (MeV)} / 5 \text{ (MeV)}$.

The number of trigger reactions (per unit time) between trapped thermal neutrons and a nucleus AZM may be calculated by the same formula as the usual collision process in vacuum but an instability parameter ξ :

$$P_f = 0.35 n_n v_n n_M V \sigma_{nM} \xi \quad (\text{A2.1})$$

Where $0.35 n_n v_n$ is the flow density of the trapped thermal neutron per unit area and time, n_M is the density of the nucleus, V is the volume where the reaction occurs, and σ_{nM} is the

cross section of the reaction.

Appendix A3. The Neutron Drop (ND) Model

Formation of the cf-matter including the neutron drop in the neutron energy band by the super-nuclear interaction between neutrons in different lattice nuclei mediated by the interstitial hydrogen isotopes, ^1H or ^2D , replaced the trapped neutrons in the square-well potential for the neutrons assumed in the TNCF model explained in Appendix A2. The ND model has more realistic bases on the properties of constituent nuclei in the CF materials and gives wider applicability to explain nuclear transmutations observed in experiments. We give here an outline of the basis of the ND model explained above.

1. Generation of the CF Material

Hydrogen isotopes and the material composed of host elements interact electrochemically through the interfaces surrounding the material. This electrochemical interaction is fundamentally including catalytic nature and has subtle nature sensitive to the nature of the interface [Bockris 1970a, 1970b, 2000, Horiuti 1970, Kita 1971, 1973]. → Qualitative reproducibility

2. Formation of the Superlattice of the Host Elements and the Hydrogen Isotope

The formation of a superlattice XH/XD of the host element X and the hydrogen isotope H/D is realized by the nonlinear process in the nonequilibrium condition as a process of the complexity [Kozima 2012b, 2013]. → Qualitative reproducibility

3. Generation of the Neutron Energy Bands through the Super-nuclear Interaction among the Neutrons in Different Lattice Nuclei Mediated by the Interstitial Hydrogen Isotope [Kozima 2006 (Sec. 3.7)]

4. Formation of the CF-matter composed of the Band Neutrons and the Itinerant Hydrogen Isotopes [Kozima 2006 (Sec. 3.7)]

5. Formation of the Neutron Drops $^A_Z\Delta$ composed of Z Protons and $(A - Z)$ Neutrons [Kozima 2006 (Sec. 3.7)]

6. Interaction of Neutrons and Neutron Drops in the Neutron Bands and Nuclei in the Disordered Sites in the CF material [Kozima 1998, 2006 (Sec. 2.4.5), 2021b (Appendix A4)]

Appendix A4. Neutrons in Exotic Nuclei

A4-1. Distribution of Valence Neutrons in Halos of Small A Nuclei**A4-2. Theoretical Distribution of Valence Neutrons in Halos of Large A Nuclei****A4-3 In Search of a New Picture of the Atomic Nucleus****Appendix A4-1. Distribution of Valence Neutrons in Halos of Small A Nuclei** [Kozima 2006 (Sec. 3.7), Riisager 1994, Mizutori 2000, Jensen 2004]

Large extension of halo neutrons outside the ordinary nuclear radius is effective to realize the super-nuclear interaction between neutrons in lattice nuclei mediated by the interstitial protons/deuterons [Kozima 2006]. The large extension of wavefunctions of halo neutrons of two-, three and many-body halos of small nucleon number (A) nuclei have been worked out recently (cf. e.g. [Jensen 2004]). These features of the valence neutrons in the exotic nuclei are favorable for the realization of the super-nuclear interactions between neutrons in lattice nuclei if they exist in the large A nuclei in the CF materials known by now. Following figures and tables show the large extension of the valence neutron wavefunctions for the small A nuclei.

Table A4-1. Halo states. For each state the excitation and separation energies and the angular momentum of the halo particle(s) are listed. [Riisager 1994 (Table I)]

Nucleus	E_x (MeV)	$S - E^a$ (keV)	Configuration	l	K
^{11}Be	g.s.	504	$n + ^{10}\text{Be}$	0	
^{11}Be	0.32	184	$n + ^{10}\text{Be}$	1	
^{17}F	0.50	105	$p + ^{16}\text{O}$	0	
^6He	g.s.	973	$n + n + ^4\text{He}$		2
^{11}Li	g.s.	310	$n + n + ^9\text{Li}$?
^{14}Be	g.s.	1340	$n + n + ^{12}\text{Be}$?

^aFrom Audi and Wapstra, 1993.

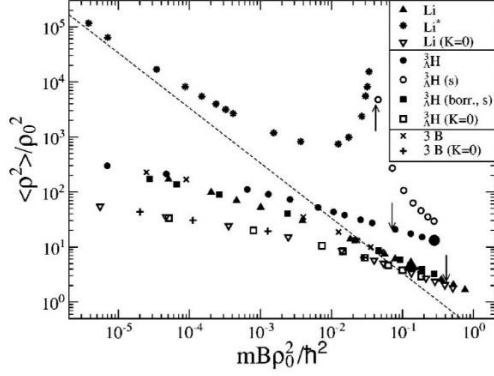


FIG. A4-3. Scaling plot for three-body halos as in Fig. 3: dashed line, the Efimov curve for $\nu = 0$ [see Eq. (8)]; ∇ , \blacktriangle , $*$, masses corresponding to ${}^{11}\text{Li}$ (${}^9\text{Li} + n + n$); \square , \blacksquare , \circ , \bullet , ${}^3_{\text{H}}\text{H}$ (${}_{\text{H}} + n + p$); realistic points are indicated by a large, closed triangle and circle; $+$, \times , three different particles with two fixed scattering lengths while the third is varied. The arrows indicate transitions between Borromean, tango, and bound-state regions. We used ρ_0 from Eq. (10). See text for further discussion. [Jensen 2004 (Fig. 5)]

In Figs. A4-1 – A-3, we used following variables for a three-cluster division with individual masses, momenta, and coordinates denoted by m_i , \mathbf{p}_i , and \mathbf{r}_i , respectively, to describe the relative motion by means of hyperspherical coordinates ($i = 1, 2, 3$). The total mass is $M = (m_1 + m_2 + m_3)$, while the average radial coordinate, the hyper-radius ρ is given by

$$m\rho^2 \equiv (1/M) \sum_{i < k} m_i m_k (r_i - r_k)^2,$$

where m is an arbitrary mass unit. And ρ_0 is defined by

$$M\rho_0^2 \equiv (1/M) \sum_{i < k} m_i m_k R_{ik}^2,$$

where R_{ik} is the two-body scaling length of the system i and k .

Table A4-2. Two-body halo candidates (only for neutron halos). The columns give cluster division of the system, excitation energy E^* (MeV), separation energy S (MeV), orbital angular momentum quantum number l of the dominating components and references. ([Jensen 2004] Table I)

System	E^*	S	l	References
${}^2_1\text{H}_1 (n+p)$	0.0	2.2	0	Audi and Wapstra, 1995
${}^{11}_4\text{Be}_7 ({}^{10}_4\text{Be}_6+n)$	0.0	0.50	0	Audi and Wapstra, 1995
${}^{14}_5\text{B}_9 ({}^{13}_5\text{B}_8+n)$	0.0	0.97	0	Ajzenberg-Selove, 1991
${}^{15}_6\text{C}_{11} ({}^{16}_6\text{C}_{10}+n)$	0.0	1.22	0	Ajzenberg Selove, 1991
${}^{19}_6\text{C}_{13} ({}^{18}_6\text{C}_{12}+n)$	0.0	0.53	0,2	Nakamura <i>et al.</i> , 1999
${}^{31}_{10}\text{Ne}_{21} ({}^{30}_{10}\text{Ne}_{20}+n)$	0.0	>0	1,3	Sakurai, 2002
${}^{34}_{11}\text{Na}_{23} ({}^{33}_{11}\text{Na}_{22}+n)$	0.0	?	1,3	Audi and Wapstra, 1995
${}^{35}_{12}\text{Mg}_{23} ({}^{34}_{12}\text{Mg}_{22}+n)$	0.0	?	1,3	Audi and Wapstra, 1995
${}^{40}_{13}\text{Al}_{27} ({}^{39}_{13}\text{Al}_{26}+n)$	0.0	>0	1,3	Sakurai, 2002
${}^{43}_{14}\text{Si}_{29} ({}^{42}_{14}\text{Si}_{28}+n)$	0.0	>0	1,3	Notani <i>et al.</i> , 2002
${}^4_2\text{He}_2 ({}^3_2\text{He}_1+n)$	20.21	0.36	0	Tilley <i>et al.</i> , 1992
${}^{10}_4\text{Be}_6 ({}^9_4\text{Be}_5+n)$	6.26	0.55	0	Ajzenberg-Selove, 1990
${}^{10}_4\text{Be}_6 ({}^9_4\text{Be}_5+n)$	5.96	0.85	0	Ajzenberg-Selove, 1990
${}^{11}_4\text{Be}_7 ({}^{10}_4\text{Be}_6+n)$	0.32	0.18	1	Endt, 1990
${}^{12}_5\text{B}_7 ({}^{11}_5\text{B}_6+n)$	2.62	0.65	0	Ajzenberg-Selove, 1990
${}^{12}_5\text{B}_7 ({}^{11}_5\text{B}_6+n)$	2.72	0.55	1	Ajzenberg-Selove, 1990
${}^{14}_5\text{B}_9 ({}^{13}_5\text{B}_8+n)$	0.74	0.23	1	Ajzenberg-Selove, 1991
${}^{17}_6\text{C}_{11} ({}^{16}_6\text{C}_{10}+n)$	0.29	0.44	0,2	Tilley <i>et al.</i> , 1993
${}^{18}_7\text{N}_{11} ({}^{17}_7\text{N}_{10}+n)$	2.61	0.22	1	Tilley <i>et al.</i> , 1995
${}^{21}_8\text{O}_{13} ({}^{20}_8\text{O}_{12}+n)$	3.08	0.73	?	Endt, 1990
${}^{25}_{10}\text{Ne}_{15} ({}^{24}_{10}\text{Ne}_{14}+n)$	3.32	0.96	?	Endt, 1990
${}^{25}_{10}\text{Ne}_{15} ({}^{24}_{10}\text{Ne}_{14}+n)$	4.07	0.11	?	Endt, 1990

Table A4-3. Three-body halo candidates (only for neutron halos). The columns give division of the system, excitation energy E^* (MeV), separation energy $S = S_{2n}$ (MeV), orbital angular momentum quantum number l of the dominating nucleon-core components, remarks (B for Borromean, T for tango) and references as in Table A2-1. Excited states are indicated by a star on the separation energy. ([Jensen 2004] Table II)

System	S	l	R	References
${}^6_2\text{He}_4$ (${}^4_2\text{He}_2 + n + n$)	0.97	1	B	Audi and Wapstra, 1995
${}^8_2\text{He}_6$ (${}^6_2\text{He}_4 + n + n$)	2.13	1	B	Audi and Wapstra, 1995
${}^{11}_3\text{Li}_8$ (${}^9_3\text{Li}_6 + n + n$)	0.30	0,1	B	Audi and Wapstra, 1995
${}^{14}_4\text{Be}_{10}$ (${}^{12}_4\text{Be}_8 + n + n$)	1.33	0,2	B	Audi and Wapstra, 1995
${}^{17}_5\text{B}_{12}$ (${}^{15}_5\text{B}_{10} + n + n$)	1.4	0,2	B	Audi and Wapstra, 1995
${}^{19}_5\text{B}_{14}$ (${}^{17}_5\text{B}_{12} + n + n$)	≈ 0.5	0,2	B	Audi and Wapstra, 1995
${}^{22}_6\text{C}_{16}$ (${}^{20}_6\text{C}_{14} + n + n$)	≈ 1	0,2	B	Audi and Wapstra, 1995;
${}^{29}_9\text{F}_{20}$ (${}^{27}_9\text{F}_{18} + n + n$)	≈ 0.9	0,1,2	B	Audi and Wapstra, 1995
${}^{31}_9\text{F}_{22}$ (${}^{29}_9\text{F}_{20} + n + n$)	> 0	0,1,2,3	B	Sakurai, 2002
${}^{32}_{10}\text{Ne}_{22}$ (${}^{30}_{10}\text{Ne}_{20} + n + n$)	≈ 1	0,1,2,3	T	Audi and Wapstra, 1995
${}^{34}_{10}\text{Ne}_{24}$ (${}^{32}_{10}\text{Ne}_{22} + n + n$)	> 0	0,1,2,3	B	Notani <i>et al.</i> , 2002
${}^{35}_{11}\text{Na}_{24}$ (${}^{33}_{11}\text{Na}_{22} + n + n$)	≈ 0.5	0,1,2,3	B	Audi and Wapstra, 1995
${}^{37}_{11}\text{Na}_{26}$ (${}^{35}_{11}\text{Na}_{24} + n + n$)	> 0	0,1,2,3	B	Notani, 2002
${}^{38}_{12}\text{Mg}_{26}$ (${}^{36}_{12}\text{Mg}_{24} + n + n$)	≈ 1	0,1,2,3	B	Audi and Wapstra, 1995; Sakurai <i>et al.</i> , 1997
${}^{41}_{13}\text{Al}_{28}$ (${}^{39}_{13}\text{Al}_{26} + n + n$)	> 0	0,1,2,3	T	Sakurai, 2002
${}^{43}_{13}\text{Al}_{30}$ (${}^{41}_{13}\text{Al}_{28} + n + n$)	?	0,1,2,3	B	
${}^{44}_{14}\text{Si}_{30}$ (${}^{42}_{14}\text{Si}_{28} + n + n$)	?	0,1,2,3	?	
${}^{46}_{14}\text{Si}_{32}$ (${}^{44}_{14}\text{Si}_{30} + n + n$)	?	0,1,2,3	?	

Table A4-4. Multibody halo candidates. The columns give cluster division of the system, four- and two-neutron separation energies (in MeV) S_{4n} , S_{2n} , indication with B if Borromean property is known, and references as in Table A2-1 and Table A2-2. ([Jensen 2004] Table III)

System	S_{4n}	S_{2n}	B?	References
${}^8_2\text{He}_6$ (${}^4_2\text{He}_2 + 4n$)	3.10	2.13	B	Audi and Wapstra, 1995
${}^{14}_4\text{Be}_{10}$ (${}^{10}_4\text{Be}_6 + 4n$)	4.00	1.33	B	Audi and Wapstra, 1995
${}^{19}_5\text{B}_{14}$ (${}^{15}_5\text{B}_{10} + 4n$)	≈ 1.9	≈ 0.5	B	Audi and Wapstra, 1995
${}^{22}_6\text{C}_{16}$ (${}^{18}_6\text{C}_{12} + 4n$)	≈ 4.7	≈ 1	B	Sakurai <i>et al.</i> , 1999
${}^{31}_9\text{F}_{22}$ (${}^{27}_9\text{F}_{18} + 4n$)	> 0	> 0	B	Sakurai, 2002
${}^{34}_{10}\text{Ne}_{24}$ (${}^{30}_{10}\text{Ne}_{20} + 4n$)	> 0	> 0	?	Lukyanov <i>et al.</i> , 2002; Notani <i>et al.</i> , 2002
${}^{37}_{11}\text{Na}_{26}$ (${}^{34}_{11}\text{Na}_{22} + 4n$)	> 0	> 0	?	Lukyanov <i>et al.</i> , 2002; Notani <i>et al.</i> , 2002
${}^{43}_{13}\text{Al}_{30}$ (${}^{39}_{13}\text{Al}_{26} + 4n$)	?	?	?	
${}^{46}_{14}\text{Si}_{32}$ (${}^{42}_{14}\text{Si}_{28} + 4n$)	?	?	?	

Appendix A4-2. Theoretical Distribution of Valence Neutrons in Halos of Large A Nuclei [Kozima 2006 (Sec. 3.7)] [Mizutori 2000]

The distribution of valence neutrons in exotic nuclei with small numbers of the nucleon number A has been determined by experiments hitherto. However, it was difficult to measure it in nuclei with large values of A and we must rely on the theoretical values in our investigation of the CFP in the CF materials containing nuclei with A larger than 20 such as Ni and Pd. We give some examples from a recent paper supporting our conjecture.

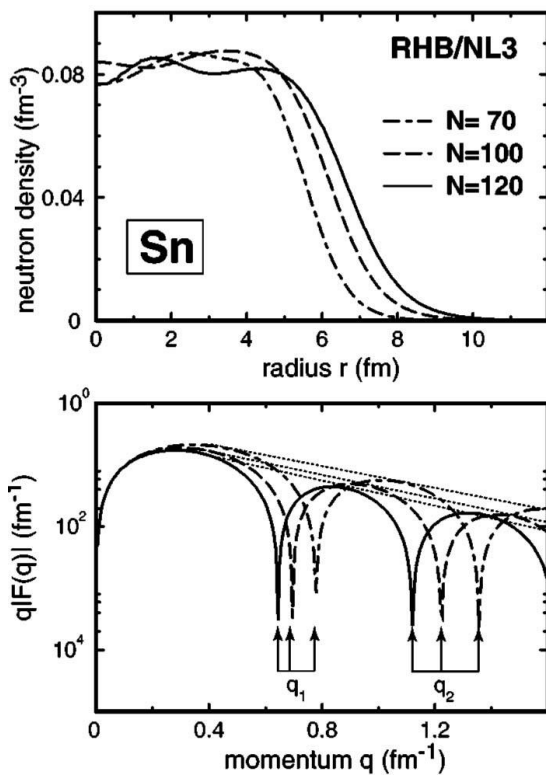


Fig. A4-4. Top: neutron densities calculated in the RHB/NL3 model for $^{120,150,170}\text{Sn}$. Bottom: the corresponding form factors. Positions of the first and second zeros in the form factors are indicated by arrows. [Mizutori 2000 (Fig. 1)]

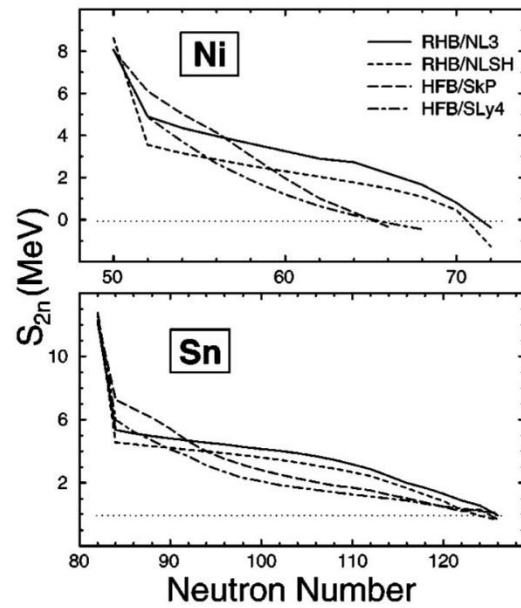


Fig. A4-5. Two-neutron separation energies S_{2n} for the neutron-rich Ni (top) and Sn (bottom) isotopes calculated in the HFB/SLy4, HFB/SkP, RHB/NLSH, and RHB/NL3 models. [Mizutori 2000 (Fig. 7)]

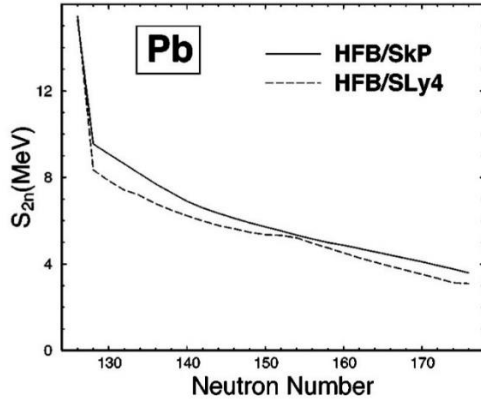


Fig. A4-6. Two-neutron separation energies S_{2n} for the neutron-rich Pb isotopes calculated in the HFB/SLy4 and HFB/SkP models. [Mizutori 2000 (Fig. 8)]

Table A4-5. Characteristics of neutron distributions in ^{40}Ca and ^{208}Pb : diffraction radius R_0 , surface thickness σ , and geometric radius R_{geom} (all in fm), obtained in the HFB and RMF models employed in this work. [Mizutori 2000 (Table I)]

Nucleus		SLy4	SkP	NL3	NLSH
^{40}Ca	R_0	3.827	3.844	3.844	3.841
	σ	0.905	0.923	0.845	0.793
	R_{geom}	4.353	4.388	4.296	4.274
^{208}Pb	R_0	6.870	6.849	7.076	7.075
	σ_n	1.022	1.033	0.971	0.929
	R_{geom}	7.252	7.244	7.409	7.374

A4-3 In Search of a New Picture of the Atomic Nucleus [Baumann 2007, Crawford 2014, Middleton 2019]

The picture of the atomic nucleus has changed from the first “structureless liquid drop of protons and neutrons” to the next “nuclear shell model where protons and neutrons experience a central potential generated by the other nucleons and therefore, as quantum particles, must exist in discrete energy levels.” [Middleton 2019]

The investigation of the exotic nuclei $^{40}_{12}\text{Mg}$ and $^{42}_{13}\text{Al}$ [Baumann 2007, Crawford 2014] opened the door to envisage a new picture of the atomic nucleus as Middleton says “When ^{40}Mg was finally observed as a bound state⁴ in 2007, it showed itself to be an even more neutron-rich Mg nuclide for studying the effects of weak binding on the nuclear structure.” [Middleton 2019]

We have now in the nuclear physics a developing story about the new picture of the atomic nucleus with new interactions between nucleons is on the nucleus in free space.

On the other hand, we have encountered a new interaction of a neutron in the lattice nucleus with a proton/deuteron at an interstitial site in the CF materials to explain the wonderful events observed in the CFP [Kozima 2006, 2019b]. We might be able to imagine a happy marriage of the two developing investigations resulting in a new solid state-nuclear physics.

Appendix A5. Neutron Energy Bands due to the Super-nuclear Interaction mediated by Interstitials and Halo Neutrons [Kozima 2006 (Sec. 3.7), 2013 (Sec. 3.3)]

We give an illustration of the essential idea of the neutron band formation due to the super-nuclear interaction between neutrons in lattice nuclei mediated by interstitial protons/deuterons.

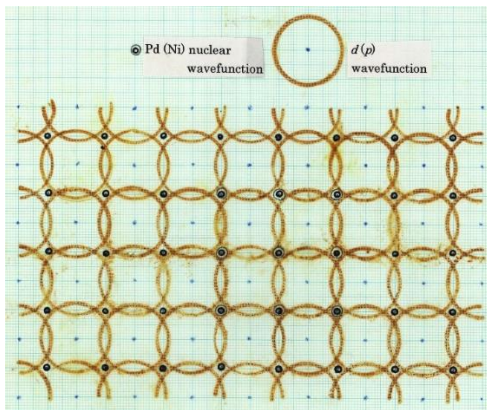


Fig. A5-1. Schematic diagram showing the optimum superlattice of host nuclei (Pd or Ni) at lattice points and hydrogen isotopes (d or p) at interstitials formed by self-organization in the open, non-equilibrium condition. Nuclear wavefunctions with extension of only a few femtometers of lattice nuclei are exaggerated largely to be seen on the figure. The extension of deuteron (proton) wavefunctions centered at interstitials is represented by a single circle in contact with nuclear wavefunctions at nearest lattice points [Kozima 2013 (Fig. 3.8)]

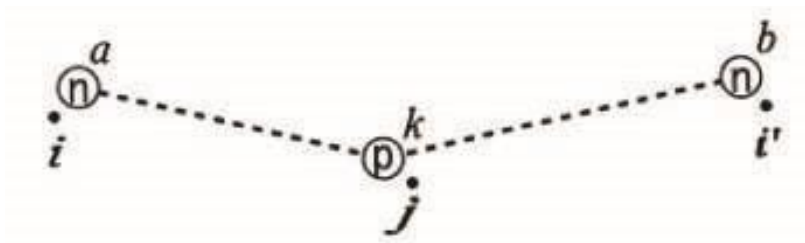


Fig. A5-2. Super-nuclear interaction of two neutrons in different lattice nuclei at site i and i' mediated by interstitial protons at sites j 's [Kozima 2006 (Fig. 3.3), 2013 (Fig. 3.9)]

Appendix A6. Electron Energy Bands in Alloys and Neutron Energy Bands in Composite CF Materials (Alloys and Ceramics) – CF Active and CF Inactive Elements

A6-1 Electron Bands in Alloys

A6-2 Neutron Energy Bands in Composite CF Materials (Alloys and Ceramics)

A6-1 Electron Bands in Alloys

We cite here an example of the theoretical justification of the electron energy band formation in alloys in (In, Ga)N alloy.

“Yet, many alloy experiments are interpreted phenomenologically precisely by constructs derived from wave vector k , e.g. effective masses or van Hove singularities.”

“Conclusions –

We have shown that, while keeping the more appropriate polymorphous picture in describing the physical properties of disordered alloy via supercells, one can still obtain an effective band structure (EBS) in the underlying primitive cell. We applied this tool to (In,Ga)N and Ga(P,N) contrasting the preservation of the band character at high symmetry points (such as Γ , L, P) of (In, Ga)N with the rapid disintegration of the valence band Bloch characteristic and the appearance of a pinned impurity band in Ga(N,P).” [Popescu 2010]

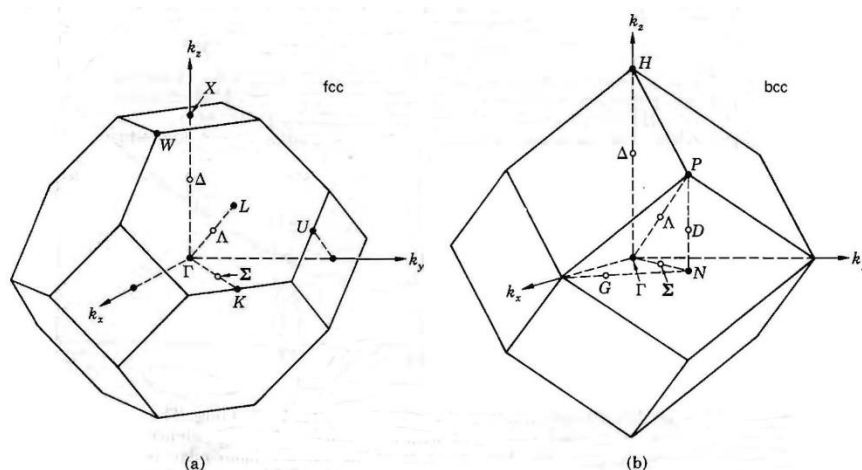


Fig. A6-1. Standard labels of the symmetry points and axes of the Brillouin zones of the fcc and bcc lattices. The zone centers are Γ . In (a) the boundary point at $(2\pi/a)(100)$ is X; the boundary point at $(2\pi/a)(1/2\ 1/2\ 1/2)$ is L, the line Δ runs between Γ and X. In (b) the corresponding symbols are H, P and Δ . [Kittel 1976 (fig. 14)]

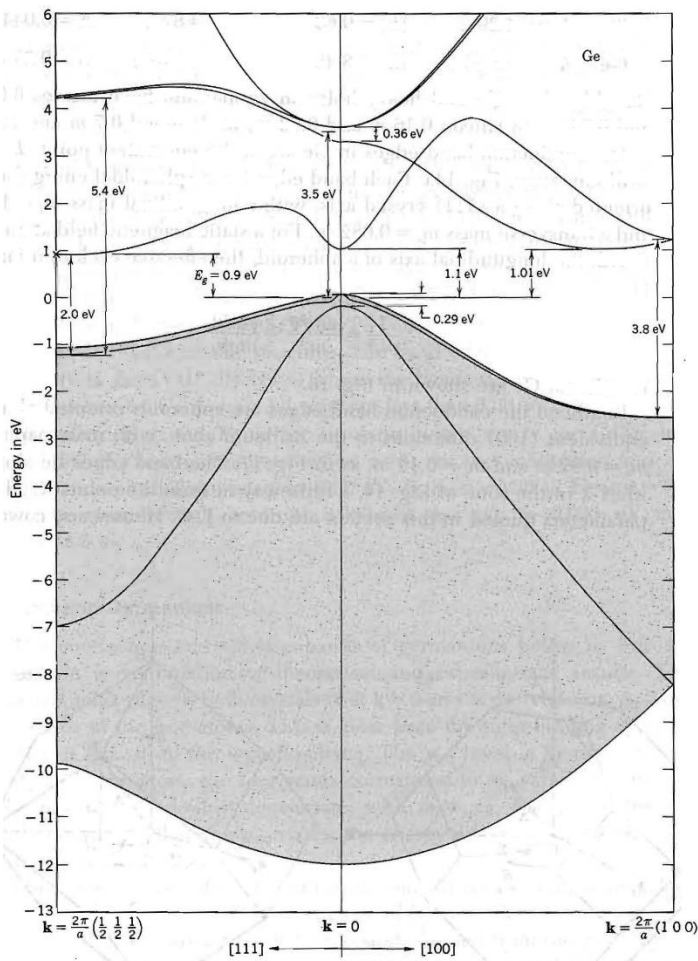


Fig. A6-2. Calculated band structure of germanium, after C.Y. Fong. The general features are in good agreement with experiment. The four valence bands are shown in grey. The fine structure of the valence band edge is caused by spin-orbit splitting. The energy gap is indirect; the conduction band edge is at the point $(2\pi/a)(1/2, 1/2, 1/2)$. The constant energy surfaces around this point are ellipsoidal. [Kittel 1976 (Fig. 15)]

A6-2 Neutron Energy Bands in Composite CF Materials (Alloys and Ceramics) – CF Active and CF Inactive Elements –

It is possible to extend the investigation of the electron bands given above to the case of the neutron bands in composite CF materials, where we could use the TNCF model successfully applied to CF materials composed of simple host elements (e.g. [Kozima 1998]) and to the case of the compound CF materials investigated in Sec. 4. In the latter case, it is necessary to assume the minor element (Cu or Co, for example) alloyed to the main element (Ni or Pd, for example) is an active element defined in Sec. 4.1.4 of [Kozima 2021a] for the use of the TNCF model.

In the program to extend the phenomenological approach to the cases of the composite CF materials, it is necessary to care about the species of minor elements added to the host elements (for instance Pd or Ni) due to the following reason.

(1) It is revealed by Claytor et al. [Claytor 1998] that addition of minor elements to a host element (Pd, for instance) causes increase of tritium generation by some element (e.g. B, Cu) and its decrease by some other (e.g. Li, Be, Hf) (cf. [Kozima 2021a (Sec. 4.1.3)]).

(2) On the other hand, there are several evidence that iron-group elements are active in the HER (hydrogen electrode reaction) [Kita 1973] and UPD (underpotential deposition) [Akiyama 1986, Fukushima 1993, Nakano 1998].

Considering the experimental data given above (1) and (2), we define tentatively (a) CF active (or constructive) elements and (b) CF inactive (or destructive) elements as follows:

(a) *CF active elements*; elements in 3d and 4d transition metals.

(b) *CF inactive elements*; other elements than those in the group (a).

Then, we may be able to use the analogy of the electron bands in the (In, Ga)N alloy given above (A6-1) to the neutron bands in the CF materials composed of Pd (or Ni) and *CF active elements*. Fortunately, these CF materials include those used in recent works by Celani et al. (Constantan $\text{Cu}_{55}\text{Ni}_{44}\text{Mn}_1$) and Kitamura et al. ($\text{Pd}_x\text{Ni}_{0.35-x}\text{Zr}_{0.65}$).

Appendix A7. Electron Energy Bands at p-n Junctions in Semiconductors

We can find out an example of the electron energy bands at around the interface between the two semiconductors in the textbook by Shockley [Shockley 1950]. Fig. A7-1 shows the distribution of holes and electrons and energy as a function of position in a p-n junction under applied biases. [Shockley 1950 (Fig. 4-4)]

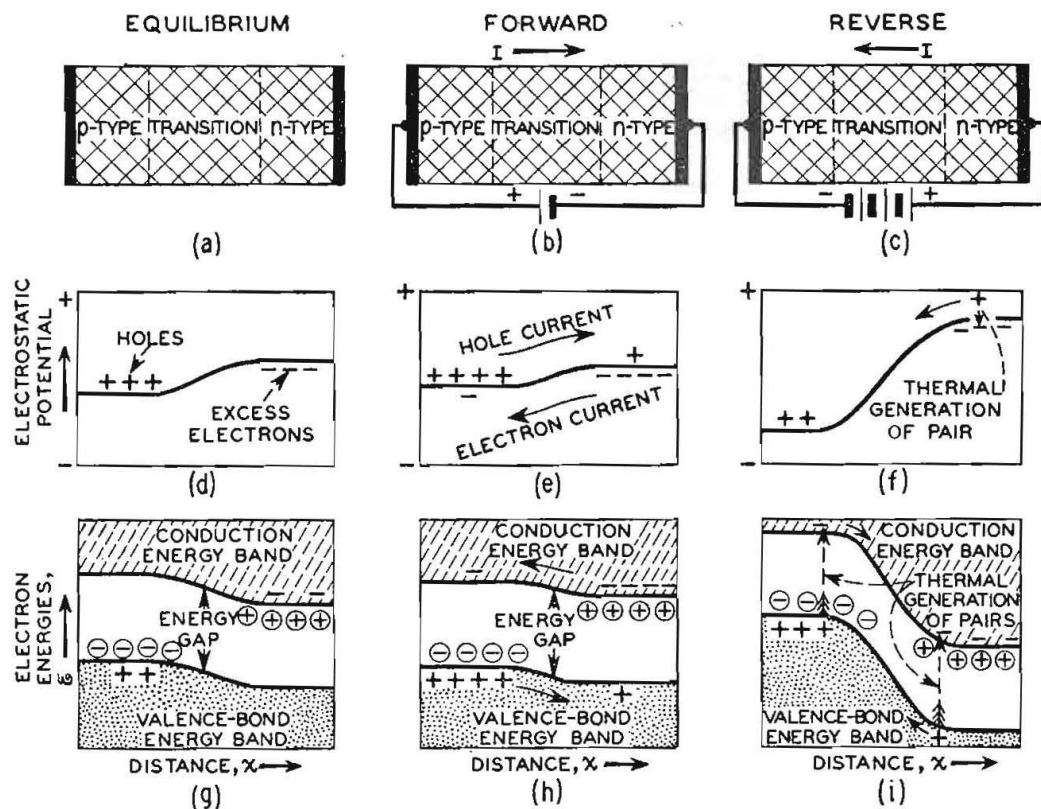


Fig. A7-1. Distribution of Holes and Electrons and Energy as a Function of Position in a p-n Junction under Applied Biases. [Shockley 1950 (Fig. 4-4)]

Appendix A8. Surface States at the Boundary between CF Material and Oxide/Ceramic

A8-1. Electron Surface States at the Boundary between Metal and Vacuum

A8-2. Neutron Surface States at the Boundary between CF Material and Substrate

A8-1. Electron Surface States at the Boundary between Metal and Vacuum

We must notice the electron surface states in the solid-vacuum interface in relation to the catalytic effect of the solid-gas interface in the CF materials in which the neutron surface state has not yet been investigated at present. The examples shown in Fig. A8-1 illustrate several features of the surface states which may be useful to speculate the corresponding features of the neutron case discussed in the next subsection.

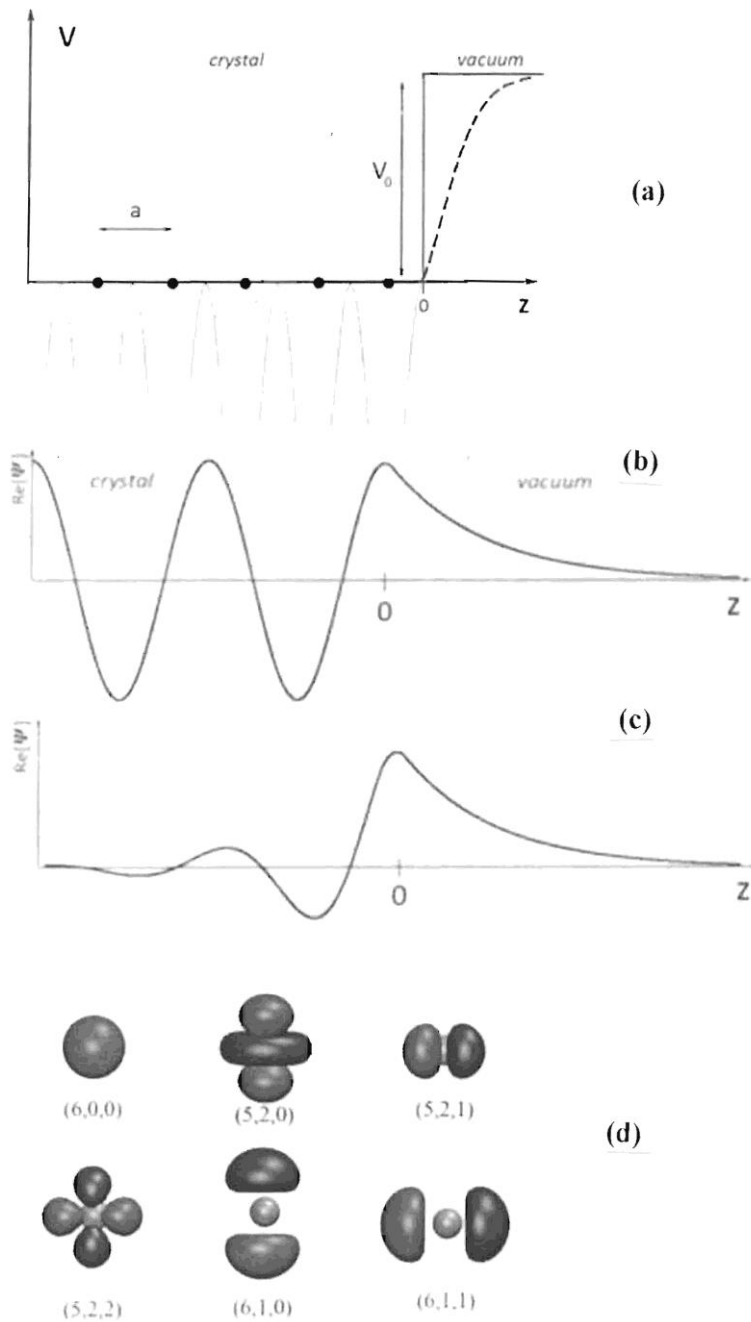


Fig. A8-1. Schematic description of electron surface states at a metal/vacuum boundary. (a) Simplified one-dimensional model of a periodic crystal potential terminating at an ideal surface. (b) Real part of the type of solution to the one-dimensional Schrödinger equation that corresponds to the bulk states. (c) Real part of the type of solution to the one-dimensional Schrödinger equation that corresponds to surface states (Shockley states). (d) Atomic like orbitals of a Pt-atom. [Wikipedia Surface-state (Figs. 1, 2, 3, 5)]

A8-2. Neutron Surface States at the Boundary between CF Material and Substrate

We can speculate the neutron surface states in analogy to the electron case shown in Fig. A8-1. We may expect the catalytic effect of the surface states in the solid-solid or solid-gas interface in the CFP.

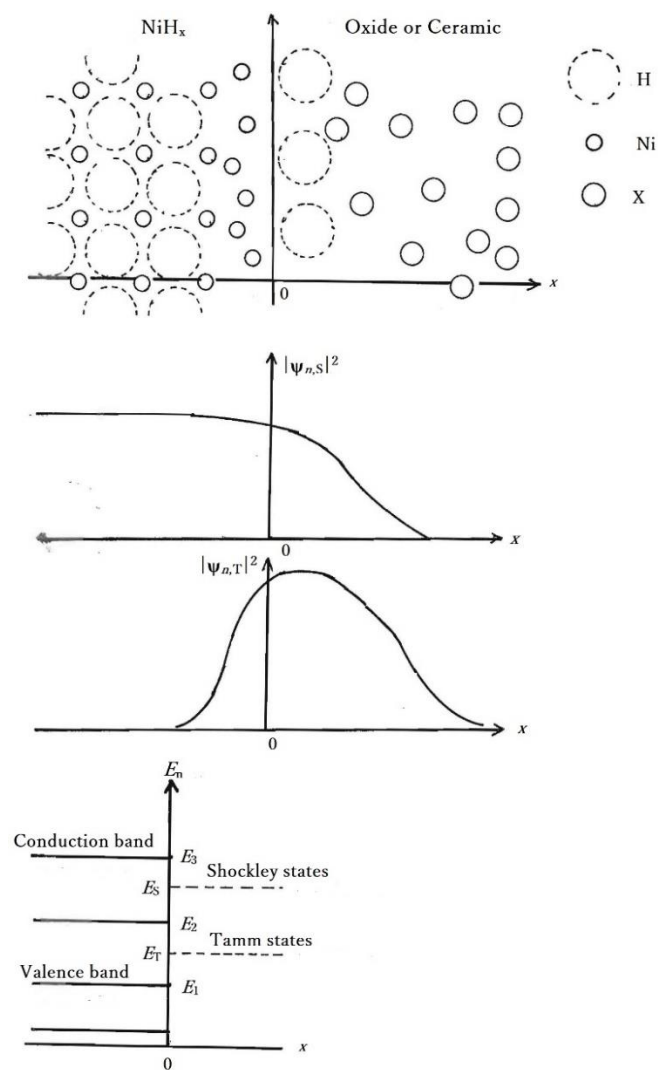


Fig. A8-2. Speculative neutron boundary states at a boundary of CF material (NiH_x)/Oxide • Ceramic. (a) Schematic of NiH_x vs. an Oxide/Ceramic boundary. The nuclei in the latter are expressed by X and the transition region at the boundary is roughly depicted as a mixture of Ni, H and X nuclei. (b) The schematics of the squares of the wavefunction $\psi_{n,S}$ of a neutron Shockley state (in upper figure) and that $\psi_{n,T}$ of a neutron Tamm state (in lower figure). (c) The schematics of the energies E_S of a Shockley state and E_T of a Tamm state in relation to the neutron conduction and valence bands in the CF material NiH_x .

Appendix A9. Neutron Energy Bands in Compound CF Materials – Pd-Ti and Ni-Pd multilayers

Using the electron energy bands around the p-n junction, we can imagine the neutron energy bands around the interface in the compound CF materials.

To make our image of the compound CF materials clear, consider the Patterson beads used in elaborate experiments by Miley et al. [Miley 1996a, 1996b]

“Experiments using 1-mm plastic and glass microspheres coated with single and multilayers of thin films of various metals such as palladium and nickel, used in a packed-bed electrolytic cell (Patterson Power Cell™ configuration), have apparently produced a variety of nuclear reaction products.” [Miley 1996b]

“Results from a thin film (500-3000A) nickel coating on 1-mm microspheres in a packed-bed type cell with 1-molar Li₂SO₄-H₂O electrolyte were reported recently at the Second International Conference on Low-Energy Nuclear Reactions (Miley and Patterson, 1996). Key new results are now presented for thin-film Pd and for multiple Pd/Ni layers.” [Miley 1996a]

“Thin-film coatings on 1-mm-diameter plastic microspheres, ranging from 500A thick single layers of **Pd** or **Ni** to multiple **Ni/Pd** layers, were used in a flowing packed-bed-type electrolytic cell with an I-molar Li₂SO₄ light water electrolyte.” [Miley 1996b]

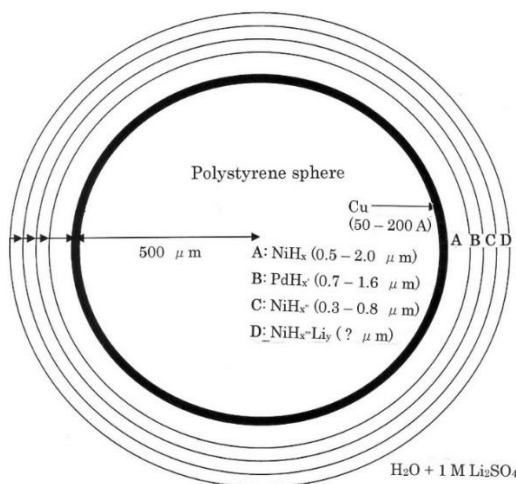


Fig. A9-1 Patterson Bead (Schematic illustration) used with H₂O + 1 M Li₂SO₄ electrolyte ([Miley 1996b]). [Kozima 2011 (Fig. 2.5)]

We can depict the neutron energy bands around the Ni/Pd interface as shown in Fig. A9-2 by analogy of the electron energy bands shown in Fig. A7-1.

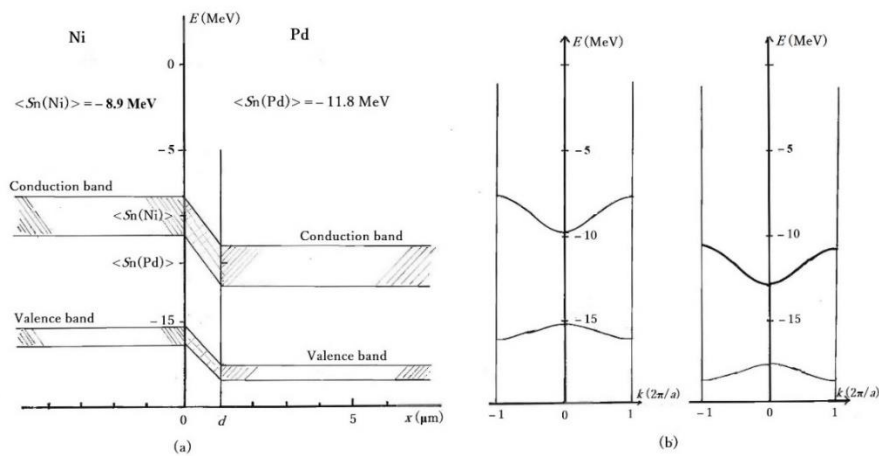


Fig. A9-2. Speculative neutron bands of a Ni-Pd compound structure. (a) The conduction and the valence bands in a Ni/(Ni+Pd)/Pd structure as a function of position at around the Ni-Pd boundary, (b) the conduction and the valence bands of Ni and Pd in the Brillouin zone.

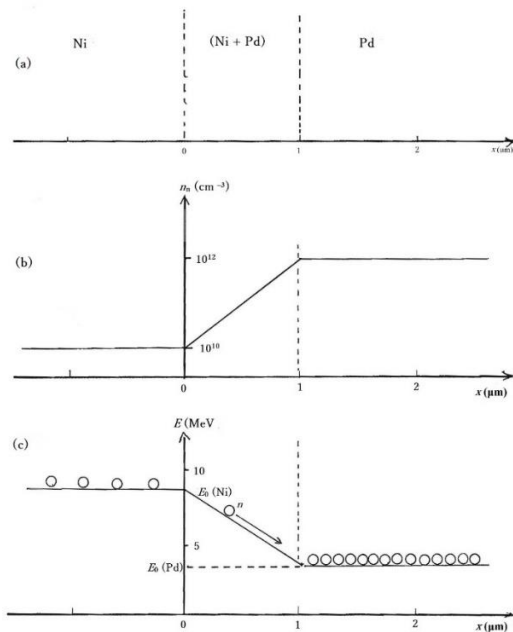
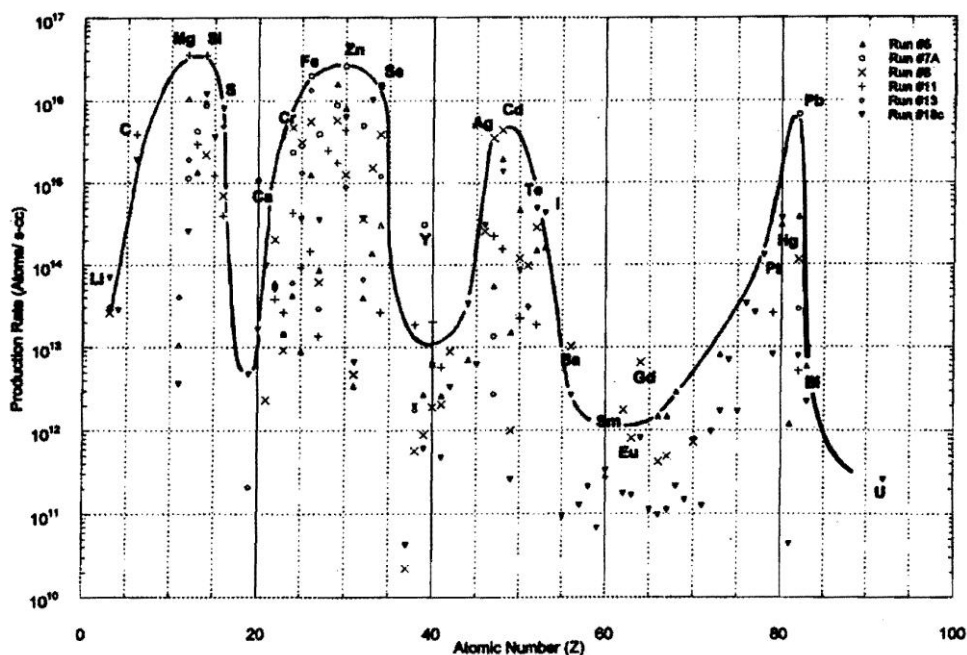


Fig. A9-3. Speculative distribution of neutrons in the neutron conduction bands around a boundary region of a Ni-Pd compound CF material as a function of position. (a) The structure of a Ni-Pd CF material at its boundary region, (b) the density of the trapped neutrons n_n (cm^{-3}) at the boundary region, and (c) the schematic distribution of the trapped neutrons in the neutron conduction bands at the boundary region.

Then, we can imagine the distribution of neutrons in the Ni/Pd interface region as depicted in Fig. A9-3.

The neutrons are accumulated in the lower potential side of the boundary region by the neutrons flowing into there from the higher potential region and the density n_n of the trapped neutron becomes very high there. Then the high density trapped neutrons constitute the neutron drops ${}^A_Z\Delta$ with large values of A and Z . The neutron drops can induce various nuclear transmutations observed in various CF materials. A classification of nuclear transmutation had been given in our book published in 2006 [Kozima 2006 (Sec. 2.5)].

One of the remarkable example is the generation of new nuclides corresponding to the natural abundances as shown in Fig. A9-4 in accordance with the stability law for the nuclear transmutation [Kozima 2006 (Section 2.15), 2012]



FigureA9-4. Comparison of atomic production rates for all runs [Miley 1996a (p. 635, Fig. 2)]

Considering the importance of the experimental data obtained by Miley et al. [Miley 1994, 1996a, 1996b], we cite a detailed reproduction of their data in Appendix A10 reliable for the bases of the ND model and existence of the neutron drops in CF materials.

the thin-film interface region.” [Miley 1994 (p. 316)]

A10-2. Ni film coated plastic microspheres [Miley 1996a] $\text{H}_2\text{SO}_4 + \text{H}_2\text{O}$

“Abstract

Experiments using 1-mm plastic and glass microspheres coated with single and multilayers of thin films of various metals such as palladium and nickel, used in a packed-bed electrolytic cell (Patterson Power Cell™ configuration), have apparently produced a variety of nuclear reaction products. The analysis of a run with 650-Å film of Ni is presented here. Following a two-week electrolytic run, the Ni film was found to contain Fe, Ag, Cu, Mg, and Cr, in concentrations exceeding 2 atoms % each, plus a few additional trace elements. These elements were at the most, only present in the initial film and the electrolyte plus other accessible cell components in much smaller amounts. That fact, combined with other data, such as deviations from natural isotope abundances, seemingly eliminates the alternate explanation of impurities concentrating in the film.” [Miley 1996a (Abstract)]

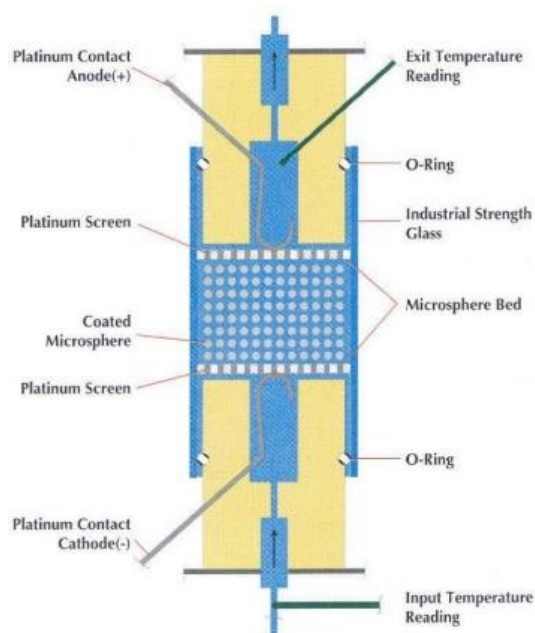


Fig. A10-2. Schematic Diagram of a Patterson Cell. The microspheres are in contact with the cathode screen, hence serve as the cathode. An electrically insulating nylon screen separates the microspheres from the upper anode screen. While platinum is shown here as screen material, titanium was used in present experiments. [Miley 1996a (Fig. 1a)]

Table A10-1. Yield Data from the Combined SIMS/NAA Analysis [Miley 1996a (Table 3)]

Data sheet for change in isotope atom % in metal film after run; comparison to natural abundance (Data from* SIMS; isotopes in **bold** use NAA element weight)

Mass No.	Element	Natural a/o	Change (Reacted-fresh) (in micro-grams)	Fresh MS Atoms	Reacted MS Atoms	Difference % Metal (atomic)	SMS a/o	Difference in a/o (SIMS-Natural)
28	Si	0.92	1.02E-01	8.14E+16	3.02E+17	1.29E+00	4.67E-01	-45.46
29	Si	0.05	9.80E-03	0.00E+00	2.04E+16	9.79E-01	3.55E-01	30.81
30	Si	0.03	5.07E-03	0.00E+00	1.02E+16	4.89E-01	1.78E-01	14.66
32	S	0.95	9.54E-03	0.00E+00	1.80E+16	8.63E-01	1.00E+00	5.00
45	Sc	1.00	4.45E-05	0.00E+00	5.96E+13	2.87E-03	1.00E+00	0.00
46	Ti	0.08	2.00E-04	0.00E+00	2.62E+14	1.26E-02	4.98E-02	-2.95
47	Ti	0.07	2.79E-04	0.00E+00	3.58E+14	1.72E-02	6.79E-02	-0.49
49	Ti	0.06	2.52E-04	0.00E+00	3.10E+14	1.49E-02	5.88E-02	0.37
50	Ti	0.05	3.60E-03	0.00E+00	4.34E+15	2.08E-01	8.24E-01	77.01
50	V	0.00	5.52E-07	3.54E+10	7.01E+11	2.79E-05	2.45E-03	0.00
51	V	1.00	2.30E-04	1.44E+13	2.86E+14	1.14E-02	9.98E-01	-0.04
52	Cr	0.84	9.22E-02	5.63E+14	1.07E+17	5.07E+00	8.70E-01	3.21
53	Cr	0.10	1.19E-02	6.27E+13	1.36E+16	6.42E-01	1.10E-01	1.51
54	Cr	0.02	2.27E-03	1.53E+13	2.55E+15	1.20E-01	2.06E-02	-0.30
54	Fe	0.06	1.34E-02	2.82E+15	1.78E+16	3.96E-01	5.72E-02	-0.10
55	Mn	1.00	7.30E-02	0.00E+00	8.00E+16	3.85E+00	1.00E+00	0.00
56	Fe	0.92	2.11E-01	.29E+16	2.70E+17	6.01E+00	8.69E-01	-4.82
57	Fe	0.02	1.24E-02	.01E+15	1.41E+16	5.14E-01	7.42E-02	5.23
59	Co	1.00	1.83E-03	.23E+14	1.99E+15	7.58E-02	1.00E+00	0.00
63	Cu	0.69	1.17E-01	.57E+15	1.16E+17	4.99E+00	7.00E-01	0.80
64	Zn	0.49	1.63E-02	.42E+15	1.67E+16	5.74E-01	3.64E-01	-12.47
65	Cu	0.31	5.19E-02	.54E+15	4.97E+16	2.14E+00	3.00E-01	-0.80
66	Zn	0.28	9.24E-03	7.82E+14	9.22E+15	3.16E-01	2.01E-01	-7.72
67	Zn	0.04	2.28E-03	1.14E+14	2.16E+15	8.55E-02	5.43E-02	1.32
68	Zn	0.19	1.41E-02	5.08E+14	1.30E+16	5.42E-01	3.44E-01	15.84
69	Ga	0.60	7.59E-05	0.00E+00	6.64E+13	3.19E-03	5.50E-01	-5.40
70	Zn	0.01	1.42E-03	1.64E+13	1.24E+15	5.70E-02	3.62E-02	3.00
71	Ga	0.40	6.39E-05	0.00E+00	5.43E+13	2.61 E-03	4.50E-01	5.40
72	Ge	0.27	5.39E-03	0.00E+00	4.51E+15	2.17E-01	4.84E-01	21.04
73	Ge	0.08	4.23E-03	0.00E+00	3.49E+15	1.68E-01	3.75E-01	29.74
74	Ge	0.37	8.94E-04	0.00E+00	7.28E+14	3.50E-02	7.81E-02	-28.69
75	As	1.00	4.89E-02	0.00E+00	3.93E+16	1.89E+00	1.00E+00	0.00
76	Ge	0.08	7.34E-04	0.00E+00	5.82E+14	2.80E-02	6.25E-02	-1.51
76	Se	0.09	1.63E-02	0.00E+00	1.29E+16	6.21 E-01	1.29E-01	3.88
77	Se	0.08	1.65E-02	0.00E+00	1.29E+16	6.21 E-01	1.29E-01	5.32
80	Se	0.50	4.29E-02	0.00E+00	3.23E+16	1.55E+00	3.23E-01	-17.54
82	Se	0.09	5.71 E-02	0.00E+00	4.20E+16	2.02E+00	4.19E-01	32.75
85	Rb	0.72	4.03E-07	0.00E+00	2.86E+11	1.37E-05	5.00E-01	-22.20
87	Rb	0.28	4.12E-07	0.00E+00	2.86E+11	1.37E-05	5.00E-01	22.20
87	Sr	0.07	0.00E+00	0.00E+00	0.00E+00	0.00E+00	0.00E+00	-7.02
88	Sr	0.83	2.13E-05	0.00E+00	1.46E+13	7.01 E-04	1.00E+00	17.40

Table 3 (continued)

Mass No.	Element	Natural a/o	Change (Reacted-fresh) (in micro-grams)	Fresh MS Atoms	Reacted MS Atoms	Difference % Metal (atomic)	SIMS a/o	Difference in a/o (SIMS-Natural)
89	Y	1.00	3.37E-05	0.00E+00	2.28E+13	1.10E-03	1.00E+00	0.00
93	Nb	1.00	8.13E-05	0.00E+00	5.27E+13	2.53E-03	1.00E+00	0.00
95	Mo	0.16	1.20E-04	0.00E+00	7.62E+13	3.66E-03	3.33E-01	17.63
96	Zr	0.03	7.85E-05	0.00E+00	4.93E+13	2.37E-03	1.00E+00	97.20
98	Mo	0.24	1.24E-04	0.00E+00	7.62E+13	3.66E-03	3.33E-01	9.53
100	Mo	0.10	1.26E-04	0.00E+00	7.62E+13	3.66E-03	3.33E-01	23.70
107	Ag	0.52	1.22E-01	7.32E+15	7.61E+16	2.47E+00	5.70E-01	5.17
108	Pd	0.27	3.27E-03	0.00E+00	1.83E+15	8.78E-02	2.73E-01	0.57
109	Ag	0.48	9.90E-02	6.68E+15	6.14E+16	1.87E+00	4.30E-01	-5.17
110	Pd	0.12	8.89E-03	0.00E+00	4.87E+15	2.34E-01	7.27E-01	60.93
111	Cd	0.13	2.33E-02	0.00E+00	1.27E+16	6.08E-01	1.12E-01	-1.60
112	Cd	0.24	5.38E-02	0.00E+00	2.89E+16	1.39E+00	2.56E-01	1.50
113	Cd	0.12	2.37E-02	0.00E+00	1.27E+16	6.08E-01	1.12E-01	-1.10
113	In	0.04	0.00E+00	0.00E+00	0.00E+00	0.00E+00	0.00E+00	-4.28
114	Cd	0.29	6.33E-02	0.00E+00	3.35E+16	1.61E+00	2.96E-01	0.70
115	In	0.96	4.86E-05	0.00E+00	2.55E+13	1.22E-03	1.00E+00	4.30
116	Cd	0.08	4.87E-02	0.00E+00	2.53E+16	1.22E+00	2.24E-01	14.82
117	Sn	0.08	8.85E-04	0.00E+00	4.56E+14	2.19E-02	1.48E-01	7.20
118	Sn	0.24	2.45E-03	0.00E+00	1.25E+15	6.02E-02	4.07E-01	16.74
119	Sn	0.09	7.87E-04	0.00E+00	3.99E+14	1.92E-02	1.30E-01	4.38
120	Sn	0.33	1.47E-03	0.00E+00	7.41E+14	3.56E-02	2.41E-01	-8.73
121	Sb	0.57	5.05E-03	0.00E+00	2.52E+15	1.21E-01	1.00E+00	42.80
124	Sn	0.06	4.69E-04	0.00E+00	2.28E+14	1.10E-02	7.41 E-02	1.47
125	Te	0.07	5.82E-03	0.00E+00	2.81E+15	1.35E-01	3.75E-01	30.51
126	Te	0.19	3.91 E-03	0.00E+00	1.87E+15	8.99E-02	2.50E-01	6.30
128	Te	0.32	5.96E-03	0.00E+00	2.81E+15	1.35E-01	3.75E-01	5.70
135	Ba	0.07	5.39E-05	0.00E+00	2.41E+13	1.16E-03	9.26E-02	2.67
137	Ba	0.11	6.93E-05	0.00E+00	3.05E+13	1.47E-03	1.17E-01	0.43
138	Ba	0.72	4.71 E-04	0.00E+00	2.06E+14	9.88E-03	7.90E-01	7.31
151	Eu	0.48	1.74E-05	0.00E+00	6.94E+12	3.34E-04	3.33E-01	-14.47
152	Sm	0.27	2.46E-05	0.00E+00	9.74E+12	4.68E-04	2.14E-01	-5.27
153	Bu	0.52	3.52E-05	0.00E+00	1.39E+13	6.67E-04	6.67E-01	14.47
154	Sm	0.23	9.12E-05	0.00E+00	3.57E+13	1.72E-03	7.86E-01	55.87
155	Gd	0.15	3.92E-04	0.00E+00	.53E+14	7.33E-03	9.09E-01	76.21
156	Gd	0.21	3.95E-05	0.00E+00	.53E+13	7.33E-04	9.09E-02	-11.41
163	Dy	0.25	2.90E-05	0.00E+00	.07E+13	5.16E-04	1.00E+00	75.00
165	Ho	1.00	3.42E-05	0.00E+00	.25E+13	6.00E-04	1.00E+00	0.00
172	Yb	0.22	5.24E-05	0.00E+00	.83E+13	8.82E-04	1.00E+00	78.20
206	Pb	0.24	2.67E-03	0.00E+00	7.82E+14	3.76E-02	2.67E-01	3.07
207	Pb	0.23	2.69E-03	0.00E+00	7.82E+14	3.76E-02	2.67E-01	4.07
208	Pb	0.52	4.75E-03	0.00E+00	1.37E+15	6.57E-02	4.67E-01	-5.63

“Most profiles peak in the nickel volume or near the film-plastic interface, suggesting an internal source rather than diffusion in from the surface. For example, the key elements Ag and Fe peak near the Ni-plastic interface, (at ~ 650 Å corresponding to about 12 min. sputtering time). Cu peaks further out in the film. However, the amplitude of the peaks is too small to draw definitive conclusions about diffusion vs. an internal source. The product concentrations decrease into the plastic substrate. However, the decrease is gradual, indicating strong interdiffusion has occurred under run conditions.” [Miley 1996a (p. 21)]

“Conclusion

The results presented here defy conventional views in many ways. First, chemically assisted nuclear reactions are not widely accepted by the scientific community. The present results not only confront that disbelief, but add a new dimension to the issue by reporting copious light and heavy element reaction products that seem to imply multi-body reactions due to the formation of heavier elements such as Cu and Ag from Ni. Further, a reaction which does not emit intense high-energy gammas is required by the experimental results. All these features are difficult to comprehend and at first glance seem to point to impurities. However, as stressed, an extensive effort to find an impurity source has not uncovered one. Also, there is other strong evidence (such as isotope shifts, the different products occurring when the coating material is changed, and the similarity in yield trends with results from other researchers), which supports the conclusion that the elements observed are reaction products.” [Miley 1996a (Conclusion)]

“The analysis of a run with 650-Å film of Ni is presented here. Following a two-week electrolytic run, the Ni film was found to contain Fe, Ag, Cu, Mg, and Cr, in concentrations exceeding 2 atom% each, plus a number of additional trace elements.” [Miley 1996a (Abstract)]

The generation of the transmuted nucleus A_ZX with largely shifted A and Z from the original nuclei in the host material has been explained by the nuclear transmutation by transformation [Kozima 2006 (Sec. 2.5.4)]. The flow of neutrons from a CF material C_1 to another C_2 through the boundary speculated in Appendix A9 will elevate the density n_n in the C_2 very much to generate the neutron drop ${}^A_Z\Delta$ with large values of A and Z there transforms into the transmuted nucleus A_ZX with largely shifted A and Z from the original nuclei in the host material.

“Most profiles peak in the nickel volume or near the film-plastic interface, suggesting an internal source rather than diffusion in from the surface. For example, the key elements Ag and Fe peak near the Ni-plastic interface, (at ~ 650 Å corresponding to about 12 min. sputtering time). Cu peaks further out in the film.” [Miley 1996a (p. 27)]

This data shows clearly the nuclear reactions are due to the neutron Bloch waves in the cf-matter formed in the superlattice of Ni and H, the neutron Bloch waves interact strongly with nuclei displaced from ordered position especially at around boundary

regions between Ni and plastics.

“In view of the large yields obtained, the reactants must involve some of the key species present, namely: Li, S, or O from the electrolyte; C and H from the plastic microsphere core; Ni from the thin films (cathode); and protons (p) from the light water.” [Miley 1996a (p. 35)]

“Other key features observed in Fig. 8 and Fig. 9 that must be accounted for by any theory include the “gaps” between high yield products and the high Ag and Cd yields. Ag (and Cd) production is particularly challenging, since Ag occurs in large quantities but is not favored energetically.” [Miley 1996a (p. 35)]

A10-3. Pd, Ni, and Pd/Ni thin film layers on plastic microspheres with electrolytic liquid H₂O + H₂SO₄ [Miley 1996b]

Abstract

Several research groups previously identified new elements in electrodes that appeared to be transmutation products (Bockris et al., 1996a; 1996b). However, due to the low concentrations involved, the distinction from possible impurities has been difficult. Now, by using a unique thin-film electrode configuration to isolate the transmutation region, plus measurements based on neutron activation analysis, the authors have achieved, for the first time, a quantitative measure of the yield of transmutation products. Results from a thin film (500-3000Å) nickel coating on 1-mm microspheres in a packed-bed type cell with 1-molar Li₂SO₄-H₂O electrolyte were reported recently at the Second International Conference on Low-Energy Nuclear Reactions (Miley and Patterson, 1996 [Miley 1996a]). Key new results are now presented for thin-film Pd and for multiple Pd/Ni layers. The transmutation products in all cases characteristically divide into four major groups with atomic number Z = 6-18; 22-35; 44-54; 75-85. Yields of ~1 mg of key elements was obtained in a cell containing ~1000 microspheres (~½ cc). In several cases over 40 atom% of the metal film consisted of these products after two weeks' operation.”

“[Bockris. 1996] Bockris, J.O'M and G.H. Lin (organizers), 1996a. Proceedings of the First International Conference on Low Energy Nuclear Reactions Conference, J. New Energy, in press.

“[Lin 1996] Bockris, J.O'M, G.H. Miley, and G.H. Lin (organizers), 1996b. Proceedings of the Second International Conference on Low Energy Nuclear Reactions Conference, J. New Energy, 1, 1, 111-118.” [Miley 1996b (Abstract)]

It is necessary to correct the citation in the above sentence from [Miley 1996b (Abstract)]. The citation “(Bockris et al. 1996a and 1996b)” does not correspond to any paper in *J. New Energy* Vol. 1 and Vol. 3 (*Proc. 1st and 2nd International Conference on Low Energy Nuclear Reactions*). Possible papers corresponding to the intention of the citation may be the following papers: [Bockris 1996] and [Lin 1996].

“Results from a thin film (500-3000A) nickel coating on 1-mm microspheres in a packed-bed type cell with 1-molar LiSO₄-H₂O electrolyte were reported recently at the Second International Conference on Low-Energy Nuclear Reactions (Miley and Patterson, 1996).” [Miley 1996b (Abstract)]

“Key new results are now presented for thin-film Pd and for multiple Pd/Ni layers. The transmutation products in all cases characteristically divide into four major groups with atomic number Z=6-18; 22-35; 44-54; 75-85.” [Miley 1996b (Abstract)]

“Thin-film coatings on 1-mm-diameter plastic microspheres, ranging from 500A thick single layers of Pd or Ni to multiple Ni/Pd layers.” [Miley 1996b (p. 629)]

Table A10-2. Summary of runs [Miley 1996b (Table 1)]

<u>Run ID</u>	<u>Packing*</u>	<u>Run 10.0 Duration (hours)</u>	<u>Excess Power (W)</u>
<u>5</u>	#59 PS/NPNPN	520	~ 2 ± 0.5
<u>7A</u>	C1 PS/PN-E	197	~ 4 ± 0.8
<u>8</u>	#60 PS/N	311	~ 0.1-0.9
<u>11</u>	#63 PS/P	211	~ 0.1-0.9
<u>13</u>	#61 GL/N	293	~ 0.1-0.9
<u>18c</u>	#76 PS/N	358	~ 0.1-0.9

*see Table 2 for microsphere data

“The coatings were found to be quite stable in this configuration, so experiments were undertaken to study reaction products using thin-films (500- to 3000-A thick) laid down by a special sputtering process.” [Miley 1996b (p. 630)]

“The following nomenclature is adopted: P: palladium, N: nickel, PS: Polystyrene, G: glass. Thus, a PS/P/N microsphere has a plastic core with a first coating of palladium and a second coating of nickel.” [Miley 1996b (p. 631)]

“Multi-layers gave larger excess power, approaching 4 W.” [Miley 1996b (pp. 631 – 632)]

This result (“Multi-layers gave larger excess power, - -.”) is interesting to test the TNCF model how we can grapple with this event. The nuclear reactions at boundaries are natural results due to the existence of many disordered nuclei in and around these regions as already had shown in the previous work [Miley 1996a]. Further, there is another possibility, as we will give a speculation in another paper on the CF materials of multilayer host elements [Kozima 2021a], the density of the trapped neutrons n_n will increase in one of the layers of the CF material and will induce much nuclear reactions in proportional to the density. This may contribute as the principal cause to the larger excess power observed in the multi-layer cases than the single layer cases.

“Most element profiles distinctly peak in the metal volume or near the metal-core interface, suggesting an internal source rather than diffusion in from the surface.” [Miley 1996b (pp. 634)]

This is a result explicable from our point of view that the neutron Bloch waves interact with nuclei at disordered position from the ordered arrangement.

Further explanation of the experimental results follows:

“The two multi-layer runs (#5 and #7a included in Fig. 2) follow the same general trend as the single-layer runs. Physically #7a differed from #5 by having fewer layers (two vs. five) and used much thicker ($\sim 1 \mu\text{m}$ vs. 300-500Å) layers made by electroplating. Run #5 shows a rich array of products (like the PS/N run #18c) whereas #7a has few products in the region of the third and fourth yield peaks. Interestingly, - - -, the multiple layers also produced the most excess heat of all six runs; see Table 1 (Table A4-1 above). The depth probe scans for the multi-layer runs confirm that the product concentrations decrease with distance from the Pd/N interface(s), suggesting that the reaction occurs preferential there, - - - .” [Miley 1996b (p. 639)]

A schematic picture of the polystyrene sphere used in the experiments explained in the above sentences is given in another paper presented at this Conference [Kozima 2021a (Appendix A8, Fig. A8-1)].

“Characteristics of the thin-film coated microspheres used are summarized in Table 2 (Table A4-2 below).” [Miley 1996b (p. 631)]

Table A10-3 Data for various thin-film microspheres [Miley 1996b (Table 2)]

PS/N/P/N/P/N (#59; used in Run #5)

Layer	Volume (cc)	Mass of layer (g)	# of atoms
PS (core)	6.22E-04	6.09E-04	-
Ni(300A)	1.06E-07	9.41E-07	9.64E+15
Pd(500A)	1.76E-07	2.11E-06	1.19E+16
Ni(400A)	1.41E-07	1.25E-06	1.29E+16
Pd(800A)	2.82E-07	3.38E-06	1.90E+16
Ni(350A)	1.23E-07	1.10E-06	1.13E+16

PS/P/N-E (#C1; used in Run #7A)

Layer	Volume (cc)	Mass of layer (g)	# of atoms
PS (core)	6.22E-04	6.09E-04	-
Pd(1micron)	3.54E-06	4.24E-05	2.39E+17
Ni(0.5 micron)	1.76E-06	1.57E-05	1.61E+17

PS/N (#60; used in Run #8)

Layer	Volume (cc)	Mass of layer (g)	# of atoms
PS	6.22E-04	6.09E-04	-
Ni(2650A)	9.34E-07	8.31E-06	8.52E+16

PS/P (#63; used in Run #11)

Layer	Volume (cc)	Mass of layer (g)	# of atoms
PS (core)	6.22E-04	6.09E-04	-
Pd(2000A)	7.05E-07	8.46E-06	4.76E+16

G/N (#61; used in Run #13)

Layer	Volume (cc)	Mass of layer (g)	# of atoms
Glass (core)	6.22E-04	1.01E-03	-
Ni(850A)	3.00E-07	2.67E-06	2.73E+16

PS/N (#76; used in Run #18C)

Layer	Volume (cc)	Mass of layer (g)	# of atoms
PS	6.22E-04	6.09E-04	-
Ni(3000A)	1.06E-06	9.41E-06	9.64E+16

“Results from a thin film (500-3000A) nickel coating on 1-mm microspheres in a packed-bed type cell with 1-molar LiSO₄-H₂O electrolyte were reported recently at the Second International Conference on Low-Energy Nuclear Reactions (Miley and Patterson, 1996).” [Miley 1996b (Abstract)]

Acknowledgement

The author would like to express his thanks to Dr. T. Ohmori for valuable discussions on the HER and UPD and also on experimental results investigated in this paper.

References

- [Akiyama 1986] T. Akiyama, H. Fukushima, K. Higashi, "Mechanism of Abnormal Type Alloy Deposition," *ISIJ International*, **72**, pp. 918 – 923 (1986), ISSN: 0021-1575 (in Japanese).
- [Aldridge 2001] S. Aldridge and A.J. Downs, "Hydrides of the Main-Group Metals: New Variations on an Old Theme," *Chem. Rev.*, **101**, pp. 3305-3365 (2001), ISSN 1520-6890.
- [Baumann 2007] T. Baumann¹, A.M. Amthor, D. Bazin, B.A. Brown, C.M. Folden et al., "Discovery of ⁴⁰Mg and ⁴²Al Suggests Neutron Drip-line Slant towards Heavier Isotopes," *Nature*, Vol. **449**|25, pp. 1022 – 1024 (2007), doi:10.1038/nature06213 1022 © 2007.
- [Belkova 2016] N.V. Belkova, L.M. Epstein, O.A. Filippov and E.S. Shubina, "Hydrogen and Dihydrogen Bonds in the Reactions of Metal Hydrides," *Chem. Rev.*, **116**, pp. 8545 – 8587 (2016), ISSN 1520-6890.
- [Bockris 1970a] J.O'M. Bockris and A.K.N. Reddy, *Modern Electrochemistry – An Introduction to an Interdisciplinary Area –*, Plenum Press, New York, 1970, Library of Congress Catalog Card Number 6819518.
- [Bockris 1970b] J. O'M. Bockris and A.R. Despić, "The Mechanism of Deposition and Dissolution of Metals," in *The Mechanism of Deposition and Dissolution of Metals, in Physical Chemistry – An Advanced Treatise –*, Vol. **IXB**/Electrochemistry, Chapter 7, Ed. Henry Eyring, Academic Press, N.Y and London, 1970, Library of Congress Catalog Card Number: 66-29951.
- [Bockris 1996] J.O'M. Bockris, B.T. Bush, G.H. Lin and R.A. Monti, "Do Nuclear Reactions take place under Chemical Stimulation?" *J. New Energy (Proceedings of the First International Conference on Low Energy Nuclear Reactions)* **1**, No. 1, pp. 1 – 8 (1996), ISSN 1086-8259.
- [Bockris 1999] J. O'M. Bockris, "Early Contributions from Workers at Texas A&M University to (so-called) Low Energy Nuclear Reactions," *J. New Energy*, **4–2**, pp. 40 – 72 (1999), ISSN 1086-8259.
- [Bockris 2000] J.O'M. Bockris, A.K.N. Reddy, M.E. Gamboa-Aldeco, *Modern Electrochemistry*, 2nd edition, Volume 2A, *Fundamentals of Electrodics*, Kluwer Academic/Plenum Publishers, 2000, ISBN 978-0-306-47605-1.

- [Bressani 1991] T. Bressani, D. Calvo, A. Feliciello, C. Lamberti, F. Iazzi, B. Minetti, R. Cherubini, A.M.I. Haque and R.A. Ricci, "Observation of 2.5 MeV Neutrons emitted from a Titanium- Deuterium Systems," *Nuovo Cimento*, **104A**, pp. 1413 – 1416 (1991), ISSN 2037-4909.
- [Celani 1992] F. Celani, A. Spallone, L. Libaratori, et al., "Search for Enhancement of Neutron Emission from Neutron-Irradiated, Deuterated High-Temperature Superconductors in a Very Low Background Environment," *Fusion Technol.*, **22**, pp. 181 – 186 (1992), ISSN 0748-1896.
- [Celani 2019] F. Celani, C. Lorenzetti, G. Vassallo, E. Purchi, et al., "Unexpected Effects due to Voltage Waveform at Anode, in Gaseous LENR Experiments based on Sub-micrometric Surface Coated Constantan Wires," Terzo Convegno "Assisi Nel Vento", 17-19 Maggio 2019; Domus Laetitia, Assisi (PG)-Italy.
- [Celani 2020a] F. Celani, C. Lorenzetti, G. Vassallo *et al.*, "First Evaluation of Coated Constantan Wires Incorporating Capuchin Knots to Increase Anomalous Heat and Reduce Input Power at High Temperatures," *J. Condensed Matter Nucl. Sci.*, **30**, pp. 25–35 (2020), ISSN 2227-3123.
- [Celani 2020b] F. Celani, C. Lorenzetti, G. Vassallo, E. Purchi, S. Fiorilla et al., "Progress toward an Understanding of LENR-AHE Effects in Coated Constantan Wires in D₂ Atmosphere: DC/AC Voltage Stimulation," *J. Condensed Matter Nucl. Sci.*, **33**, pp. 46 – 73 (2020), ISSN 2227-3123.
- [Claytor 1991a] [T. N. Claytor](#), [D. G. Tuggle](#), [H. O. Menlove](#), [P. A. Seeger](#), [W. R. Doty](#) and [R.K. Rohwer](#), "Tritium and neutron measurements from deuterated Pd-Si," *AIP Conference Proceedings*, **228**, 467 – 480 (1991); <https://doi.org/10.1063/1.40668>
- [Claytor 1991b] T.N. Claytor, D.G. Tuggle and H.O. Menlove, "Tritium Generation and Neutron Measurements in Pd-Si under High Deuterium Gas Pressure," *Proc. ICCF2*, pp. 395 – 408 (1991), ISBN 88-7794-045-X.
- [Claytor 1993] T.N. Claytor, D.G. Tuggle, and S.F. Taylor, "Evolution of Tritium from Deuterided Palladium Subject to High Electrical Currents," *Proc. ICCF3*, pp. 217 – 229 (1993), ISBN 4-946443-12-6.
- [Claytor 1996] T. Claytor, D. Jackson and D. Tuggle, "Tritium Production from a low Voltage Deuterium Discharge on Palladium and Other Metals," *J. New Energy*, **1**, No. 1, pp. 111 – 118 (1996), ISSN 1086-8259.
- [Claytor 1998] T. N. Claytor, M. J. Schwab, D. J. Thoma, D. F. Teter and D. G. Tuggle, "Tritium Production from Palladium Alloys," *Proc. ICCF7*, pp. 88 - 93 (1998), ENECO Inc., Salt Lake City, Utah 84108, USA.
- [Crawford 2014] H. L. Crawford, P. Fallon, A.O. Macchiavelli, R.M. Clark, B. A. Brown

et al., “Shell and Shape Evolution at $N = 28$: The ^{40}Mg Ground State,” *Phys. Rev., C* **89**, pp. 041303-1 – 5 (2014).

[Dash 1994] J. Dash, G. Noble and D. Diman, “Surface Topography and Microcomposition of Palladium Cathodes after Electrolysis in Acidified Light and Heavy Water: Correlation with Excess Heat,” *Proc. ICCF4*, Vol. **2**, pp. 25-1 – 25-11 (1994).

[Dufour 1993] J. Dufour, “Cold Fusion by Sparking in Hydrogen Isotopes,” *Fusion Technology*, **24**, pp. 205 – 228 (1993), ISSN 0748-1896.

[Einstein 1031] A. Einstein, *Cosmic Religion: With Other Opinions and Aphorisms*, 1931.

[Endo 2020] M. Endo, K. Ishikawa, S. Kikuchi, S. Narita, K. Negishi et al., “Deuterium Desorption Experiment Using Surface-Coated Pd Foil with a Fine-Structured Interface,” *Proc. JCF20*, **20-5**, pp. 67 – 79 (2020), ISSN 2187-2260.

[Fleischmann 1989] M. Fleischmann, S. Pons and M. Hawkins, "Electrochemically induced Nuclear Fusion of Deuterium," *J. Electroanal. Chem.*, **261**, 301 – 308 (1989).

[Forsley 1998] L. Forsley, R. Auguste, J. Jorne, J. Khim, F. Mis and F. Phillips, “Analyzing Nuclear Ach from the Electrocatalytic Reduction of Radioactivity in Uranium and Thorium,” *Proc. ICCF7*, pp. 128 – 132 (1998), ENECO Inc., Salt Lake City, Utah 84108, USA.

[Fukushima 1993] H. Fukushima, T. Akiyama, A. Yano, T. Ishikawa and R. Kammel, “Electro-deposition Behavior of Zn – Iron-group Metal Alloys from Sulfate and Chloride Baths,” *ISIJ International*, Vol. **33**, No. 9, pp. 1009 – 1015 (1993), ISSN: 1883-2954.

[Horiuti 1970] J. Horiuti, “Gas Evolution Reactions,” pp. 543 – 610, in *The Mechanism of Deposition and Dissolution of Metals, in Physical Chemistry – An Advanced Treatise* – , Vol. **IXB**/Electrochemistry, Chapter 6, Ed. Henry Eyring, Academic Press, N.Y and London, 1970, Library of Congress Catalog Card Number: 66-29951.

[Hosokawa 2013] G. Hosokawa, M. Kawashima, N. Oikawa, H. Yamada and S. Narita, “Characterization of Deuterium Loading/Unloading Behavior for Various Types of Multi-layered Metal Sample,” *Proc. JCF13*, **13-6**, pp. 188 – 195 (2013), ISSN 2187-2260.

[Iwamura 2006a] Y. Iwamura, T. Itoh, M. Sakano *et al.*, “Observation of Nuclear Transmutation Reactions Induced by D_2 Gas Permeation through Pd Complexes” *Proc. ICCF11*, pp. 339 – 350 (2006), ISBN 981-256-640-6.

[Iwamura 2006b] Y. Iwamura, T. Itoh, M. Sakano *et al.*, “Observation of Surface Distribution of Products by X-ray Fluorescence Spectrometry during D_2 Gas Permeation through Pd Complexes” *Proc. ICCF12*, pp. 178 – 187 (2006), ISBN 981-256-901-4.

[Jensen 2004] AS. Jensen, K. Riisager and D.V. Fedorov, “Structure and Reactions of Quantum Halos,” *Rev. Mod. Physics*, **76**, pp. 215 – 261 (2004), ISSN 0034-6861.

[Jones 1994] Jones et al., “Search for Neutron, Gamma and X-ray Emission s from

- Pd/LiOD Electrolytic Cells: A Null Result” *Proc. ICCF4*, Vol. **3**, pp. 26-1 – 26-14 (1994).
- [Kataoka 2016] S. Kataoka, H. Kudou, K. Ota and S. Narita, “Deuterium Desorption Experiments using Multi-layered Metal Samples with Fine-structured Surface,” *Proc. JCF16*, **16-4**, pp. 29– 40 (2016), ISSN 2187-2260.
- [Kita 1971] H. Kita, “Catalytic activity and the reaction mechanism on the hydrogen electrode reactions” *Nihon Kagaku Zasshi*, **92**, pp. 99 – 114 (1971), ISSN: 0369-5387 (in Japanese).
- [Kita 1973] H. Kita and T. Kurisu, “Electroanalysis by *d*- and *sp*- Metals,” *J. Res. Inst. Catalysis, Hokkaido Univ.*, **21**, No.3, pp. 200 – 246 (1973), ISSN 0034-530X.
- [Kitamura 2014] A. Kitamura, A. Takahashi, R. Seto, Y. Fujita, A. Taniike and Y. Furuyama, “Comparison of Some Ni-based Nano-composite Samples with Respect to Excess Heat Evolution under Exposure to Hydrogen Isotope Gases,” *Proc. JCF15*, pp. 1 – 16 (2014), ISSN 2187-2260.
- [Kitamura 2018] A. Kitamura et al., “Excess heat evolution from nanocomposite samples under exposure to hydrogen isotope gases” *Int. J. of Hydrogen Energy*, **43**. Issue 33, pp. 16187 – 16200 (2018), ISSN: 0360-3199.
- [Kittel 1976] C. Kittel, *Introduction to Solid State Physics*, Fifth Edition, John Wiley and Sons, New York, 1976, ISBN 0-471-49024-5.
- [Kozima 1990] H. Kozima, “On the Mechanism of the Electrochemically Induced Nuclear Fusion,” *Rep. Fac. Science, Shizuoka Univ.*, **24**, pp. 19 – 21 (1990), ISSN 05830923.
- [Kozima 1994] H. Kozima, “Trapped Neutron Catalyzed Fusion of Deuterons and Protons in Inhomogeneous Solids,” *Transactions of Fusion Technology*, **26**, No. **4T**, Part 2 FUSTE8 (4), pp. 508 – 515 (1994), ISSN 0748-1896.
- [Kozima 1997] H. Kozima, K. Kaki and M. Ohta, "The Physics of the Cold Fusion Phenomenon," *Cold Fusion*, **22**, 58 – 78 (1997), ISSN 1074-5610.
- [Kozima 1998] H. Kozima, *Discovery of the Cold Fusion Phenomenon – Development of Solid State-Nuclear Physics and the Energy Crisis in the 21st Century –*, Ohtake Shuppan Inc., 1998, ISBN 4-87186-044-2. The “References” in this book is posted at the CFRL (Cold Fusion Research Laboratory) Website.
<http://www.kozima-cfrl.com/Books/bookse/bookse.html>
- [Kozima 1999] H. Kozima, M. Fujii, M. Ohta, K. Arai, H. Kudoh and K. Kaki, “Analysis of Energy Spectrum of Neutrons Measured in Cold Fusion Experiment on the TNCF Model,” *Il Nuovo Cimento*, **112A**, pp. 1431 – 1438 (1999), ISSN 2037-4909.
- [Kozima 2000] H. Kozima, “Electroanalytical Chemistry in Cold Fusion Phenomenon” *Recent Res. Development in Electroanalytical Chemistry* **2**, pp. 35 – 46 (2000). ISBN:

81-86846-94-8).

[Kozima 2004] H. Kozima, “Quantum Physics of Cold Fusion Phenomenon,” *Developments in Quantum Physics – 2004*, pp. 167 – 196, Ed. V. Krasnoholovets, Nova Science Publishers, Inc., New York, 2004. ISBN 1-59454-003-9.

[Kozima 2005] H. Kozima, “Cold Fusion Phenomenon,” *Rep. Fac. Science, Shizuoka Univ.*, **39**, pp. 21 – 90 (2005), ISSN 05830923.

[Kozima 2006] H. Kozima, *The Science of the Cold Fusion Phenomenon, – In Search of the Physics and Chemistry behind Complex Experimental Data Sets –*, 1st Edition, Elsevier, Amsterdam, 2006, ISBN-13: 978-0-08045-110-7, ISBN-10: 0-080-45110-1.

[Kozima 2009] H. Kozima, “Non-localized Proton/Deuteron Wavefunctions and Neutron Bands in Transition-metal Hydrides/Deuterides,” *Proc. JCF9*, pp. 84 – 93 (2009), ISSN 2187-2260.

[Kozima 2012a] H. Kozima, “Three Laws in the Cold Fusion Phenomenon and Their Physical Meaning,” *Proc. JCF12*, pp. 101 – 114 (2012), ISSN 2187-2260.

[Kozima 2012b] H. Kozima, “Cold Fusion Phenomenon in Open, Nonequilibrium, Multi-component Systems,” *Reports of CFRL (Cold Fusion Research Laboratory)* **12-1**, pp. 1 – 14 (January 2012): <http://www.kozima-cfrl.com/Papers/paperr/paperr.html>.

[Kozima 2013] H. Kozima, “Cold Fusion Phenomenon in Open, Nonequilibrium, Multi-component Systems – Self-organization of Optimum Structure,” *Proc. JCF13*, **13-19**, pp. 134 - 157 (2013), ISSN 2187-2260.

[Kozima 2014a] H. Kozima and K. Kaki, “Atomic Nucleus and Neutron—Nuclear Physics Revisited with the Viewpoint of the Cold Fusion Phenomenon,” *Proc. JCF14*, **14-5**, pp. 47 -76 (2014), ISSN 2187-2260.

[Kozima 2014b] H. Kozima, “Nuclear Transmutations (NTs) in Cold Fusion Phenomenon (CFP) and Nuclear Physics,” *Proc. JCF14*, **14-15**, pp. 168 - 202 (2014), ISSN 2187-2260.

[Kozima 2016] H. Kozima, “From the History of CF Research – A Review of the Typical Papers on the Cold Fusion Phenomenon –,” *Proc. JCF16*, **16-13**, pp. 116-157 (2016), ISSN 2187-2260.

[Kozima 2018] H. Kozima, “Nuclear Transmutations and Stabilization of Unstable Nuclei in the Cold Fusion Phenomenon,” *Reports of CFRL (Cold Fusion Research Laboratory)*, **18-1**, pp. 1 – 32 (June 2018): <http://www.kozima-cfrl.com/Papers/paperr/paperr.html>

The contracted version of this paper with the same title is published as *J. Condensed Matter Nucl. Sci.*, **28**, pp. 28 – 49 (2019), ISSN 2227-3123 in the *Proceedings of the International Conference on the Application of Microorganisms for the Radioactive Waste Treatment* posted at the CMNS website; <http://www.iscmns.org/CMNS/CMNS.htm>

This *Proceedings* is also posted at the LENR website:

<https://www.lenr-canr.org/acrobat/BiberianJPjcondensedza.pdf>

[Kozima 2019a] H. Kozima, “Inductive Logic and Meta-analysis in the Cold Fusion Phenomenon,” *Proc. JCF19*, **19-14**, pp. 85 - 111 (2019), ISSN 2187-2260.

[Kozima 2019b] H. Kozima, “Development of the Solid State-Nuclear Physics,” *Proc. JCF19*, **19-15**, pp. 112 – 147 (2019), ISSN 2187-2260.

[Kozima 2020] H. Kozima, “The “anomalous heat effect” is a normal event in the cold fusion phenomenon – On the paper “Excess heat evolution from nanocomposite samples under exposure to hydrogen isotope gases” by Kitamura et al. published in the *Int. J. Hydrogen Energy* **43**, pp. 16187 – 16200 (2018) –, “*Int. J. Hydrogen Energy*, **45** (38), pp. 19577 – 19582 (2020), ISSN 2187-2260.

[Kozima 2021a] H. Kozima, “Cold Fusion Phenomenon in the Composite CF Materials – Mixed Hydrogen Isotopes, Alloys, Ceramics and Polymers –,” *Proc. JCF21*, **21-2** (2021), ISSN 2187-2260, (to be published).

[Kozima 2021b] H. Kozima, “Cold Fusion Phenomenon in the Compound CF Materials – Effects of Interface –,” *Proc. JCF21*, **21-3** (2021), ISSN 2187-2260, (to be published).

[Kozima 2021c] H. Kozima and T. Ohmori, “The Effects of the Catalytic Action on the Cold Fusion Phenomenon,” (to be published).

[Lin 1996] G.H. Lin and J.O'M. Bockris, “Anomalous Radioactivity and Unexpected Elements as a Result of Heating Inorganic Mixtures,” *J. New Energy*, **1**, No. 3, pp. 100 – 105 (1996), ISSN 1086-8259.

[McKubre 1993] M.C.H. McKubre, S. Crouch-Baker, Riley, S.I. Smedley and F.L. Tanzella, "Excess Power Observed in Electrochemical Studies of the D/Pd System," *Proc. ICCF3*, pp. 5 – 19 (1993), Universal Academy Press, Inc., Tokyo.

[Middleton 2019] C. Middleton, “Neutron-rich Magnesium Undergoes Unexpected Transitions,” *Physics Today*, **72**, 4, pp. 14 – 18 (2019).

<https://doi.org/10.1063/PT.3.4177>

[Miley 1994] G.H. Miley, H. Hora, E.G. Batyrbekov and R.L. Zich., “Electrolytic Cell with Multilayer Thin-Film Electrodes.” *Trans. Fusion Technol.*, **26**(4T), pp. 313 – 340 (1994), ISSN 0748-1896.

[Miley 1996a] G.H. Miley and J.A. Patterson, “Nuclear Transmutations in Thin-film Nickel Coating undergoing Electrolysis,” *J. New Energy*, **1**(3), pp. 5 – 39 (1996), ISSN 1086-8259.

[Miley 1996b] G.H. Miley, G. Name, M.J. Williams, J.A. Patterson, J. Nix, D. Cravens, and H. Hora, “Quantitative Observation of Transmutation Products occurring in Thin-film Coated Microspheres during Electrolysis,” *Proc. ICCF6*, pp. 629 – 644 (1996), NEDO and Institute of Applied Energy, Tokyo, Japan, 1996.

- [Mizutori 2000] S. Mizutori, J. Dobaczewski, G. A. Lalazissis, W. Nazarewicz, and P.-G. Reinhard, "Nuclear skins and halos in the mean-field theory," *Phys. Review*, **C61**, pp. 044326-1 – 044326-13 (2000), ISSN 2469-9985.
- [Morrey 1990] J.R. Morrey, M.R. Caffee, H. Farrar, IV, N.J. Hoffman, et. al., "Measurements of Helium in Electrolyzed Palladium," *Fusion Technol.*, **18**, pp. 659 – 668 (1990), ISSN 0748-1896.
- [Nakano 1998] H. Nakano, T. Akiyama and H. Fukushima, "Underpotential Deposition of Zn with Iron-group Metals," *J. Surf. Finish. Soc. Jpn*, **49**, No. 11, pp. 1209 – 1214 (1998), ISSN: 0915-1869 (in Japanese).
- [Narita 2008] S. Narita, H. Yamada, M. Sakuraba and Y. Fukuda "Investigation of Nuclear Phenomena in Deuterium Diffusion from Pd Heterostructure," *Proc. JCF8*, **8-2**, pp. 5 – 9 (2008), ISSN 2187-2260.
- [Okamoto 1994] M. Okamoto, H. Ogawa, Y. Yoshinaga, T. Kusunoki., and O. Odawara, "Behavior of Key Elements in Pd for the Solid State Nuclear Phenomena Occurred in Heavy Water Electrolysis," *Proc. ICCF4*, Vol. **3**, pp. 14-1 – 14-8 (1993).
- [Oya 1996] Y. Oya, H. Ogawa, T. Ono, M. Aida and M. Okamoto, "Hydrogen Isotope Effect Induced by Neutron Irradiation in Pd-LiOD (H) Electrolysis," *Proc. ICCF6*, pp. 370 – 376 (1996), NEDO and Institute of Applied Energy, Tokyo, Japan, 1996.
- [Plato 1966] Plato (Plato in Twelve Volumes), Vol. **7**, translated into English by R.G. Bury. Cambridge, MA, Harvard University Press; London, William Heinemann Ltd. 1966.
<http://www.perseus.tufts.edu/hopper/text?doc=Perseus:text:1999.01.0164:letter=7>
- [Popescu 2010] V. Popescu and A. Zunger, "Effective Band Structure of Random Alloys" *Phys. Rev. Letters*, **104**, pp. 236403-1 – 236403-4 (2010), ISSN 0031-9007.
- [Qiao 1997] G.S. Qiao, Z.M. Han, L.C. Kong and X.Z. Li, "Nuclear Transmutation in a Gas Loading H/Pd System," *J. New Energy*, **2-2**, pp. 48 – 52 (1997), ISSN 1086-8259.
- [Quaino 2007] P.M. Quaino, M.R. Gennero de Chialvo, A.C. Chialvo, "Hydrogen Electrode Reaction: A Complete Kinetic Description," *Electrochimica Acta*, **52**, pp. 7396–7403 (2007), ISSN 0013-4686.
- [Riisager 1994] K. Riisager, "Nuclear Halo States," *Reviews of Modern Physics*, **66**, No. 3, pp. 1105 – 1116 (1994), ISSN 0034-6861
- [Romodanov 1993] V.A. Romodanov, V.I. Savin, Y.B. Skuratnik and Y. Timofeev, "Nuclear Fusion in Condensed Matter," *Proc. ICCF3*, pp. 307 – 319 (1993), ISBN 4-946443-12-6,
- [Romodanov 1998a] V.A. Romodanov, V.I. Savin and Y.B. Skuratnik, "Nuclear Reactions at Effect of Ions Deuterium on Ceramic Materials from Plasmas of Glow Discharge," *Proc. ICCF6*, pp. 590 – 594 (1998), NEDO and Institute of Applied Energy, Tokyo, Japan,

1996.

[Romodanov 1998b] V.A. Romodanov, V.I. Savin, Y.B. Skuratnik and V.N. Majorov, "Tritium Generation in Metals at Thermal Activation," *Proc. ICCF7*, pp. 319 – 324 (1998), ENECO, Inc, Salt Lake City, Utah 84108, USA.

[Sato 2018] Y. Sato, K. Ota, K. Negishi and S. Narita, "Deuterium Desorption Experiments using Pd–Zr and Pd–Ni–Zr Multi-layered samples," *Proc. JCF18*, **18-1**, pp. 1– 13 (2018), ISSN 2187-2260.

[Shockley 1950] W. Shockley, *Electrons and Holes in Semiconductors with Applications to Transistor Electronics*, Van Nostrand Co., Inc., Princeton, New Jersey, 1950, ISBN-13: 978-044-2075-934.

[Seo 2012] M. Seo, "Underpotential Deposition and Metallic Corrosion Reaction," *Corrosion Engineering of Japan*, **61**, No.9, pp. 341 – 348 (2012), ISSN: 1884-1155 (in Japanese).

[Shani 1989] G. Shani, C. Cohen, A. Grayevsky and S. Brokman, "Evidence for a Background Neutron Enhanced Fusion in Deuterium Absorbed Palladium," *Solid State Comm.*, **72**, pp. 53 – 57 (1989), ISSN: 0038-1098.

[Shockley 1950] W. Shockley, *Electrons and Holes in Semiconductors: with Applications to Transistor Electronics*, Princeton, N. J.: Van Nostrand, 1950, ISBN-13: 978-044-2075-934.

[Shull 1951] C.G. Shull and E.O. Wollan, "Coherent Scattering Amplitudes as Determined by Neutron Diffraction," *Phys. Rev.*, **81**, No. 4, pp. 527 – 536 (1951), ISSN 1536-6065.

[Shull 1956] C.G. Shull and E.O. Wollan, "*Applications of Neutron Diffraction to Solid State Problems*", in *Solid State Physics*, Vol. **2**, Ed. Seitz and Turnbull, pp. 137 – 217, (1956), ISBN: 9780080864662.

[Srinivasan 1990] M. Srinivasan, A. Shyam, T. C. Kaushik, R. K. Rout, L. V. Kulkarni et al., "Observation of Tritium in Gas/Plasma Loaded Titanium Samples," *AIP Conference Proceedings* **228**, pp. 1 – 21 (1990). Brigham Young Univ., Provo, UT: American Institute of Physics, New York.

[Srinivasan 1993] M. Srinivasan, A. Shyam, T.K. Sankaranarayanan, M.B. Bajpai, H. Ramamurthy, U.K. Mukherjee, M.S. Krishnan, M.G. Nayar and Y.P. Naik, "Tritium and Excess Heat Generation during Electrolysis of Aqueous Solutions of Alkali Salts with Nickel Cathode," *Proc. ICCF3*, pp. 123 – 138 (1993), ISBN 4-946443-12-6.

[Stella 1993] B. Stella, M. Corradi, F. Ferrarotto, V. Malone, F. Celani and A. Spallone, "Evidence for Stimulated Emission of Neutrons in Deuterated Palladium," *Frontiers of Cold Fusion (Proc. ICCF3)*, pp. 437 – 440 (1993), ISBN 4-946443-12-6.

- [Takagi 2017] S. Takagi, Y. Iijima, T. Sato et al., “Formation of Novel Transition Metal Hydride Complexes with Ninefold Hydrogen Coordination,” *Scientific Reports*, **7**:44253, (2017), DOI: 10.1038/srep44253 www.nature.com/scientificreports/
- [Takahashi 1991] A. Takahashi, T. Iida, T. Takeuchi, A. Mega, S. Yoshida and M. Watanabe, “Neutron Spectra and Controllability by PdD/Electrolysis Cell with Low-High Current Pulse Operation” *Proc. ICCF2*, pp. 93 – 98 (1991), ISBN 88-7794-045-X.
- [Wikipedia Catalysis] <https://en.wikipedia.org/wiki/Catalysis>
- [Wikipedia Surface-state] https://en.wikipedia.org/wiki/Surface_states
- [Yamaguchi 1993] E. Yamaguchi and T. Nishioka, “Direct Evidence for Nuclear Fusion Reactions in Deuterated Palladium,” *Proc. ICCF3*, pp. 179 – 188 (1993), ISBN 4-946443-12-6.
- [Yuhimchuk 1992] A.A. Yuhimchuk, V.I. Tichonov, S.K. Grischechkin, et al., “Registration of Neutron Emission in Thermocycle of Vanadium Deuterides,” (in Russian) *Kholodnyi Yadernyi Sintez*, p. 57, ed. R. N. Kuz'min, Sbornik Nauchnykh Trudov (Kariningrad) 1992.
- [Yvon 1998] K. Yvon, “Complex Transition-Metal Hydrides,” *Chimia*, **52** (10), pp. 613 – 619 (1998), ISSN 2673-2424.
- [Zaera 1995] F. Zaera, “An Organometallic Guide to the Chemistry of Hydrocarbon Moieties on Transition Metal Surfaces,” *Chem. Rev.*, **95**, pp. 2651-2693 (1995), ISSN 1520-6890.